Alma Mater Studiorum – Università di Bologna

DOTTORATO DI RICERCA IN

SCIENZE DELLA TERRA

Ciclo: XXVIII

Settore Concorsuale di afferenza: 04/A2

Settore Scientifico disciplinare: GEO/02

Drivers of continental margin growth. Examples from the Quaternary Adriatic Basin.

Presentata da: Claudio Pellegrini

Coordinatore Dottorato

Prof. Jo De Waele

Relatore

Dr. Fabio Trincardi

Correlatore
Dr. Vittorio Maselli

Esame finale anno 2016

Preface

The growth of continental margins typically results in the development of large-scale sedimentary units with sigmoidal-shaped profiles, termed clinothems. Clinothems occur at a variety of spatial and temporal scales, are recognized from shelfal to basin regions and represent one of the fundamental building blocks of prograding successions. This Ph.D. thesis is based on four datasets from different case histories along an hypothetical sediment routing system of the Adriatic continental margin. The four case histories allow to investigate how the sediment is transferred from river to continental margin and to document the depositional architecture of a set of prograding successions developed in three different environments, from coastal-deltaic to deep marine settings. The datasets available consist of orthophotos, multibeam bathymetry, Chirp sonar and multichannel profiles, sediment cores and well logs data. The main goal of this Ph.D. thesis is to investigate how the interaction of allogenic and autogenic processes impacts on river morphodynamics and drives clinothems development and growth, and ultimately the formation of modern continental margins. The first case history is a portion of the Po River upstream the Isola Serafini dam. This area may be considered as a natural laboratory where investigate and quantify the impact of the backwater effect on river morphodynamics. The second case history is the Mid Adriatic Deep during the Last Glacial Maximum, where in a river-dominated system developed a 350 m thick succession in a very short-time window. This area allows to investigate the internal architecture, geometric relation and facies distribution of a lowstand delta with high chronological resolution. The third case history, offshore the Gargano Promontory, offers the possibility to investigate how genetically-related coastal and subaqueous progradations, i.e. a compound delta, may develop at sub-millennial time scale. The fourth case history, the southern Adriatic Basin, gives opportunity to investigate the impact of the oceanographic regime on sediment transport, where, far from direct sediment feeding sources, lateral advection and current deposition became the dominant mechanism of margin progradation.

Working on the Adriatic Quaternary succession it was possible to document the effect of a paramount control on margin feed and progradation, to discriminate short-lived phases of extremely rapid deposition during the margin construction, and to document the importance of oceanographic processes on margin growth.

Content

“The same parts of the earth are not always moist or dry, but they change according as rivers come into existence and dry up. And so the relation of land to sea changes too and a place does not always remain land or sea throughout all time, but where there was dry land there comes to be sea, and where there is now sea, there one day comes to be dry land. But we must suppose these changes to follow some order and cycle. The principle and cause of these changes is that the interior of the earth grows and decays, like the bodies of plants and animals...”

(From Meteorology, Aristotele 340 BC ca.)

1) Introduction

1.1) Continental margins

The boundary between continents and the oceans occurs in a physiographic region known as *continental margin*. Continental margins extend from coastal plains to deep-sea basins and encompass shorelines, shallow shelves and steep slopes (Fig. 1.1). Passive continental margins attain the largest sediment accumulation rates on Earth, which results in thick successions that have the potential for resolving signals of change in accommodation, oscillation in sediment flux and variation in oceanographic regime paced over a range of time-scales. For these reasons stratigraphic successions of continental margins represent extraordinary archives from which extract the record of continental-margin processes, climate and paleoceanography (e.g. Pratson et al., 2007).

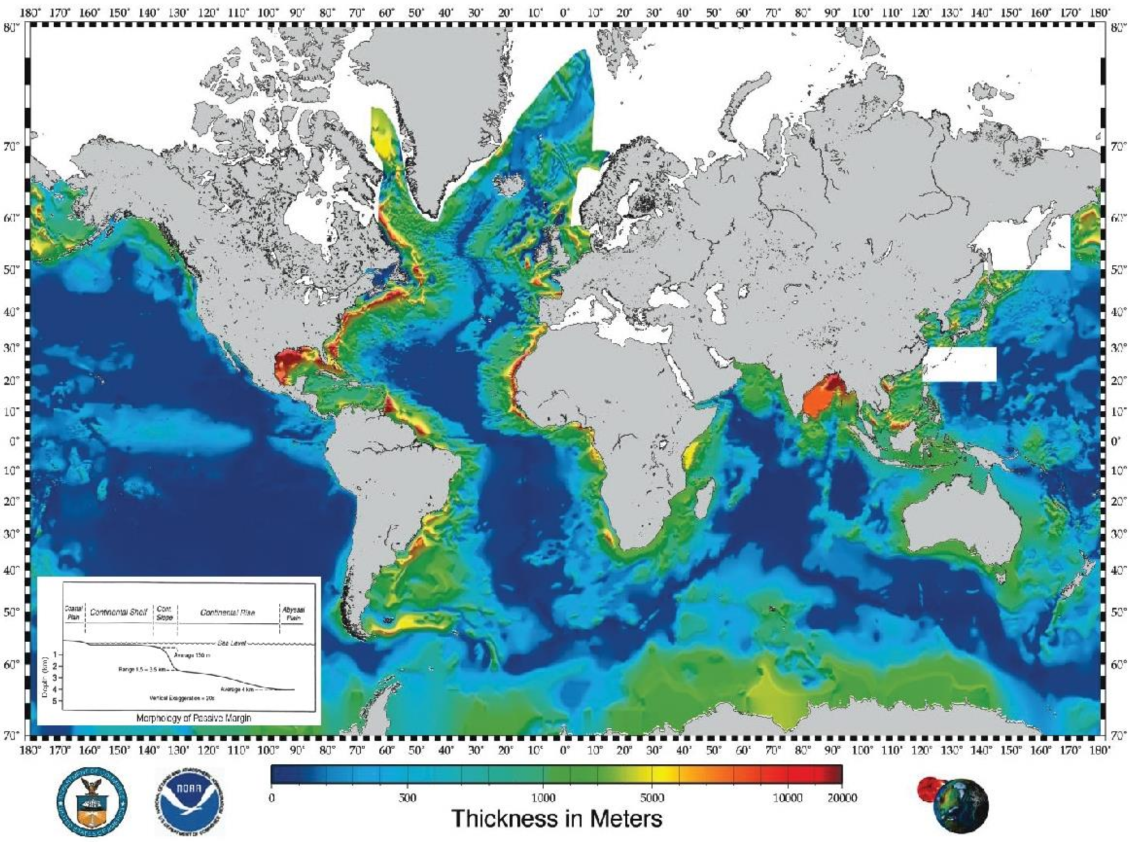

Figure 1.1: map of the total sediment thickness of the World's oceans and Marginal Seas (modified from https://www.ngdc.noaa.gov/mgg/sedthick/sedthick.html). Bottom left: the passive continental margin profiles with coastal plain, broad continental shelf, and continental rise (from Brink *et al.*, 1992).

Rivers deliver some 84% of the total sediment load that reaches the oceans (Milliman and Meade, 1983) and are the dominant means by which clastic sediments are transported to continental margins. Rivers have been active in delivering sediments to continental margins since their inception, but individual rivers are ephemeral on geological timescales. Tectonics, glaciations and stream pirating among other processes alter river courses or have created new rivers from old ones. So, while fluvial input to margins may be considered continuous, the cast of rivers responsible for this input is subject to change (Bridge, 2003). Large individual rivers, such as the Amazon, Indus, Yangtze and Mississippi, often act as a single point source of sediment to a continental margin. Where multiple rivers feed a margin, they can combine to form a line source (Jaeger and Nittrouer, 2000; Walsch et al., 2004; Cattaneo et al., 2007; Liu et al., 2009; Patruno et al., 2015). Sediment emanates from the mouth of each river, but on the shelf these contributions are smeared together by waves and currents, making it very difficult to define where the input sediment comes from.

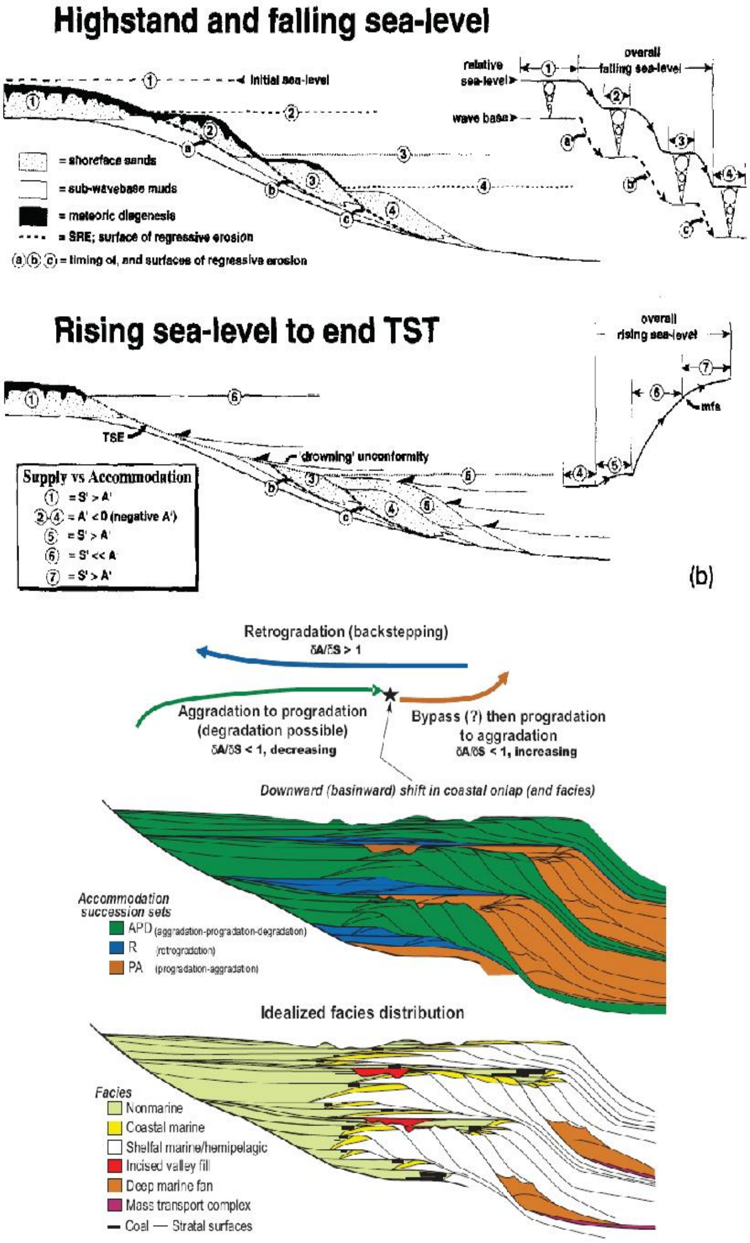

Figure 1.2: stratal stacking patterns associated with changing rates of coastal accommodation creation (δA) and sediment fill (δS) (modified from Hunt and Tuker, 1992; Neal and Abreu, 2009).

The integration of seismic and sequence stratigraphy is a powerful method in revealing the main factors that govern the outbuilding of continental margins (Vail et al., 1977; Vail, 1987; Van Wagoner, 1988). Sequence stratigraphy is focused on analyzing changes in geometric characters and seismic facies of strata packages and on the identification of key bounding surfaces to determine the chronological order of basin fill and erosional events (Catuneanu et al., 2009). Stratal stacking patterns respond to the interplay of changes in the rate of sediment supply and base level (through tectonic subsidence, isostasy, sediment compaction and eustasy), and reflect combinations of depositional trends (Steckler al., 1999). Each stratal stacking pattern defines a particular genetic type of deposit defined as *transgressive*, *normal regressive* and *forced regressive* (Hunt and Tucker, 1992); alternatively, strata packages can be defined as sets of *retrogradation*, *progradation to aggradation*, *aggradation to progradation to degradation* deposit (Fig. 1.2; Neal and Abreu, 2009).

The relationship between stratal stacking pattern and cyclic change in base level is a fundamental theme of sequence stratigraphy; the concept of “base level” delineates a dynamic surface of balance between erosion and deposition (Neal and Abreu, 2009), and is strictly related to the concept of ‘accommodation’, i.e. the amount of space available for sediment accumulation (Jervey, 1988; Neal and Abreu, 2009): a rise in base level creates accommodation, whereas a fall in base level destroys accommodation. Base level is commonly approximated to relative sea level (e.g., Jervey, 1988), although it can lie below sea level depending on the energy of the marine system, especially waves and currents (Pirmez et al., 1998; Swenson et al., 2005). When base level approximates sea level, the concept of ‘base-level change’ becomes equivalent to the concept of ‘sea-level change’ (Posamentier et al., 1988; Swenson et al., 2005) and may become a powerful tool for reconstructing the paleo sea-level oscillations up to a global scale (Haq et al., 1987).

After the early to middle Pleistocene transition, high-amplitude (100 m) sea level fluctuations, among other factors, played a crucial role in continental margins outbuilding (Vail et al., 1977; Haq et al., 1987; Trincardi and Coreggiari, 2000; Schlager, 2004; Rabineau et al., 2005; Ridente et al., 2009; Schattner et al., 2010; Lobo and Ridente, 2014). These fluctuations have many impacts, in particular forcing the migration of the shoreline hundreds of kilometers basinward until reaching the shelf edge during periods of sea level lowstand, promoting coarse-sediment delivery to the deep sea (Covault and Graham, 2010). Conversely, sea level rise causes landward migration of the shoreline (defined as the region from the low-tide shoreline to ca. 10 m water depth), leading to the development of backstepping coastal lithosomes (e.g. Cattaneo and Steel, 2003). The slowing of the rate of sea level rise at the end of each cycle allows most river systems to fill their estuaries, and is followed by a broadening of the sediment dispersal system onto the continental shelf to form deposits with a prominent morphological expression. During periods of sea level highstand a great amount of sand delivered by rivers is trapped on the inner shelf forming subaerial and coastal deposits while finer sediment fractions are transported farther seaward forming subaqueous depocenters (e.g. Michels et al., 1998; Goodbred and Kuehl, 2000; Liu et al., 2009; Korus and Fielding, 2015). Modern deltas and subaqueous clinoforms, originated during the last 5-6 thousands of years (Stanley and Warne, 1994) are observed in different tectonic settings: on passive margins, such as the Amazon deltaic system (Nittrouer et al., 1986); on active-margins, such as the margin where the Ganges-Brahmaputra deltaic system is located (Goodbred et al., 2003); and broad epicontinental shelves such as the Yellow River deltaic system (Alexander et al., 1991). Moreover, these deposits usually exhibit an asymmetrical thickness distribution with respect to their feeding system(s) and reflect the influence or dominance of lateral sediment dispersion through advection (McCave, 1972; Nittrouer et al., 1996; Bhattacharya and Giosan, 2003; Cattaneo et al., 2007).

Eustatic oscillations have occurred in association with climatic fluctuations throughout the Quaternary (Shackleton et al., 1984; Mix and Ruddiman, 1985; Chapman and Shackleton, 1998; Mix et al., 2001), and in turn affected changes in sediment supply to the basin (Mulder et al., 2013), variations in oceanographic regime (Toucanne et al., 2007), and basin interconnectivity (Hernández-Molina et al., 2014). Among all the sedimentary bodies present on continental margins, bottom-current-deposits (i.e. contourites) represent excellent archives for paleoclimatic and paleoceanographic reconstructions because of their fairly continuous sedimentation rate and their high potential in offering high-resolution chronostratigraphy (Faugères et al., 1999; Rebesco et al., 2014 for a review).

Recent advances in geophysical-survey and techniques, especially the use of very high-resolution seismic and 3D multibeam bathymetry, provided the opportunity to analyze the stratigraphic succession of continental margins with higher detail and improved accuracy, both in shallow and deep waters. These advances in knowledge led to a better understanding of the main processes that control the formation of stratigraphic successions and of the evolution of continental margins as a whole.

The overarching aim of this thesis is to contribute to the understanding of the main processes that, by interacting with each other, governed the dispersion of sediments and the final architectural motif of the Quaternary sedimentary succession of the Adriatic continental margin. A wealth of geophysical and core data from the region were analyzed in a multi-methodological approach in order to:

- ✓ understand the hydrodynamics of a modern river with the ultimate aim to provide new insights on the impact of backwater dynamics on the construction of river deltas (chapter 3);
- ✓ evaluate the main factors that generated changes in accommodation on millennial time scales, in a very high sediment supply deltaic system during a lowstand sea level (chapter 4);
- ✓ understand the role of lateral advection in delta construction during the post glacial maximum sea level rise (chapter 5);
- ✓ unravel the role of changing bottom current intensity and pathways from the Pliocene to late Holocene on the construction of a continental margin (chapter 6).

1.2) High-frequency cyclicity in the sedimentary record of continental margins

It is widely accepted that climatic fluctuations reflect the variations in the astronomic parameters that define the Earth's motion around the Sun (eccentricity, obliquity and precession; Milankovitch, 1930), as expressed in the modulation of solar radiation with periodicities of ca. 100, 40 and 20 kyr, respectively (Chappell and Shackleton, 1986; Schwarzacher, 2000). Since their first detection in the marine geological record (Emiliani, 1995), these Milankovitch cycles have been shown to drive sea level variations as expressed in Marine Isotopic Stage (MIS), and Substages, of Quaternary records (e.g. Hays et al., 1976; Siddal et al., 2003). The Milankovitch cyclicity can be identified in a variety of sedimentary records, as documented during the last two decades (Mitchum and Van Wagoner, 1991; Hernández-Molina et al., 2000; Jouet et al., 2006; Ridente et al., 2009; Zhu et al., 2012; Lobo and Ridente, 2014 among others), and on continental margins, as major high-frequency base level changes. Base level cycles were predominantly paced by 40 kyr interval during the Pliocene and Lower Pleistocene (Carter et al., 1998), while sea level and hence sediment deposition has been strongly controlled by 100 and 20 kyr cyclicity after the early to middle Pleistocene transition (Fig. 1.3; Maslin and Ridgwell, 1995).

Most of the sedimentary successions on modern continental margins show a dominant influence of 100 kyr glacial-interglacial cycles, including well-studied Mediterranean areas (e.g. Cattaneo and Trincardi, 1999; Amorosi and Colalongo, 2005; Rabineau et al., 2005). Each sequence is bounded by shelf-wide unconformities recording subaerial erosion (e.g. Hernandez-Molina et al., 1994; Trincardi and Correggiari, 2000; Tesson et al., 1998; Ridente and Trincardi, 2002; Bernè et al., 2007).

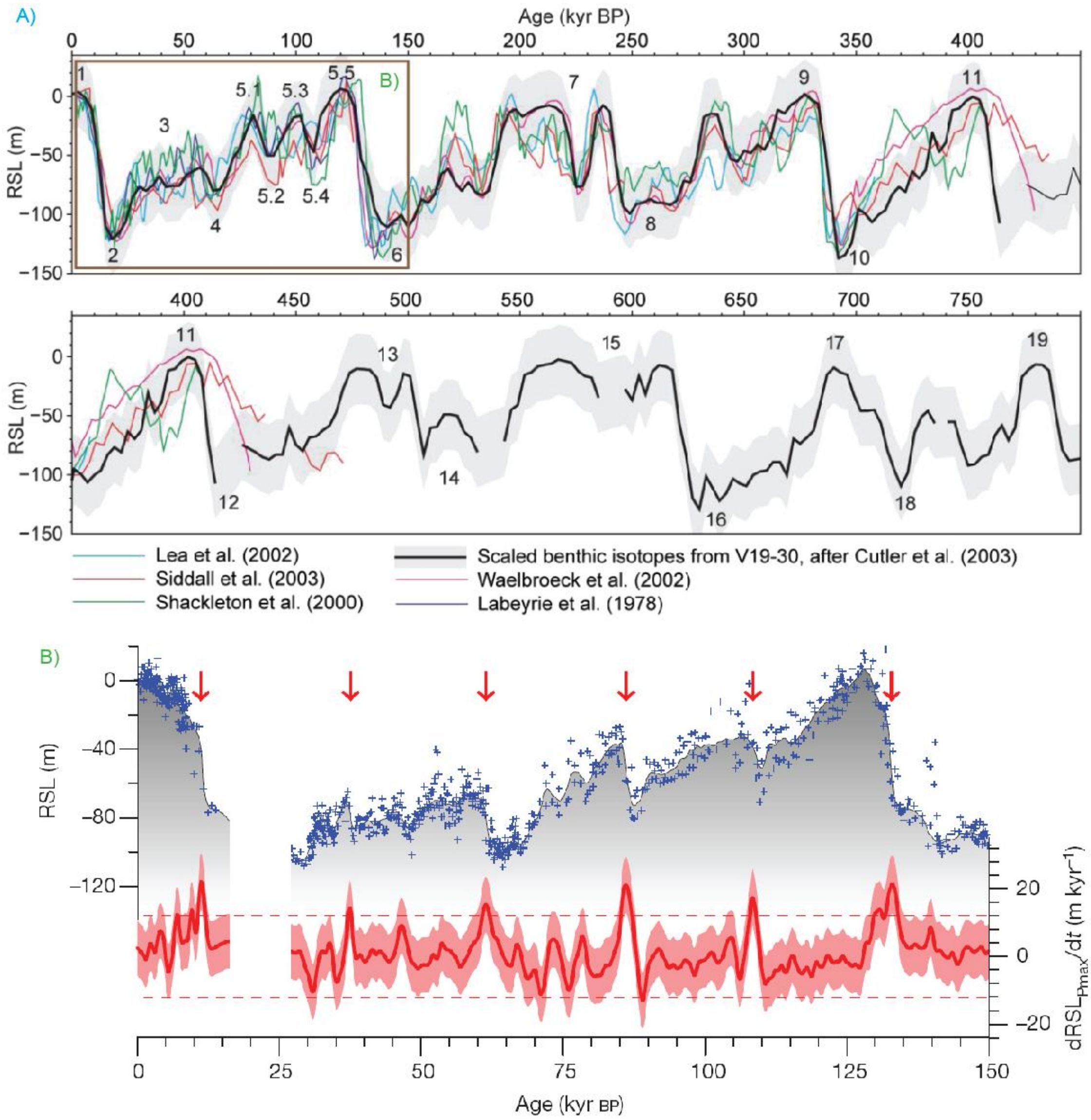

Figure 1.3: A) sea level curves reflect astronomic cycles at Milankovian and sub-Milankovian time scales; numbers represent Marine Isotope Stage and Substage. B) detail of sea level curve for the last 150 kyr (from Grant et al., 2012). Blue crosses mark relative sea-level data, while grey shading indicates the maximum probability of relative sea-level. The red line displays respective rates of sea-level change with 95% confidence interval (pink shading). Rates of sea level change of +12 and -8 m/kyr are indicated by dashed lines. Red arrows mark peaks in sea level rises of more than 12 m/kyr. Data from the Red Sea aplanktonic interval (14-23 kyr BP) are omitted. Modified from Lobo and Ridente (2014).

Recently, sub-Milankovich climate and sea level fluctuations have been documented in the Gulf of Lions, where short-lived prograding sequences could be linked to 5-10 kyr cycles matching the occurrence of Heinrich events (Bassetti et al 2008; Sierro et al., 2009); while changes in the inflow, ventilation and vertical fluctuation punctuated the Levantine Intermediate Water and variations in temperature impacted the deep-water formation along the Western Mediterranean margin, matching the timing of Dansgaar-Oeschger cycles (Cacho et al., 2006; Toucanne et al., 2007; Minto'o et al., 2015). Throughout the Holocene climatic fluctuations known as *Bond events* occurring every ca. 1.5-2 kyr were identified primarily from fluctuations in ice-rafted debris by studying petrologic traces of drift ice in the North Atlantic; these Bond events may be viewed as the interglacial counterpart of the glacial Dansgaard-Oeschger events (Bond et al., 1997). A similar cyclicity was documented to affect discharge rates of the Po delta in the Adriatic Sea through the Holocene (Piva et al., 2008).

A peculiar example of abrupt climate change occurred within late Pleistocene during the cold spell of the Younger Dryas (Fairbanks, 1989). The Younger Dryas stadial, between 12.8-11.6 ka BP (Severinghaus et al., 1998), was a major cooling event linked to an abrupt interruption of the thermohaline oceanographic circulation in the North Atlantic (Berger, 1990) that marked the transition between two steps of deglacial warming characterized by pulses of meltwater input (Bard et al., 1990). The meltwater pulse 1A (MWP-1A), at about 14.08-13.61 ka BP, centered with the Older Dryas, and the MWP-1B, centered at 11.4–11.1 BP during the last phases of the deglaciation (Berger, 1990; Camoin et al., 2012). The Younger Dryas event was recorded in the stratigraphy of Mediterranean margins by a set of shelf-phase deltas and subaqueous progradations, offshore, accompanied by the re-incision of channel-belt deposits by rivers, on land (Trincardi et al., 1996; Cattaneo and Trincardi, 1999; Labaune et al., 2005; Berné et al., 2007; Hernández-Molina et al., 1994; Amorosi and Milli, 2001; Maselli et al., 2011; Sømme et al., 2011).

The identification of bounding surfaces relating to Milankovitch- and Sub-Milankovitch-type depositional units is of great importance in the investigation of prograding sequences since, as mentioned above, these may reflect eustatic oscillations, sudden changes in sediment supply, and shifts in the oceanographic regime. The combination of these fluctuating environmental factors becomes especially important in river-dominated systems (chapter 4), supply- and advection-dominated deltaic systems (chapter 5) and bottom-current-dominated systems (chapter 6), where climatically-induced perturbations may be recorded by changes in sedimentary stacking pattern.

1.3) Adriatic geological setting

1.3.1) Physiographic setting of the Adriatic basin

The Adriatic Sea is an epicontinental basin elongated about 800 km long in NW-SE direction and about 200 km wide, with a present day surface area of ca. 138, 600 km^2 (Cushman-Roisin, 2001) that represents the northernmost part of the Mediterranean Sea extending as far as 45°47’ North. The northern Adriatic Sea is characterized by a low-gradient profile (ca. 0.02°) that reaches its maximum depth of about 252 m in the Mid Adriatic Deep (MAD), a remnant slope basin aligned in a SW-NE (Fig. 1.4). South of the MAD, localized bathymetric irregularities, such as the Tremiti Islands, the Gargano Promontory, the Gallignani Ridge and the Pelagosa Sill, are the morphological expression of recent tectonic activity (Fig. 1.4). The southern Adriatic Sea, beyond the Pelagosa Sill, reaches depths of ca. 1200 m and is flanked by a steep slope and a broad shelf, about 70-80 km south of the Gargano Promontory (Fig. 1.4).

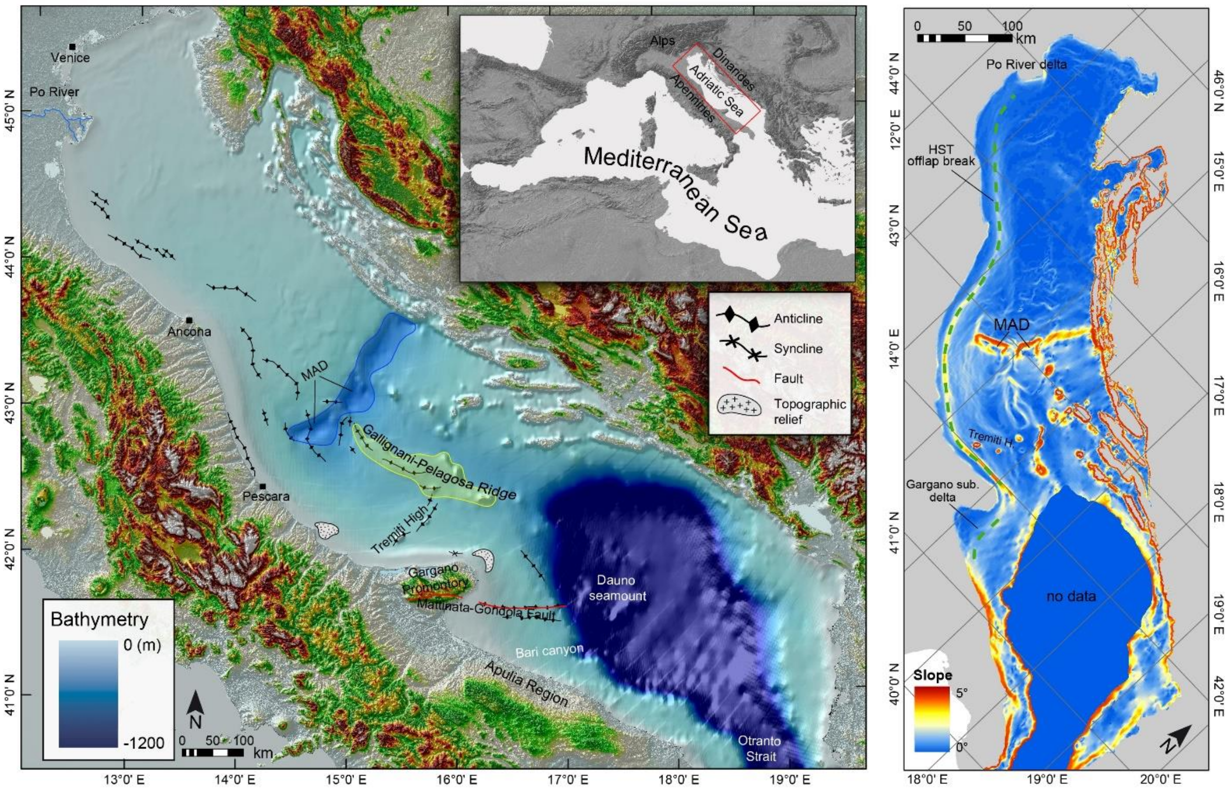

Figure 1.4: Left: Digital elevation model of the Adriatic Sea with main structural elements. MAD stands for Mid Adriatic Deep. Right: slope angle map of the Adriatic Sea floor shallower than 300 m. The green dashed line indicates the offlap break of the Late Holocene deposits (Cattaneo et al., 2007). Note that the shelf is steeper in the study area than in the northern Adriatic. The digital elevation model of the land surface is derived from SRTM 90 m Digital Elevation Data (http://srtm.csi.cgiar.org). Modified after Maselli et al., 2011.

The steep and irregular western slope of the southern Adriatic Sea is characterized by an uneven morphology related to several structural highs (e.g. the Gondola anticline and the Dauno sea mount), and large incisions, as the Bari Canyon (Fig. 1.4). The southern Adriatic Sea is connected with the Ionian Sea through the Otranto Strait, a relatively narrow and deep sill (72 km wide and 780 m deep), which plays a fundamental role in determining the present-days circulation pattern of the whole Mediterranean Sea (Artegiani et al., 1997a,b).

1.3.2) Tectonic setting of the Adriatic basin

The Adriatic basin lies on a continental crust (Adria), located between the East-verging Apennine and the West-verging Dinarides (Ori et al., 2009; Royden et al., 1987). The structural setting and sedimentary architecture of the Adriatic basin reflect a long-term evolution from a passive margin during the Mesozoic to a foreland domain during the Cenozoic (D'Argenio and Horvath, 1984). The western Adriatic margin of the Adriatic basin represents the Oligo-Miocene to early Pleistocene Apennine foreland basin (Fig. 1.5; Ricci Lucchi, 1986; Argnani et al., 1993, 2001, 2009; Doglioni et al., 1994, 1996).

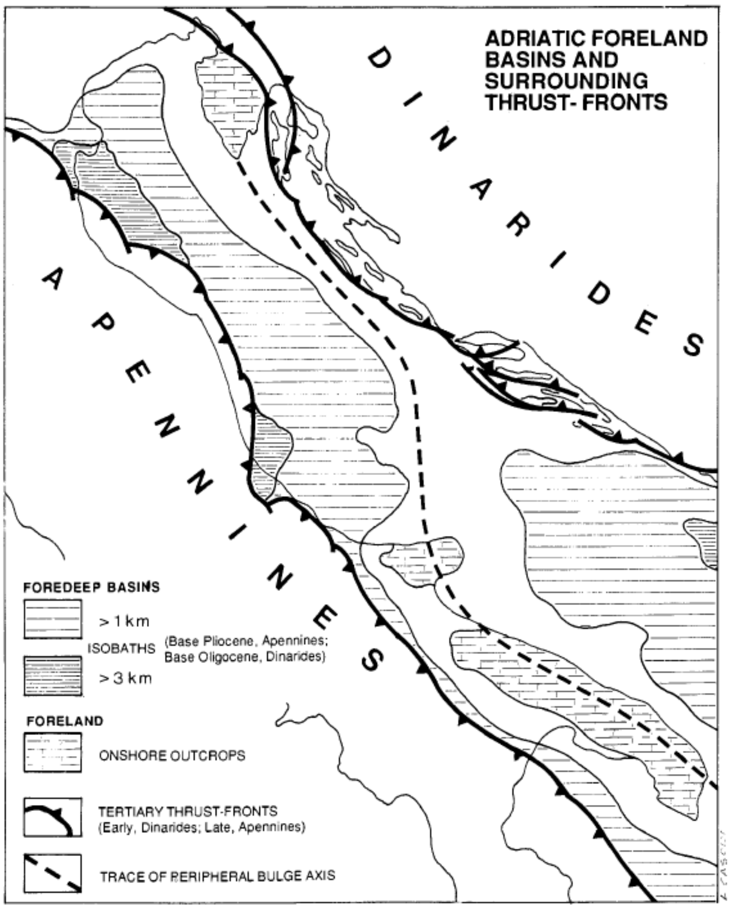

Figure 1.5: sketch map of the Adriatic foreland with an outline of the flexural bulge resulting from the double load of the Apennines and Dinarides fold and thrust belts (from Argnani et al., 1993).

The emerged sectors of the Gallignani Ridge, the Gargano Promontory and the Apulia ridge correspond to the flexural bulge resulting from the subduction activity connected to the Apennine and Dinaric-Ellenic belts. (Argnani et al., 1993, de Alteriis, 1995; Bertotti et al., 1999). North of the Gargano Promontory, the central Adriatic shelf area is bounded by NW-SE trending Gallignani and Pelagosa ridges, which correspond to regional folds along this peripheral bulge (de Alteriis, 1995).

The tectonic domain provides evidence of marked structural differentiation from North to South of the Gargano, likely related to deep crustal discontinuities and variations in lithosphere thickness of the westward dipping Adriatic plate (Doglioni et al., 1994; de Alteriis, 1995). Transpressive structures occur in the North within the NE-SW oriented Tremiti-Pianosa High (Argnani et al., 1993;

de Alteriis, 1995) and along the Gargano Deformation Belt, extending offshore in the W-E trending Gondola fault (Ridente et al., 2008).

The tectonic evolution of the central Adriatic Sea since the Oligocene shows that the highest subsidence values are confined landward, toward the Apennine foredeep, as highlighted by the flexure of the Messinian datum (e.g. Scrocca, 2006) and the average subsidence rates of 0.3 mm/yr calculated from the PRAD 1-2 borehole placed in the central Adriatic Sea (Maselli et al., 2010). Since the middle Pleistocene, the units infilling the foredeep basin have changed from a dominant turbidite fill into a progradational margin wedge that records the Milankovich glacial-eustatic cyclicity (Ridente et al., 2009; Ghielmi et al., 2010).

South of the Gargano Promontory the South Adriatic Margin corresponds to the present days Dinarides Foredeep and the Bradanic trough, on the western side of the Apulia ridge, corresponds to the Apennine foredeep (Argnani et al., 1996). Combined seismic and outcrop data suggest that, during the Pliocene, a large and subsiding foredeep basin encompassed the areas North and South of the Gargano Promontory (Torre et al., 1988). In the late Pliocene, the growth of structural highs mainly related to the establishment of the Tremiti transfer zone, separated this foredeep into two distinct basins: the Adriatic foredeep basin and the Bradanic foredeep basin, respectively North and South of the Gargano Promontory (Capuano et al., 1996). These two sectors were then further decoupled with the growth of the Apulia Ridge, during the middle-late Pleistocene (Doglioni et al., 1994).

In the southern Adriatic Sea, deformation since the Pliocene was likely related to the re-activation and inversion of inherited Mesozoic extensional faults (Argnani et al., 1993). These faults form the Gargano Deformation Belt, which develops both on land with the Monte S. Angeolo-Mattinata fault, and offshore where the W-E-trending deformation zone related to the Gondola fault and anticline are the most evident features (Billi and Salvini, 2000; Ridente et al., 2008).

1.3.3) Oceanographic setting of the Adriatic basin

The Adriatic Sea is a micro-tidal epicontinental sea dominated by a cyclonic circulation driven by thermohaline processes (Artegiani et al., 1997a, b; Poulain, 2001). Three water masses define the general oceanographic setting (Fig. 1.6; Paschini et al. 1993): (1) a surficial temperature-mixed layer (0-30 m); (2) a Levantine Intermediate Water (LIW); (3) and the Northern Adriatic Deep Water (NAdDW).

The cyclonic circulation of surficial waters, with the upper 10 m of less saline and cooler waters of coastal origin, mainly formed by the Po River runoff, forces the fresh waters to flow along the western side of the basin. Fluvial sediment sources are located almost exclusively along the north and western side of the Adriatic basin, with a combined modern delivery of 51.7 10^6 t yr-1 of mean suspended load with contributions of 3 10^6 t y-1 from eastern Alpine rivers, 15 10^6 t y-1 from the Po river, 32.2 10^6 t y-1 from the eastern Apennine rivers and 1.5 10^6 t y-1 from rivers south of the Gargano promontory (Frignani et al., 1992; Milliman and Syvitski, 1992; Cattaneo et al., 2003). In this shallow part of the basin, hypoxic events occur, typically, between September and November and reflect low current velocities at the gyre centre, enhanced water stratification, which reduces vertical mixing, and high turbidity which prevents light penetration. Currents are stronger away from the gyre centre, resulting in a prevailing flow to the SE along the Italian coast, a flow that appears consistent with the overall shore-parallel thickness

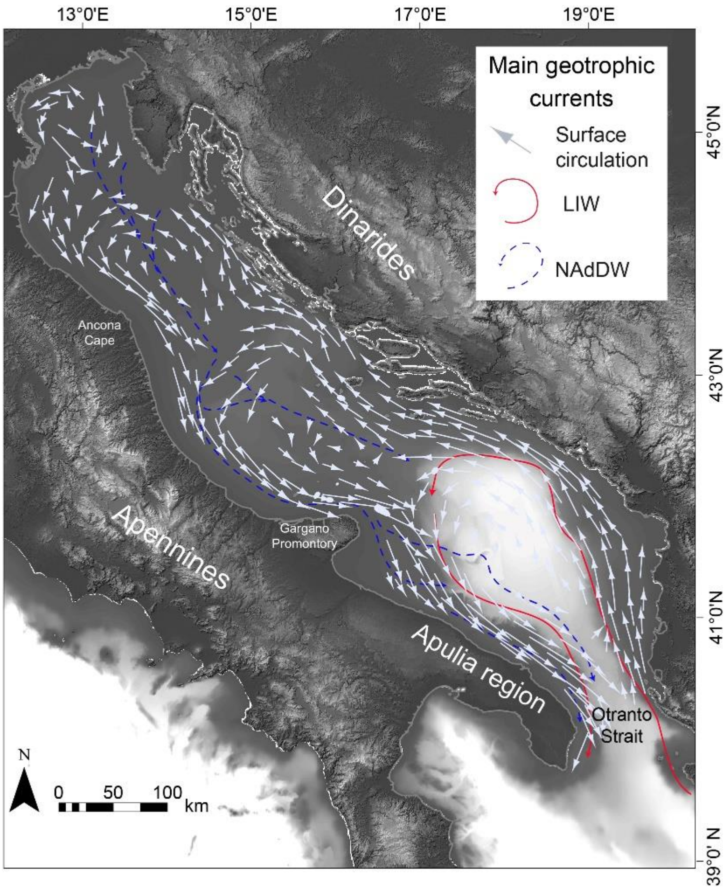

Figure 1.6: Pathways of surface circulation, North Adriatic Dense Waters (NAdDW) and Levantine Intermediate Waters (LIW) in the Adriatic Sea (from Poulain et al., 2001; Cattaneo et al., 2003; Bonaldo et al., 2015; Marini et al., 2015).

distribution of the late-Holocene clinoform (Cattaneo et al., 2003 and 2007). Sediment transport is enhanced in the northern Adriatic by the northeasterly Bora wind that enhances waves and currents especially in winter, with an average southward transport along the shelf and reduced across-shelf transport (Lee et al., 2005).

The LIW, a denser and salty water mass (29.0 kg/m^3) that forms in the Levantine Basin through evaporation during the summer and cooling during winter (Lascaratos et al., 1999), enters in the Adriatic Sea through the Otranto Strait and flows with a cyclonic path in a water depth range between 200 and 700 m (Fig. 1.6; the so-called South Adriatic Gyre: e.g. Artegiani et al., 1997a, b; Mantziafou and Lascaratos, 2008).

The North Adriatic Dense Water (NAdDW), the densest water in the whole Mediterranean with densities up to 1.030 kg/m^3 and mean temperatures of ~ 11 °C during extreme events (Vilibič, 2003), is generated on the broad and shallow (< 40-m-deep) North Adriatic shelf (Fig. 1.6) through intense cooling and evaporation during January and February and is largely affected by severe winter outbreaks of the cold and dry northeast Bora wind (Ivančan-Picek and Tutiš, 1996; Grubišič, 2004), and by river runoff. Due to its spatial heterogeneity, the Bora wind produces a coupled cyclonic–anticyclonic gyre system in the North Adriatic (Hendershott and Rizzoli, 1976; Artegiani et al., 1997a, b), thus increasing vertical mixing in the area, especially in the centre of the cyclonic gyre. The newly formed NAdDW flows southward as different water branches along the Italian coast, towards the MAD and the South Adriatic Margin (SAM; Artegiani and Salusti, 1987). On its routing, the NAdDW may sink and flow as a bottom-trapped current underneath the older water masses present in the MAD: lifting and pushing the older water masses through Pelagosa Sill, and promoting water exchange among the basin and the migration of small-scale sediment drifts (Marini et al., 2015). Typically, the NAdDW reaches the South Adriatic slope two months after its generation (Vilibič and Orlič, 2001), strongly interacts with the slope topography by enhanced turbulent mixing, and finally sinks to the bottom of the SAM (Trincardi et al., 2007; Benetazzo et al., 2014). Through this process the NAdDW cascades obliquely across the south Adriatic slope along the steepest sector reaching below the depth range impacted by the contour parallel LIW (Trincardi et al., 2007; Canals et al., 2009). On the other side, due to its dynamical properties (buoyancy and kinetic energy), a portion of the NAdDW remains trapped on the shelf, flowing as a contour-parallel bottom current over several hundreds of kilometers (Fig. 1.6; Benetazzo et al., 2014; Bonaldo et al., 2015).

Both the contour-parallel LIW and the NAdDW interact with the seafloor morphology along preferred paths, leading to the formation of depositional and erosional features in water depths between ca. 100 and 1.200 m (Fig. 1.6; Verdicchio et al., 2007; Foglini et al., 2015). Recent analysis of erosional and depositional features highlighted how the process of bottom-hugging currents concur to a thorough “restyling” of the submarine landscape markedly differentiated morphologies and sediment distribution (Foglini et al., 2015). These processes were active, or become re-activated, after the end of the last glacial maximum (Verdicchio et al., 2007), likely in response to the sea level rise that flooded the Adriatic shelf thereby permitting the formation of dense shelf waters by rapid winter cooling of an extensive shallow-water region (less than 50 m deep).

2) Overview of own research

The purpose of this PhD project is to understand the main processes that governed the evolution of the Adriatic basin during the Quaternary and to define allogenic and autogenic signals preserved in the stratigraphic record. To achieve this goal, four case histories were selected along the Adriatic basin (Fig. 2.1) where relative impact of sediment flux and basin dynamic are markedly differentiated: 1- (northern Adriatic Po plane): the effect of backwater on the morphodynamic evolution of a river (chapter 3): 2- central Adriatic margin (Adriatic shelf and Mid Adriatic Deep): river-dominated system with very high sediment supply, where direct supply from the catchments is the major controlling process (chapter 4); 3- central Adriatic margin (offshore the Gargano Promontory): a supply-and advection-dominated system, where fine grain sediments are transported far from the main feeding point (chapter 5); 4- south Adriatic margin (outer shelf, slope and basin): a current-dominated system, where, far from direct sediment feeding sources, the oceanography of the basin controls the stacking of stratigraphic units (chapter 6).

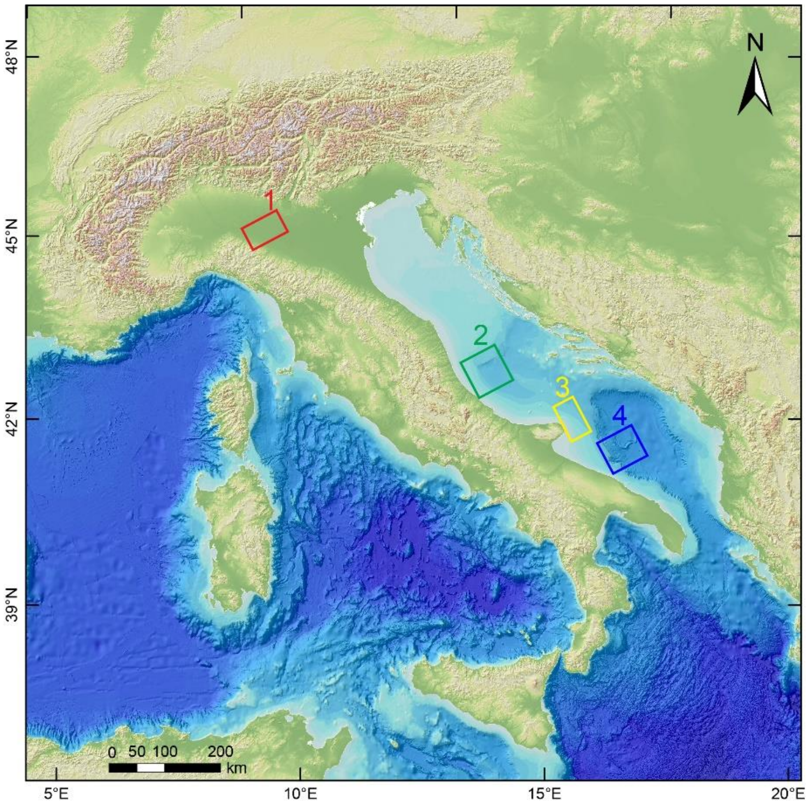

Figure 2.1: the four case histories along the Adriatic continental margin.

The results obtained for each study area have been documented in four research paper (that have either been published, are under peer review, or as in the case of chapter 4 is currently under internal review by Exxon-Mobil researchers for submission to a peer-reviewed international journal) and are presented in chapters 3 to 6. Each chapter consists of a manuscript (edited following the style of the journal) and a brief introduction on the topic of the research and the open questions to which the manuscript aims to address. In addition, chapter 4 is accompanied by the supplementary material that take into account the age model of PRAD 1-2 borehole done under the guidance of Dr. Alessandra Asioli (IGG-CNR, Padua) and the stratigraphic analysis performed at the Upstream Research Company of the Exxon-Mobil (Houston, TX).

Finally, chapter 7 reports the main conclusion of this dissertation.

The manuscript I (chapter 3),

River morphodynamic evolution under dam-induced backwater: an example from the Po River (Italy)

concerns on a portion of the Po River upstream of the Isola Serafini dam (Northern Italy). The trunk of the Po River is viewed as a natural laboratory where investigate and quantify the impact of a backwater zone on river morphodynamics. This analysis helps understanding how the sediment is exported to the ocean and highlights the potential of backwater effect in governing river morphology and sediment partitioning along the channel axis.

The manuscript II (chapter 4),

Stratal architecture, shelf-edge trajectories and sand bypass on the rapidly accumulated Po River lowstand delta forced by high-frequency base level change

focuses on the late Quaternary stratigraphic succession of the Mid Adriatic Deep provides the opportunity to investigate with high spatial and temporal resolutions the relation between clinoform progradation and sediment bypass to the basin and refer it to the late-Quaternary global eustatic curve. The high-resolution chronostratigraphy framework of the Po River lowstand wedge provides peculiar insights into shelf-edge architecture and growth phases, which can be applied to models of continental-margin evolution.

The manuscript III (chapter 5),

Anatomy of a compound delta from the post-glacial transgressive record in the Adriatic Sea

reports on a supply-dominated system offshore the Gargano Promontory, where the oceanography of the receiving basin regulates sediment dispersion through advection and a markedly skewed thickness distribution of the resulting stratigraphic units. The interplay between sediment supply and sediment advection governed the development of a compound delta with a markedly asymmetric subaqueous clinoform during a short interval of relative sea level still stand during the Younger Dryas cold reversal.

The manuscript IV (chapter 6),

Pliocene–Quaternary contourite depositional system along the south-western Adriatic margin: changes in sedimentary stacking pattern and associated bottom currents

investigates a system far from a direct river-born sediment input where the activity of contour-parallel and cascading oceanographic currents govern the formation of the stratigraphic units and their architecture. In particular, at the shelf-edge and upper slope of the south-western Adriatic the interaction between oceanographic currents and the seafloor morphology, which in turn reflects local tectonic deformation, favored the development of contourite systems within the Pliocene-Quaternary succession.

3) Rivers and backwater effect

Sediment flux from rivers to the ocean is the main driver of continental sedimentation with significant implications for land use, construction of hydrocarbon reservoirs, and unraveling Earth history and global climate change from sedimentary strata (e.g. Nittrouer, 1999; Blum and Törnqvist, 2000; Paola et al., 2011). Rivers transfer the sediment to continental margins delivering up to 84% of the total sediment load that reaches the oceans (Milliman and Meade, 1983). River mouths represent fundamental transition zones in the sediment source-to-sink pathway where rivers hand off to marine transport processes. Despite the importance of this transfer, there exists considerable uncertainty about the controls on erosion and deposition of sediment near river mouths (e.g., Fagherazzi et al., 2004). Across the river mouth zone, river flow tends to decelerate downstream due to channel deepening; the segment of river where this response occurs defines the backwater zone (Chow, 1959). At the backwater zone a river behave in fundamentally different ways than further upstream because is affected by the static body of water beyond the shoreline (Fig. 3.1).

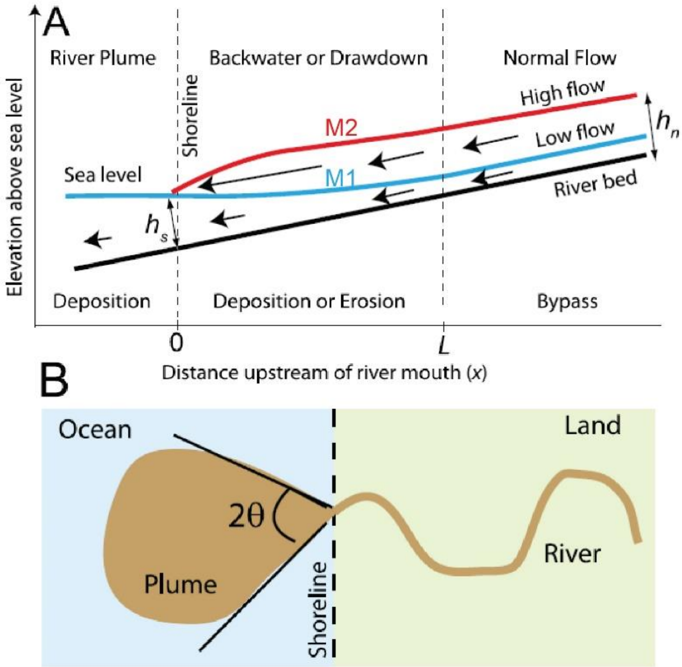

Figure 3.1: cartoon showing a river entering an ocean with three zones of interest: normal flow (x > L), a transitional region (0 < x <L), and the offshore river plume (x < 0) in (a) cross section and (b) plan view. After Lane (1957).

Depending on the channel depth at its mouth and on river-bed slope (Paola, 2000), the backwater effect may propagate for tens to hundreds of kilometer upstream, and can influence the gravel-sand and the sand-mud transition of the river (Venditti and Church, 2014), and the river plume hydrodynamics. Together these changes impact the formation of distributary networks and the evolution of delta plains (Jerolmack and Swenson, 2007; Chatanantavet et al., 2012).

The backwater zone can be affected by erosion or deposition depending on river discharge. At low flow the transitional region is a zone of backwater, where the water depth at the shoreline (hs) is greater than the normal flow depth (hn), and the water surface (blue) and bed (black) diverge downstream (i.e., M1 curve [e.g., Chow, 1959]) resulting in deceleration (shown by length of arrows in Fig. 3.1) and deposition. At high flow hn > hs and the water surface (red in Fig. 3.1) is convex (i.e., M2 curve [e.g., Chow, 1959]), resulting in spatial acceleration of flow and erosion. In both cases, the elevation of the water surface at the river mouth is relatively insensitive to discharge due to lateral spreading of the plume (Fig. 3.1b). This concept suggests that backwater dynamics may be important in shaping channel morphology through deposition and erosion (as suggested in Nittrouer et al., 2011; Whipple et al., 2000). Moreover, many backwater zones and estuaries are interpreted to be transient features that result from flooding due to Holocene sea level rise that created accommodation space faster than could be balanced by fluvial sediment infilling (e.g., Anderson and Rodriguez, 2008). This notwithstanding, many rivers have backwater zones that persist despite the formation of Holocene highstand deltas (e.g., Mississippi River, United States).

The next chapter focuses on a portion of the Po River (northern Italy) as a natural laboratory where a backwater zone was created upstream of the construction of the Isola Serafini dam; in the absence of external forcing such as waves or tides avoiding amplification through resonance with waves and tides the area is an ideal study site. By using an integrated approach based on the analysis of geophysical, sedimentological and hydrological data, this study quantifies how river hydrodynamics change through the backwater zone and its impact on river morphology and sediment partitioning along the channel axis. In essence, the backwater and drawdown effects show a paramount control on the river hydrodynamics and are fundamental in controlling the morphodynamic evolution of rivers, deltas and estuaries. The results obtained may be applied to source-to-sink studies and will help understanding how oscillations in the backwater zone, in response to the allogenic forcing of changing base-level, influence the evolution of channel belts, control sediment export to the ocean and, ultimately, continental margin growth.

3.1) Manuscript I

"River morphodynamic evolution under dam-induced backwater: an example from the Po River (Italy)"

Authors: Vittorio Maselli (Istituto di Scienze Marine, ISMAR-CNR, Bologna, Italy)

Claudio Pellegrini (Istituto di Scienze Marine, ISMAR-CNR, Università di Bologna, Dipartimento di Scienze della Terra e Geologico-Ambientali, Bologna, Italy)

Fabrizio Del Bainco (Istituto di Scienze Marine, ISMAR-CNR, Bologna, Italy)

Alessandra Mercorella (Istituto di Scienze Marine, ISMAR-CNR, Bologna, Italy)

Luca Crose (Agenzia Interregionale per il Fiume Po, AIPO)

Status: Submitted to *Journal of Geophysical Research*

Title

River morphodynamic evolution under dam-induced backwater: An example from the Po River (Italy).

Authors

Vittorio Maselli[1,*], Claudio Pellegrini[1,2], Fabrizio Del Bianco[3], Alessandra Mercorella[1], Luca Crose[4].

[1] Institute of Marine Science, ISMAR-CNR, Bologna, Italy.
[2] University of Bologna, Bologna, Italy.
[3] Consorzio ProAmbiente, Bologna, Italy.
[4] AIPO, Agenzia Interregionale per il Fiume Po, Settore Navigazione Interna.
[*]: Corresponding Author.

Keywords

Po River, backwater, lateral river migration, gravel-sand transition.

Highlights

The Isola Serafini dam interrupts the Po River continuity at 300 km upstream of its river mouth.

The dam creates a backwater zone that modifies river hydrodynamics for up to 40 km upstream.

Lateral migration rates progressively reduce across the backwater zone.

The size of river-bed sediment decreases across the backwater zone, and coarse-grained channel-bars are progressively drowned and reworked through time.

The dam-induced backwater affected the gravel-sand transition of the river.

Abstract

River dynamics is the product of a combination of autogenic processes and allogenic forcing that may affect the entire fluvial systems, from the source to the downstream end. Among external controls, the backwater effect created by the presence of a standing body of water at the river outlet plays an essential role in the evolution of coastal rivers and delta plains. In natural systems the backwater effect propagates from tens to hundreds of kilometer upstream of the river mouth, and its effect may be amplified through resonance with waves and tides. Here we use a portion of the Po River (Italy) upstream of the Isola Serafini dam, as a natural laboratory to investigate and quantify the impact of a backwater zone on river morphodynamics, where the effect of waves and tides are absent. The analysis of orthophotos and longitudinal cross-sections in pre- and post-dam conditions allows understanding how the Po River adjusts its profile in response to the backwater, quantifying areas of net river bank erosion and deposition in meanders, defining river-bed sediment partitioning. Lateral migration rate is high at the transition from normal to gradually-varied flows, where the river-bed slightly aggrades and bed material is coarser. Moving downstream, across the backwater zone, lateral migration rate progressively reduces; this trend is accompanied by the drowning of channel-bars, by the

reduction of river competence, testified also by deposition of fine grained sediment, and by the increase in bedforms length. These results may be of help in understanding the evolution of natural river systems near the coastlines and in interpreting fluvial-deltaic deposits preserved in stratigraphic sequences.

1. Introduction

Understanding how river systems may evolve in response to external forcing has fundamental implications in predicting the fate of sediment, its final sink and the evolution of continental, shallow-marine and abyssal systems (Pratson et al., 2007). In the last decades an increasing attention has been dedicated to the study of late Quaternary examples, due to the possibility of identifying the signature of tectonic, climatic or eustatic forcing in the fluvial evolution (Blum and Törnqvist, 2000). Moreover, the study of modern systems, with the help of numerical simulations and flume tank experiments, allowed to link the hydrodynamics of the river to the evolution of the deltaic and marine environments, and, ultimately, to the stratigraphic record (Paola, 2000; Van Heijst and Postma, 2001; Edmonds and Slingerland, 2009; Jerolmack, 2009; Kim et al., 2014). An important step forward for more accurate modeling results has been the introduction of a backwater zone upstream of the river mouth, where the flow velocity decelerates until reaching the standing body of water of the ocean (Parker et al., 2008; Hoyal and Sheets, 2009). Numerical simulations and field observations demonstrated that the so-called backwater effect has a paramount control on the evolution of the environments along the sediment routing system, from the continental realm to the open marine. Depending on the channel depth at its mouth and on river-bed slope (Paola, 2000), the backwater effect may propagate for tens to hundreds of kilometer upstream, and may influence the gravel-sand transition of the river (Venditti and Church, 2014), the river plume hydrodynamics (Lamb et al., 2012), and the formation of distributary networks and the evolution of delta plains (Jerolmack and Swenson, 2007; Chatanantavet et al., 2012).

The present study uses a portion of the Po River (Italy) as a natural laboratory where a backwater zone was created by the construction of the Isola Serafini dam (Fig. 1). By using an integrated approach based on the analysis of geophysical, sedimentological and hydrological data, this study quantifies how river hydrodynamics change through the backwater zone, in absence of external forcing such as waves or tides, and its impact on river morphology and sediment partitioning along the channel axis. The results obtained are discussed in the light of understanding modern hydrodynamics of the river with the ultimate aim to provide new insights for the interpretation of ancient deposits and stratigraphic sequences.

2. Study area

The Po River flows roughly West-East from the Western Alps toward the Northern Adriatic Sea, draining an area of ca. 74.500 km^2 with a 652 km long river (Fig. 1). The watershed can be divided into three sectors on the basis of lithology and maximum elevation: an Alpine sector of crystalline and carbonate rocks (maximum relief ~4500 meters above mean sea level, m amsl), an Apennine sector mostly composed of sedimentary rocks with high clay content (maximum relief ~2000 m amsl) and a central alluvial area including the Po Plain and the Po River delta (Fig. 1).

The annual Po River hydrograph shows two peaks in discharge normally in autumn and spring, generated by rainfall and snowmelt, respectively. The mean annual discharge recorded at the Piacenza gauging station is 959 m^3/s (period 1924-2009; Montanari, 2012), while the total annual sediment and freshwater discharges to the Northern Adriatic Sea are ~13x10^9 kg and ~40-50 km^3, respectively (Syvitski and Kettner, 2007; Cozzi and Giani, 2011).

The Isola Serafini dam, built for hydroelectricity production and completed in the 1962 AD, interrupts the river continuity at ca. 300 km upstream of its river mouth (Figs. 1 and 2). The dam consists of a gate structure with eleven openings of 30 m each that maintain a normal retention level of 41.5 m amsl through a constant flux of water downstream. Depending on the intensity of the floods, the gate can be opened, preventing river overflow and allowing the flux of extra waters. The construction of the dam affected both upstream and downstream river hydrology, morphology, and consequently the flux of sediment, nutrients and dissolved material to the Sea (Davide et al., 2003; Surian and Rinaldi, 2003).

In the 250 km upstream of the dam (watershed of about 45x10^3 km^2), the Po River course changes from multi-channel braided to wandering to single thread meandering, with a bed slope decrease from 1.4‰ to 0.22‰ and a fining of river bed sediments from coarse gravel to medium/fine sand (Figure 1; Colombo and Filippi, 2010; Lanzoni, 2012). The present study focused on the 70 km of river course upstream of the dam, where channel morphology is characterized by a sequence of meander bends both upstream- and downstream-skewed (Fig. 2). This portion of the river is characterized by a sinuosity index of 1.82, a water surface elevation between 45 m and 41.5 m amsl, a mean and maximum thalweg depth of ca. 6 m and 22 m, respectively (AIPO, 2005). The present-day river bathymetry (Fig. 2) is the result of the interaction between natural processes and anthropic activities, the latter, with a greater impact, in particular related to gravel and sand mining in the years between 1960 and 1970 AD (Lanzoni et al., 2012). The gravel-sand transition has been recognized between the confluence of the Po River with the Tidone and Trebbia tributaries (Fig. 2), where a subtle decrease in slope was created by deformation of the pre-Quaternary substrate (ADBPO, 2005).

3. Material and methods

The morpho-planimetric evolution of the Po River within the study area was quantified by using a combination of orthophotos (years 1954, 1962, 1991 AD) and satellite images (years 2004, 2005, 2014 AD), with the year 1954 AD as a reference for the quantification of river migration rates. Orthophotos were acquired by the IGM (Istituto Cartografico Militare) since the first decades of the ’900 Century, and are available online at http://www.igmi.or/voli. Each photo, at 1:33000 scale, was rectified as WGS84 UTM33 N in ArcGIS® by using 150 control points. Satellite images came from Landsat TM (years 2004 and 2005 AD) and Landsat 8 (year 2014 AD), both with 30 m of spatial resolution (data available at http://earthexplorer.usgs.gov). The thalweg depth for the year 1954 AD, used for the numerical simulation of the critical shear stress, came from AIPO (Agenzia Interregionale per il Fiume Po); the data, referenced to mean sea level, are available at http://geoportale.agenziapo.it/cms. The modern thalweg depth came from the multibeam bathymetry of the river, acquired by AIPO in the years 2004-2005 AD by using a multibeam echosounder Kongsberg 3002 equipped with a DGPS Racal Landstar (Colombo and Filippi, 2010).

Samples of river bed sediment, collected by using a Van Veen grab, and water surface elevation data were acquired during two cruises in July and August 2014, both during low flow conditions (Fig. 3). Positioning and river water surface elevation data were obtained by the using of Trimble Marine SPS461 GPS receiver equipped by an internet-based (via GSM) VRS RTK for real-time corrections that allows to obtain vertical and horizontal resolutions of 10 cm. Water elevation data are normalized for a reference stream height corresponding to a discharge of 1000 $m^3 s^{-1}$, measured at the Piacenza gauging station located about 30 km upstream of the dam (data available at http://arpa.emr.it). Elevation data are converted in water discharge by using the rating curve presented in Cesi (2004).

Grain-size analyses were performed with a set of sieves for the >63 mm fraction (from mesh no. 7 to no. 230) and with Micromeritics SediGraph 5120 for finer fractions at ISMAR-CNR sedimentary laboratory. All the samples were treated with 30% diluted H_2O_2 to remove organic matter and washed with distilled water to dissolve salts. Before SediGraph analyses the samples were dispersed in sodium hexametaphosphate and the flocculation were avoided also with mechanical agitation. Grain-size distributions were interpreted by using the software Gradistat and are presented according to the software graphics (Blott and Pye, 2001).

4. Field observations

4.1. Morpho-planimetric evolution

The morphologic and planimetric evolution of the Po River along the 70 km of river course within the study area have been quantified through orthophotos and satellite images available since 1954 AD, few years before the construction of the Isola Serafini dam. The pattern of the river surface area was obtained through pixel analysis in ArcGIS®, although this approach neglects small planimetric variations associated to the river stage, with larger channel widths during high-flow conditions. The data show that the river course changed continuously through time in the upstream portion, with lateral migrations of few hundreds of meters (Fig. 4). Bend instability progressively reduces downstream, and in the final reaches, from the dam to ca. 30 km upstream, the river almost maintained its position. This tendency of the river is highlighted also by lateral shifts of the river centerline (Fig. 5), positioned with horizontal errors in the order of few meters, depending on the resolution of the images available. Centerline migration rate, low in the most upstream portion of the river, increases between ca. 55 and 30 km, with values up to 45 m/yr in the years spanning the construction of the dam, and starts to reduce at ca. 30 km upstream of the dam, where the river flows close to the city of Piacenza. Migration rates decrease over time along the entire section, until reaching extremely low values in the final reaches of the river (Fig. 5). The condition of river bank stability detectable along the 30 km of river course upstream of the dam persisted during the entire time-interval investigated, between 1954 and 2014 AD.

The planimetric evolution of the river has been accompanied by morphological changes of channel bars, as detected in 4 snapshots between 1954 and 2004/2005 AD (Fig. 4). The most upstream portion of the river, meander loop 1, shows the most energetic conditions, with side bars that start to accumulate between

1954 and 1962 AD (see yellow arrows in Figure 4), most likely after the construction of the dam, and continuously growing since that. The point bar, furthermore, is progressively reworked and reshaped, testifying the dynamism of this trunk of the river (see orange arrows in Figure 4). Moving downstream, meander loop 2, sand transport is progressively reduced, as testified also by the gradual drowning of side bars (between 1962 and 1991 AD, red arrows in Figure 4) and by the slower reshaping of the point bar, with strengthened banks by riparian vegetation (blue arrows in Figure 4). Further downstream, in full backwater conditions, side bars disappear soon after the construction of the dam (between 1954 and 1962 AD in both meander loops 3 and 4, red arrows in Figure 4), whereas sandy point bars are drowned faster close to the dam: between 1962 and 1991 AD in meander loop 3, and between 1951 and 1962 AD in meander loop 4 (red arrows in Figure 4).

5.2. Downstream change in river bed sediment and bedforms

The general trend of downstream reduction in shear stress, emphasized by the morpho-planimetric change of the river, is confirmed by grain size analyses of river-bed material. Bed sediments, collected along the 70 km of river course, with more detailed sampling in meander loops 1, 3 and 4 (Fig. 6), show the presence of coarse-grained material (D_{50} up to 10 cm) only in the upstream portion of the river (along about 40 km): pebble to cobble river beds develop with a patchy distribution and alternate with sandy beds with mean D_{50} of 600 μm. Pebbles and cobbles accumulate in particular where flow velocity increases, inhibiting the deposition of fine-grained particles (see meander loop 1 in Figure 6), or at the confluence with the main tributaries entering from the South. Here cobbles, characterized by an Apennine provenance, remain in situ without being carried by the Po River (ADBPO, 2005). Cobbles were also found in few samples further downstream, in areas subjected to anthropic interventions for channel bank stabilization. Approaching the meander loop 3, the samples are almost entirely characterized by sand-size particles, with mean D_{50} between 500 μm and 300 μm. Finer deposits, with high clay content, can be found in low-velocity zones, as the inner side of the meander toward the drowned point bar (Fig. 6). Further downstream, within the final reaches of the river next to the dam (meander loop 4, Fig. 6), bed sediment becomes finer and dominated by silt-size fractions, with mean D_{50} between 200 μm and 10 μm. This trend is well highlighted by the grain size distribution of the river-bed sediment sampled in the thalweg along the final 15 km of the river (Fig. 7). A quick comparison between aerial views of the final reaches of the river acquired before and 50 yr after the construction of the dam (1954 AD and 2004-2005, during low flow conditions) highlights clearly how this downstream decrease of particles size is accompanied by the drowning of the system and the disappearance of coarse-grained channel bars. Furthermore, this change is also reflected by an increase in the dimension of river bedforms (Fig. 8). Dune length, in particular, shows a mean value of ca. 5 m in the upstream portion of the river and, starting at circa 30 km from the dam, increases downstream until reaching values up to 25 m.

5. Po River sediment transport capacity

In order to quantify the impact of a backwater zone on river flow velocity, bed shear stress and, ultimately, sediment transport capacity of the river, it is needed to introduce a hydrodynamic model that describes the downstream change of the river surface height approaching a standing body of water.

5.1. 1-D backwater curve

Under the assumption of the conservation of fluid mass and momentum, the depth-averaged gradually-varied flow equation is:

$$\frac{dh_x}{dx} = \frac{S_0 - S_f}{1 - Fr^2} \qquad (1)$$

with h_x flow depth, x downstream distance, S_0 river bed slope, S_f friction slope and Fr Froude number (Chow, 1959). Since the flow is only gradually varying, it is possible to calculate the friction slope at any given point (with flow depth h_x) under the backwater influence by using the Manning's equation $U = \frac{1}{n} R_h^{\frac{2}{3}} S_f^{\frac{1}{2}}$. Far upstream from the backwater influence, where the condition of steady and uniform flow is reached, the friction slope is constant and equal to the bed slope ($S_0=S_f$), and the Manning's equation allows the calculation of the normal flow depth. In rectangular channel (H=depth, L= width), with the approximation for the hydraulic radius $R_h \cong H$ (as L>>H), the normal flow depth is $H_n = \left(\frac{U^2}{C_z^2 g S_{0=f}} \right)$, where the mean flow velocity U is given by the continuity equation ($U=Q/HL$), with Q is the water discharge, L is the mean channel length, g is the gravitational acceleration, C_z is the Chezy resistant coefficient (Chow, 1959).

For subcritical normal flow regime (Fr<1) on mild slope ($h_1>H_n>H_c$), and considering a single discharge with no delta progradation, Eq. (1) can be solved with an iterative procedure starting with the depth $h_{x=1}$ at the ponded water and integrating upstream (Chow, 1959); the computation allows to have a preliminary estimate of the backwater curve for 1-D open channel flow on a flat sand bed (e.g. Parker, 2004).

The river surface height for pre-dam and post-dam conditions, therefore with a backwater zone, is quantified by using: 1- a constant bed slope of 0.2063 10^{-3}, calculated from the linear fit of thalweg depths derived from cross-sectional channel profiles (Fig. 9); 2- three Chezy resistant coefficient (10 in red, 20 blue, 30 green); 3- a water discharge of 1000 m^3 s^{-1}, derived the mean annual discharge measured at the Piacenza gauging station; 4- a channel width of 250 m, a mean value calculated along the 70 km of the study area; 5- a starting depth of 10 m, as the depth at the normal retention level of the reservoir (41.5 m amsl). Figure 4 compares the normal flow depth for pre-dam conditions (left column) and the M1 river profile for post-dam conditions (center column), calculated for the three Chezy coefficients, to the modern channel depth and river surface height for a discharge of 1000 m^3 s^{-1} (right column in Figure 9).

5.2. Total boundary shear stress

Once calculated theoretical channel depth in pre and post-dam conditions, and considering the resistance of the alluvial bed only related to the presence of grains, the total boundary shear stress can quantified using the equation: $\tau_b = \rho_w \frac{U^2}{C_z^2}$ (Einstein and Barbarossa, 1952; Wright and Parker, 2004). The channel deepening in consequence of dam-induced backwaters creates an exponential reduction of the shear stress that in turn affects the sediment transport capacity of the river (Fig. 9).

The shear stress calculated for the present configuration of the Po River (right column in Figure 9) is quantified by using the thalweg depth surveyed by AIPO in the years 2004-2005 AD (Colombo and Filippi, 2010). The water surface profile, acquired in this study, shows a sharp decrease in slope from 3 $\times 10^{-4}$ to 0.5 $\times 10^{-4}$ in the most upstream portion of the study area (between 70 and 45 km), where the gravel-sand transition is recognized (ADBPO, 2005). Further slight changes in slope are in correspondence of the confluence with the main tributaries Tidone, Lambro and Trebbia rivers (Fig. 2).

5.3. Sediment transport capacity

In order to quantify the mobility of specific grain size, it is possible to compare the non-dimensional shear stress (i.e. the Shields parameter τ^*, estimated from the total boundary shear stress; Bunte et al., 2010) of each grain size to its critical value τ_c^*, estimated from Brownlie (1981) as a function of a modification of the Reynolds particle number:

$$\tau_c^* = 0.22 R_p^{-0.6} + 0.06 \cdot 10^{-7.7 R_p^{-0.6}} \text{ with } R_p = \left[\left(g\frac{\rho_s - \rho_w}{\rho_w}\right) D_{50}\right]^{\frac{1}{2}} \cdot \frac{D_{50}}{\nu} \quad (2)$$

with $\rho_s = 2650 \text{ kg m}^{-3}$ and $\rho_w = 1000 \text{ km m}^{-3}$ particle and water density, respectively, and $\nu = 1.004 \cdot 10^{-6} \text{ m}^2 \text{ s}^{-1}$ kinematic viscosity at 20 °C.

The downstream change in sediment mobility has been calculated for 12 grain-sizes (Fig. 10), spanning from cobble to silt, and considering a Chezy resistant coefficient of 30, the value that best represents this portion of the Po River, characterized by a clean bed with little to absent vegetation on the walls. The model well estimates the upstream influence of the backwater zone compared to field observations, and well approximates the reduction of the sediment transport capacity of the river for the post-dam conditions. Along the 30 km of river course upstream of the dam, the particle size carried by the river decreases from few millimeters to less than 100 μm; this value is in agreement with the competence of the river calculated for modern conditions, and also with the results from river-bed sediment sampling collected during normal flow conditions.

6. Discussion

The downstream hydrodynamic change of a river entering into the coastal ocean has fundamental implications for the formation and evolution coastal landscapes (Edmonds and Slingerland, 2006; Geleynse et al., 2011). In the last years many efforts have been made to understand how, how much, and how far upstream, the presence of a standing body of water at a river mouth affects the behavior of the river, its sediment transport capacity, and the morphodynamics of deltas and estuaries (Jerolmack and Swenson, 2007; Edmonds et al., 2009; Chatanantavet et al., 2012; Lamb et al., 2012; Bolla Pittaluga et al., 2015). We used a trunk of the Po River where a backwater zone was induced by the construction of a dam, as a natural laboratory to investigate the morphodynamic evolution of the river under gradually-varied flow conditions, in comparison with the observations made in river systems toward their outlets to the ocean (Nittrouer et al., 2012).

6.1. Morphological change within the backwater zone

When river flow velocity is forced to reduce at the river outlet, the perturbation induced in the river hydraulics migrates upstream for distances that are typically approximated by $L \approx H/S$ (S: channel bed slope, H: flow depth at the river mouth; Paola, 2000). Throughout the backwater zone, the morphology and kinematics of the Po River changes downstream, reflecting the non-linear reduction in the sediment transport capacity of the river. At the transition from normal to gradually-varied flow conditions under the backwater influence (between 45 km and 30 km, approximately), the lateral migration rate is high and accompanied by a slight tendency of the river to aggrade (Figs. 2 and 5), in marked contrast with the scenario further upstream, where river incision may be the consequence of reduced sediment supply from tributaries and river-bed mining. This tendency of the river, explored also by the Exner model results in Nittrouer et al. (2012), reflects the spatial divergences in river-bed sediment transport associated to non-uniform water flow, and has fundamental implications for the onset of distributary network on deltas (Edmonds et al., 2009; Chatanantavet et al., 2012). Along the final reaches of the Po River, downstream of 30 km and, in particular, close to the Isola Serafini dam, lateral migration rate collapses to extremely low values, sandy channel bars disappear and the river progressively erodes its bed along the thalweg. This tendency of the river has been observed also in the Mississippi River, where lateral migration rate decrease from more than 120 m/yr to less than 20 m/yr along the last 600 km upstream its outlet (Hudson and Kesel, 200). To fully understand the morphodynamic of this trunk of the Po River it is necessary to evaluate the hydrodynamic conditions during both normal flow and high-discharge events. In the first case, a reduction in flow velocity, typical of M1 river profiles, corresponds to a drop of the bed shear stress below critical thresholds for both suspended-load and bed-load transport and to the accumulation of fine-grained material, up to clay size, in the channel axis and along channel bars. During floods and high-discharge events, conversely, the channel-bed kinematics change drastically: when the normal-flow depth of the river becomes larger than the water depth at its downstream end, and this is because the normal retention level of the dam is maintained at a constant elevation by opening the gates, the river flow velocity accelerates due to the drawdown of the fluvial water close to the dam (as described by an M2 profile), the shear stress increases and the river becomes erosional. This phenomenon, first observed by Lane (1957) and quantified by Lamb et al. (2012), explains the reduction in lateral river migration, the deep incision of the channel thalweg, that may promote the formation of armored beds, and the partial removal of the sediment accumulated in channel bars and in the final reaches of the river. Similar processes have been observed in the Teshio River (Ikeda, 1989) and in the Mississippi River (Nittrouer et a., 2012); in the Lower Mississippi River, in particular, a 100-fold increase in sand transport has been observed during high-discharge events, when the drawdown of fluvial water forced an up to 13-fold increase in shear stress respect to backwater conditions (Nittrouer et al., 2011). The decrease in lateral migration, favoured by the stabilization of river banks through riparian vegetation (Wickert et al., 2013), coupled with the deepening of the channel toward its outlet, promotes the narrowing of the channel belt. This concept may be useful when interpreting ancient fluvial systems, as low values of the width-thickness ratio of the channel belt associated to limited lateral migration rate (up to few channel widths) may be diagnostic of distributary channels (Blum et al., 2013).

6.2. Sedimentological change within the backwater zone

The hydrodynamic behavior of the Po River throughout the backwater/drawdown zone can be quantified not only by considering spatial informations such as lateral river migration, channel deepening and widening, but also by considering the morphological evolution of channel bars and the grain-size partitioning along the channel axis. Repeated aerial surveys of the Po River during the last 60 years, since dam-induced backwater has been created, show that point bars and side bars, continuously evolved through time between 70 and 45 km (Fig. 4), as the river-bed shear stress is high enough to transport coarse sands also during moderated flow conditions (1000 m^3 s^{-1}, Figure 10). Further downstream, and in particular along the 30 km of river upstream of the dam, the establishment of a backwater zone forced channel deepening, while repeated oscillations backwater/drawdown associated to the transit of high discharge events progressively eroded the channel bars and further increased thalweg depth (Figs. 2 and 4). The morphological changes associated to the kinematics and transport capacity of the river is reflected in channel-bed grain size data: coarse sediment characterizes the upstream portion of the river and accumulates in the trunk of the river where the transition from normal-flow to gradually-varied flow is observed (between 45 km and 30 km, approximately), and that, interestingly, corresponds to the gravel-sand transition of the river. Further downstream pebbles and coarse sand are gradually replaced by fine sand, silt and, close to dam or where the flow velocity is extremely low, by clay. River-bed samples from the drowned point bars in meander loops 3 and 4 (Fig. 6), in detail, show a coarsening trend toward deeper water, with clay-rich sediment accumulating at the inner point bar (Fig. 6). This situation is in marked contrast with the morphology of both meanders observed in 1954 AD, before the dam, where sandy point bars are subaerially exposed (Fig. 7). On the basis of the lithology observed in meander loops 3 and 4, it is possible to speculate that a fining upward trend, with more frequent mud-drapes, should characterize the vertical sedimentary succession of a point bar where the river enters the backwater zone. As the backwater zone penetrates further upstream respect to the tidal influence and to the intrusion of brackish waters (Blum et al., 2013), this finding may be useful when interpreting ancient river deposits at outcrop or sediment core scales, where the presence of fine-grained beds are normally associated to tidal influence (Shanley et al., 1992; Labrecque et al., 2011).

The change in river hydraulics and river-bed material observed throughout the backwater zone is reflected also in the evolution of river bedforms, showing a downstream increase in length (Fig. 8). This trend may be connected to a combination of the general fining of bed sediments and the high flow velocity during high-discharge events, as both factors contribute positively to increase the size of the dunes (Southard and Boguchwal, 1990). Therefore, it is possible that only large-scale dunes formed during high-discharge events and remain as relict features (i.e. not in equilibrium) during low flow conditions, as observed in the Yangtze River (Chen et al., 2012).

6.3. Implication for the gravel-sand transition

It is widely recognized that the size of bed sediments in alluvial rivers decreases exponentially downstream (Church and Kellerhals, 1978), and among such variation the transition from gravel to sand is a fundamental boundary in the fluvial geomorphology, as it marks the key change from gravel-bed to sand-bed rivers. Several mechanisms, both autogenic and allogenic, have been proposed to explain the emergence of a gravel-sand transition (Schumm and Stevens, 1973; Hoey and Ferguson, 1994; Ferguson et al., 1996; Ferguson, 2003), and among external controls the backwater influence on river capacity plays a fundamental role (Sambrook Smith and Ferguson, 1995; Venditti and Church, 2014). The gravel-sand transition in the Po River has been recognized between the confluences with the Tidone and Trebbia tributaries, where river hydrodynamics start feeling the effect of backwater (Fig. 2), and has been associated to a slight decrease in river bed slope due the deformation of the pre-Quaternary substrate (ADBPO, 2005). Combining the morphological evidences of the Po River derived from the orthophoto acquired in 1954 AD (Fig. 7), showing the presence of large point bars, side bars and both vegetated and un-vegetated mid-channel bars, with the sedimentological informations available within the study area and further downstream of the Isola Serafini dam, where armored gravel beds have been recognized below the modern sedimentary cover (ADBPO, 2005), it is possible to argue that, before the construction of the dam, the gravel-sand transition was located kilometers downstream respect to the modern position. Therefore, the modern location of the gravel-sand transition is not as it would be for a pristine system, but it is consequence of the upstream effect of dam-induced backwater. This result adds value to the importance of the backwater effect in controlling not only the evolution of the downstream end of the river, with its impact on the genesis of distributary network on deltas and on the morphodynamics of estuaries (Jerolmack and Swenson, 2007; Edmonds and Slingerland, 2009; Chatanantavet et al., 2012; Lamb et al., 2012; Bolla Pittaluga et al., 2015), but also the kinematics and morphology of the river for kilometers upstream.

7. Conclusions

The hydrodynamic behavior of a river changes radically from its mountain reaches to downstream toward the ocean. The presence of a standing body of water at the river outlet exerts a fundamental control on the river morphodynamics through the formation of a backwater zone that may propagate for hundreds of kilometers upstream. Quantifying the morphologic evolution of a trunk of the Po River when entering in a dam-induced backwater zone allows understanding the effect of the transition from normal to gradually-varied flow regimes on the river dynamics, without introducing assumptions on the effect of waves and tides. From upstream to downstream the lateral migration rate of the river reduces, accompanied by a general fining of bed sediments and increase in dune length. When the river enters the backwater zone, a strong decrease in water surface slope and associated bed shear stress allows the deposition of coarse-grained material, promoting the gravel-sand transition of the river and the aggradation of the river bed. Further downstream, where the water surface oscillates from M1 to M2 profiles during low-flow and high-discharge events, respectively, bed shear stress increases promoting the erosion of channel bars and the deepening of the channel thalweg. In essence, the backwater and drawdown effects show a paramount control on the river hydrodynamics and are fundamental in driving the morphodynamic evolution of rivers, deltas and estuaries. This concept, applied to source to sink studies of continental margin evolution, will help understanding how oscillations in the backwater zone in response to the allogenic forcing of changing base-level govern the evolution of channel belts, control sediment export to the ocean and, ultimately, continental margin growth.

Acknowledgments

References

Autorità di Bacino del Fiume Po (ADBPO), 2005. Programma generale di gestione dei sedimenti alluvionali dell'alveo del Fiume Po. Stralcio confluenza Tanaro-confluenza Arda.

Agenzia Interregionale per il Fiume Po (AIPO), 2005. Rilievo sezioni topografiche trasversali nella fascia B del Fiume Po, dalla confluenza con il Ticino al Mare.

Blott, S.J., Pye, K., 2001. Gradistat: a grain size distribution and statistics package for the analysis of unconsolidated sediments. Earth Surf. Process. landf. 26, 1237-1248.

Bolla Pittaluga, M., Tambroni, N., Canestrelli, A., Slingerland, R.L., Lanzoni, S., Seminara, G., 2015. When river and tide meet: The morphodynamic equilibrium of alluvial estuaries. Journal of Geophysical Research 120, 75-94.

Brownlie, W.R., 1981. Prediction of flow depth and sediment discharge in open channels. Rep. no. KH-R-43A, W.M. Keck Lab. of Hydraulics and Water Resources, California Institute of Technology, Pasadena, CA, 232 pp.

Bunte, K., Abt, S.R., Swingle, K.W., potyondy, J.P., 2010. Bankfull mobile particle size and its prediction from a shields-type approach. 2nd Joint Federal Interagency Conference, Las Vegas, Nevada.

Cesi, 2004. Monitoraggio della qualità delle acque del nodo Po-Lambro. Anno 2003 Rapporto A4/000662 del 27 gennaio 2004.

Chatanantavet, P., Lamb, M.P., Nittrouer, J.A., 2012. Backwater controls of avulsion location on deltas. Geophysical Research Letters 39, L01402.

Chen, J., Wang, Z., Li, M., Wei, T., Chen, Z., 2012. Bedform characteristics during falling flood stage and morphodynamic interpretation of the middle-lower Changjiang (Yangtze) River chanel, China. Geomorphology 147-148, 18-26.

Chow, V.T., 1959. Open-channel hydraulics, 680 pp., McGraw-Hill, New York.

Colombo, A., Filippi, F., 2010. La conoscenza delle forme e dei processifluviali per la gestione dell'assetto morfologico del fiume Po. Biologia Ambientale 24, 331-348.

Cozzi, S., Giani, M., 2011. River water and nutrient discharge in the Northern Adriatic Sea: current importance and long term changes. Continental Shelf Research 31, 1881-1893.

Davide, V., Pardos, M., Diserebs, J., Ugazio, G., Thomas, R., Dominik, J., 2003. Characterization of bed sediments and suspension of the river Po (Italy) during normal and high flow conditions. Water Research 37, 2847-2864.

Edmonds, D.A., Slingerland, R., 2006. Mechanics of river mouth bar formation: Implications for the morphodynamics of delta distributary networks. Journal of Geophysical Research 112, F02034.

Edmonds, D.A., Slingerland, R.L., 2009. Significant effect of sediment cohesion on delta morphology. Nature Geoscience 3, 105-109.

Edmonds, D.A., Hoyal, D.C.J.D., Sheets, B.A., Slingerland, R.L., 2009. Predicting delta avulsions: Implications for coastal wetland restoration. Geology 37, 759-762.

Einstein, H.A., Barbarossa, N.L., 1952. River channel roughness. Trans. Am. Soc. Civ. Eng. 117, 1121-1146.

Fagherazzi, S., Howard, A.D., Wiber, P.L., 2004. Modeling fluvial erosion and deposition on continental shelves during sea level cycles. Journal of Geophysical Research 109, F03010.

Ferguson, R., Hoey, T., Wathen, S., Werritty, A., 1996. Field evidence for rapid downstream fining in alluvial rivers. Journal of Geology 106, 661-675.

Ferguson, R.I., 2003. Emergence of abrupt gravel to sand transitions along rivers through sorting processes. Geology 31, 159-162.

Geleynse, N., Storms, J.E.A., Walstra, D-J. R., Jagers, H.R., Wang, Z.B., Stive, M.J.F., 2011. Controls on river delta formations; insights from numerical modelling. Earth and Planetary Science Letters 302, 217-226.

Hoey, T.B., Ferguson, R., 1994. Numerical simulation of downstream fining by selective transport in gravel bed rivers: Model development and illustration. Water Resources Research 30, 2251-2260.

Hoyal, D.C.J.D., Sheets, B.A., 2009. Morphodynamic evolution of experimental cohesive deltas. Journal of Geophysical Research 114, F02009.

Hudson, P.F., Kesel, R.H., 2000. Channel migration and meander-bend curvature in the Lower Mississippi River prior to human modificatios. Geology 28, 531-534.

Ikeda, H., 1989. Sedimentary Controls on Channel Migration and Origin of Point Bars in Sand–Bedded Meandering Rivers, in River Meandering (eds S. Ikeda and G. Parker), American Geophysical Union, Washington, D. C. doi: 10.1029/WM012p0051

Kim, W., Petter, A., Straub, K., Mohrig, D., 2014. Investigating the autogenic process response to allogenic forcing: experimental geomorphology and stratigraphy. In: Depositional Systems to Sedimentary Successions on the Norwegian Continental Margin, IAS Special Publication 46, (Eds.) Martinius, A.W., Ravnås, R., Howell, J.A., Steel, R.J., Womham, J.P., Blackwell Publishing Ltd., Oxford, UK.

Jerolmack, D.J., Swenson, J.B., 2007. Scaling relationships and evolution of distributary networks on wave-influenxed deltas. Geophysical Research Letters 34, L23402.

Jerolmack, D.J., 2009. Conceptual framework for assessing the response of delta channel networks to Holocene sea level rise. Quaternary Science Reviews 28, 1786-1800.

Labrecque, P.A., Hubbard, S.M., Jensen, J.L., and Nielsen, H., 2011. Sedimentology and stratigraphic architecture of a point bar deposit, Lower Cretaceous McMurray Formation, Alberta, Canada. Bulletin of Canadian Petroleum Geology 59, 147-171.

Lamb, M.P., Nittrouer, J.A., Mohrig, D., Shaw, J., 2012. Backwater and river plume controls on scour upstream of river mouths: Implications for fluvio-deltaic morphodynamics. Journal of Geophysical Research 117, F01002.

Lane, E.W., 1957. A study of the Channels Formed by Natural Streams Flowing in Erodible Material. U.S. Army Corps of Eng., Mo.River Div., Omaha, Nebraska.

Lanzoni, S., 2012. Evoluzione morfologica recente dell’asta principale del Po. Atti dei Convegni dei Lincei, Giornata Mondiale dell’Acqua, Accademia Nzionale dei Lincei.

Montanari, A., 2012. Hydrology of the Po River: Looking for changing patterns in river discharge. Hydrol Earth Syst. Sciences 16, 3739-3747.

Nittrouer, J.A., Shaw, J., Lamb, M.P., Mohrig, D., 2012. Spatial and temporal trends for water-flow velocity and bed-material transport in the lower Mississippi River. Geol. Soc. Am. Bull. 124, 400-414.

Nittrouer, J.A., Mohrig, D., Allison, M., 2011. Punctuated sand transport in the lowermost Mississippi River. Journal of Geophysical Research 116, F04025.

Paola, C., 2000. Quantitative models of sedimentary basin filling. Sedimentology 47, 121-178.

Parker, G., 2004. Review of 1D open channel hydraulics. In: online book “1D Sediment transport morphodynamics with applications to rivers and turbidity currents”.
Parker, G., Muto, T., Akamatsu, Y., Dietrich, W.E., Wesley Lauer, J., 2008. Unrevelling the conundrum of river response to rising sea-level from laboratory to field. Part II. The Fly-Strickland River system, Papua New Guinea. Sedimentology 55, 1657-1686.
Pratson, L.F., Nittrouer, C.A., Wiberg, P.L., Steckler, M.S., Swenson, J.B., Cacchione, D.A., Karson, J.A., Murray, A.B., Wolinsky, M.A., Gerber, T.P., Mullenbach, B.L., Spinelli, G.A., Fulthorpe, C.S., O'grady, D.B., Parker, G., Driscoll, N.W., Burger, R.L., Paola, C., Orange, D.L., Field, M.E., Friedrichs, C.T., Fedele, J.J., 2007. Seascape Evolution on Clastic Continental Shelves and Slopes. In: Continental Margin Sedimentation: From Sediment Transport to Sequence Stratigraphy, IAS Special Publication 37, (Eds.) Nittrouer, C.A., Austin, J. A., Field, M. E., Kravitz, J. H., Syvitski, J.P.M., Wiberg, P.L., Blackwell Publishing Ltd., Oxford, UK.
Sambrook Smith, G.H., Ferguson, R.I., 1995. The gravel to sand transition along river channels. Journal of Sedimentary Research A65, 423-430.
Schumm, S.A., Stevens, M.A., 1973. Abrasion in place: a mechanism for rounding and size reduction of coarse sediments in rivers. Geology 1, 37-40.
Shanley, K.W., McCabe, P.J., Hettinger, R.D., 1992. Tidal influence in Cretaceous fluvial strata from Utah, USA: a key to sequence stratigraphic interpretation. Sedimentology 39, 905-930.
Southard, J.B., Boguchwal, L.A., 1990. Bed configuration in steady unidirectional water flows. Part 2. Synthesis of flume data. Journal of Sedimentary Petrology 60, 658-679.
Syvitski, J.P.M., Kettner, A.J., 2007. On the flux of water and sediment into the Northern Adriatic Sea. Continental Shelf Research 27, 296-308.
Surian, N., Rinaldi, M., 2003. Morphological response to river engineering and management in the alluvial channels in Italy. Geomorphology 50, 307-326.
Swenson, J.B., Muto, T., 2007. Response of coastal plain rivers to falling relative sea-level: allogenic controls on the aggradational phase. Sedimentology 54, 207-221.
Van Heijst, M.W.I.M., Postma, G., Fluvial response to sea-level changes: a quantitative analogue, experimental approach. Basin Research 13, 269-292.
Venditti, J.G., Church, M., 2014. Morphology and controls on the position of a gravel-sand transition: Fraser River, British Columbia. Journal of Geophysical Research 119, 1959-1976.
Wickert, A.D., Martin, J.M., Tal, M., Kim, W., Sheets, B., Paola, C., 2013. River channel lateral mobility: metrics, time scales, and controls. Journal of Geophysical Research 118, 396-412.
Wright, S., Parker, G., 2004. Flow resistance and suspended load in sand-bed rivers: Simplified stratification model. J. Hydraul. Eng. 130, 796-805.

Figure

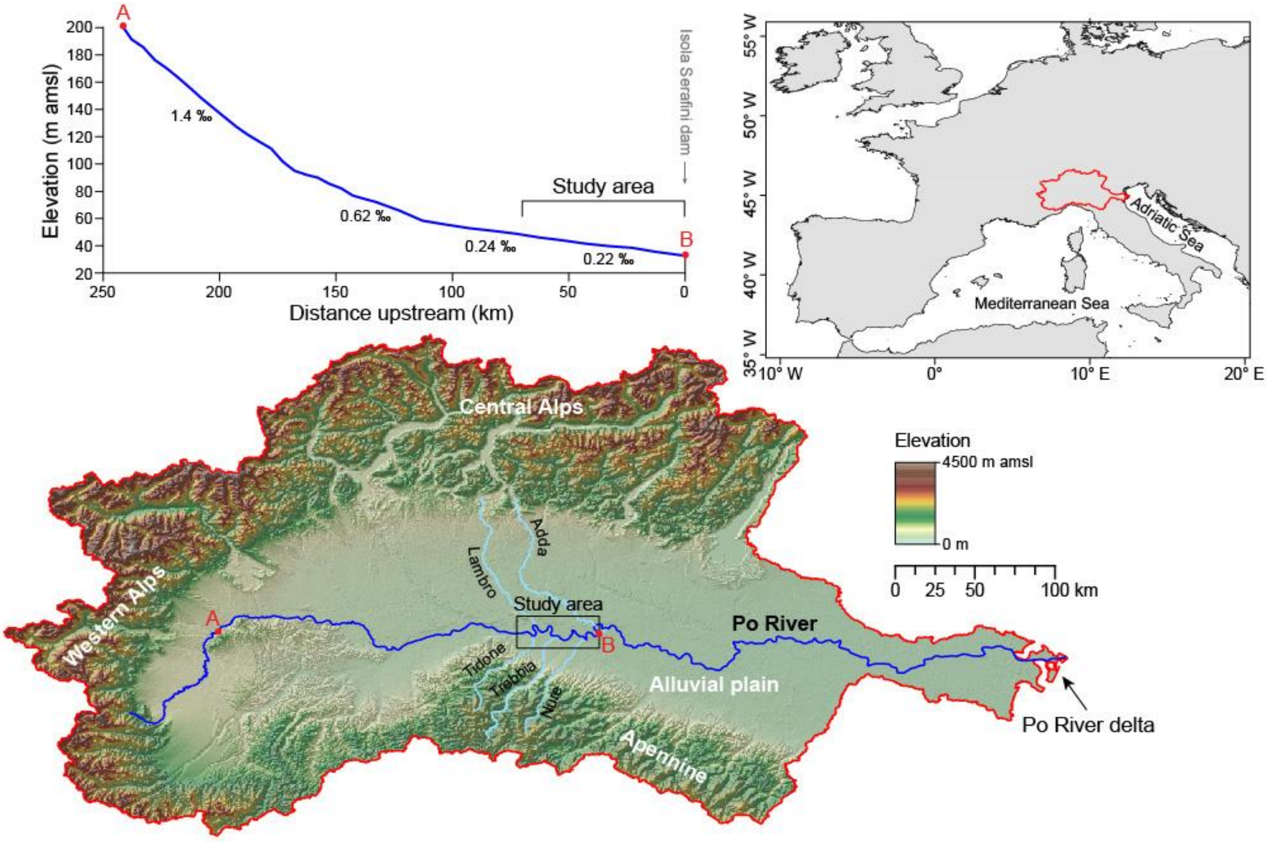

Figure 1. Po River course and its catchment basin, with reported the main tributaries entering the river in the study area (black box). River bed elevation and mean slopes, calculated for the 250 km of river course upstream of the dam (between point A and B; modified from Colombo and Filippi, 2010). Point B marks the location of the Isola Serafini dam.

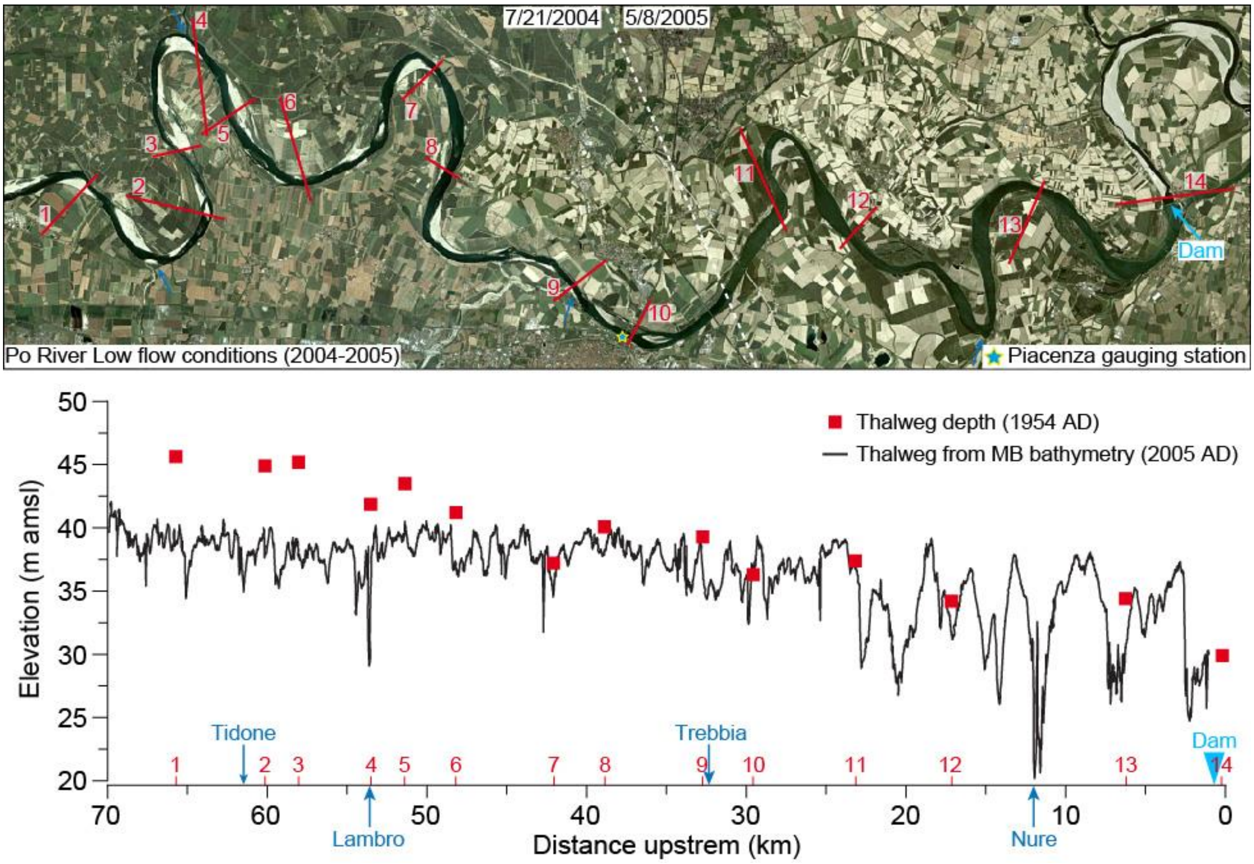

Figure 2. Top: Aerial view of the study area derived from a combination of two images (date 7/21/2004 and 5/8/2005, left and right sides of the white dashed line, respectively) acquired during low flow conditions, see Figure 3 for details. Red lines represent the location of river cross sections acquired in 1954 AD (source AIPO: http://geoportale.agenziapo.it/cms). Bottom: thalweg elevation from multibeam bathymetry (black line; source AIPO, 2005) and from 1954 AD river cross sections (squares and numbers reported in red). Blue arrows are the four main tributaries (Tidone, Lambro, Trebbia and Nure rivers). The blue star marks the location of the gauging station near the city of Piacenza.

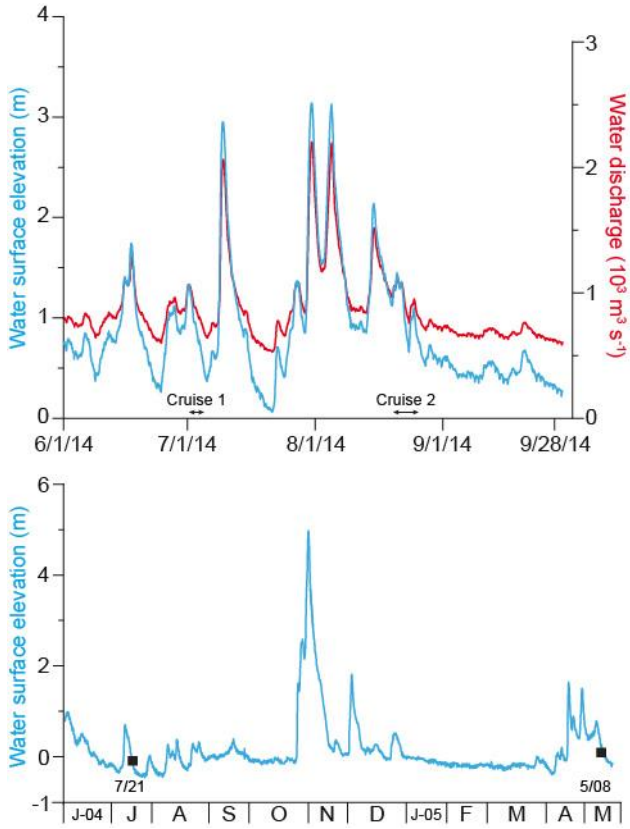

Figure 3. Top: Water surface elevation (blue) and water discharge (red) data from the Piacenza gauging station (source: http://arpa.emr.it) during June-September 2014; cruise time is reported below. Bottom: water surface elevation of the Po River during the acquisition of the aerial views presented in Figure 2; both images are acquired during low flow conditions (black squares).

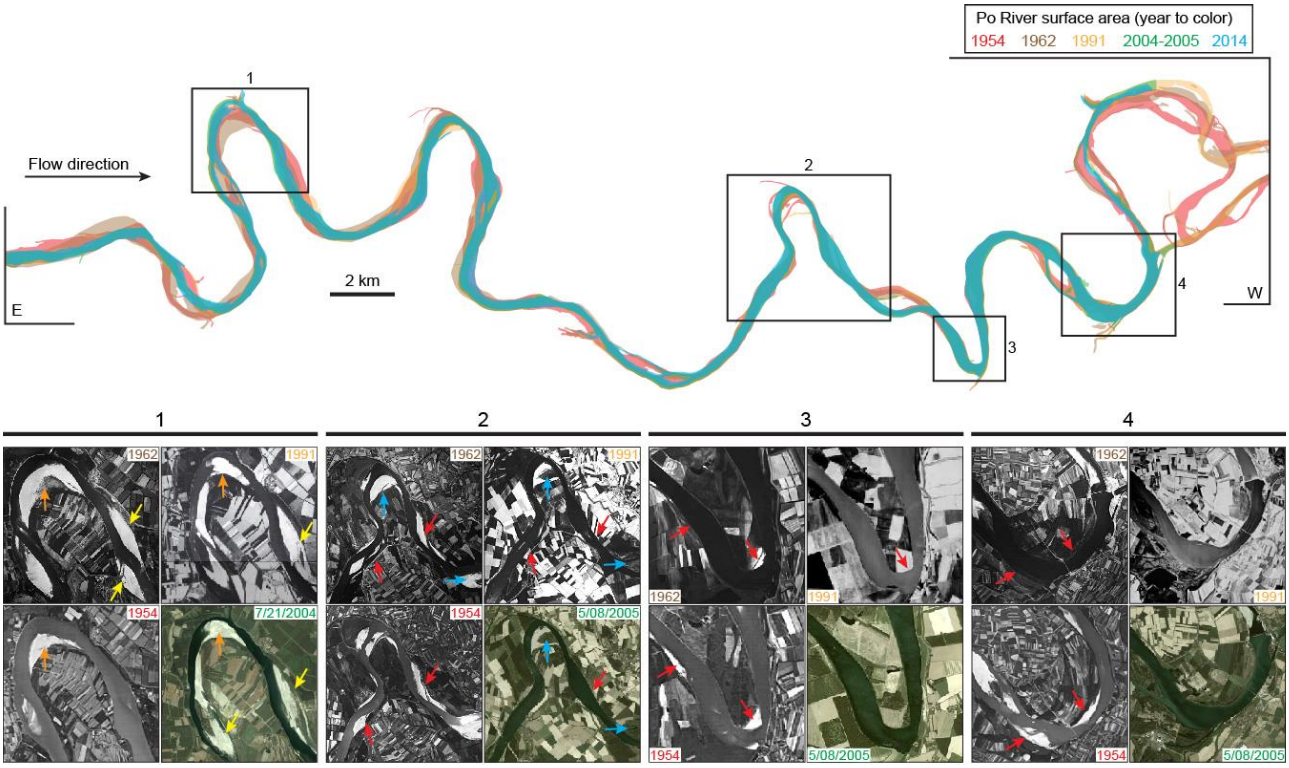

Figure 4. Top: Extent of the Po River surface area obtained from five aerial surveys since 1954 AD (before the construction of the Isola Serafini dam) highlighting the downstream change in lateral migration of the river. Bottom: The detailed view (age reported in years AD) of four-selected meander loops (1 to 4 moving downstream) shows the morphological evolution of river banks and channel bars. In detail: orange and yellow arrows in meander loop 1 indicate channel bar and point bar accretion through time, respectively; blue arrows in meander loop 2 mark river banks with increasing vegetation cover; red arrows in meander loop 2, 3 and 4, highlight channel bars that are progressively eroded until disappear.

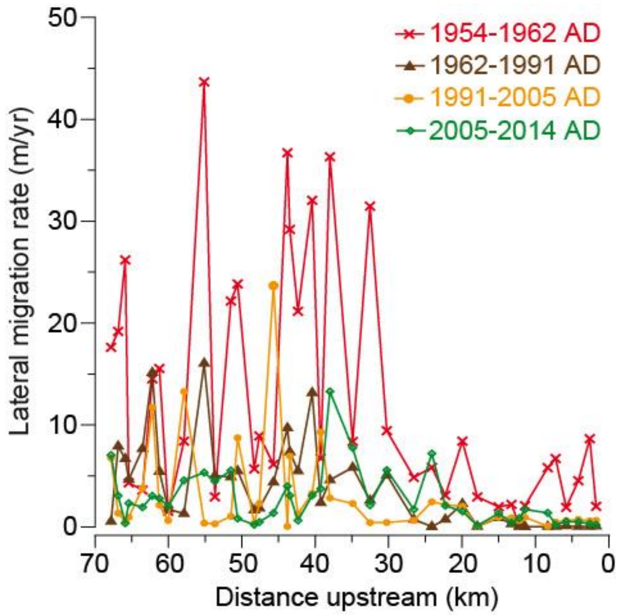

Figure 5. Lateral migration rate of the Po River centerline, calculated in four time intervals, plotted versus distance upstream. The data show a marked drop of the lateral migration of the Po River along the 30 kilometers upstream of the Isola Serafini dam, in the interval 1954-1962 AD. During the last sixty years lateral migration reduce both in space (downstream) and in time (toward nowadays).

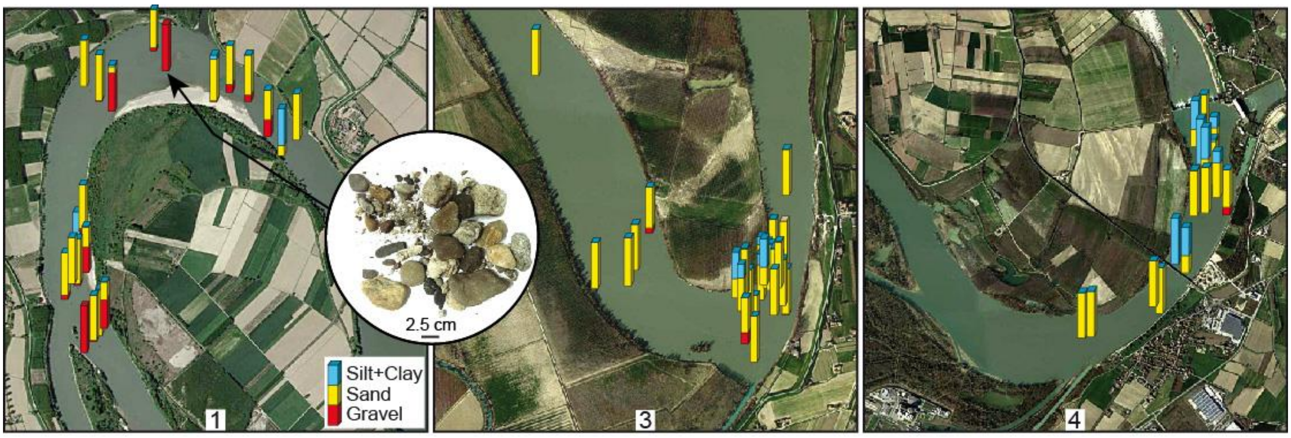

Figure 6. Detailed view of meander loops 1, 3 and 4 (see location in Figure 4) showing the grain-size variability of river bed sediment. Blue (sediment < 63µm), yellow (sediment between 63-2000 µm) and red (>2000 µm), with color proportions reflecting the amount of a specific grain size. Note the overall decreasing in grain size toward the inner side of the meander loop 3 and approaching the Isola Serafini dam.

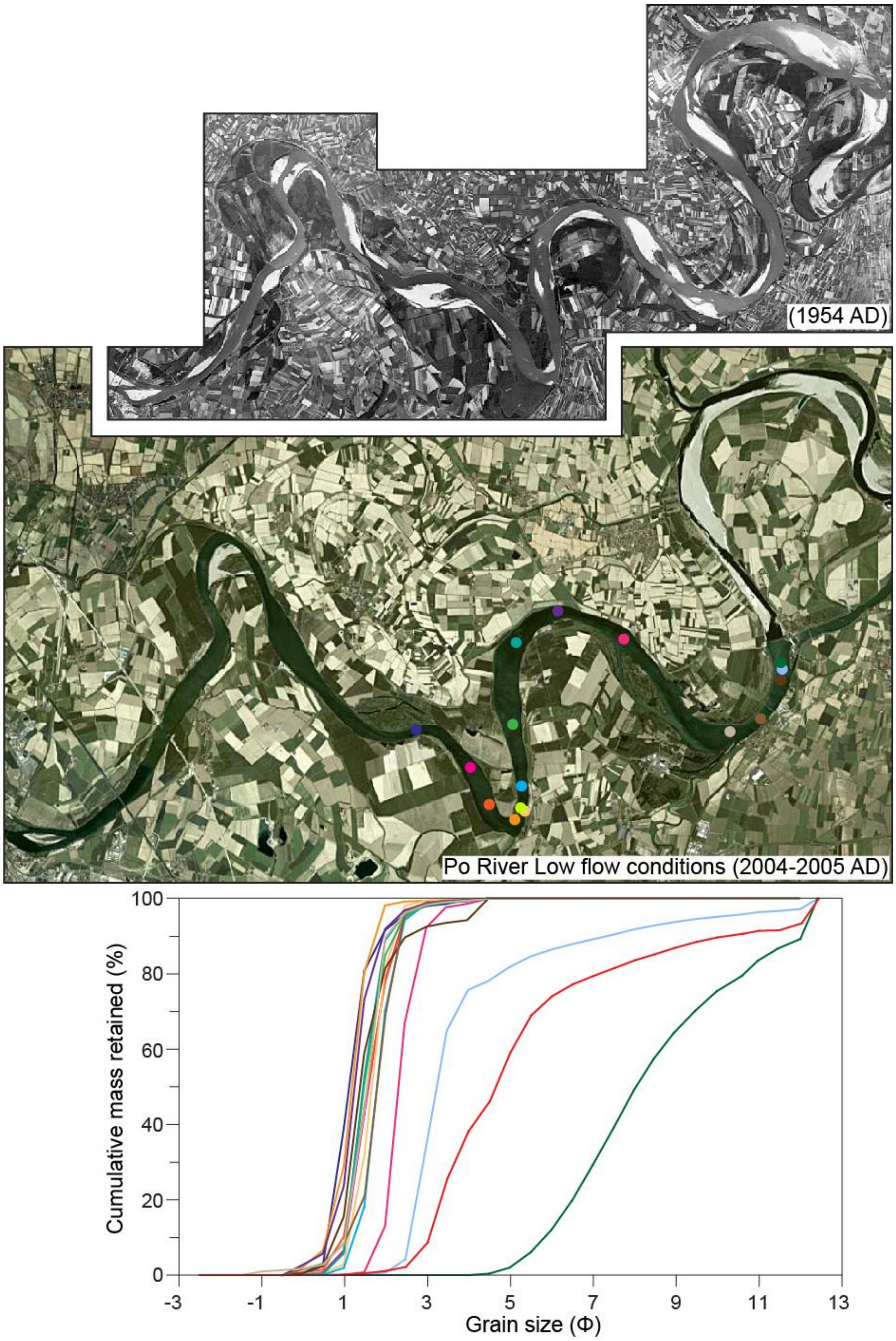

Figure 7. Morphology of the Po River along the final reaches located upstream of the Isola Serafini dam in 1954 AD and 2005 AD. Note the presence of extensive coarse-grained deposits along the river course before the establishment of backwater conditions in marked contrast with the modern river channel physiography lacking of channel bars. River-bed samples acquired in this study (colored dots reported on the 2005 AD satellite image) highlight the general downstream fining of sediment particles, as summarized by the grain size distributions (each color refers to a specific sediment sample).

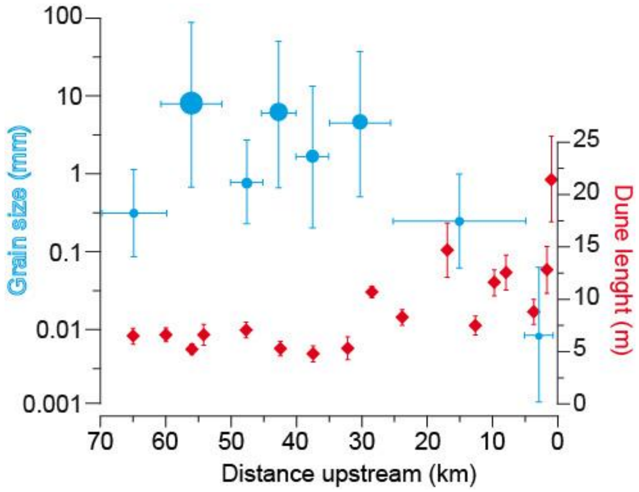

Figure 8. Variability of river bed sediments along the 70 kilometers of the Po River upstream of the Isola Serafini dam (blue dot, dimensions scale with D_{50} grain sizes). Vertical blue bars represent the range of grain sizes, while horizontal bars their spatial distribution along the river. Red diamonds represent average dune length derived from 300 m long 2D profiles extracted from multibeam bathymetry. Vertical red bars represent the maximum and minimum dune length in each transect.

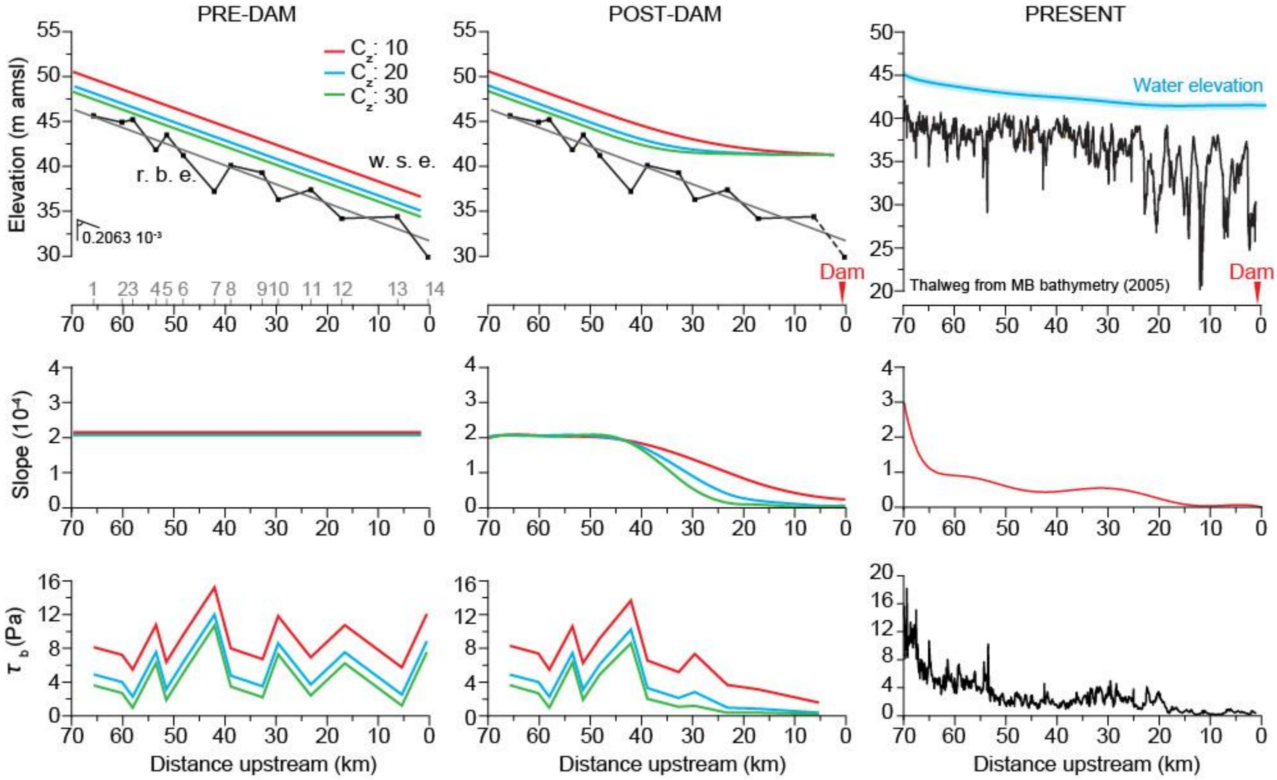

Figure 9. Theoretical water surface elevations (w.s.e.) for normal flow (pre-dam) and gradually-varied flow (post-dam) conditions, calculated by introducing three Chezy coefficients (10 in red, 20 in blue, 30 in green). Water surface slope is equal to the bed slope (obtained through linear fit of the thalweg depths derived from river cross-sectional profiles, see Figure 2) in the normal-flow regime, while is derived from the M1 river profiles in the post-dam conditions. Total boundary shear stress (t_b) is by using a channel depth derived from river bed elevation (r.b.e.) and theoretical water surface profiles, and shows the gradual downstream decrease in response to the establishment of dam-induced backwater. The right column represents the modern river physiography, with thalweg depth in black and water surface elevation in blue; the water surface slope in red; and, below, the total boundary shear calculated by using a water discharge of 1000 $m^3 s^{-1}$. The drop in shear stress, between kilometers 45 and 30, coincides with the upstream limit of the backwater zone.

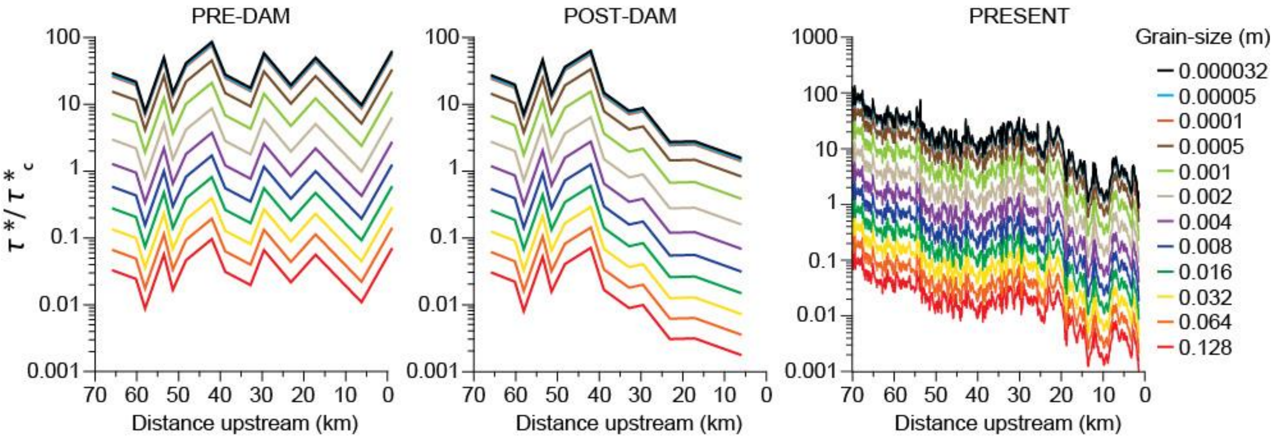

Figure 10. The sediment transport capacity of the river has been quantified through change in frictional mobility estimated by comparing the non-dimensional shear stress of specific grain sizes to its critical value. The post-dam scenario, with a marked downstream reduction of the ratio t^*/t_c^* compared to pre-dam conditions, is in agreement with the modern river transport capacity. River bed profile in pre- and post-dam scenarios are obtained from thalweg depths in river cross-sectional profiles; the modern river profile is derived from the 2005 AD multibeam bathymetric survey (Colombo and Filippi, 2010) while water surface elevation are acquired in this study and scaled for water discharge of 1000 m^3 s^{-1}.

4) Clinoforms and trajectory analysis

Clinoform is the term originally introduced by Rich (1951) to describe the shape of a depositional surface at the scale of an entire continental margin (Fig. 4.1). Clinoforms are widely recognized as one of the fundamental building blocks of the stratigraphic record (Pirmez et al., 1998) and are characterized by three geometric elements: the topset (undaform) represents the most low-angle and shallow-water sector; the foreset (clinoform) diagnostic of the steepest sector; the bottomset (fondoform) the almost flat and distal basinward sector (Fig. 4.1). The morphological break in slope at the topset-foreset transition is called rollover-point and in margin-scale clinoforms it coincides with the shelf edge (Fig. 4.1).

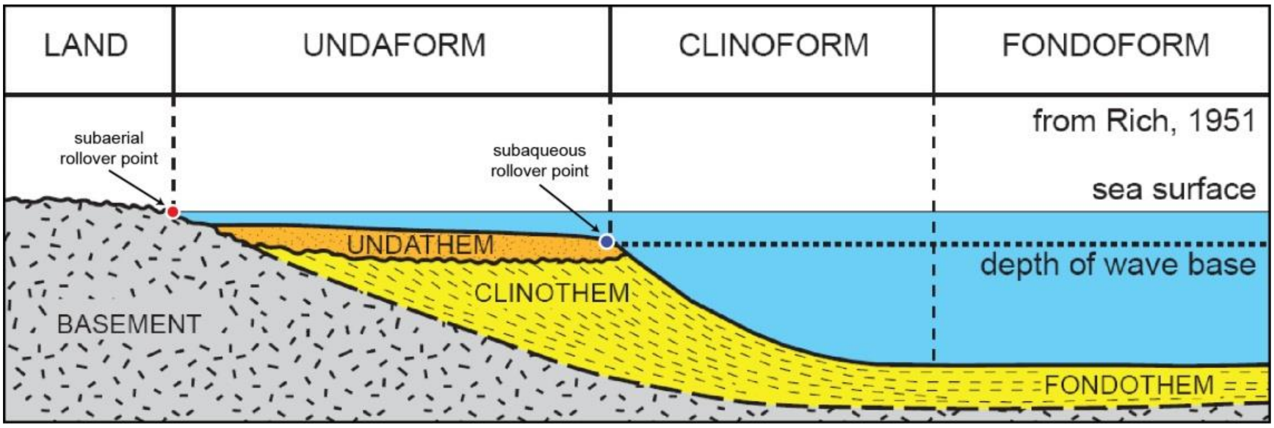

Figure 4.1: Diagram showing the original definition of clinoform from Rich (1951). Note the position of subaerial and subaqueous rollover points.

Since the advent of seismic stratigraphy, clinoforms have been observed over several spatial and temporal scales ranging from shoreline accretion to continental margin progradation (Vail et al., 1991), and encompassing intervals from hundreds of thousands to millions of years (Helland-Hansen and Hampson, 2009). Further advances in understanding of the migration of clinoforms through time derive from the application of the rollover-point trajectory analysis (Fig. 4.2; Helland-Hansen and Martinsen, 1996). The trajectory analysis is the study of lateral and vertical migration of geomorphological features and associated sedimentary environments, with emphasis on the paths and direction of migration of the shoreline and shelf edge (Henriksen et al., 2009). This information can be used to gain enhanced understanding of changing paleoenvironmental conditions and lithological distributions through time.

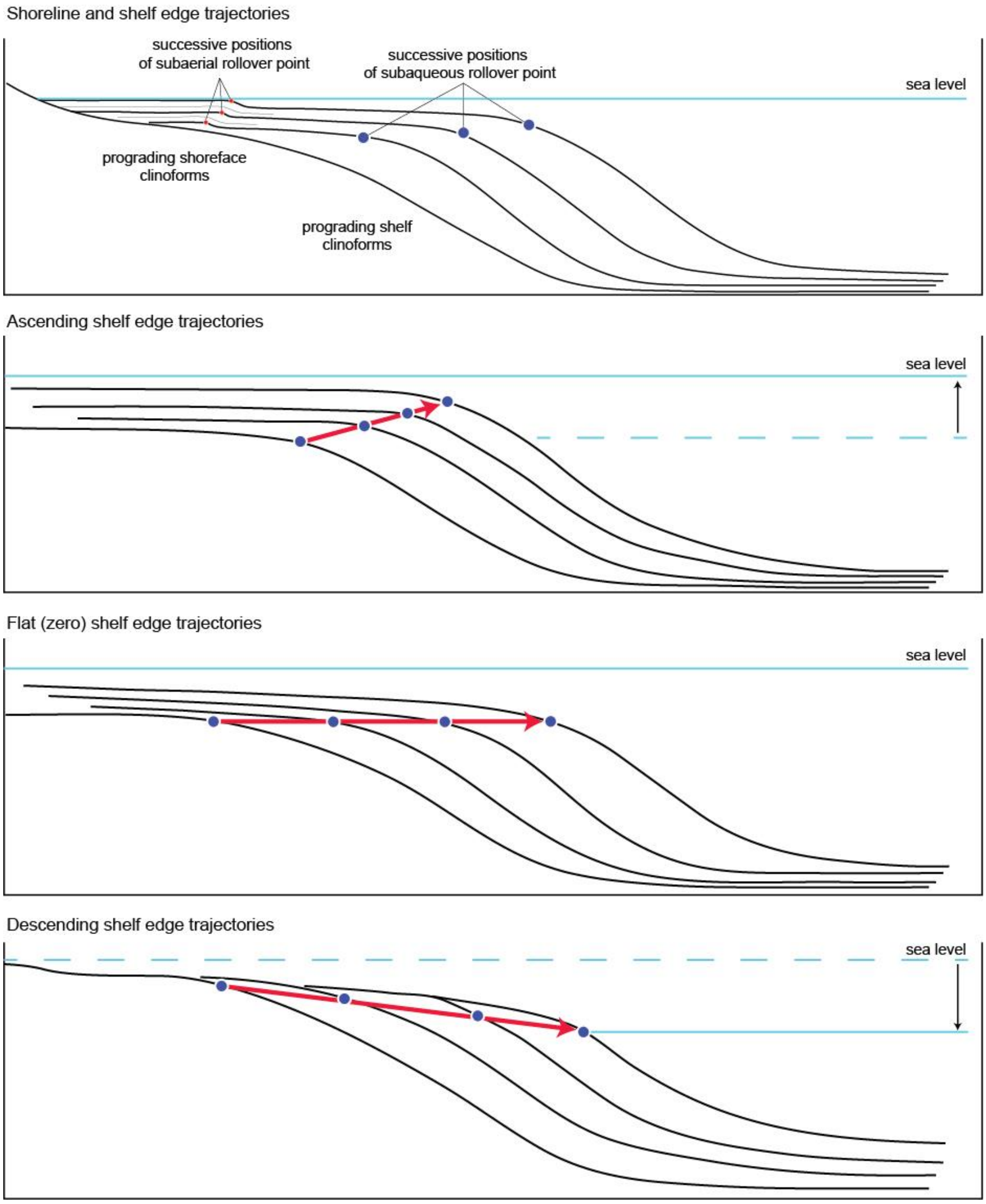

Figure 4.2: schematic diagram showing the different prograding shoreface and shelf clinoform. Note that the successive positions of the shoreline allows for the identification of a shoreline trajectory, which, in this example, shows normal regressive trend. The shelf edge trajectory is determined by the successive positions of the migrating shelf-slope break and may exhibit a ascending, flat or descending trend (modified after Steel and Olsen, 2002; Patruno et al., 2015).

More precisely, clinoform trajectory analysis has been applied to constrain the migration pattern of shorelines and associated coastal depositional systems (Helland-Hansen and Martinsen, 1996), or to describe the cross-sectional pathway of the shelf-edge during the accretion of shelf-slope-basin clinoforms (Mellere et al., 2002; Johannessen and Steel, 2005; Mahon et al., 2015). Trajectory analysis has been mostly applied to two-dimensional (2D) studies of widely-exposed dip-oriented successions, both in outcrop (Mellere et al., 2002, among others) and on seismic profiles (Patruno et al., 2014, among others), to progradational successions encountered in the geological record and ascribed to base level cycles of 100-500 kyr duration (Hampson, 2010) or even lower frequency (Midtkandal and Nystuen, 2009). The integrated approach of trajectory analysis and traditional sequence stratigraphy allows a better understanding of how changes in base level, subsidence and sediment supply affected the depositional architecture of continental margins (Fig. 4.2). While the shoreline trajectory is determined by the interplay among sediment supply, 4th and 5th order sea level changes, and basin physiography (Helland-Hansen and Gjelberg 1994; Helland-Hansen and Martinsen 1996), the shelf-edge trajectory seems more influenced by lower order changes of relative sea level and sediment flux (Mellere et al., 2002; Bullimore et al., 2005; Helland-Hansen and Hampson, 2009). Earlier publications suggest that descending/flat shelf-edge trajectories are associated with more fluvial-dominated depositional systems and that ascending shelf-edge trajectories are associated with wave-dominated processes; in addition, flat/negative shelf-edge trajectories have coeval deepwater slope and basin floor sandy deposits, whereas positive trajectories tend to associate with muddy slopes and basin floors coupled with the sand storage on the shelf and coastal plain (Steel el al. 2000; Plink-Björklund et al. 2001; Mellere et al. 2002; Plink-Björklund and Steel 2002; Bullimore et al., 2005).

The next manuscript is focused on the integrated approach of traditional stratigraphy with shelf-edge trajectory analysis of the Po River Lowstand delta that developed during the Last Glacial Maximum in the central Adriatic Sea. The additional material that accompanies the manuscript document the age model built for the interested stratigraphic interval through the analysis of the PRAD 1-2 borehole (paragraph 4.1.2) and the stratigraphic analysis of one of the clinothems that recorded the formation of deep-sea sandy lobes (paragraph 4.1.3). The stratigraphic interpretation takes into account surface, isochronal and seismic facies maps of each elementary clinothems that were analyzed through Petrel 3D platform at the Upstream Research Center (ExxonMobil, Houston, Texas).

This study offers the opportunity to resolve the internal geometry of clinothems that compose a lowstand sediment wedge and verify the presence of a systematic depositional motif. The high spatial and temporal framework gives helps establishing predictive relationships between shelf edge trajectories and the occurrence of sand-rich slope deposits.

4.1) Manuscript II

“Architectural motif, shelf-edge trajectories and sand bypass in short lived low-stand clinothems: the late-Pleistocene Po delta”

Authors: Claudio Pellegrini (Istituto di Scienze Marine, ISMAR-CNR, Università di Bologna, Dipartimento di Scienze della Terra e Geologico-Ambientali, Bologna, Italy)

Vittorio Maselli (Istituto di Scienze Marine, ISMAR-CNR, Bologna, Italy)

Fabiano Gamberi (Istituto di Scienze Marine, ISMAR-CNR, Bologna, Italy)

Alessandra Asioli (Istituto di Geoscienze e Georisorse, CNR-UOS Padova, Italy)

Kevin Bohacs (ExxonMobil Upstream Research Company, Spring, Texas, U.S.A)

Tina Drexler (ExxonMobil Upstream Research Company, Spring, Texas, U.S.A)

Fabio Trincardi (Istituto di Scienze Marine, ISMAR-CNR, Bologna, Italy)

Status: Submitted to ExxonMobil for internal peer review processes before the submission to *Geology Journal*

Architectural motif, shelf-edge trajectories and sand bypass in short lived low-stand clinothems: the late-Pleistocene Po delta

Authors: Pellegrini, C., Maselli, V., Gamberi, F., Asioli, A., Bohacs, K., Drexler, T., M., Trincardi, F.

Abstract

The Late Pleistocene Po River lowstand delta rapidly filled the Adriatic foredeep through a 350 m thick set of longitudinally prograding clinothems, causing a margin encroachment of 60 km during an extremely short time window, between 31.8 and 14.4 kyr BP. The resulting very expanded stratigraphic succession allows investigation of the spatial relations and internal architecture of each composing clinothem, in a high-resolution chronostratigraphic framework constrained by a continuous-recovery borehole (PRAD1-2) in the distal bottomset area. Based on topset geometry, shelf-edge trajectories and seismic facies, three types of clinothems can be recognized, each associated with different amounts and mechanisms of sand transport offshore. In Type 1, characterized by descending shelf-edge trajectories and eroded topset, sand is transported to slope channels and bottomset lobes; in Type 2, associated with ascending trajectories and topset aggradation, sand is transported beyond the shelf-edge by thin-skinned mass failures; in Type 3, characterized by ascending trajectories, maximum topset aggradation and major landward shifts of the coastal onlap, sand is almost entirely trapped on the shelf, and can reach the basin through hyperpycnal flows of decreasing competence through time, as recorded by cm thick sharp-based sandy layers on the slope. While the alternation of Type 1 and 2 clinothems, formed during overall sea level falls of about 25-30 meters, is associated with high-frequency accommodation cycles (mostly driven by the compaction of rapidly-accumulated sediment), Type 3 heralds the abandonment of the system close to the LST to TST transition (onset of Terminantion I), when sand transport to deeper water is progressively hampered by enhanced alluvial plain aggradation.

Our findings and chronological constraints document that subsiding foredeep settings at lowstand may record the typical stack of parasequences encountered in other subsiding realms, like the

Cretaceous successions of the Book Cliffs, but with durations one to two orders of magnitude shorter. Moreover, in over-supplied basins like the Po, repeated high-frequency accommodation cycles of only few thousands years duration may lead to the stacking of disconnected sand bodies in slope and bottomset settings, resulting in compartmentalized reservoirs even within one single Milankovitch-scale lowstand wedge.

Introduction

Clinothems are the major building block of continental margins and their variable morphological profile reflects the interplay between sediment supply and available accommodation space (Pirmez et al., 1998). Being the shape of a clinotheme somehow independent from its physical scales, attempts have been made to define a hierarchy of stratal patterns and key surfaces to interpret the conditions for clinotheme growth virtually on any time scale (Neal and Abreu, 2009). A major advance in understanding the evolution of clinothems and continental margin growth came from the integration of sequence stratigraphy with the trajectory analysis of morphological breaks-in-slope, often referred to as rollover points in the literature (i.e. the topset-foreset transition; Steel and Olsen, 2002). This integrated approach led to a better quantification of the temporal range of creation/destruction of accommodation space and its bearing on the prediction of lithology and facies partitioning at a sequence scale (Henriksen et al., 2009 and references there in).

The Po River lowstand delta (ca. 200,000 km^2 drainage area debouching on a ca. 20,000 km^2 basin; Fig. 1), accumulated in a over-supplied epicontinental sea during the Last Glacial Maximum (LGM), offers the unique opportunity to disentangle how allogenic and autogenic processes drive clinotheme growth, sediment export toward the slope/basin and sand bodies compartmentalization within a single progradational event and with a very high chronological resolution.

Results

The interval between the former interglacial (Eemian, 123-119 kyr BP) and the onset of the LGM at ca. 23 kyr BP (LGM Chronozone Level 1, 19,000-23,000 cal yr B.P. according to Mix et al., 2001) led to a substantial shrinkage of the Adriatic basin and the concurrent broadening of the Po River drainage area, with a seaward shift of the shoreline of ca. 200 km (Maselli et al., 2011; Amorosi et al., 2015 and Fig. 1). During the LGM, the Po River discharged directly into the Mid Adriatic Deep (MAD), a structurally-confined slope basin that remained connected to the Mediterranean Sea, thereby keeping a link to global sea level.

The chronology of the progradation into the MAD was assessed in the borehole PRAD1-2, recovered in its distal toe region (Ridente et al., 2009), by a combination of new and already available ^{14}C AMS dates (Piva et al., 2008), tephrochronology (Bourne et al., 2010), bio- and event-stratigraphy (Piva et al., 2008; see Supplementary material for details) (Fig. 2): the delta started its growth at ca. 31.8 cal kyr BP and was drowned at ca. 14.4 cal kyr BP, when a major flooding event brought the basin into fully marine waters (Asioli et al., 2001). In this very short time-window, encompassing the MIS 2 sea level fall (about 25-30 meters, Siddal et al., 2003) to the early stages of the post-glacial sea level rise, the Po River outbuilt its coastal plain 60 km basin-ward, forming a lowstand delta that reached a thickness of 350 m, an estimated total volume of 650-700 km^3 (Amorosi et al., 2015; Fig. 3), where 45 m of topset aggradation resulted from the stacking of of coastal/delta plain and paralic deposits.

In detail, clinothems are characterized by repeated changes in rollover-point trajectory accompanied by concurrent changes in the distance between the coastal onlap and the correlative rollover point (Fig. 3). Based on seismic facies, topset geometry, rollover-point trajectory, and occurrence vs. absence of mounded deposits in the bottomset (taken as a proxy of sand bypass across the shelf and slope), three types of clinothems are recognized (Fig. 3 and 4).

Type 1: topset characterized by truncated toplap reflectors that pass vertically to seaward dipping shingled reflectors reminiscent of shelf-phase delta (Suter and Berryhill, 1985). These deposits are connected to discontinuous high amplitude and mounded reflector packages in the bottomset interpreted as sand lobes; occasionally, these lobes show small channels with modest levee wedges. These clinothems show minimal aggradation in the topset and a descending trajectory of the rollover point (Fig. 3 and 4); in such context it may prove difficult to estimate the amount of sediment removed from the topset region and, ultimately, quantify the relative sea level fall intervened.

Type 2: topset characterized by continuous high amplitude reflectors that pass toward the bottomset into discontinuous and low amplitude reflectors, interpreted as mass-transport deposits. Type 2 clinothems show an ascending rollover point trajectory and maximum aggradation in the order of 10-15 m, calculated through the vertical component in the rollover point trajectory (Fig. 3 and 4). Type 3: topset characterized by plane-parallel landward-onlapping reflectors with high lateral continuity accompanied by weakly reflective foreset with continuous reflectors at the toe region. Type 3 clinotheme shows aggradation at the topset with a maximum component at the rollover point (10-15 m), an ascending rollover point trajectory and a maximum distance between the landward pinch out and its time equivalent rollover point (Fig. 4).

Type 1 clinothems pass continuously, with no detectable break in sedimentation, into Type 2 clinothems, forming a typical progradational-degradational to progradational-aggradational sequence (APD-PA, Neal and Abreu, 2009). The end of a Type 2 progradation is marked by a flooding surface that has a clear physical expression in seismic profiles and can be traced to borehole PRAD1.2. The seismic facies configuration and the sediment cores (Fig. 2) sampled from Type 3 documents the presence of sharp-based cm-thick sandy layers in the foreset, even if the system is aggrading on a large shelf portion, while sand lobes in the bottomset are absent.

Overall, the height of each clinothems (vertical distance between rollover point and the inflection point at the toe of the foreset; Pirmez et al., 2008) decreases from the oldest (260 m) to the youngest (80 m) during the development of the Po River lowstand wedge; this trend reflects the progressive fill of the basin through continuous bottomset aggradation, in turn favored by the structural confinement of the slope basin (Fig. 3).

In less than 15 kyr, the Po River lowstand delta recorded three APD-PA sequences (three couples of Type 1+Type 2 clinothems), each separated by a minor flooding surface; this succession is topped by a set of Type 3 clinothems (Fig. 4). The first sequence formed in about 10 kyr (between 31.8 and 21.1 kyr BP) and is characterized by the lowest values in the ratio of Ca/Ti obtained from borehole PRAD1-2 (Fig. 2), indicating a reduce influence of the catchment on the sediment supply. The bulk of the progradation (sequences 2 and 3) occurred between 21.1 and 18 kyr BP and is accompanied by higher Ca/Ti values implying an increasing supply of clastic sediment from the Alps and Apennines during the LGM chronozone (an increased biogenic production is excluded by the very low content of carbonate biosomes); furthermore, the presence of the benthic foraminifera *Sigmoilina sellii* throughout the entire section confirms that this phase of the progradation occurred during an overall cold period, while the increasing content of organic matter in PRAD 1.2 suggests hypoxic to anoxic conditions at the sea floor (Fig. 2). The Type 3 clinotheme started accumulating at ca. 18 kyr BP (at ca. 6.5 m in PRAD1-2), during the early phases of the post-glacial sea level rise; the drowning and abandoned of the system at ca. 14.4 kyr (at ca. 2.5 m in PRAD1-2) is accompanied by an increasing rate in the number of benthic specimens and a lighter $\delta^{18}O$ values (*Bulimina marginata*), and the last occurrence of *S. sellii* within the uppermost strata (Figs. 2 and 4).

Discussion and Conclusion

The Po River lowstand delta is composed by a combination of forestepping clinothems that mimic those commonly ascribed to base level cycles of 100-500 kyr of duration or even lower frequency (Helland-Hansen and Martinsen, 1996; Johannessen and Steel, 2005; Helland Hansen and Hampson, 2009; Midtkandal and Nystuen, 2009; Hampson, 2010). In addition, the descending trajectory of Type 1 clinothems composing the Po River lowstand delta are accompanied by sand leakage through the coastal system and bypass to the upper slope area and are diagnostic of the presence of significant storage of sand in the bottomset, similarly to what is suggested for clinothems that develop on longer time scales (Steel et al., 2000; Gong et al., 2015). Our data therefore show that the geometry and the thickness of prograding clinotheme packages are not sufficient to discriminate their hierarchy and the duration of the cycle during which deposition has occurred. As observed originally by Boyd et al. (1989) for the entire Mississippi River lowstand delta, also in the case of the Po River lowstand delta the physical scale of the lithosomes recorded in the stratigraphic succession has no implication on the time elapsed during their deposition.

Although, the formation of the Po River lowstand delta was driven by the allogenic control of eustasy that was also responsible for part of the topset aggradation, in detail its stratal architecture and facies distribution were dictated by a combination of changes in sediment supply, mostly driven by climatic oscillations (as suggested elsewhere by Fuller et al., 1998), and high-frequency accommodation cycles, related to the compaction of rapidly accumulated sediment. Three APD-PA sequences formed during an overall sea level fall, as witnessed by the descending trajectory of Type 1 clinothems, but among each sequence the compaction of Type 1 clinothems results in increased accommodation space on the shelf that allows the formation of the PA reflector packages within the overlying Type 2 clinothems, indicating that sediment supply was able to keep pace with 5-10 m base-level rises. Recent estimates of the compaction rates from the rapidly accumulated (30 m in 400 yr) modern Po River delta (Teatini et al., 2011) are in agreement with the results obtained from the PRAD1-2 borehole, where sediment compaction is calculated in about 15% of the total vertical section (Maselli et al., 2010). These figures appear consistent with the accommodation space needed for the topset aggradation of each PA sequences. The formation of Type 2 clinothems is also characterized by the presence of mass-transport deposit in the bottomset, probably generated by the high accumulation rates at the shelf edge. At the end of the cycle, rapid basin-ward and downward shifts of the shoreline generate a bypass surface on the shelf (where accommodation space is at a minimum) and to the formation of Type 1 clinothems in the basin, where the descending rollover point trajectories reflect the general sea level fall (Fig. 4). During the formation of Type 1 clinothems, sea level fall forced the shoreline close to the shelf edge, allowing a more efficient sand transport toward the basin with the formation of channels and lobes. Changes in sediment accumulation rate obtained from the borehole

PRAD1-2 may reflect climate variability, as indicated by phases of Apennine and Alpine glaciers advances and retreats (Giraudi, 2011; Florineth and Schluchter, 1998), and variations in the sediment storage and bypass toward the basin related to the fluvial response time and autogenic processes (Muto and Steel, 2002; Nijhuis, et al., 2015). The finding from the Po River lowstand delta highlights that, although coarse-sediment delivery to the deep sea is expected principally during periods of sea level fall and lowstand (Covault and Graham, 2010), sand bypass toward the basin may not be continuous even on very short times: high-frequency base level oscillations may force the development of sandy deposits separated by flooding surfaces and relatively thick muddy clinothems (Fig. 4). In this scenario, stacked sandy deposits separated by mud drapes constitute discrete-individual sedimentary bodies and may represent an interesting case of compartmentalization within a single high-frequency lowstand deposit (Ainsworth, 2010).

References

Ainsworth, R. B., 2010, Prediction of stratigraphic compartmentalization in marginal marine reservoirs: Geological Society, London, Special Publications, v. 347(1), p. 199-218.

Amorosi, A., Maselli, V., Trincardi, F., 2015. Onshore to offshore anatomy of a late Quaternary source-to-sink system (Po Plain–Adriatic Sea, Italy): Earth-Science Reviews.

Asioli, A., Trincardi, F., Lowe, J.J., Ariztegui, D., Langone, L., and Oldfield, F., 2001, Sub-millennial scale climatic oscillations in the central Adriatic during the Lateglacial: palaeoceanographic implications: Quaternary Science Reviews, v. 20(11), p. 1201-1221.

Bourne, A.J., Lowe, J.J., Trincardi, F., Asioli, A., Blockley, S.P.E., Wulf, S., Matthews I.P., Piva, A., and Vigliotti, L., 2010, Distal tephra record for the last ca 105,000 years from core PRAD 1-2 in the central Adriatic Sea: implications for marine tephrostratigraphy: Quaternary Science Reviews, v. 29(23), p. 3079-3094.

Boyd, R., Suter, J., and Penland, S., 1989, Relation of sequence stratigraphy to modern sedimentary environments: Geology, v. 17, p. 926-929.

Covault, J.A., and Graham, S.A., 2010, Submarine fans at all sea-level stands: tectono-morphologic and climatic controls on terrigenous sediment delivery to the deep sea: Geology, v. 38(10), p. 939-942.

Florineth, D., and Schluchter, C., 1998, Reconstructing the Last Glacial Maximum (LGM) ice surface geometry and flowlines in the Central Swiss Alps: Eclogae Geologicae Helvetiae, v. 91(3), p. 391-407.

Fuller, I.C., Macklin, M.G., Lewin, J., Passmore, D.G., and Wintle, A.G., 1998, River response to high-frequency climate oscillations in southern Europe over the past 200 k.y: Geology v. 26, p. 275-278.

Giraudi, C., 2011, Middle Pleistocene to Holocene glaciations in the Italian Apennines: Developments in Quaternary Science, v. 15, p. 211-219.

Gong, C., Wang, Y., Steel, R.J., Olariu, C., Xu, Q., Liu, X., and Zhao, Q., 2015, Growth Styles of Shelf-Margin Clinoforms: Prediction of Sand-and Sediment-Budget Partitioning Into and Across The Shelf: Journal of Sedimentary Research, v. 85(3), p. 209-229.

Hampson, G.J., 2010, Sediment dispersal and quantitative stratigraphic architecture across an ancient shelf: Sedimentology, v. 57(1), p. 96-141.

Helland-Hansen, W., and Martinsen, O.J., 1996, Shoreline trajectories and sequences: description of variable depositional-dip scenarios: Journal of Sedimentary Research, v. 66(4), p. 670-688.

Helland-Hansen, W., and Hampson, G.J., 2009, Trajectory analysis: concepts and applications: Basin Research, v. 21(5), p. 454-483.

Henriksen, S., Hampson, G.J., Helland-Hansen, W., Johannessen, E.P., and Steel, R.J., 2009, Shelf edge and shoreline trajectories, a dynamic approach to stratigraphic analysis: Basin Research, v. 21(5), p. 445-453.

Johannessen, E.P., and Steel, R.J., 2005, Shelf-margin clinoforms and prediction of deepwater sands: Basin Research, v. 17(4), p. 521-550.

Maselli, V., Trincardi, F., Cattaneo, A., Ridente, D., and Asioli, A., 2010, Subsidence patterns in the central Adriatic and its influence on sediment architecture during the last 400 kyr: Journal of Geophysical Research: Solid Earth, v. 115, no. B12, doi: 10.1029/2010JB007687.

Maselli, V., Hutton, E.W., Kettner, A.J., Syvitski, J.P., and Trincardi, F., 2011, High-frequency sea level and sediment supply fluctuations during Termination I: an integrated sequence-stratigraphy and modeling approach from the Adriatic Sea (Central Mediterranean): MarineGeology, v. 287(1), p. 54-70.

Midtkandal, I., and Nystuen, J.P., 2009, Depositional architecture of a low-gradient ramp shelf in an epicontinental sea: the lower Cretaceous of Svalbard: Basin Research, v. 21(5), p. 655-675.

Mix, A.C., Bard, E., and Schneider, R., 2001, Environmental processes of the ice age: land, oceans, glaciers (EPILOG): Quaternary Science Reviews, v. 20(4), p. 627-657.

Muto, T., and Steel, R.J., 2002, In Defense of Shelf-Edge Delta Development during Falling and Lowstand of Relative Sea Level: The Journal of Geology,v. 110(4), p. 421-436.

Neal, J., and Abreu, V., 2009, Sequence stratigraphy hierarchy and the accommodation succession method: Geology, v. 37(9), p. 779-782.

Nijhuis, A.G., Edmonds, D.A., Caldwell, R.L., Cederberg, J.A., Slingerland, R.L., Best, J.L., Parson, D.R., and Robinson, R.A.J., 2015, Fluvio-deltaic avulsions during relative sea-level fall: Geology, v. 43(8), p. 719-722.

Pirmez, C., Pratson, L.F., and Steckler, M.S., 1998, Clinoform development by advection-diffusion of suspended sediment: Modeling and comparison to natural systems: Journal of Geophysical Research: Solid Earth (1978–2012), v. 103, p. 24141-24157, doi: 10.1029/98JB01516.

Piva, A., Asioli, A., Schneider, R. R., Trincardi, F., Andersen, N., Colmenero-Hidalgo, E., Dennielou, B., Flores, J.A., and Vigliotti, L., 2008, Climatic cycles as expressed in sediments of the PROMESS1 borehole PRAD1-2, central Adriatic, for the last 370 ka: 1. Integrated stratigraphy: Geochemistry, Geophysics, Geosystems, v. 9(1), doi: 10.1029/2007GC001713.

Ridente, D., Trincardi, F., Piva, A., Asioli, A., 2009. The combined effect of sea level and supply during Milankovitch cyclicity: Evidence from shallow-marine δ18O records and sequence architecture (Adriatic margin). Geology,37(11), 1003-1006.

Siddall, M., Rohling, E.J., Almogi-Labin, A., Hemleben, C., Meischner, D., Schmelzer, I., and Smeed, D.A., 2003, Sea-level fluctuations during the last glacial cycle: Nature, v. 423(6942), p. 853-858.

Steel, R.J., Crabaugh, J., Schellpeper, M., Mellere, D., Plink-Björklund, P., Deibert, J., and Loeseth, T., 2000, Deltas vs. rivers on the shelf edge: their relative contributions to the growth of shelf-margins and basin-floor fans (Barremian and Eocene, Spitsbergen): Deepwater Reservoirs of the World, v. 33, p. 981-1009.

Steel, R.J., and Olsen, T., 2002, Clinoforms, clinoform trajectories and deepwater sands. Sequence Stratigraphic Models for Exploration and Production: Evolving Methodology, Emerging Models and Application Histories, p. 367-381.

Suter, J.R., and Berryhill Jr, H.L., 1985, Late Quaternary shelf-margin deltas, northwest Gulf of Mexico: AAPG Bulletin, v. 69(1), p. 77-91.

Teatini, P., Tosi, L., and Strozzi, T., 2011, Quantitative evidence that compaction of Holocene sediments drives the present land subsidence of the Po Delta, Italy: Journal of Geophysical Research, v. 116, B08407, doi: 10.1029/2010JB008122, 2011.

Figure captions (2933 characters)

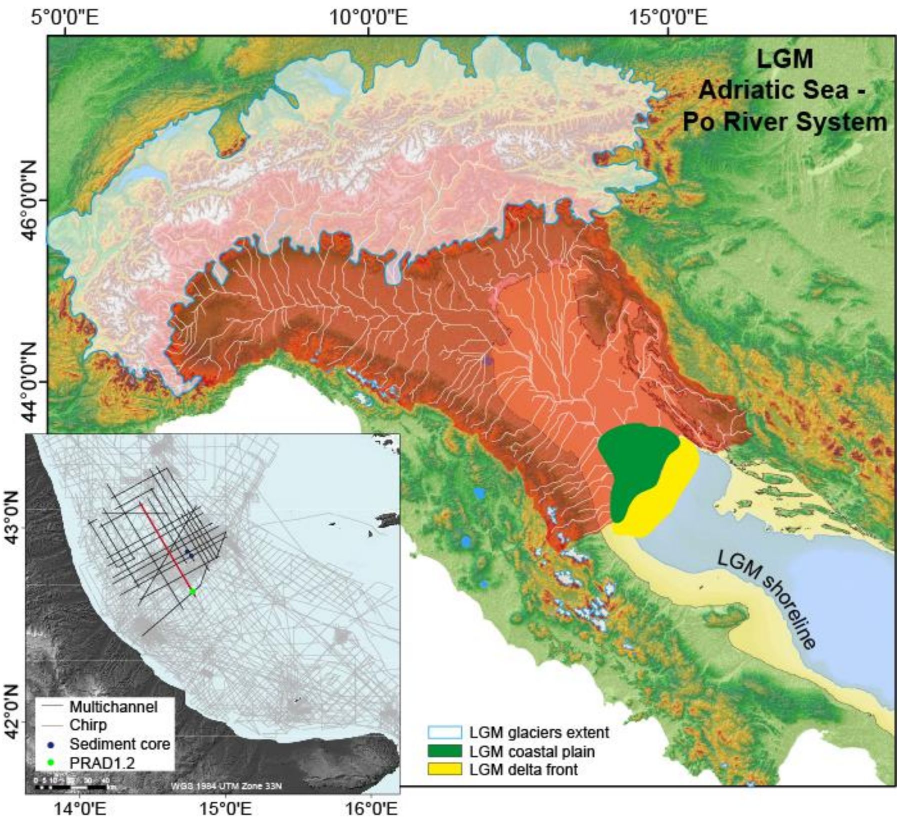

Fig. 1: A) Study area with ISMAR high-resolution seismic data (gray lines) and the location of multichannel seismic lines (note the location of seismic line LSD22 in red) and PRAD1.2 borehole (large green dot). B) Po River drainage area during LGM (modified after Maselli et al., 2011) and Alpine and Apennines glaciers extent (modified after Florineth and Schlüchter, 1998; Giraudi, 2011). White lines represent the ancestral Po River and its tributaries; Green and yellow polygons depict Po River coastal plain and delta front, respectively.

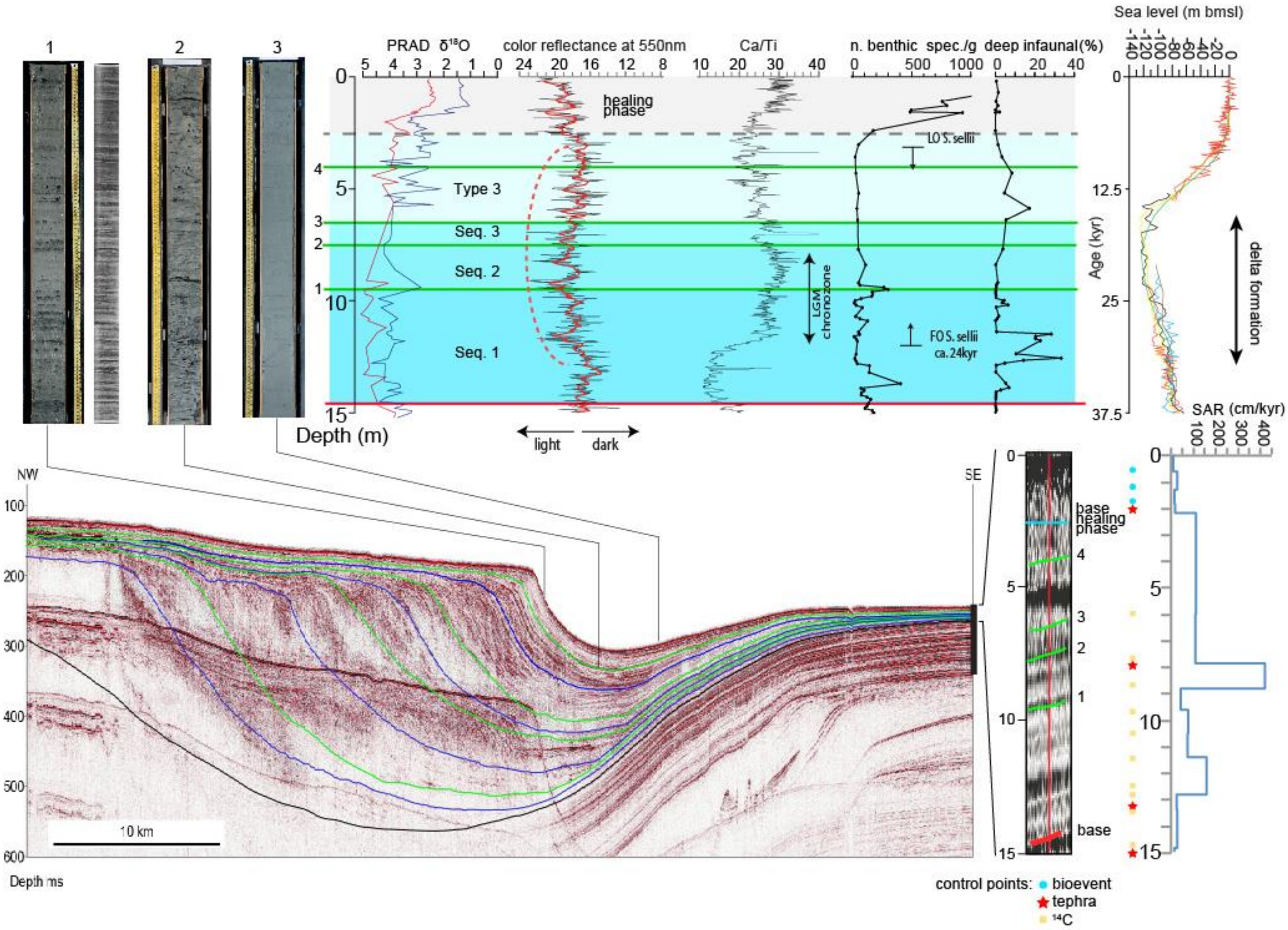

Fig. 2: Core images illustrate respectively, 1: the sharp-based sand beds in the proximal foreset and 2: the bioturbated organic-rich etherolitic sediment of the bottomset of Type 3 Clinotheme; in Type 3 the "healing phase" uniform mud records the last 14.4 kyrs (Asioli et al., 2001). Borehole PRAD1-2 in the distal correlative (right) allows dating individual flooding surfaces that partition the expanded lowstand wedge of the LGM (left); ^{14}C constrained stable isotope curves on planktonic and benthic foraminifera allow correlation to global sea-level curves. Even in the distal location of borehole PRAD1-2, peaks of supply occur consistently during the formation of Type 1 Clinothems, characterized by descending trajectory and sand bypass to the slope basin.

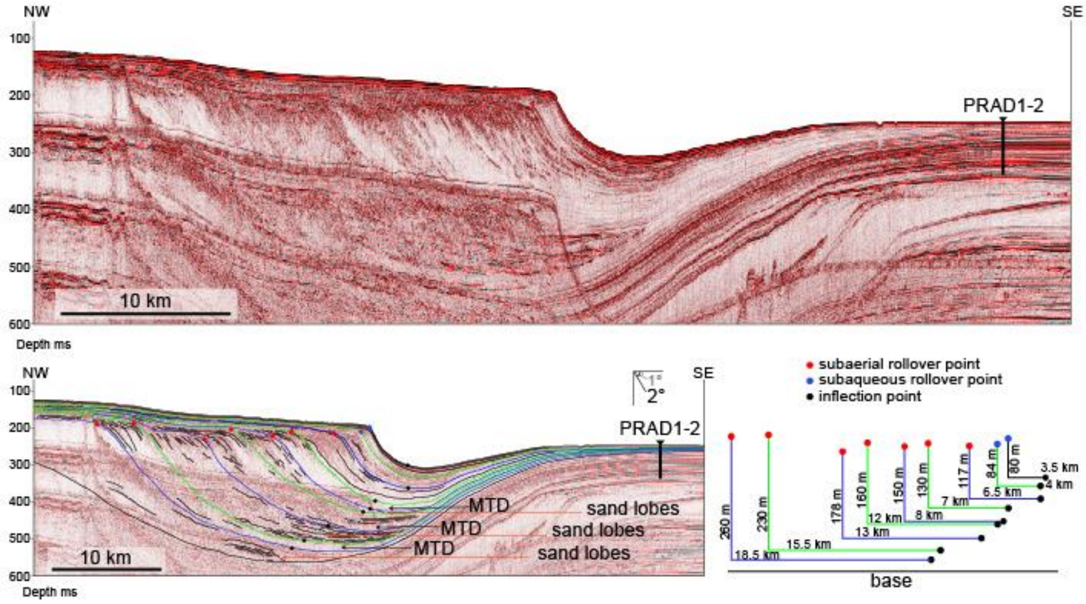

Fig. 3: Multichannel seismic profile LSD22 and line drawing (bottom left). Subtle changes in the topset geometry and shelf-edge trajectories reflect changes in accommodation accompanied by changes in the foreset and bottomset stratal geometry, primarily related to the amount of sand bypass off shelf. Above the sequence boundary (at ca. 31 kyr), individual clinothems show a decreasing height (from 260 m to 80 m) and seaward extent (18.5 km to 3.5 km) as the bottomset area aggrades substantially filling the slope basin and rising significantly the foundation surface for the clinothems. The youngest clinotheme, above the green reflector and records a major landward shift of the shoreline accompanied by high supply to maintain shelf-edge progradation and occurs just before 15.7 kyr BP.

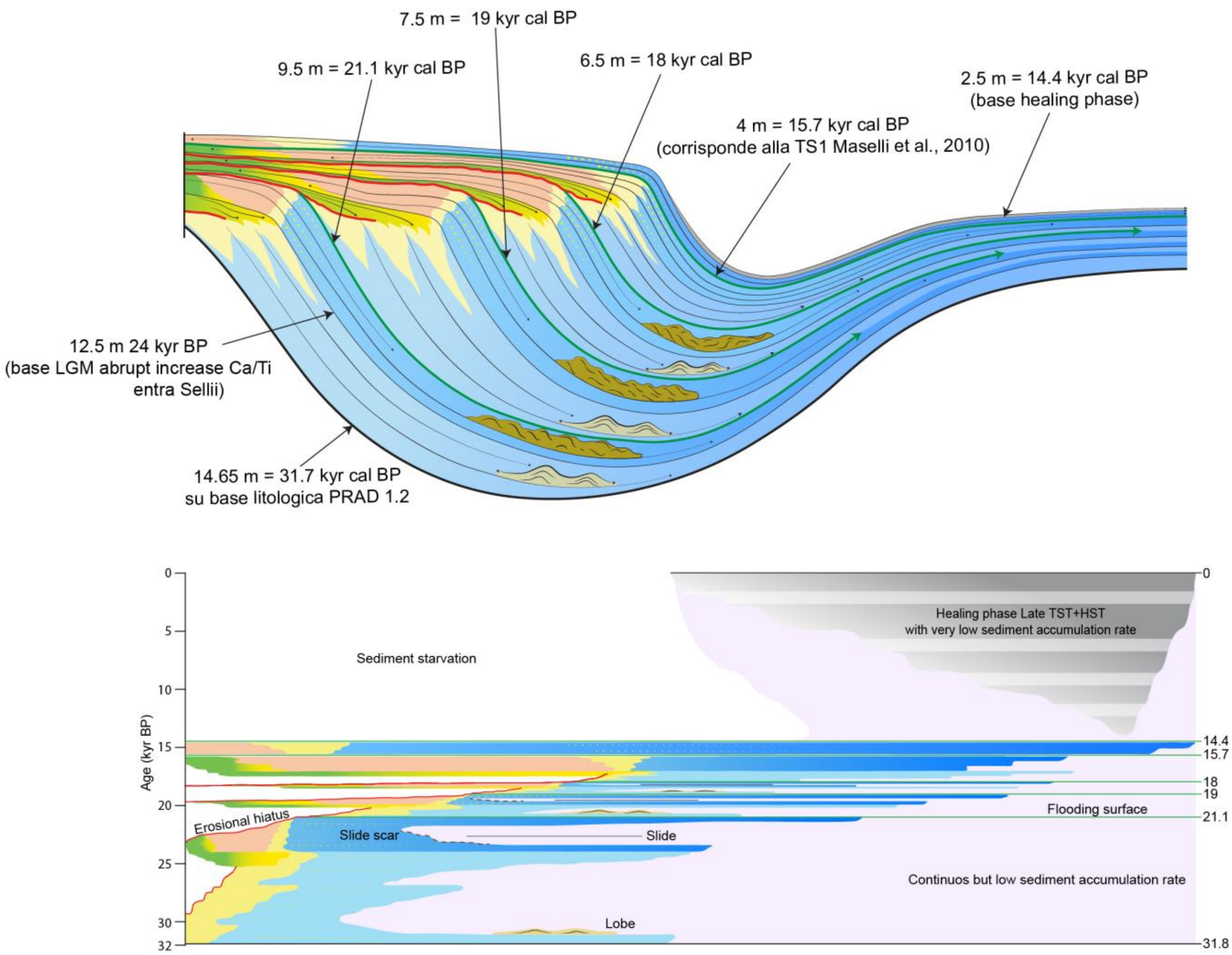

Fig. 4: Idealized Po River lowstand wedge architecture and chronostratigraphic (Wheeler) diagram. Type 1 and Type 2 alternate repeatedly. Type 1 records the destruction of accommodation (expressed by the erosional topset surface), associated with sandy lobes in the bottomset, and is capped by flooding surfaces that record landward shifts of the coastal onlap in the order of tens of kilometers. Type 2 records constructional accommodation phases (as suggested by ascending rollover point trajectories) coupled with the presence of mass transport deposits in the basin. Type 3 develops at the end of the lowstand and heralds the drawn of the system with maximum aggradation rates on the shelf and the greatest landward migration of coastal onlap; even in these conditions cm-scale sand layers reach the slope as hyperpycnal flows (see Fig. 3).

4.2) Additional Material

4.2.1) Chronology of the PRAD 1-2 borehole

The chronology of the investigated interval of borehole PRAD1-2 relies on the integration of both new and already available in literature (Table 4.1; Piva et al., 2008) ^{14}C AMS dates, accompanied by tephrochronology on macro and cryptotephra (Bourne et al., 2010) as well as on bio- and event-stratigraphic control points (Piva et al., 2008). The six radiocarbon dates available from literature were performed on benthic monospecific samples, on either *Elphidium crispum* or *Hyalinea balthica*, at the Poznan Radiocarbon Laboratory, Poland, while the five new ones were performed on benthic monospecific samples, on either *Elphidium crispum, or Glandulina laevigata* at the NOSAMS National Ocean Sciences Accelerator Mass Spectrometry Facility, Department of Geology and Geophysics, Woods Hole Oceanographic Institution, USA and at Poznan Laboratory. The specimens were picked up from the size fraction >0.250 mm.

All the ages were calibrated for the present study using the online Calib 7.1.0 Radiocarbon Calibration Program (Stuiver and Reimer, 1993) and the calibration data set Marine13.14c by Reimer et al. (2013). ΔR (reservoir) of 135.8 years with a standard deviation of 40.8 years, was obtained by two sites on the western side of the Adriatic: one from the Northern Adriatic (487 years, Rimini) and another from the Southern Adriatic (483 years, Barletta), avoiding data from Dalmatia and Croatia (Rovigne, 262 and 254 years, respectively), because from a different geological context dominated by karst structures. We assume that, during the last climate cycle at least, the area where PRAD1-2 borehole was recovered was mostly influenced by the western Adriatic catchment area.

Level	Core depth (mbsf)	Lab. n.	^{14}C age (yr BP)	Species	Calibrated age (range) yr BP
PRAD1-2 S8 cm 40-42	5.976	Poz-16129	14930 ± 90	*E. crispum*	17226 - 17845
PRAD1-2 S10 cm 60-62	7.80	Poz-16130	16530 ± 100	*E. crispum*	18991 - 19569
PRAD1-2 S12 cm 0-2	8.80	OS-121214	17000 ± 50	*E. crispum*	19628 - 20065
PRAD1-2 S13 cm 0-2	9.60	OS-121280	18200± 85	*E. crispum*	21024 - 21681
PRAD1-2 S14 cm 10-12	10.50	OS-121215	19200± 40	*E. crispum*	22376 - 22680
PRAD1-2 S15 cm 20-22	11.40	OS-121496	20300±110	*E. crispum*	23471 - 24098
PRAD1-2 S15 cm 70-72	11.90	Poz-25365	21140 ± 180	*G. laevigata*	24301 - 25314
PRAD1-2 S16 cm 50-52	12.48	OS-121281	22100± 130	*E. crispum*	25602 - 26076
PRAD1-2 S16 7/8	12.78	Poz-25366	20990 ± 260	*E. crispum*	23978 - 25313
PRAD1-2 S17 cm 60-62	13.40	Poz-16131	24130 ± 150	*E. crispum*	27458 - 27959
PRAD1-2 S17 cm 60-62	13.40	Poz-16132	23390 ± 150	*H. balthica*	26741 - 27505
PRAD1-2 S19 cm 40-42	14.8	Poz-17321	28960 ± 270	*E. crispum*	31536 - 33163

Table 4.1: dates available from the literature (labeled Poz; from Piva et al., 2008) and six new dates performed for this study (labeled OS and Poz-25365); the ages are expressed as range 2σ.

Five tephra layers determined by geochemical analysis occur within the investigated interval offering an independent cross check for the radiocarbon dates, and were included in the age model as additional control points. The five tephra were analyzed by Bourne et al. (2010) and the reader is referred this paper for further details about the tephra ages obtained independently from the ^{14}C dates above described. Finally, three dated bio-events were used as additional control points (Piva et al. 2008) were used for the uppermost 2 m of the PRAD 1-2 borehole section and they include: 1) the Last Occurrence of the planktic foraminifer *Globorotalia inflata* at 6 cal. kyr BP, a biomarker recognized in the whole Adriatic basin and pre-dating the attainment of the maximum flooding during the Holocene (Trincardi et al., 1996); 2) the recognition of the time equivalent deposit of the Sapropel 1 in the eastern Mediterranean, a major oceanographic event centered at 8.5 cal. kyr according to the astronomical tuning by Lourens (2004); and 3) the paleoenvironmental change related to the end of the GS-1 event well recognized in the Adriatic basin and dated at 12 cal yr by Piva et al. (2008). In Table 4.2 all the available control points are listed. The control points obtained from of the radiocarbon ages are mid points.

Sample top (m)	Age range (yr BP)	Source	Reference		Control points	SAR (cm/ka)
0	0	modern time	Piva et al. (2008)	accepted	0	10
0.6	6000	LO *G. inflata*	Piva et al. (2008)	accepted	6000	28
1.288	8500	Sapropel equivalent 1	Piva et al. (2008)	accepted	8500	15
1.8	12000	Top GS-1	Piva et al. (2008)	accepted	12000	18
2.18	14320 - 13900	Neapolitan Yellow Tuff	Bourne et al. (2010)	accepted	14110	111
5.976	17226 - 17845	^{14}C	Piva et al. (2008)	accepted	17540	108
7.8	18991 - 19569	^{14}C	Piva et al. (2008)	mean	19275	420
7.84	19480 - 19050	Greenish/Verdoline	Bourne et al. (2010)	mean		
8.8	19628 - 20065	^{14}C	this study	accepted	19498	43
9.6	21024 - 21681	^{14}C	this study	accepted	21350	76
10.50	22376 - 22680	^{14}C	this study	accepted	22528	72
11.40	23471 - 24098	^{14}C	this study	accepted	23780	160
12.48	25602 - 26076	^{14}C	this study	rejected		
12.78	23978 - 25313	^{14}C	Piva et al. (2008)	accepted	24725	25
13.32	28255 - 26302	VRa	Matthews et al. (2015)	mean	27200	27
13.4	26741 - 27505	^{14}C	Piva et al. (2008)	mean		
14.8	31536 - 33163	^{14}C	Piva et al. (2008)	accepted	32350	15
14.94	33965 - 32630	Codola (base)	Matthews et al. (2015)	accepted	33300	26
16.53	39390 - 39170	Campanian Ignimbrite	Bourne et al. (2010)	accepted	39500	

Table 4.2: the age model of the study encompassing the ^{14}C dates on benthic species and tephra layers.

The radiocarbon dating at 12.48 m has been rejected as producing an inversion with the underlying age. The higher value may reflect interval-time with river input of older carbon-rich sediments. In two cases the age provided by ^{14}C has shown an age overlapping with the age of a tephra positioned very close (within 4 to 8 cm), and therefore, to avoid possible distortions due to a too short integrating time interval, depth and age of the control points were calculated by averaging the values of the levels above and below. The age of the flooding surfaces has been calculated by linear interpolation between two successive control points, assuming constant the sediment accumulation rates between them. Finally, the sediment accumulation rates (SAR) have been calculated for each discrete interval.

4.2.2) Short-lived clinothem from the late Pleistocene Po River sediment wedge: an example of sand bypass to the basin

The late Pleistocene clinothem 300-400 is bounded by surfaces 300 and 400 at its top and base, respectively. Surfaces 300 and 400 are characterized by high amplitude and continuous reflectors (Fig. 4.1). Clinothem 300-400 is characterized by high amplitude and chaotic reflectors in the topset that pass to high amplitude chaotic and dipping and to low amplitude discontinuous and dipping reflectors at the foreset sector (Fig. 4.1).

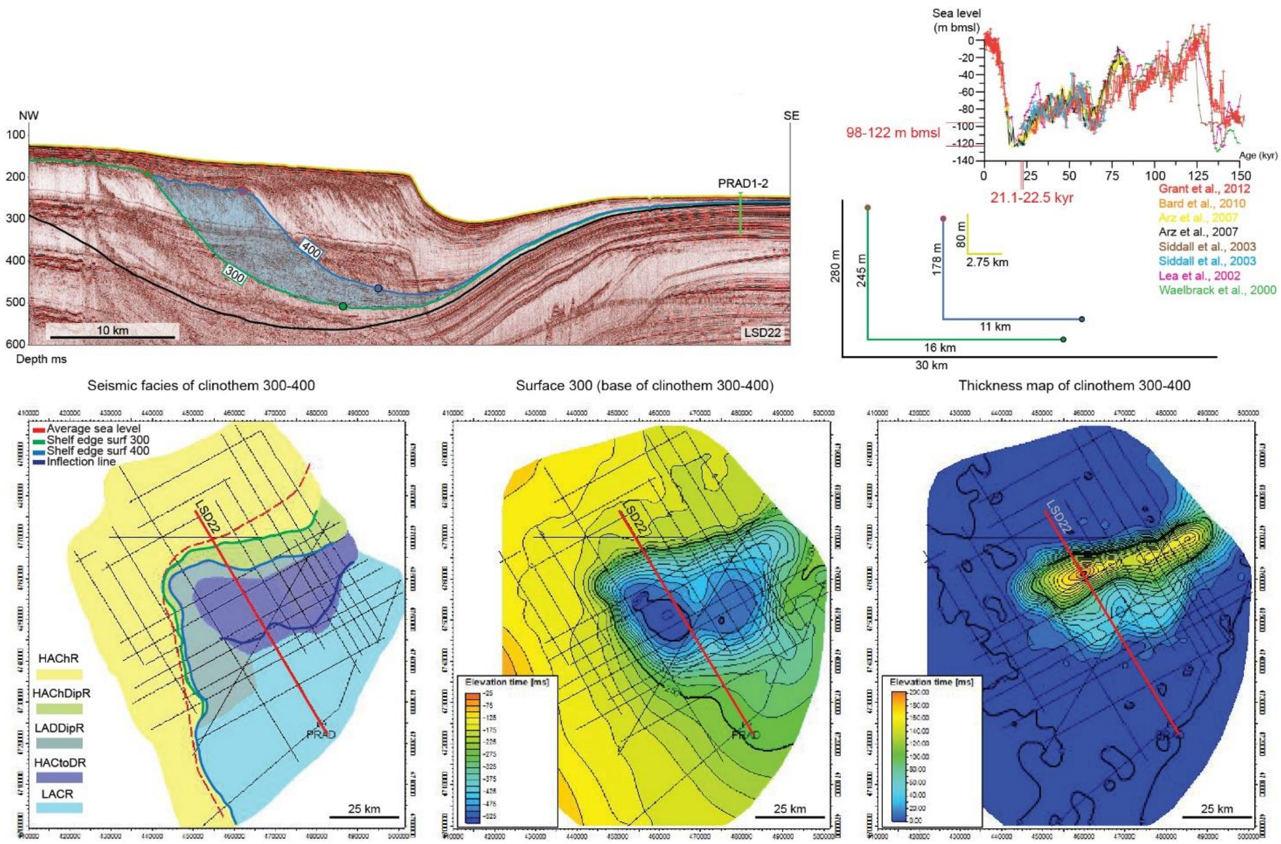

Figure 4.1. Top left: seismic line LSD22 and clinothem 300-400; note the base of the late-Pleistocene sediment wedge (black line); note the subaerial rollover points (*red dots*) and the inflection points (*black dots*) of the clinothem 300-400. Note the location of the borehole PRAD1-2. Top right: Sea level curve: note the time interval and the depth interval of the paleo-shoreline where clinothem 300-400 developed. Below the sea level curves, the geometric measures of the clinothem 300-400 are reported (the time-depth conversion considers a mean of 1600 m/s in the sediment). Bottom left: seismic facies map of clinothem 300-400 (HA=high amplitude; LA= low amplitude; Ch= chaotic; D=discontinuous; CtoD= continuous-to-discontinuous; Dip= dipping; R= reflectors); note the average position of the paleo-shoreline during the development of clinothem 300-400. Bottom central: isochronal map of surface 300 (base of clinothem 300-400); note the presence of anticline structures in the central part of basin). Bottom right: thickness map of clinothem 300-400; note the minimum value at the shelf sectors and the depocenters developed along the strike axis of the basin, where two main depocenters are observable.

Across its bottomset sector, clinothem 300-400 is characterized by high amplitude continuous-to-discontinuous reflectors (semi-continuous reflectors), while at the toe, the clinothem 300-400 shows low amplitude continuous reflectors (Fig 4.1).

The isochronal map of surface 300 shows a gently dipping shelf, a curvilinear shelf edge, a steeper slope and a pronounced uneven topography at the basin sector characterized by a regional-scale convex-down geometry interrupted by convex-up geometries denoting a buried anticline in the central sector of the basin (Fig. 4.1). The thickness map of clinothem 300-400 shows a minimum thickness in the topset region (0-10 ms) and a prevalent accumulation in the foreset sector with depocenters elongated on E-W direction. Two main depocenters are located at the western and eastern side of the anticline. The western depocenter shows its maximum thickness up to 210 ms, while the eastern depocenters attains 150 ms (Fig. 4.1).

Clinothem 300-400 shows a descending rollover point trajectory with depths of the rollover point at 155 m at surface 300 and a depth of 175 m at surface 400 (Fig. 4.1). The height of the clinothem 300-400, taken as the vertical distance between the rollover point and the inflection point at the toe of the foreset (i.e. the foreset-bottomset transition: Pirmez er al., 2008), changes from 245 m on surface 300 to 178 m on surface 400; concurrently the horizontal distances between the rollover points and the inflection points decrease from 16 to 11 km (Fig. 4.1). The maximum vertical thickness of clinothem 300-400, measured at the forest, is 150 m. Surfaces 300 and 400 are intercepted by the PRAD1-2 borehole at 10.5 and 9.5 m below sea floor (bsf), respectively. Based on the age model from the PRAD1-2 (Table 4.2) the surface 300 have an age of 22.5 cal. kyr BP and the surface 400 have an age of 21.1 cal. kyr BP.

During the deposition of clinothem 300-400 the sea level was between -98 and -122 m compared to modern and likely the feeding system was close to the MAD as suggested by the vicinity of the paleo-shoreline to the rollover points (from few tens of meters to ca. 15 km; Fig. 4.1) and the presence in the topset sector of chaotic reflectors that are interpreted as amalgamated channels (*chaotic fill* sensu Mitchum et al., 1977; (Fig. 4.1). The very low aggradation recorded in the topset sector coupled with descending trajectories of the rollover points confirms that clinothem 300-400 developed during a fall in the base level. The base level fall was governed by the global fall in the sea level (Lea et al., 2002, among others) coupled with sediment compaction (measured up to 15% in the last 400 yr in modern Po delta, Teatini et al., 2015), whereas tectonic subsidence can be considered negligible for that interval of time (Maselli et al., 2010).

Clinothem 300-400 shows a depocenter developed along the strike of the clinoform with two main depocenters on the western and eastern sides of an anticline. This evidence and the map of the surface 300 suggest that during its evolution the clinothem 300-400 conveys the structural confinement of the MAD (Fig. 4.1). Moreover, the depocenter tends to remain constricted on the northern part of the basin suggesting deposition under the influence of wave field (Fig. 4.4). The depocenters are characterized by semi-continuous high amplitude reflectors that resemble seismic facies encountered in intra-slope basins and interpreted as turbidite lobes and sheet-like turbidite (e.g. Normark et al., 1993; Gervais et al., 2006; among others). This finding implies that during the evolution of clinothem 300-400 sand was capable to bypass the shelf edge forming gravity-flow deposits at the base of the slope.

Based on the age model of table 3.2, clinothem 300-400 developed in a very short time-window of ca. 1.4 cal. kyr BP. During its deposition clinothem 300-400 reached very high accumulation rates up to 11.6 cm/yr at the foreset sector, two order of magnitude higher than 0.85 cm/yr of the modern Po Pila prodelta, and one order of magnitude higher than 1.8 cm/yr of the modern Po River subaqueous clinoform (Cattaneo et al., 2007). The very high accumulation rate may be explained by the enlargement of the catchment area of the ancestral Po River (ca. 200,000 km^2 against the modern ca. 74,000 km^2) and may reflect climate variability and increasing sediment flux during retreat phases of Apennine and Alpine glaciers (Giraudi, 2011; Florineth and Schluchter, 1998).

5) Compound clinoforms

Seaward of major deltas worldwide, modern continental margins exhibit extensive muddy clinoforms, up to several tens of meters thick (Korus and Fielding, 2015). These clinoforms typically have sediment accumulation rates exceeding 1.5 cm/yr and have been building since the mid Holocene (stratigraphically above the maximum flooding surface attained at ca. 7-5 kyr BP), when sea level reached approximately its present position (Stanley and Warne, 1994; Nittrouer et al., 1996; Asioli et al., 1996; Yi et al., 2003; Walsh et al., 2004; Amorosi et al., 2005; Liu et al., 2009; Korus and Fielding, 2015). Furthermore, such modern deltaic systems are characterized by compound clinoforms where progradation mainly takes place in two distinct areas: the coastal plain delta with a subaerial topset, and the subaqueous clinoform, composed of three geometric elements: topset, foreset and bottomset (Fig. 5.1; Nittrouer et al., 1996; Steckler, 1999). The subaqueous deltas exhibit thickness distributions that appear strongly asymmetric with respect to their parent deltas, as a function of fluvial input and basin hydrodynamics (Korus and Fielding, 2015); because the effect of oceanographic processes redistributes river-borne sediment predominantly along the shelf, such clinoforms extend hundreds of kilometers away from major deltas, as far as 1500 km as in the case of the Amazon River (Nittrouer et al., 1996).

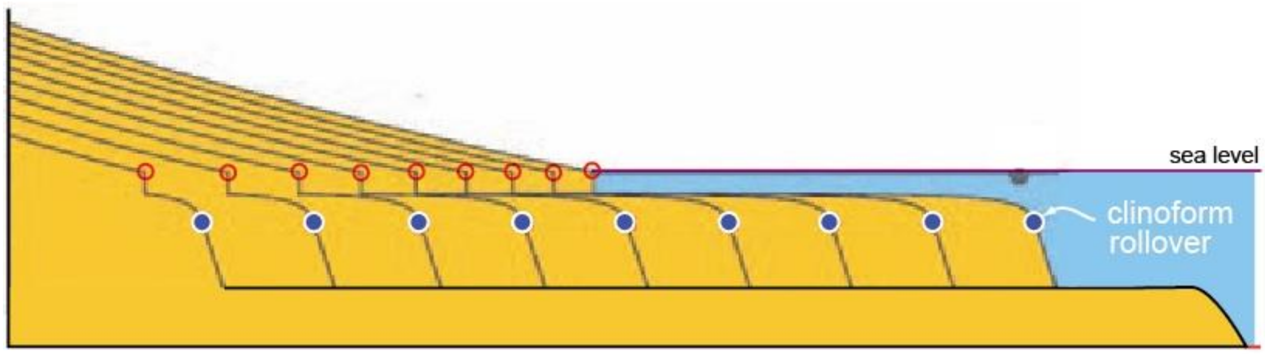

Figure 5.1: conceptual sketch for model of delta progradation and associated compound clinoform development: the shoreline rollover point (red circles) and shelf-clinoform rollover point (blue circles) are critical boundaries on continental margins (modified after Swenson et al., 2005; Nittrouer et al., 2007).

In the last few decades compound delta systems have been received many attentions from both academy and oil companies because they represent a peculiar paleo-environment archive and potential reservoir of the continental margin. Worldwide examples of compound delta systems may be found in both open continental margin settings and in semi-enclosed basins (Fig. 5.2), where subaqueous clinoforms develop tens of meter thick sediment successions with kilometric alongshore distributions: e.g., Amazon, (Kuehl et al., 1986); Eel river (Goff et al., 1999; Wheatcroft et al., 1997); Ganges-Brahmaputra (Kuehl et al., 1997); Yellow river – Shandong subaqueous clinoform (Alexander et al., 1991); Fly river (Walsh et al., 2004); Po river – Gargano subaqueous delta (Cattaneo et al., 2003); Rhone delta (Fanget et al., 2014). While subaqueous and compound deltas are increasingly recognized on modern continental margins (stratigraphically above the maximum flooding surface), their identification in the ancient rock record is hampered due to their reduced thickness and low angle of progradation that is difficult to detect at outcrop scales (typically less than 1° for muddy successions).

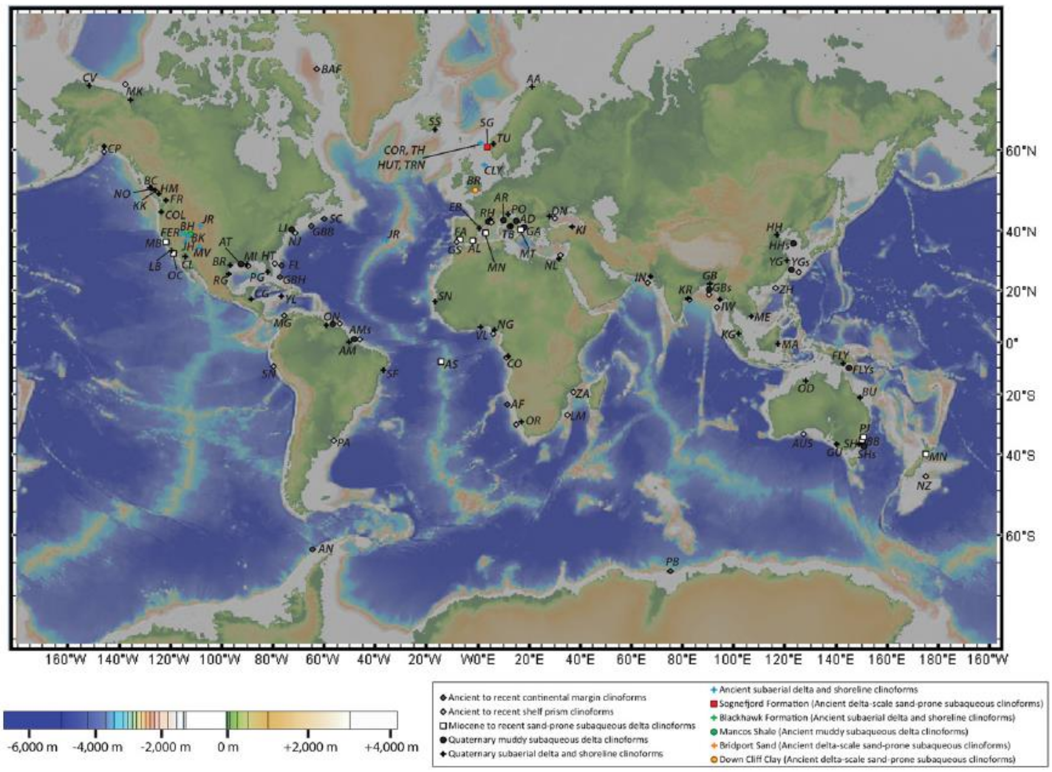

Figure 5.2: location of modern, and ancient, clinoform sets, from Patruno et al. (2015).

Earlier sequence stratigraphic models predict, during an overall seal level rise, dominant deposition on alluvial and coastal plain areas and sediment starvation conditions toward the shelf and in the basin (Posamentier et al., 1988). Conversely, among late Pleistocene to Holocene examples, a growing body of evidence suggests that thick shelf progradations may form during an overall sea level rise. Examples of this came from Mediterranean continental shelves where seaward prograding deltaic to shallow marine successions formed during the short-term Younger Dryas climatic spell (Rabineau et al., 1998; Cattaneo and Trincardi 1999; Hernandez-Molina et al., 2000; Lobo et al., 2001; Aksu et al., 2002; Labaune et al., 2005, Berné et al., 2007; Jouet et al., 2006; Sømme et al., 2011).

The aim of the next manuscript is to understand if oceanographic condition similar to the modern one was already active in the Adriatic Sea promoting the development of a compound progradation. The stratigraphic record presented here shows, for the first time, the documentation of a well-preserved compound delta formed offshore the Gargano Promontory, offering the opportunity to characterize both coastal and subaqueous deposits developed during the Younger Dryas. The main goal in studying the Gargano compound delta can be summarized in three points: 1. Propose the possibility of a compound delta forming in a rapidly developed TST record to be used to re-evaluate cases of possible compound deltas recognized in outcrop or seismic surveys from ancient geological records; 2. Document a case of formation of a compound delta that encompasses even a shorter time than in the modern "high-stand" best-documented cases worldwide; 3. Infer the balance between oceanographic redistribution of fine-grained sediment and short-term climate-driven supply fluctuations from mainland.

5.1) Manuscript III

"Anatomy of a compound delta from the post-glacial transgressive record in the Adriatic Sea"

Authors: Claudio Pellegrini (Istituto di Scienze Marine, ISMAR-CNR, Università di Bologna, Dipartimento di Scienze della Terra e Geologico-Ambientali, Bologna, Italy)

Vittorio Maselli (Istituto di Scienze Marine, ISMAR-CNR, Bologna, Italy)

Antonio Cattaneo (Insitu Français de Recherche de la Mer, Ifremer, Brest, France)

Andrea Piva (Eni, Exploration and Production Division, S. Donato Milanese, Italy)

Alessandro Ceregato (Istituto di Scienze Marine, ISMAR-CNR, Bologna, Italy)

Fabio Trincardi (Istituto di Scienze Marine, ISMAR-CNR, Bologna, Italy)

Status: Published in *Marine Geology*, edited by M. Rebesco volume 362, pages 43-59, doi:10.1016/j.margeo.2015.01.010.

Marine Geology 362 (2015) 43–59

Contents lists available at ScienceDirect

Marine Geology

journal homepage: www.elsevier.com/locate/margeo

Anatomy of a compound delta from the post-glacial transgressive record in the Adriatic Sea

Claudio Pellegrini [a,b,*], Vittorio Maselli [a], Antonio Cattaneo [c], Andrea Piva [d], Alessandro Ceregato [a], Fabio Trincardi [a]

[a] ISMAR (CNR), v. Gobetti 101, 40129 Bologna, Italy
[b] University of Bologna, Dipartimento di Scienze della Terra e Geologico-Ambientali, Piazza di Porta San Donato 1, 40126 Bologna, Italy
[c] IFREMER, Géosciences Marines Centre de Brest, BP70, 29280 Plouzané, France
[d] Eni, Exploration and Production Division, Sedimentology, Petrography & Stratigraphy Dpt., 20097 S. Donato Milanese, Italy

ARTICLE INFO

Article history:
Received 4 July 2014
Received in revised form 21 January 2015
Accepted 25 January 2015
Available online 28 January 2015

Keywords:
Compound delta
Mediterranean Sea
Younger Dryas
Subaqueous clinoform
Transgressive deposits

ABSTRACT

On the Mediterranean continental shelves the post-glacial transgressive succession is a complex picture composed of seaward progradations, related to sea level stillstands and/or increased sediment supply to the coasts, and minor flooding surfaces, associated with phases of enhanced rates of sea level rise. Among Late Pleistocene examples, major mid-shelf progradations have been related to the short-term climatic reversal of the Younger Dryas event, a period during which the combination of increased sediment supply from rivers and reduced rates of sea level rise promoted the formation of progradations up to tens-meter thick. While the documentation of coastal and subaqueous progradations recording the Younger Dryas interval is widely reported in literature, the model of compound progradation within transgressive deposits has not yet been proposed. Here we present the documentation of a deltaic system where both delta front sands and related fine-grained subaqueous progradations (prodeltaic to shallow marine) have been preserved. The Paleo Gargano Compound Delta (PGCD) formed offshore the modern Gargano Promontory (southern Adriatic Sea), and is composed of a coastal coarse-grained delta of reduced thickness and a muddy subaqueous clinoform, up to 30 m thick. The PGCD, probably the first worldwide documentation of a compound delta within the transgressive record, provides the opportunity to investigate the processes controlling the formation of a compound delta system during an overall sea level rise and the factors that allowed its preservation. The finding of the PGCD provides the opportunity for a comparison with modern worldwide compound systems.

1. Introduction

Modern and ancient river deltas represent one of the most intriguing sedimentary archives in the geological record, as their internal geometry and evolution reflects the interplay between river dynamics, sediment availability, grain size distribution and the oceanographic regime of the receiving basin (Orton and Reading, 1993; Cross et al., 1993; Trincardi et al., 2004; Slingerland et al., 2008). After the first process-driven classification of Wrigth and Coleman (1972), and Galloway (1975), another important step in understanding delta dynamics was introduced with the concept of compound deltas (Swenson et al., 2005), i.e., deltas composed by shallow-water progradations that are genetically related to deeper subaqueous clinothemes. The transition in grain-size, mostly related to the oceanographic regime of the basin, is also reflected by the overall geometry, characterized by two main roll-over points (i.e., breaking in slope at the topset/foreset transition; Swenson et al., 2005; Cattaneo et al., 2007; Walsh and Nittrouer, 2009). The depth of the subaqueous rollover point is assumed to reflect the seaward limit beyond which wave-current shear stress decreases allowing sediment deposition (e.g., Nittrouer et al., 1986; Kuehl et al., 1986; Alexander et al., 1991; Pirmez et al., 1998; Walsh et al., 2004).

Along the western Adriatic basin, the modern highstand deposits are organized in shelf-wide progradations that locally show variations in the stratal geometry; from North to South on bidimensional profiles it is possible to identify: 1) a single rollover point, where the delta front and the prodelta are "attached" (Fig. 1 section A–A′); 2) two rollover points (coastal and subaqueous rollover point), where the delta front and the prodelta are separated, and their distance is governed by the oceanographic regime (Fig. 1 section B–B′, the 2D compound delta); 3) a single subaqueous rollover point where the subaqueous delta disconnected from the delta front (Fig. 1 section C–C′, purely subaqueous delta). In a section parallel to the modern shoreline from the modern Po River delta down to the Gargano Promontory, the Adriatic subaqueous clinoform has been interpreted as a "distorted" compound system (Fig. 1 section D–D′; Cattaneo et al., 2007).

The understanding of the physiographic parameters of the compound system is crucial to explaining the main processes and physical

* Corresponding author at: ISMAR (CNR), v. Gobetti 101, 40129 Bologna, Italy.
E-mail address: claudio.pellegrini@bo.ismar.cnr.it (C. Pellegrini).

http://dx.doi.org/10.1016/j.margeo.2015.01.010

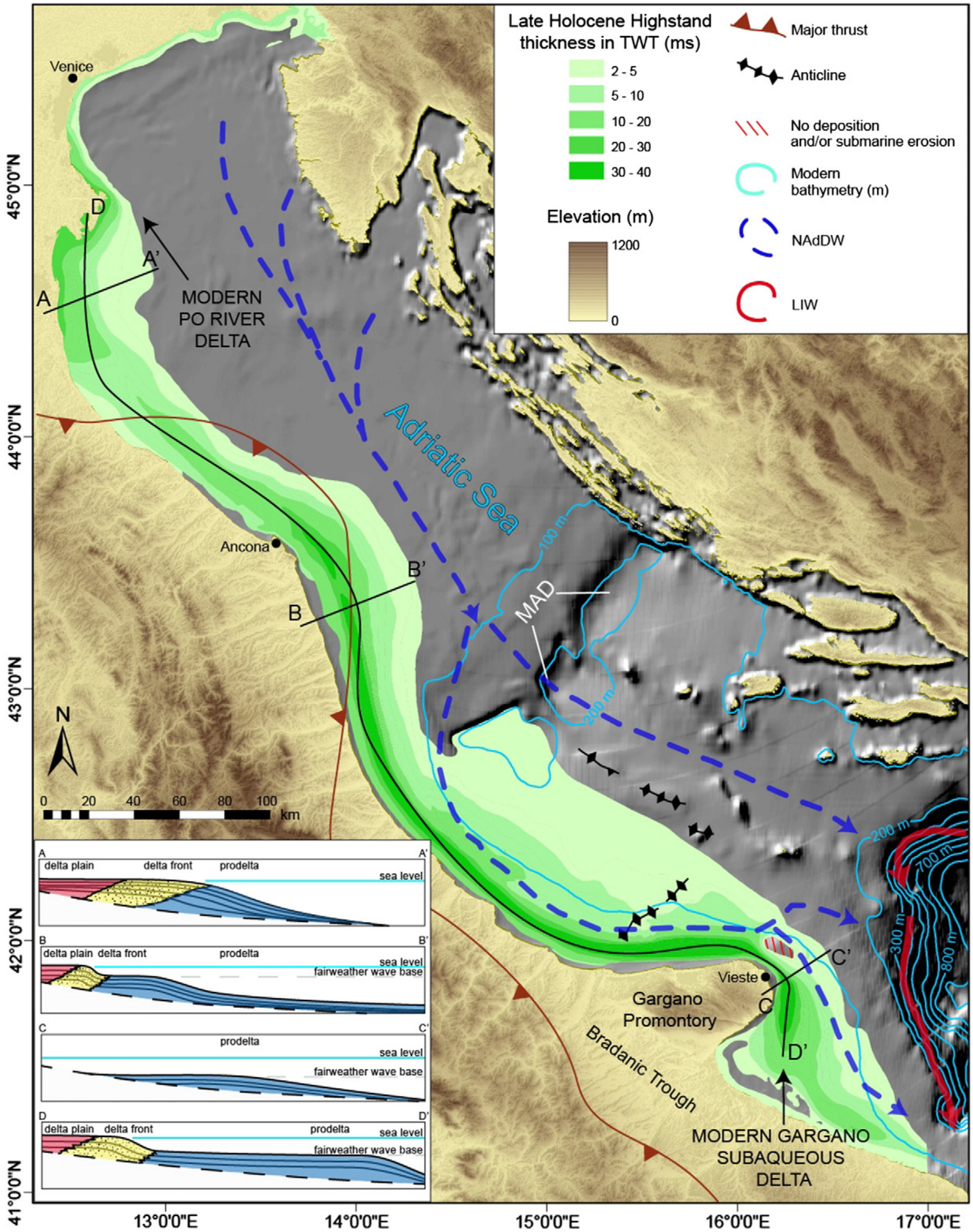

Fig. 1. Thickness distribution of the Late-Holocene HST wedge (from Correggiari et al., 2001; Cattaneo et al., 2007). Note the area of no deposition NE of Gargano Promontory. The bathymetry of the Adriatic is from Trincardi et al. (2013) and is shown with a 100 m contour on a DTM. The pathways of the NAdDW and LIW currents are highlighted by a blue dashed line and a dark red line, respectively. Bottom left: schematic stratigraphic sections illustrating the difference in delta configurations seaward of the Italian coast.

laws that govern a couplet progradation (Patruno et al., 2015). Steckler et al. (1999) noticed that a subaqueous clinoform may prograde simultaneously with the costal delta system depending on the oceanographic regime of the receiving basin; Swenson et al. (2005) highlighted that such genetically-connected clinoforms (coastal and subaqueous) may be geometrically disconnected depending on fair-weather and storm wave bases (10/15 m to 30 m water depth, respectively; Cattaneo et al., 2003) exhibiting a dominantly along-shore thickness distribution and a typical convex seaward morphology (Cattaneo et al., 2003). Examples of compound delta systems may be found in both open ocean settings and enclosed basins: e.g., Amazon River, (Nittrouer et al., 1996); Ganges–Brahmaputra River (Goodbred and Kuehl, 2000); Yellow River — Shandong subaqueous clinoform (Liu et al., 2004); and Po River — Gargano subaqueous delta (Cattaneo et al., 2003). Furthermore, many authors focused on the subaqueous clinoforms that constitute tens of meter thick sediment successions with kilometric alongshore distributions far from the main Rivers: e.g.; Ganges–Brahmaputra Rivers subaqueous delta (Kuehl et al., 1997; Palamenghi et al., 2011); Fly, Kikori and Purari Rivers (Walsh et al., 2004); Yellow River subaqueous delta (Yang and Liu, 2007); Mekong River subaqueous delta (Xue et al., 2010); Rhone River subaqueous delta (Fanget et al., 2014). While compound and subaqueous deltas are increasingly recognized on modern continental margins, their identification in ancient sedimentary records is more difficult, mainly for two reasons: the difficulty in pinpointing the position of the feeder system and the poor geometric resolution in depicting the low angle of muddy subaqueous progradations (Mellere et al., 2002; Morris et al., 2006; Hampson, 2010).

The aim of this paper is to document a compound delta system (the Paleo Gargano Compound Delta, PGCD), formed during the post-glacial sea level rise, offshore the Gargano Promontory in the South Adriatic continental shelf. This study provides the opportunity to investigate the conditions that led to the formation and preservation of a complex deltaic system during a period of overall sea level rise and to develop new concepts for the study of ancient sedimentary archives. Among Late Pleistocene to Holocene examples, a growing body of evidence suggests that mid-shelf progradational deposits of variable thickness developed during the overall last post-glacial sea level rise (Fig. 2; Cattaneo and Trincardi, 1999; Hernández-Molina et al., 1994; Aksu et al., 2002; Labaune et al., 2005; Berné et al., 2007; Maselli et al., 2011; Sømme et al., 2011) although no documentation of compound deltas has been proposed so far in these contexts.

2. Background

2.1. Geological setting

The Gargano Promontory peaks at 1050 m above sea level and has constituted a morphologic relief since the Middle Pliocene (Bertotti et al., 1999). The outcropping stratigraphic succession consists of Mesozoic carbonate rocks and includes four main lithostratigraphic units: the Maiolica Formation (Fm), the Marna a Fucoidi Fm, the Scaglia Fm and the Peschici Fm, characterized by thin- to thick-bedded lime mudstone, with Calcarenite and Breccia intervals (Eberli et al., 1993). The same lithology extends offshore the Gargano Promontory to form the Gargano Structural High (GSH) of the study area: a shallow plateau in ca. 50 m of modern water depth with steep flanks to the North and to the East (Fig. 1). The GSH represents an area of no or reduced sediment deposition during the modern highstand (Fig. 1; Cattaneo et al., 2003), where carbonate related karst features are exposed on the sea floor (Taviani et al., 2012).

2.2. Modern hydrology of the Adriatic Sea and sedimentation patterns

The oceanographic circulation of the Adriatic Sea is dominated by three main elements (Artegiani et al., 1997a,b): 1- a superficial cyclonic gyre with a component that flows parallel to the western Adriatic shoreline, mainly generated by the wind pattern; 2- the Levantine Intermediate Water (LIW), a salty water that forms in the Eastern Mediterranean Sea (Levantine Basin) and intrudes in the Adriatic basin flowing at depths of 200–600 m (Lascaratos, 1993); and 3- the North Adriatic Dense Water (NAdDW), that forms in the northern Adriatic through winter cooling (Vilibich and Supich, 2005; Benetazzo et al., 2014) and then, once a density threshold is reached, flows southward until cascading toward the deep southern Adriatic Basin (Trincardi et al., 2007; Canals et al., 2009). The overall thermohaline circulation, under the Coriolis apparent force, runs along the Italian coast constraining the main sediment flux to deposit in a prism parallel to the Apennine coast (Fig. 1; Correggiari et al., 2001; Cattaneo et al., 2003).

2.3. Stratigraphic setting of Adriatic TST deposits

In the Adriatic basin the Late Pleistocene–Holocene transgressive units comprise backstepping barrier lagoon deposits with large reworked sand dunes, in the northern low-gradient shelf (Trincardi et al., 1994; Correggiari et al., 1996), and subaqueous progradational deposits, in the western Adriatic shelf and in the Mid Adriatic Deep (MAD, Trincardi et al., 1996; Cattaneo and Trincardi, 1999; Maselli et al., 2011), where continuous chronological controls are available (Asioli, 1996; Blockley et al., 2004; Lowe et al., 2007). The transgressive systems tract (TST) is floored by an unconformity of regional extent (lowstand unconformity ES1) and topped by the maximum flooding surface (mfs).

On the central Adriatic shelf, the TST unit records the impact of sea level and sediment supply fluctuations on sub-millennial scales resulting in a tripartite TST (Cattaneo and Trincardi, 1999; Maselli et al., 2011). The lower and upper TST units (lTST and uTST unit, respectively) record an abrupt landward shift of the shoreline, while the middle unit (mTST unit) is prograding seaward and represents a regressive sedimentary body within the TST (Cattaneo and Trincardi, 1999). The three TST units are separated by two prominent, and extensively erosional, surfaces (S1 and S2 surface, Cattaneo and Trincardi, 1999;

Fig. 2. Map of Mediterranean examples of transgressive (stars; Hernández-Molina et al., 1994; Jouet et al., 2006; Sømme et al., 2011; Chiocci et al., 1991; Lykousis et al., 2005; Aksu et al., 2002; Giosan et al., 2009; Lericolais et al., 2010; Schattner et al., 2010; Zecchin et al., 2011; Durán et al., 2013) and highstand clinothemes (green patches; Díaz and Ercilla, 1993; Lobo et al., 2006; Fanget et al., 2014; Cattaneo et al., 2007; Hiscott et al., 2002; Giosan et al., 2013).

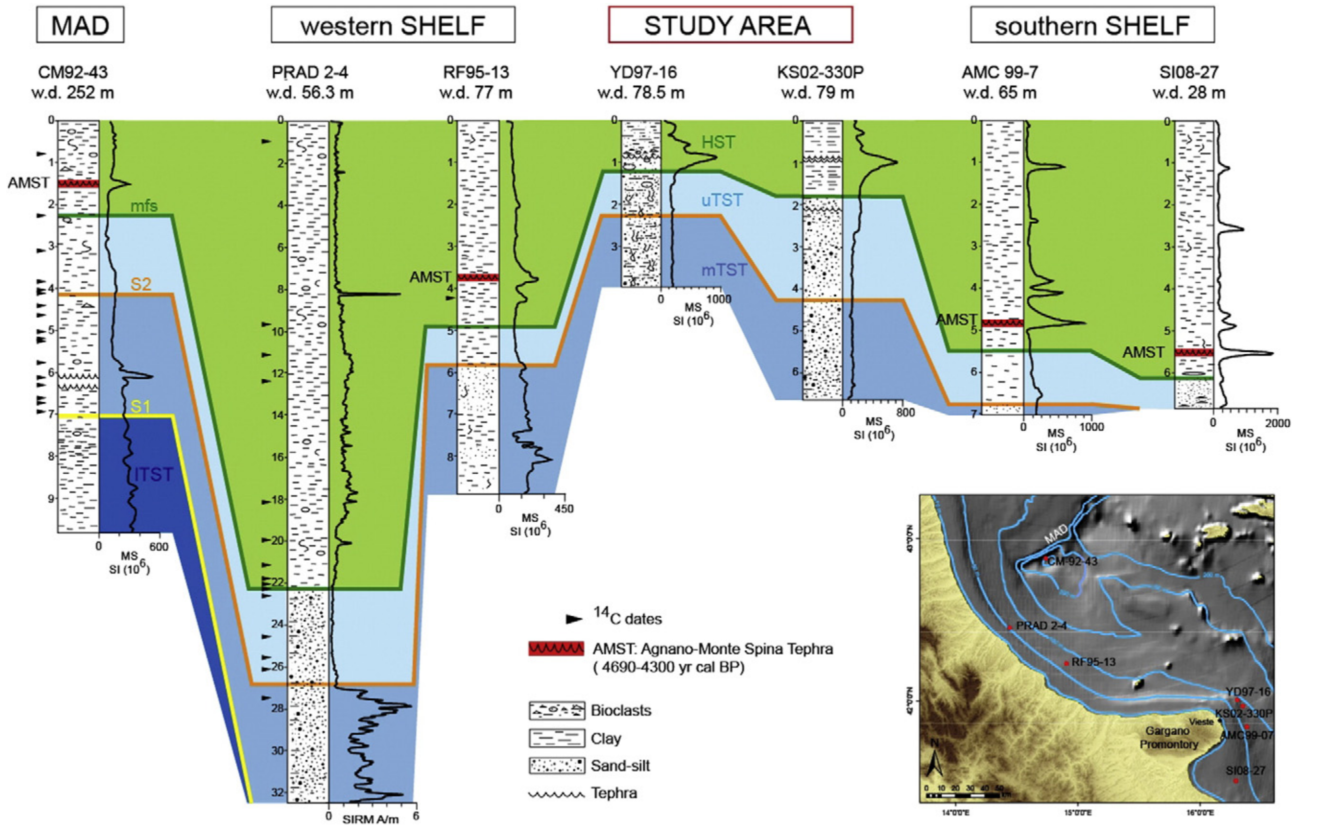

Fig. 3. Along shelf correlation of the TST and HST deposits. The mTST unit is completely sampled in the MAD (core CM92-43). In the inner shelf the mTST expands into a thick section, that is partially sampled by borehole PRAD 2–4. The transition from the uTST to the mTST units is marked by an abrupt change in the saturation isothermal remnant magnetization SIRM, due to the transition from fine to coarse-grained sediments (Vigliotti et al., 2008). In deeper environments, the top of the unit is sampled by cores RF95-13, YD9716 and KS02-330P (study area), and AMC99-7. High-resolution chronostratigraphic correlation, obtained by ^{14}C dates and tephra chronologies, support the hypothesis that the mTST unit deposited before the Meltwater Pulse 1B (Asioli, 1996). The vertical scale of the PRAD 2–4 is double.

Maselli et al., 2011; see Fig. 3 and Table 1 for a summary of the main stratigraphic surfaces and depositional units within the Late Pleistocene-Holocene TST record). In particular, the mTST unit is characterized by two sub-units (mTST-1 and mTST-2 sub-units) separated by an erosional surface (Si) that, possibly, records a minor sea level fall during the Younger Dryas interval (Maselli et al., 2011). The mTST-1 unit records the Bölling–Allerød interval, while the mTST-2 unit progrades during the Younger Dryas interval (Maselli et al., 2011).

From the central Adriatic to the southern Adriatic shelf the lTST and mTST units are organized in depocenters which reflect the interaction between sediment distribution, oceanographic processes and sea floor morphology. In particular, the Gargano Promontory is characterized by an articulated slope morphology and approaching the GSH the low TST and the mTST-1 units tend to diminishing in thickness and disappear, locally.

3. Data and methods

The database is composed by a dense network of high-resolution chirp-sonar profiles (acquired with a 16-transducer hull-mounted Benthos sound source), and sediment cores (both piston and gravity corers) acquired during the last decades by ISMAR-CNR with R/V URANIA (Cruises YD97, AMC99, CSS00, COS01, KS02 and SA03). The seismic profiles analyzed in the study area offshore Gargano Promontory sum to a total length of 1300 km over an area of 3200 km^2, with an average spacing between the lines of 2.5 km. A D-GPS allowed accurate positioning of the profiles and sediment cores.

Chirp profiles are imaged with a metric vertical scale assuming a 1500 m/s propagation sound velocity within sediment. By using a total length of 1300 km of seismic profiles, we constructed the structural map of the ES1 surface (the sequence boundary above which the transgressive record developed, Fig. 4), and the isopach maps of the main stratigraphic units composing the post-glacial stratigraphy offshore the GSH. The maps are stored in a GIS and projected in UTM with a WGS84 datum. In the lack of more precise velocity analyses on the sediments, volumes are quantified by assuming a constant 1500 m/s propagation sound velocity through superficial sediment.

Piston cores YD97-16 and KS02-330P were recovered on the GSH flank in 78.5 m and 79 m water depth using a 10 m barrel. The penetration of the corer was 7 m in the first site, and 11 m in the second, with a core recovery of 3.91 m and 6.6 m, for a total recovery of 70% in both cases. Both cores were sampled every 10 cm; core KS02-330P for grain size analysis and both cores for lithological and paleo-environmental reconstructions based on micro and macro faunal assemblages. Calcimetry and grain size analyses were performed at Ifremer; the sampled fractions were disaggregated with a Retsch MM200 mixer mill at 17 cycles per second for 4 min. The $CaCO_3$ content was measured with an automatic pressure calcimeter (Dream Electronique model 2.1) while grain size analyses were made using a Coulter LS200 laser microgranulometer. Radiographies of the lowermost 3 m of core KS02-330P allow detection of bottom-current structures.

The correlation between cores and seismic profiles is performed after decompacting the total recovery versus the total penetration by assuming a linear compaction (the compaction is given by the ratio between the total penetration and the total core length). Correlation

Table 1
Synthesis tables of seismic units, surfaces and their interpretation proposed by Cattaneo and Trincardi (1999), Trincardi and Correggiari (2000), Maselli et al. (2011).

Seismic surface/ age (yr BP)	Seismic unit and subunit	Corresponding sediment core depth (m bsf)	Description	Paleo-environment interpretation and sea level variation	Graphic sketch LAND SEA
	HST	YD97-16 0-1.20 KS02-330P 0-1.70	Prograding unit of the modern Po delta system and Gargano subaqueous muddy clinoform	Shelf-slope	
Mfs (ca.5500)		YD97-16 1.20 KS02-330P 1.70	Maximum flooding surface	Maximum adriatic sea ingression	
	uTST	YD97-16 1.20-2.20 KS02-330P 1.70-4.20	Mud drape unit characterized by marine-onlap terminations onto preexisting sea floor structures	Outershelf-upper slope	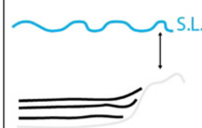
S2 (ca. 11300)		YD97-16 2.20 KS02-330P 4.20	Regional erosional surface	MWP-IB	
	mTST-2	YD97-16 2.20-3.91 KS02-330P 4.20-6.60	High-angle prograding unit	Inner-shelf (less than 30m water depth)	
Si (12200-12800)		YD97-16 No recorded KS02-330P No recorded	Localerosional surface	Possiblesea level fall during the YD interval	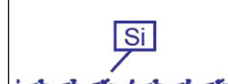
	mTST-1	YD97-16 No recorded KS02-330P No recorded	Very low-angle prograding unit	Inner-shelf(melting of Alpine and Apennine glaciers; increased sediment delivery)	
S1 (ca. 14800)		YD97-16 No recorded KS02-330P No recorded	Regional erosional surface	MWP-IA	
	lTST	YD97-16 No recorded KS02-330P No recorded	Prograding unit with shingled reflectors	Early phases of the last sea level rise; influenced by fresh water input	
ES1 (ca.18000)		YD97-16 Not reached KS02-330P Not reached	Regional erosional surface	Lowstand subaerial exposure (Sequence Boundary)	

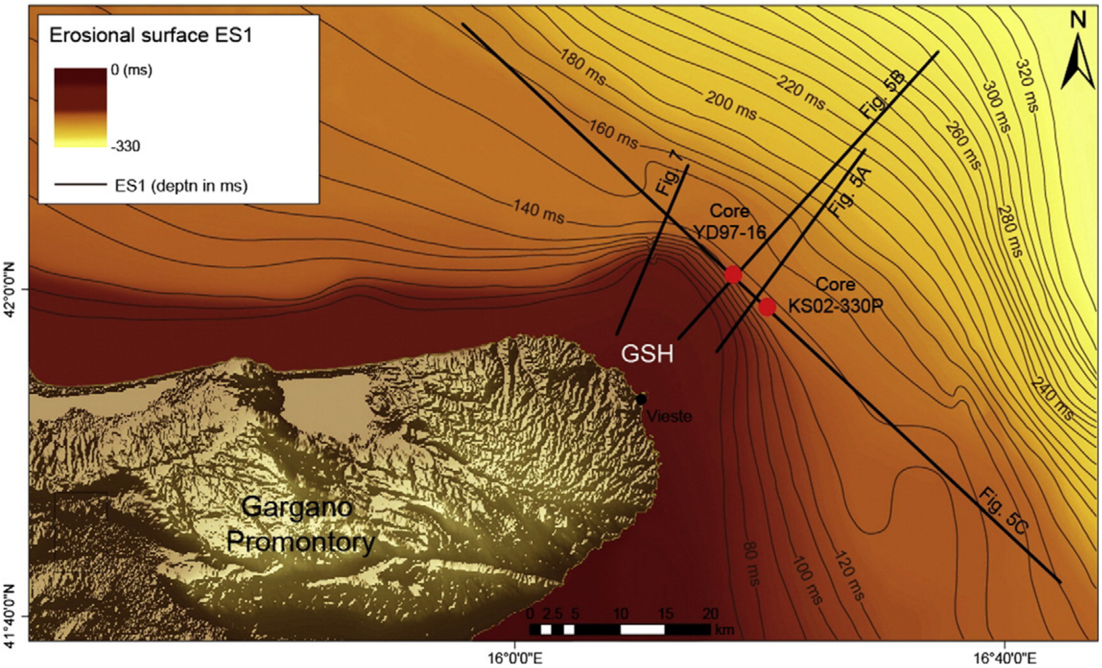

Fig. 4. Digital Elevation Model (DEM, SRTM 90 m, from http://srtm.csi.cgiar.org) and structural map of the ES1 erosional surface at the base of the post-glacial TST record (grid 100 × 100 m), with contours every 10 ms. The Gargano Structural High (GSH) represents the drowned part of the Gargano Promontory. The map shows also the location of the seismic lines and cores discussed in this paper.

among YD97-16 and KS02-330P cores relied on wiggle matching of the magnetic susceptibility logs.

4. Results

4.1. The middle TST unit offshore the Gargano Promontory

Offshore Gargano Promontory a prominent erosional surface (ES1), characterized on seismic profiles by a continuous and high amplitude seismic reflector, formed during the last glacial sea level lowstand, when the shelf underwent subaerial exposure, as highlighted for the northern and central Adriatic shelf by Trincardi and Correggiari (2000) and Ridente and Trincardi (2002). On the steep flanks of the GSH the lTST unit and the mTST-1 unit are not recorded and consequently the ES1 coincides with the S1 and Si surfaces (ES1 ≡ S1 ≡ Si, Fig. 5A, B, C). Locally, the recognition of ES1 surface is hampered by the occurrence of biogenic gas in the upper TST deposits (Fig. 5A, B).

In this setting the mTST unit is confined between surface ES1 (below) and surface S2 (above), the latter corresponding to a high amplitude reflector of regional extent (Fig. 5A, B). In the proximal area of GSH the coastal deposits of the mTST unit show seismic facies with opaque discontinuous reflectors characterized by local and small scale steep reflectors (Fig. 5B). The seismic pattern of the costal deposits shows high-angle foresets with a pronounced costal rollover point at ca. 60 m bsl (below sea level; Fig. 5A, B). The transition area between coastal and subaqueous deposit of the mTST unit is characterized by discontinuous reflectors in part due to the presence of gas charged sediment (Fig. 5A, B). In the area seaward of the GSH the subaqueous deposits of the mTST unit are characterized by complex sigmoid-oblique seismic pattern reflector (sensu Mitchum et al., 1977; Fig. 5A, B). Within this subaqueous progradational deposits the subaqueous rollover point is detected at an average water depth of 90 m bsl (Fig. 5A, B, C). The subaqueous rollover point shows an ascending trajectory that may suggest the onset of a relative sea level rise (Fig. 5A, B; Helland-Hansen and Hampson, 2009).

The mTST unit develops in the proximal area and seaward of GSH over an area of 5×10^5 km^2 and with a total volume of about 4.6 km^3. This unit reaches a maximum thickness of up to ca. 30 m close to the GSH, where a bidirectional progradation develops (Fig. 5C), and then becomes thinner and spread over a broader area further to the south (Fig. 6). The bidirectional downlap is accompanied by an asymmetric internal geometry with steeper foresets (up to 2.2°), and a reduced seaward progradation toward the NW and gentler foresets (0.7°), with a greater seaward progradation toward the SE. Furthermore, the direction of progradation within the clinothemes (sensu Slingerland et al., 2008), determined from apparent angles measured along perpendicular profiles, is parallel to the coast. Interestingly, the mTST unit partly developed in the area where no HST units develop and presents two features indicative of highly energetic environments: a karst zone submerged about 12.500 years ago (Taviani et al., 2012), and a wave-cut terrace lie in the upper slope of the GSH at a modern water depth of about −55 m bsf (detail in Fig. 7).

In the YD97-16 and KS-330P sediment cores the mTST unit, below 2.20 m downcore and below 4.20 m downcore, respectively, is composed by fine to medium poorly-sorted sand (Fig. 8). The benthic assemblage shows the occurrence of species tolerating a high content of organic matter, i.e., *Stainforthia complanata*, *Melonis padanum*, *Bulimina marginata*, and *Globobulimina spinescens*, in addition to the inner shelf benthic species of *Ammonia* and *Elphidium* genera and miliolids, possibly indicating enhanced dysoxic conditions at the sea floor. The mTST unit is characterized by very few planktonic foraminifera typical of cold climate conditions (e.g., *Neogloboquadrina pachyderma*, *Globigerina bulloides*, *Turborotalita quinqueloba*). The discontinuous occurrence of opportunistic species like *Valvulineria complanata* and *Nonionella turgida*, coupled with episodes of dysoxic conditions, could either highlight an open mud-belt setting, characterized by a substantial content of organic matter and by reductive conditions at the sea floor, or be a consequence of repeated depositional events linked to river floods. The overall assemblage suggests that deposition occurred in an inner shelf environment. X-ray analysis highlights the pronounced cross

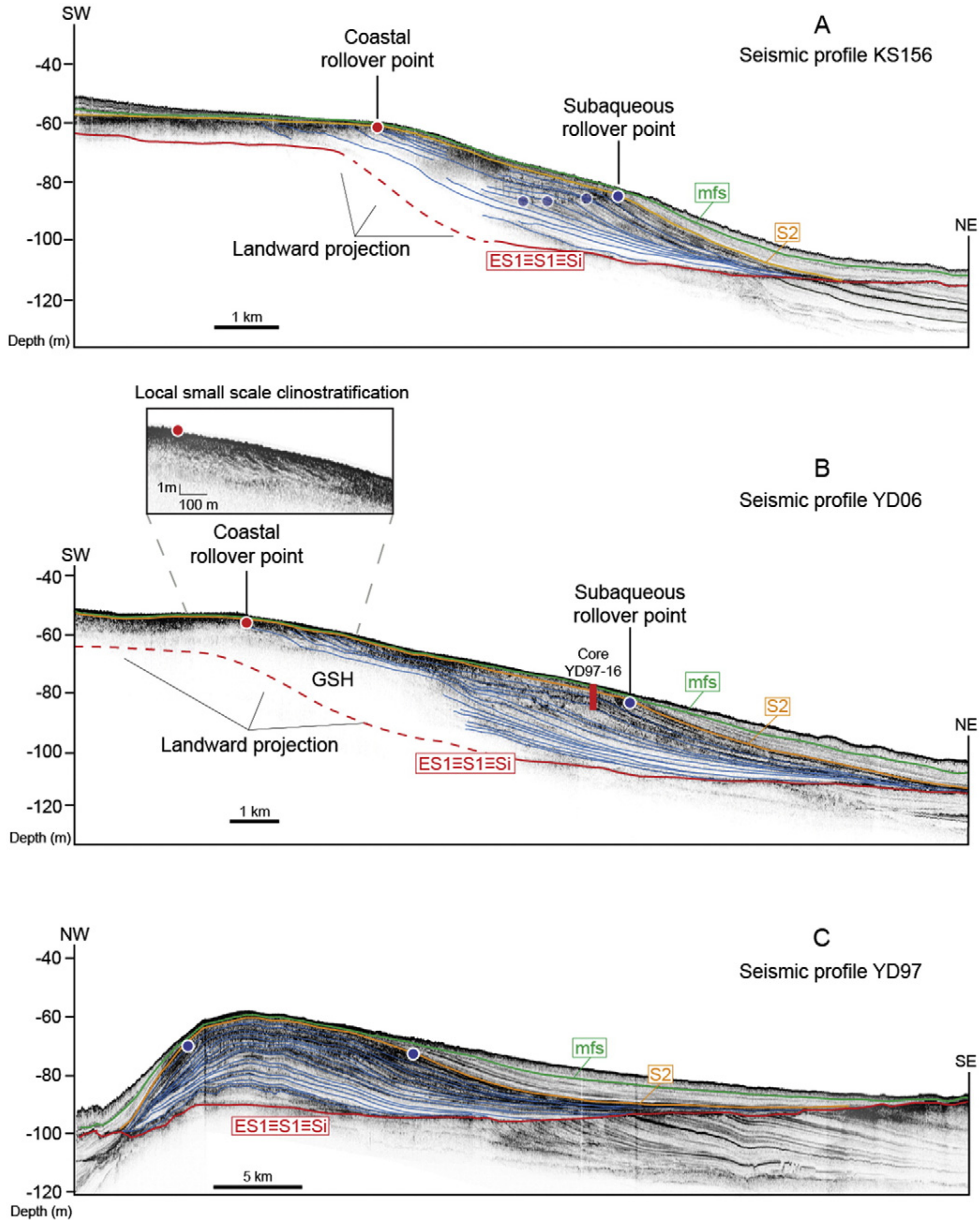

Fig. 5. Seismic profiles (see Fig. 3 for location), showing the internal subdivision of the transgressive deposits atop and seaward the GSH, between ES1 and S2 surfaces. Top: seismic profile KS156 (A) across the GSH showing the correlation between the subaerial clinotheme and its subaqueous counterpart. Note the ascending trajectory of the subaqueous rollover point. Center: seismic profile YD06 (B) showing the correlation between the subaerial and subaqueous delta and the position of core YD97-16. Note local small scale subaerial clinostratifications of the coastal deposits within mTST unit. Bottom: seismic profile YD57 (C), seaward the GSH, illustrating the bidirectional downlap of the subaqueous delta that constitutes the marine component of the compound delta; note that the steepness of the clinothemes is higher to the North (up-current) and gentler to the South (down-current) where the deposit becomes thicker and more spread across shelf. Coastal and subaqueous rollover points are highlighted by red and blue dots, respectively. Note the possible presence of gas-charged sediments in the GSH area. Note the ascending trajectory of the subaqueous rollover point (transparent blue dots).

lamination possibly reflecting the influence of tractive bottom currents (see detail in Fig. 8) and high sediment accumulation rates (Rhoads et al., 1985; Kuehl et al., 1986).

4.2. The upper TST unit offshore the Gargano Promontory

The uTST unit is confined by surface S2, at the base, and the maximum flooding surface, on top. In the central Adriatic Sea, the uTST unit is a mud drape characterized by marine-onlap terminations onto pre-existing morphological structures (Cattaneo and Trincardi, 1999; Maselli et al., 2011). Offshore the GSH, the uTST unit shows subparallel and low-angle continuous reflectors with a progradational stacking pattern (Fig. 5A, B, C and detail in Fig. 7). The maximum flooding surface at the top of the uTST unit constitutes a prominent and continuous regional surface above which the highstand system tract develops (Fig. 5A, C and detail in Fig. 7). The maximum flooding surface displays an erosional character in the area close to the GSH, where the uTST unit shows a toplap termination (Fig. 5A, C). This evidence is indicative of a strong interaction between coast parallel currents and the pre-existing topography, resulting in an area of no deposition and or submarine erosion of the uTST unit (Fig. 7).

The thickness distribution of the uTST defines distinct depocenters separated from each other (Fig. 7). In the north-eastern portion of the GSH an area of no deposition or submarine erosion is evidenced by

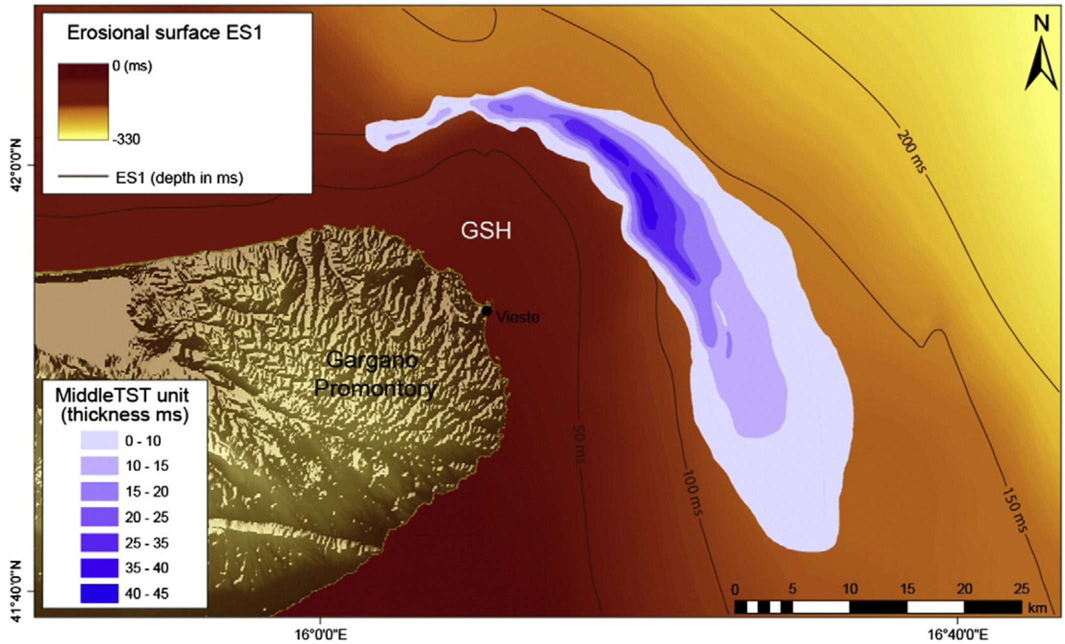

Fig. 6. Thickness distribution of mTST unit. The mTST unit (more than 40 ms in thickness in two-way time offshore Vieste) is elongated parallel to the depth contour of the underlying ES1 surface.

the lack of the uTST unit. Because of the presence of this bypass area the uTST unit shows a detached geometry separated by the edge of the GSH (Fig. 7). The uTST unit advances mainly in southward direction, where the GSH is less prominent, showing a depocenter elongated in a N–S direction reaching ca. 21 m of thickness (Fig. 7). At regional scale the uTST depocenter marks a landward migration of the depositional area with respect to the underlying mTST unit, indicating a possible jump of the relative sea level (Fig. 7).

In the YD97-16 and KS-330P sediment cores the uTST unit, between 1.20–2.20 m and 1.70–4.20 m, respectively, consists of fine to medium

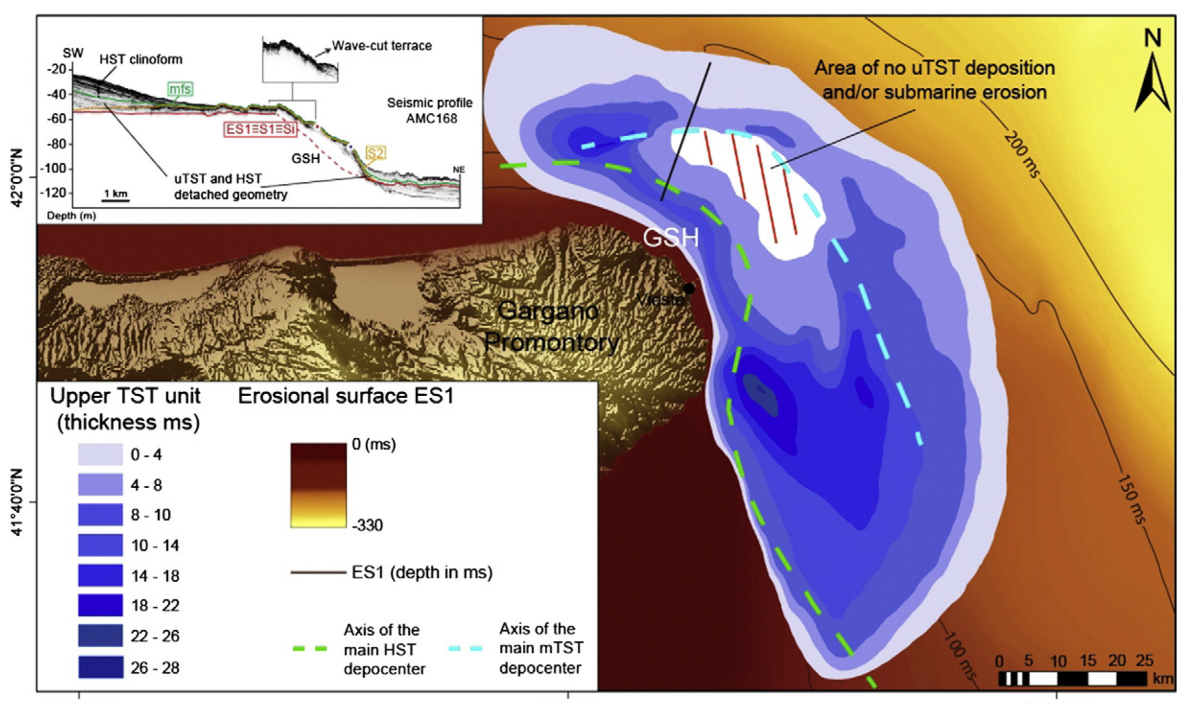

Fig. 7. Map of the shore-parallel uTST wedge (in ms two-way travel time). The dashed lines represent the main axis along which the depocenters of the mTST and HST around the Gargano Promontory. Note the landward shift of the depocenters main axes from the mTST unit (dashed blue line, offshore) passing by the uTST unit (darkest blue) to the HST unit (dashed green line, inshore). The area characterized by no deposition NE of Vieste is in the same position of the modern one (see Fig. 1). A simplified bathymetric contour of the lowstand unconformity ES1 is provided for reference. Inset: seismic profile AMC168 investigated an area adjacent to the GSH where the mTST unit is less developed, and the uTST and HST units did not form or were eroded.

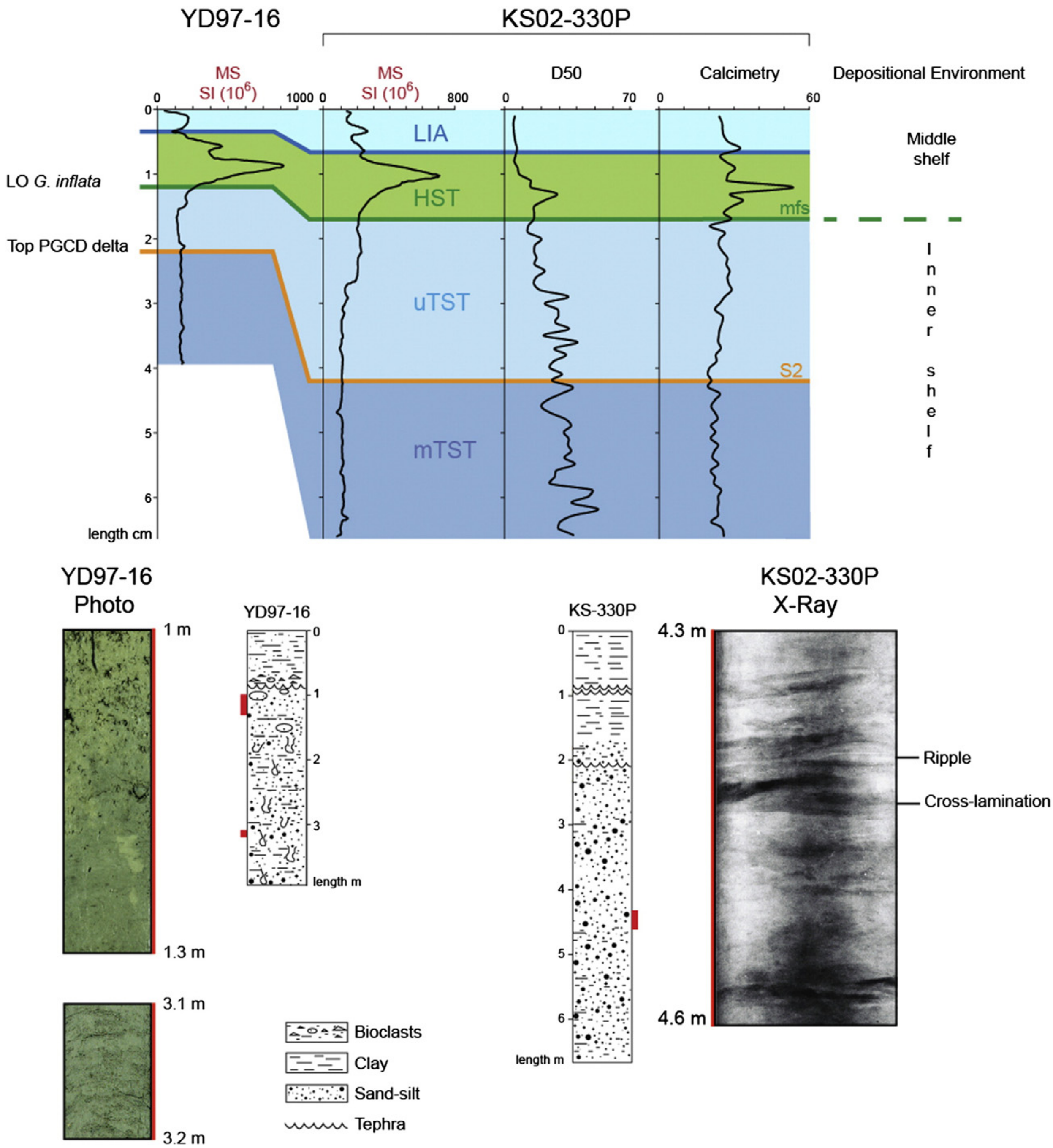

Fig. 8. Cores YD97-16 and KS02-330P through the HST, the uTST and the upper portion of mTST unit. The correlation of the cores is based on seismic data and whole-core magnetic susceptibility profiles. The regional erosional surface S2, the maximum flooding surface, the minor flooding surface associated with the onset of the Little Ice Age (LIA) unit and identified tephra layers provide timelines that support the proposed stratigraphic correlation. The last occurrence (LO) of *G. sacculifer* marks the base of the Little Ice Age (Fig. 10; Piva et al., 2008), while the LO of *G. inflata* marks to the attainment of the maximum marine ingression, ca 5.5 kyr B.P. in the Adriatic Sea (Asioli, 1996). On core KS02-330P the calcimetry curve shows the highest concentration above the mfs, the D50 curve shows a fining upward trend with a core bottom characterized by a unimodal grain-size distribution; the X radiography suggests current-generated structures during the deposition of the mTST unit. The photograph detail of core YD97-16 shows an increase in bioturbation rate across the mfs and alternating sandy silt layers characterizing the mTST unit. The depositional environment, deduced from micro and macro paleontological analysis was inner shelf and middle shelf respectively below and above the mfs. The unit subdivision is supported by changes in seismic facies on seismic profiles at the corresponding depths.

poorly sorted sand (Fig. 8). The foraminifera assemblage of *Ammonia* spp., *Elphidium* spp., *Nonion* spp., agglutinated taxa and miliolids testified a shallow water depositional environment. The uTST unit is characterized by a benthic fauna of *S. complanata*, *M. padanum*, *B. marginata*, *Ammonia tepida*, *Ammonia perlucida*, *Ammonia papillosa*, *Ammonia beccarii*, *Elphidium decipiens* and Miliolidae. This faunal assemblage is typical of a inner-shelf environment with nearby sediment input.

4.3. Chronological framework of the mTST unit

On the Adriatic margin, seismic stratigraphic correlations supported by ^{14}C dating and biostratigraphic reconstructions allowed the correlation of the main TST units, and bounding surfaces, at a basin scale (Fig. 3 and Table 1; Trincardi et al., 1994, 2011; Cattaneo and Trincardi, 1999; Asioli, 1996; Asioli et al., 2001; Correggiari et al.,

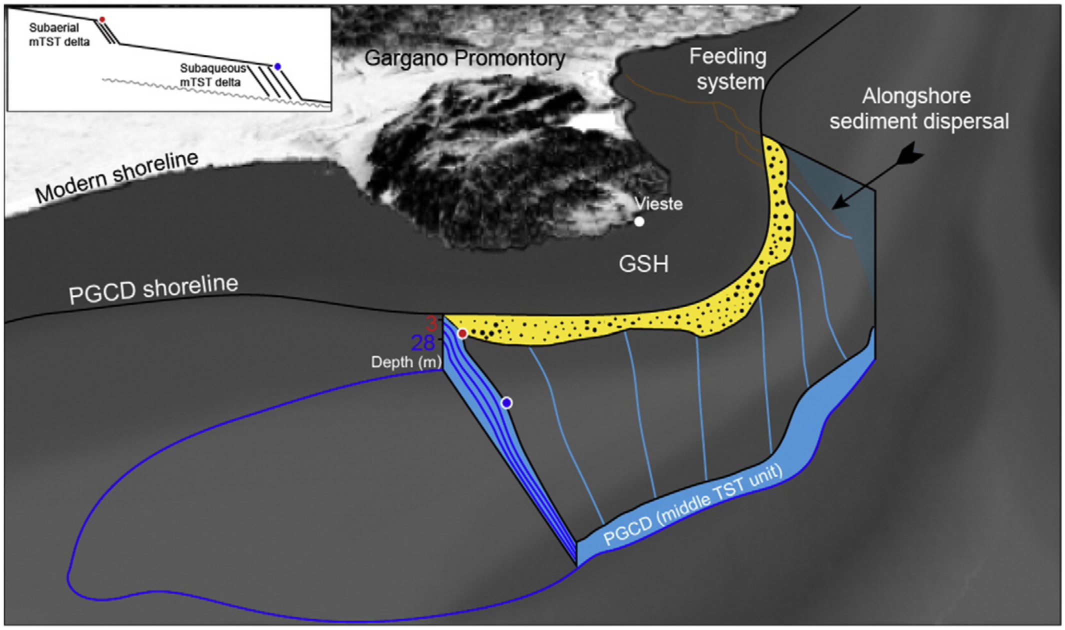

Fig. 9. Conceptual scheme for the PGCD showing the interplay between costal sediment flux and alongshore sediment dispersal. The paleo-shoreline rims the GSH flank where down-drift current deflection leads to an asymmetrical compound systems characterized by a coastal and subaqueous rollover point at paleo-water depth of 3 and 28 m (red and blue dots, respectively). Inset: schematic compound delta modified after Nittrouer et al. (1996), and Swenson et al. (2005).

2001; Cattaneo et al., 2003; Piva et al., 2008; Maselli et al., 2010). In the central Adriatic the mTST unit comprises two subunits each recording two intervals of sea level rise during the Bölling–Allerød and Younger Dryas events; these two mTST sub-units are separated by the Si erosional surface that developed during a minor sea level fall within the Younger Dryas cold spell (Maselli et al., 2011).

In the south Adriatic, offshore the Gargano Promontory, the ES1, S1 and Si surfaces coincide and the lower TST and mTST-1 sub-units are not recognized (Fig. 5). This may be related to a total cannibalization of the lower transgressive deposit during the Younger Dryas sea level fall proposed by Maselli et al. (2011) or a reduced deposition during the first phases of the post-glacial sea level rise, that may suggest that only the upper mTST unit proposed by Maselli et al. (2011), formed offshore the Gargano Promontory. As suggested by several authors, transgression do not necessarily coincide in time along every part of a basin margin (Helland-Hansen and Gjelberg, 1994; Posamentier and Allen,

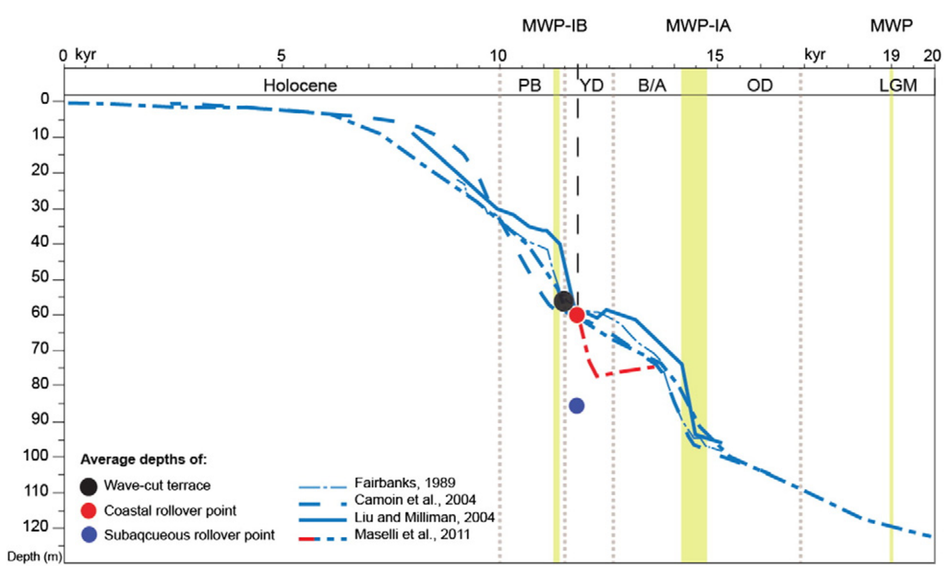

Fig. 10. Correlation between mTST unit and sea level curve (modified after Fairbanks, 1989; Camoin et al., 2004; Liu and Milliman, 2004; Maselli et al., 2011). Average depths of seismic facies interpreted as possible wave-cut terraces (black circle), coastal rollover point (red dot) and subaqueous rollover point (blue dot) record a progradation phase during the Younger Dryas interval. Note that the coastal rollover point and wave-cut terrace occurred at average depths that implies their formation after the minor sea level fall proposed by Maselli et al., 2011, and during a phase of possible still stand in the sea level curve of Liu and Milliman, 2004. The water column between the coastal and the subaqueous rollover point was about of 25 m deep.

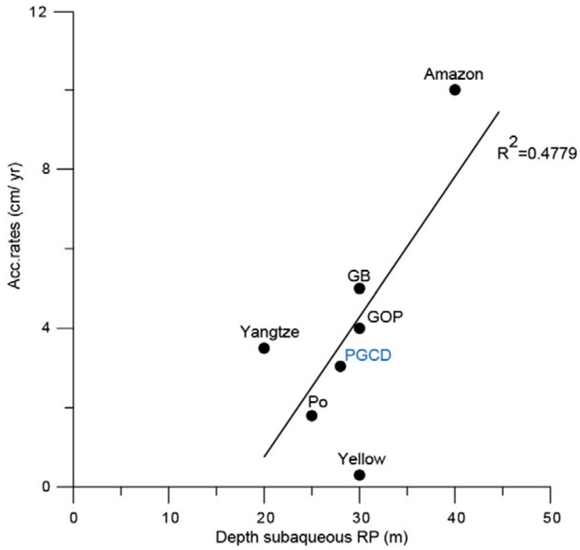

Fig. 11. The comparison between sediment accumulation rates against depth of subaqueous rollover point shows that main worldwide delta and PGCD are characterized by a similar subaqueous rollover point depth of ca. 30 m, and slight similar accumulation rates (with the exception of the Amazon subaqueous delta).

1999) and, in turn, the related transgressive deposits may be characterized by different expressions in terms of the presence or absence of ravinement surfaces and facies (Cattaneo and Steel, 2003).

Seaward the GSH the mTST unit shows its maximum stratigraphic variability and complexity, with a well-preserved sandy costal deltaic deposit spatially-connected and genetically related to a progradation wedge deeper on the shelf (Fig. 5). By analogy of modern compound systems, we propose that coarse-grained deposits formed at the shoreline, while fine-grained sediments accumulate in deeper shelf environments (typically in water depths of 25–30 m or deeper; Fig. 9). Given that the coastal rollover point of this compound delta is in a modern water depth of ca. 60 m, we can approximate its age to be ca. 11.8–12.6 kyr BP (Fig. 10, PGCD), by correlating the depth of the subaerial delta to global sea level curves (Fairbanks, 1989; Camoin et al., 2004; Liu and Milliman, 2004; Maselli et al., 2011), assuming that the vertical movements of the substrate in the area are negligible compared with the eustatic component.

As demonstrated for other Mediterranean margins, changes in precipitation rates and vegetation cover related to the Younger Dryas event may have resulted in enhanced sediment production in the catchments and/or enhanced rates of sediment export to the sea that favored the formation of thick progradational deposits (Cattaneo and Trincardi, 1999; Labaune et al., 2005; Berné et al., 2007; Sømme et al., 2011). Within this short time interval (ca. 800 years), the mTST subaqueous clinotheme offshore the Gargano Promontory recorded a short phase of higher sediment accumulation rates (0.5 cm yr^{-1}, with a maximum of ca. 3 cm yr^{-1} in the area where bidirectional downlap develops; Fig. 5C). The increased sediment supply in a relatively small interval of time can be explained by referring to the climatic reversal of the Younger Dryas event that promoted increased rates of sediment discharge from the rivers draining the high altitude areas of the Gargano Promontory that favored the development of compound delta (Fig. 9). In

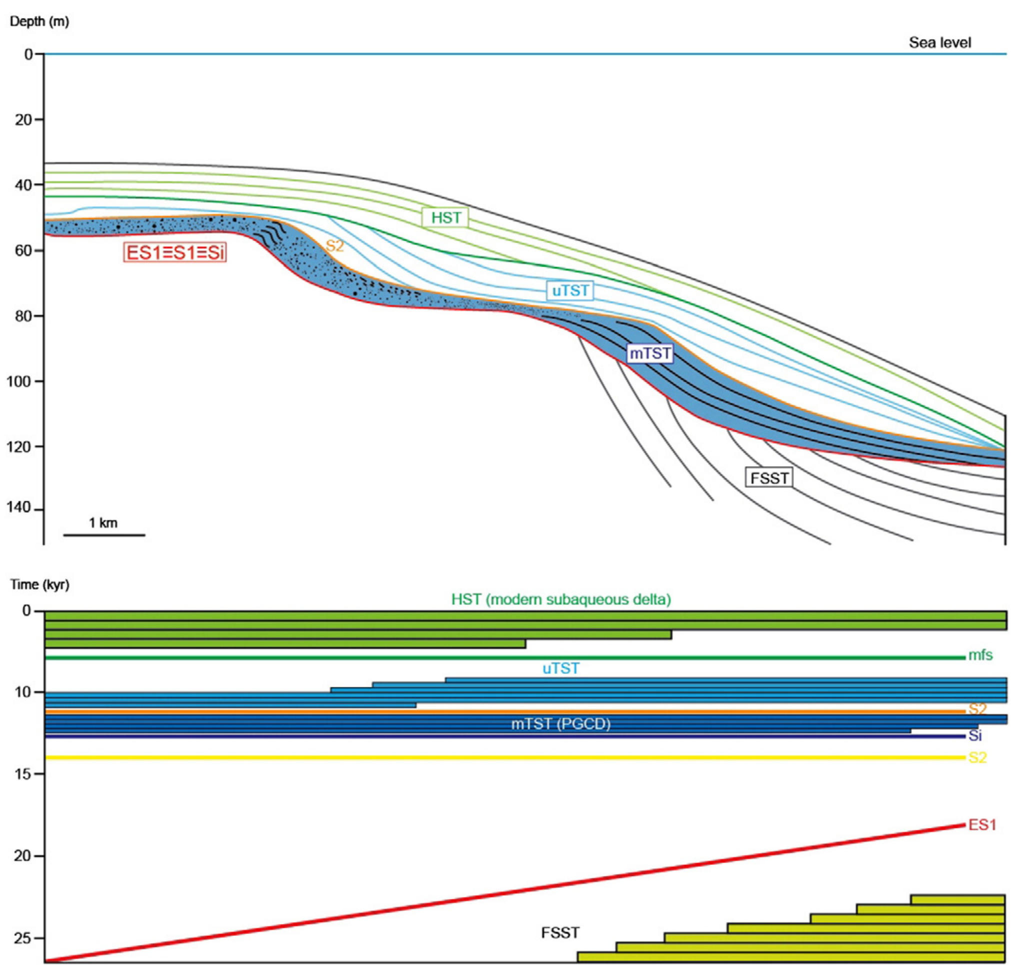

Fig. 12. Top: idealized stratigraphic section perpendicular to the coast offshore Gargano Promontory. Bottom: wheeler diagram of the same idealized section.

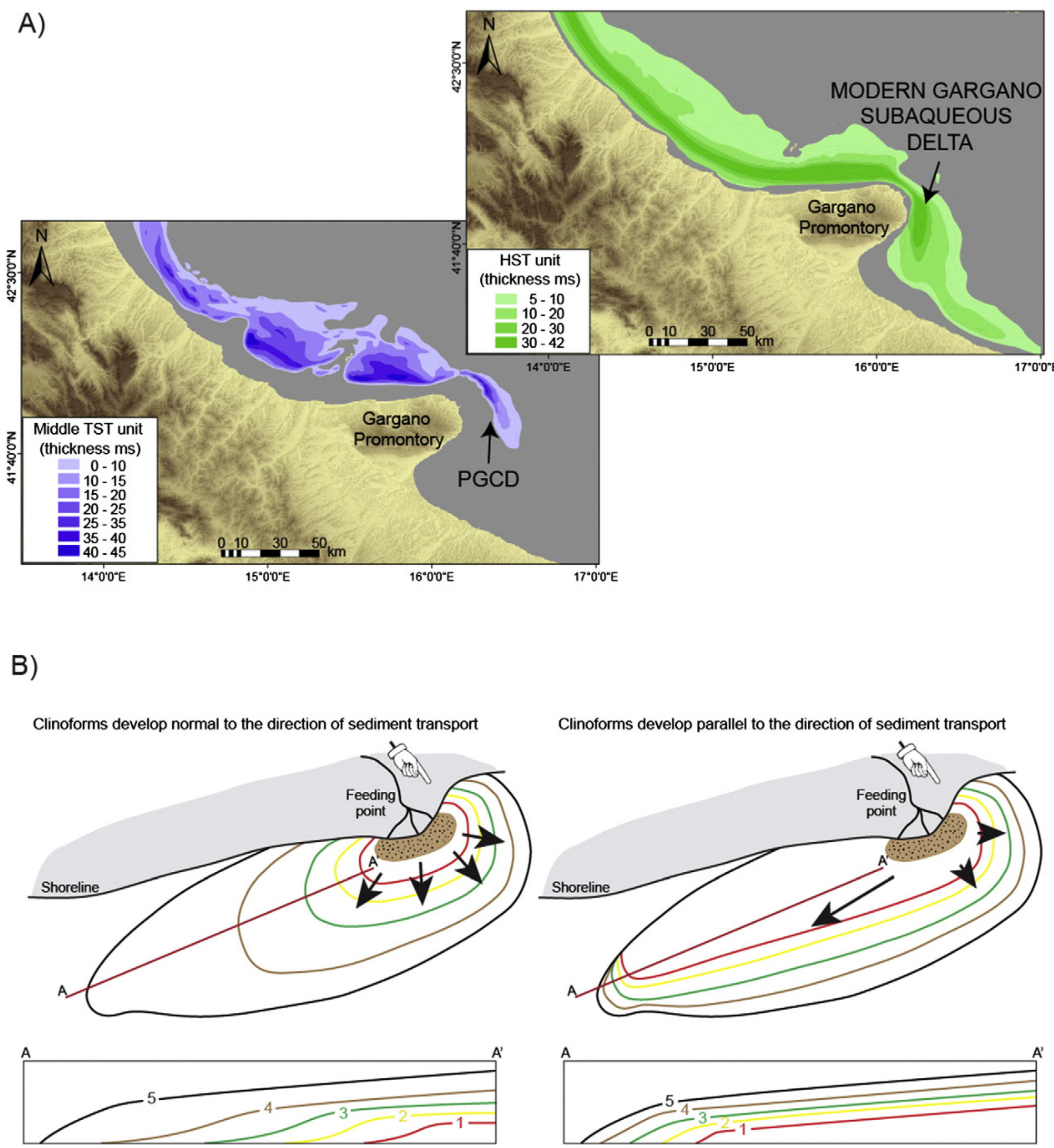

Fig. 13. Top (A): comparison of the thickness distributions of the mTST (left) and the modern HST deposits (right). The middle TST unit is characterized by main depocenters reflecting local deltaic entry points and along-shore sediment redistribution. Right: maps of the HST (thickness more than 6 ms, modified from Cattaneo and Trincardi, 1999: Cattaneo et al., 2007). Compared to the mTST, the HST shows a more continuous depocenter from the Po delta to the area south of the Gargano Promontory (see also Fig. 1). Bottom (B): conceptual scheme of clinoform progradation of river-dominated "Gilbert-type" delta against subaqueous "advective-type" delta. In the first case (left side) the direction of progradation is parallel to the sediment transport because fluvial energy prevails on along-shore transport. In the second case (right side), the direction of progradation is perpendicular to the sediment transport, as the oceanographic regime dominates on river processes.

particular the subaqueous counterpart consists of basinward downlapping strata, indicating, for some time, that the sediment supply was able to counteract with the new accommodation space created by the ongoing sea level rise. Moreover, a greater sediment accumulation rate is also favored by focused deposition against the GSH: in this area the thickness of mTST unit reached ca. 30 m. Similar examples of focused sedimentation in depocenters down-current of obstacles like the GSH come from the modern subaqueous delta south of the Shandong Peninsula (Yang and Liu, 2007; Liu et al., 2009). These values are comparable with the sediment quantified accumulation rates recorded in modern subaqueous deltas worldwide (Fig. 11: at least 5 cm yr^{-1} in the Ganges Brahmaputra foreset area, Michels et al., 1998; 7 cm yr^{-1} in the Indus clinoform foreset, Giosan et al., 2006; up to 10 cm yr^{-1} in the Amazon foreset area, Nittrouer et al., 1986).

5. Discussion

5.1. Compound delta progradation and oceanographic regime

Seminal papers in seismic stratigraphy suggested that the presence of a rollover point at the topset–foreset transition may occur in marine environments and thus does not necessarily represent the shoreline

(Mitchum et al., 1977; Vail et al., 1977; Pratson et al., 2007), and that the rollover point may form at different water depths with several trajectories for a given trend of relative sea level rise, depending on sediment supply rates and oceanographic regime. Following this concept, Steckler et al. (1999) underlined that the ratio between sediment supply and accommodation space plays a fundamental control on the distance between the shoreline and its time equivalent subaqueous rollover point and assumed this distance to be at a minimum during intervals of sea level lowstand. While in these models the oceanographic regime is scarcely considered, Swenson et al. (2005) highlighted the importance of the wave and current fields as the main factor affecting the lateral separation between the coastline and the subaqueous rollover point. The extent of this separation depends on the shear stress on the seafloor that prevents the deposition in the foreset region, as pointed out by Pirmez et al. (1998). In Cattaneo et al. (2007), the compound delta model proposed by Swenson et al. (2005), was modified into a "distorted geometry" where the energetic geostrophic circulation limits the accommodation of sediment in the clinoform bottomset; in this view the seaward progradation is not limited by the lack of sediment but by increased energetic conditions.

The concept of compound delta can be applied also to the mTST unit offshore the Gargano Promontory, where a coastal sandy deposit is genetically linked to a distal subaqueous progradation (Figs. 9, 12). The difference in water depth of ca. 25 m between the coeval coastal and subaqueous rollover points is similar to the distance found in the modern Adriatic compound delta (ca. 25–30 m; Cattaneo et al., 2007). The two systems show comparable directions of progradation, with the two subaqueous clinothemes elongated parallel to each other and to their shorelines (Fig. 13A). This evidence suggest that during the deposition of the PGCD the oceanographic regime was characterized by a wave-current field similar to the modern one, and the interaction between wave energy and along-shore currents governed sediment partitioning between the subaerial and its subaqueous counterpart.

5.2. The main factors favored the PGCD preservation

The variability of transgressive deposits, driven by numerous factors influencing the shoreline migration, may be high for coeval deposits over relatively small distances within the same sedimentary basin (Heward, 1981). Minor changes in one controlling factor or a combination of the controlling factors may modify the preservation of transgressive deposits. The preservation of transgressive deposits is strongly influenced by a number of factors such as the depth of erosion, the wave-energy, the rate of relative sea level rise, the sediment supply, the along shore transport and the erosion resistance of bed material (Belknap and Kraft, 1981). Notwithstanding the preservation of coastal transgressive deposits is considered unlikely as a result of intense ravinement during shoreline transition, example of costal deposits within transgressive units on worldwide shelves are reported in the literature by several authors (e.g., Steel et al., 2000; Aksu et al., 2002; Salzmann et al., 2013; Gamberi et al., 2014). Finally, progradational (regressive) coastal deposits are more likely to be fully preserved than those of transgressive coasts (Davis and Clifton, 1987); indeed if the sediment supply compensates or overwhelms the increasing accommodation space related to relative sea level rise an aggradational or progradational succession is expected, respectively (Curray and Moore, 1964; Galloway and Hobday, 1983).

The costal counterpart of the PGCD is characterized by an along-coast sandy deposit connected to a muddy subaqueous clinoform (Fig. 9). We suggest that the preservation of this shallower unit may be related to a prevailing vertical component of submergence rather than the horizontal component of reworking deposits during the shoreface retreat. This is possible in contexts where the rates of sea level rise and sediment supply overwhelm the sediment dispersion rates of the currents (Davis and Clifton, 1987). This interpretation is in agreement with the "cliff overstep" model proposed by Zecchin et al. (2011) for steep shelves where relative high sea level rise connected to the Meltwater pulses promotes a rapid drowning of cliff portions with related rapid excursion of the shoreline; and with the documentations of the high sediment supply recorded on the Mediterranean shelves during the Younger Dryas interval (e.g., Labaune et al., 2005; Berné et al., 2007; Lericolais et al., 2010; Maselli et al., 2011; Sømme et al., 2011). The further jump in sea level highlighted by the subsequent landward migration of the uTST unit depocenter (Fig. 7) leads to the burial of the mTST unit and, in turn, promotes its preservation. Furthermore, the internal reflector architecture and the external geometry of the uTST unit highlight that an along-shore currents governed the directions of the subaqueous clinotheme progradation, as observed for the underlying mTST unit and the overlaying HST unit. In this view, the PGCD highlights a peculiar case study where the interaction between a step-like sea level rise and a pre-existing morphology may have favored the preservation of coupled progradations in the area present down-current in respect to the structural high.

5.3. The PGCD in three dimensions

The PGCD and the modern Gargano subaqueous delta share also a comparable internal geometry with the strike of the clinoform subparallel to the axis of the depocenters. This evidence implies that the transport of sediment occurs over significant distances parallel to the clinoform strike instead of perpendicular (or at high angle) to it. Fig. 13B shows an interesting implication of this concept: in a depocenter growing from a feeding point located upcurrent (the subaerial delta) the successive steps of deposition may lead to the formation of clinoforms that are normal to the direction of sediment transport and, therefore, have the youngest reflector located further away downcurrent (Fig. 13B, left). In this case, the time lines are progressively younger ride off the subaerial delta in a fashion that is reminiscent of a subaerial Gilbert type delta. In the Adriatic basin, both modern and TST examples, instead, show time lines with a more radial pattern and display an increasing distance moving downdrift from the entry points. Examples of a similar progradation pattern are documented for the submarine delta of the Ganges–Brahmaputra (Michels et al., 1998), the modern clinoform of Gulf of Papua (Walsh et al., 2004) and the deglacial deposits of the Gulf of Lyon (Labaune et al., 2005).

When a subaqueous delta is recognized on the continental shelf, it is genetically linked to a time equivalent deltaic or estuarine deposit, through which sediment is fed to the subaqueous counterpart (two examples come from the delta Po-Gargano, Cattaneo et al., 2007; and the Amapa coastal plain-Amazon compound systems, Nittrouer et al., 1996). The morphologic profiles of compound systems are characterized by a couple of rollover points (i.e., coastal and subaqueous rollover points); this evidence is confirmed also in profile of worldwide rivers characterized by an estuarine outflow (e.g., Amazon and Columbia Rivers, Fig. 14A). Moreover, depending on the morphology of the basin, compound systems may be nourished by several point sources, captured by an alongshore current (e.g., Apennine and Po Rivers for the Po-Gargano deltaic systems, Cattaneo et al., 2003; Fly, Kikori and Purari Rivers, for the Gulf of Papua deltaic systems, Walsh et al., 2004). In compound systems where a well developed costal delta grows, marine currents lead to an asymmetric progradation of both costal and subaqueous systems (Bhattacharya and Giosan, 2003; Cattaneo et al., 2003; Correggiari et al., 2005). Despite all the differences in the oceanographic regime among different systems, subaqueous deltas can always be viewed as the marine components of compound deltas which coastal counterpart may be located hundreds of kilometers away (e.g., Shandong subaqueous delta and subaerial Yellow River delta, Alexander et al., 1991; Yangtze subaqueous delta and tidal subaerial delta, Hori et al., 2002; Gulf of Papua subaqueous delta and Fly, Kiori and Purari subaerial delta, Slingerland et al., 2008; Indus mid-shelf subaqueous

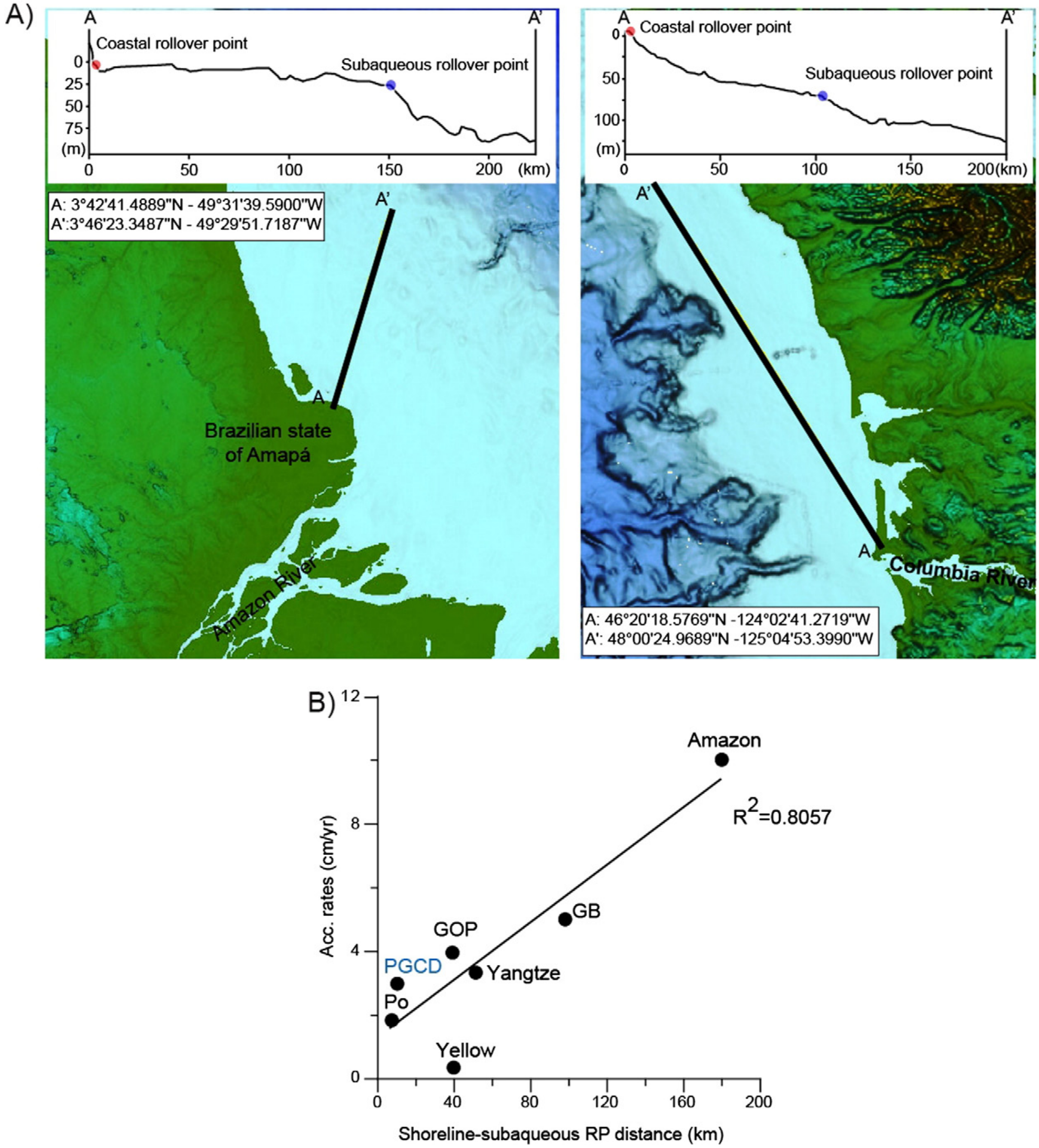

Fig. 14. Top (A): down-drift profile of the Amazon and Columbia Rivers' deposits highlights the presence of both costal and subaqueous rollover points (bathymetry from GEBCO.net). Bottom (B): correlation between sediment accumulation rates and shoreline-subaqueous rollover point; the PGCD records a small distance between shoreline and subaqueous progradation, suggesting a limited sink area during the Younger Dryas interval.

delta and subaerial delta, Giosan et al., 2006; Ganges–Brahmaputra shallow subaqueous delta and subaerial delta, Palamenghi et al., 2011).

5.4. Sedimentation patterns of the PGCD

Modern compound deltas developed during the last ca. 5–8 kyr BP, and substantially after the post LGM sea level highstand was attained (e.g., Goodbred et al., 2003; Yi et al., 2003; Walsh et al., 2004; Cattaneo et al., 2007). In modern examples of compound systems, sediments carried by rivers are dispersed alongshore far from the river mouths, and accumulated in subaqueous clinoforms 20–40 m thick in water depth ranges of 30–90 (Liu et al., 2009). Fluvial sediment dispersed alongshore may be transported as far as 300 km (Mekong River, Ta et al., 2002), 700 km (Yellow River, Yang and Liu, 2007), and as much as 1500 km (Amazon River, Nittrouer et al., 1996). A particular case comes from the Yellow Sea, where the subaqueous clinoform is characterized by a bidirectional progradation (omega-shaped) due to the interplay between long-shore sediment transport and the physiographic constriction by the Shandong Peninsula (Yang and Liu, 2007).

The sediment accumulation rates calculated on the foreset region of the subaqueous delta is linearly related to the distance between the shoreline and the subaqueous rollover point, as highlighted for modern compound systems in Fig. 14B. Interestingly, the PGCD recorded slightly higher accumulation rates compared to the modern Gargano subaqueous delta (3 mm/yr and 1.28 mm/yr respectively), possibly because of a smaller distance between the source and the subaqueous clinotheme during the Younger Dryas interval. The post-Younger Dryas sea level rise led to the drowning of the shelf and widening of the basin that triggered the formation of an alongshore current acting as a linear sediment source for the modern compound delta system. For this reason, in the modern Adriatic compound delta the distance between the feeder source and the subaqueous depocenter is larger (in order of 600 km).

During the deposition of the mTST unit, a sandy deposit about 12 m thick and its subaqueous counterpart developed asymmetrically over 50 km (Fig. 6), with the coastal and subaqueous rollover points separated by ca. 10 km, along a down-current dip section. As for modern analogs, this evidence may suggest the presence of an alongshore current that prevented the seaward progradation of the PGCD. In the up-drift side of the GSH the PGCD appears less developed. Conversely, in the down-drift side of the GSH, the PGCD reaches its greatest thickness (Fig. 6). This evidence suggests a strong interaction between sediment transport from land, alongshore circulation, and pre-existing topography, and underlines a down-drift deflection of the marine currents, as suggested by Bhattacharya and Giosan (2003). The impact of southeasterly currents has been stronger at the up-drift side of the GSH: conversely the lower energy current has characterized the down-drift side of the GSH leading to a greater sediment accumulation of the PGCD.

The substantial absence of microfauna in the PGCD deposits offshore GSH suggests the influence of freshwater discharge, flowing from the continent and nourishing a delta NE of Vieste (Fig. 9). Considering an average sediment density of 2.5 g cm^{-3}, the total sediment load of the river was in the order of less than 10×10^6 t yr^{-1}, a value of one order of magnitude greater than the modern value of Apennine rivers (Frignani et al., 2005). These values may reflect the impact of a rejuvenated fluvial incision excavated during the Younger Dryas cold event documented on land (Amorosi and Milli, 2001).

6. Conclusions

In the southern Adriatic basin, mid-shelf deposits document the first case of a compound delta deposited within a period of overall sea level rise. Offshore the Gargano Promontory, the landward backstepping architecture of the Late Pleistocene to Holocene transgressive deposits was punctuated by the progradation of a compound delta system characterized by a sandy costal unit of reduced thickness and a subaqueous muddy clinotheme up to 30 m thick. Seismic–stratigraphic correlations support the hypothesis that the Paleo Gargano Compound Delta (PGCD) formed in a short time window including the Younger Dryas cold spell, when slow rates of sea level rise and enhanced sediment production in the catchments promoted both coastal and subaqueous progradations. Likely, the increased rates of sea level rise during the post-Younger Dryas interval allowed the rapid drowning and preservation of the PGCD. More in general, our findings support the following conclusions:

- The formation of the PGCD within an overall transgressive record implies that the time required for the development of such deposit may take place during very short windows, likely in the order of centuries; this notion may be useful in interpreting ancient stratigraphic records where a much lower geochronological resolution may lead to assume or imply much slower rates of sediment accumulation.
- Depending on internal reflector geometries and overall architecture, the PGCD may be viewed as the transgressive, small-scale, analog of the modern highstand Adriatic compound delta, as both records reflect progradations influenced by similar alongshore sediment dispersion with sediment transport occurring dominantly along the strike of the clinoform.
- The findings from the PGCD, in agreement with documentation from the literature (especially for the Amazon delta), suggest that subaqueous deltas are always connected to a coastal deposit, characterized by a coastal rollover point, that may be interpreted as the genetically linked subaerial counterpart of a compound delta systems.

Acknowledgments

We are grateful to the Editor for its suggestions, the anonymous reviewer for his detailed comments and suggestions and to the reviewer Liviu Giosan for his comments and suggestion. We thank Captain, the Crew of campaigns and all the researches on board R/V Urania (CNR) that during the last decades acquired chirp sonar profiles and sediment cores. We thank Gwenael Jouet, Bernard Dennielou, and Elda Miramontes García for their insights, and Mickael Rovere and Angelique Roubi for their skilled assistance in calcimeter and grain size analysis at Ifremer GM-LES in Brest. We thank Andrea Gallerani for the X radiography at ISMAR-CNR in Bologna. We thank Alessandra Asioli for her consulting and Elisabetta Campiani and Federica Foglini for their support on GIS. This is ISMAR-CNR contribution number 1857.

References

Aksu, A.E., Hiscott, R.N., Yas, D., Is, F.I., 2002. Seismic stratigraphy of Late Quaternary deposits from the southwestern Black Sea shelf: evidence for non-catastrophic variations in sea-level during the last ca. 10,000 yr. Mar. Geol. 190, 61–94.
Alexander, C.R., DeMaster, D.J., Nittrouer, C.A., 1991. Sediment accumulation in a modern epicontinental-shelf setting: the Yellow Sea. Mar. Geol. 98, 51–72.
Amorosi, A., Milli, S., 2001. Late Quaternary depositional architecture of Po and Tevere river deltas (Italy) and worldwide comparison with coeval deltaic successions. Sediment. Geol. 144 (3), 357–375.
Artegiani, A., Paschini, E., Russo, A., Bregant, D., Raicich, F., Pinardi, N., 1997a. The Adriatic Sea general circulation. Part I: air–sea interactions and water mass structure. J. Phys. Oceanogr. 27, 1492–1514.
Artegiani, A., Paschini, E., Russo, A., Bregant, D., Raicich, F., Pinardi, N., 1997b. The Adriatic Sea general circulation. Part II: baroclinic circulation structure. Phys. Oceanogr. 27, 1515–1532.
Asioli, A., 1996. High resolution foraminifera biostratigraphy in the central Adriatic basin during the last deglaciation: a contribution to the PALICLAS project. Mem. Ist. Ital. Idrobiol. 55, 197–217.
Asioli, A., Trincardi, F., Lowe, J.J., Ariztegui, D., Langone, L., Oldfield, F., 2001. Sub-millennial climatic oscillations in the Central Adriatic during the last deglaciation: paleoceanographic implications. Quat. Sci. Rev. 20, 33–53.
Belknap, D.F., Kraft, J.C., 1981. Preservation potential of transgressive coastal lithosomes on the US Atlantic shelf. Dev. Sedimentol. 32, 429–442.
Benetazzo, A., Bergamasco, A., Bonaldo, D., Falcieri, F.M., Sclavo, M., Langone, L., Carniel, S., 2014. Response of the Adriatic Sea to an intense cold air outbreak: dense water dynamics and wave-induced transport. Prog. Oceanogr. 128, 115–138.
Berné, S., Jouet, G., Bassetti, M.A., Dennielou, B., Taviani, M., 2007. Late Glacial Preboreal sea-level rise recorded by the Rhône deltaic system (NW Mediterranean). Mar. Geol. 245, 65–88.
Bertotti, G., Casolari, E., Picotti, V., 1999. The Gargano Promontory: a Neogene contractional belt within the Adriatic plate. Terra Nova-Oxford 11 (4), 168–173.
Bhattacharya, J.P., Giosan, L., 2003. Wave-influenced deltas: geomorphological implications for facies reconstruction. Sedimentology 50, 187–210.
Blockley, S.P.E., Lowe, J.J., Walker, M.J.C., Asioli, a., Trincardi, F., Coope, G.R., Donahue, R.E., 2004. Bayesian analysis of radiocarbon chronologies: examples from the European Late-glacial. J. Quat. Sci. 19, 159–175.
Camoin, G.F., Montaggioni, L.F., Braithwaite, C.J.R., 2004. Late glacial to post glacial sea levels in the Western Indian Ocean. Mar. Geol. 206 (1), 119–146.
Canals, M., Danovaro, R., Heussner, S., Lykousis, V., Puig, P., Trincardi, F., Calafat, A., de Madron, X., D., Palanques, A., Sánchez-Vidal, A., 2009. Cascades in Mediterranean submarine grand canyons. Oceanography 22 (1), 26–43.
Cattaneo, A., Steel, R.J., 2003. Transgressive deposits: a review of their variability. Earth Sci. Rev. 62 (3), 187–228.
Cattaneo, A., Trincardi, F., 1999. The late-Quaternary transgressive record in the Adriatic epicontinental sea: basin widening and facies partitioning. Soc. Sediment. Geol. Spec. Publ. 64, 127–146.
Cattaneo, A., Correggiari, A., Langone, L., Trincardi, F., 2003. The late-Holocene Gargano subaqueous delta, Adriatic shelf: sediment pathways and supply fluctuations. Mar. Geol. 193, 61–91.
Cattaneo, A., Trincardi, F., Asioli, A., Correggiari, A., 2007. The western Adriatic shelf clinoform: energy-limited bottomset. Cont. Shelf Res. 27, 506–525.
Chiocci, F.L., Orlando, L., Tortora, P., 1991. Small-scale seismic stratigraphy and paleogeographical evolution of the continental shelf facing the SE Elba Island (northern Tyrrhenian Sea, Italy). J. Sediment. Res. 61 (4).
Correggiari, A., Field, M.E., Trincardi, F., 1996. Late Quaternary transgressive large dunes on the sediment-starved Adriatic shelf. Geol. Soc. Spec. Publ. 117, 155–169.
Correggiari, A., Trincardi, F., Langone, L., Roveri, M., 2001. Styles of failure in heavily-sedimented highstand prodelta wedges on the Adriatic shelf. J. Sediment Res. 71, 218–236.

Correggiari, A., Cattaneo, A., Trincardi, F., 2005. The modern Po Delta system: lobe switching and asymmetric prodelta growth. Mar. Geol. 222–223, 49–74.

Cross, T.A., Baker, M.R., Chapin, M.A., Clark, M.S., Gardner, M.H., Hanson, M.S., Lessenger, M.A., Little, L.D., McDonough, K.-J., Sonnenfeld, M.D., Valasek, D.W., Williams, M.R., Witter, D.N., 1993. Applications of high-resolution sequence stratigraphy to reservoir analysis. Subsurface Reservoir characterization from Outcrop observation 51, pp. 11–33.

Curray, J.R., Moore, D.G., 1964. Holocene regressive littoral sand, Costa de Nayarit, Mexico. Dev. Sedimentol. 1, 76–82.

Davis Jr., R.A., Clifton, H.E., 1987. Effects of sea-level rise on preservation potential of wave- and tide-dominated coasts. In: Nummedal, D., et al. (Eds.), Sea-level Fluctuations and Coastal Evolution. Society for Sedimentary Geology Special Publication 41, pp. 167–178.

Díaz, J.I., Ercilla, G., 1993. Holocene depositional history of the Fluviá–Muga prodelta, northwestern Mediterranean Sea. Mar. Geol. 111 (1), 83–92.

Durán, R., Canals, M., Lastras, G., Micallef, A., Amblas, D., Pedrosa-Pàmies, R., Sanz, J.L., 2013. Sediment dynamics and post-glacial evolution of the continental shelf around the Blanes submarine canyon head (NW Mediterranean). Prog. Oceanogr. 118, 28–46.

Eberli, G.P., Bernoulli, D., Sanders, D., Vecsei, A., 1993. From aggradation to progradation: the Maiella Platform, Abruzzi, Italy, Carbonate Platforms. AAPG Mem. 56, 213–232.

Fairbanks, R.G., 1989. A 17,000-yr glacio-eustatic sea level record: influence of glacial melting rates on the Younger Dryas event and deep-ocean circulation. Nature 342, 637–642.

Fanget, A., S., Berné, S., Jouet, G., Bassetti, M.A., Dennielou, B., Maillet, G.M., Tondut, M., 2014. Impact of relative sea level and rapid climate changes on the architecture and lithofacies of the Holocene Rhone subaqueous delta (Western Mediterranean Sea). Sediment. Geol. 305, 35–53.

Frignani, M., Langone, L., Ravaioli, M., Sorgente, D., Alvisi, F., Albertazzi, S., 2005. Fine-sediment mass balance in the western Adriatic continental shelf over a century time scale. Mar. Geol. 222–223, 113–133.

Galloway, W.E., 1975. Process framework for describing the morphologic and stratigraphic evolution of deltaic depositional systems, 87–98. In: Broussard, M.L. (Ed.), Deltas: Models for Exploration. Houston Geological Society, Houston, TX, pp. 87–98.

Galloway, W.E., Hobday, D.K., 1983. Terrigenous clastic depositional systems. Applications to Petroleum, Coal and Uranium Exploration.

Gamberi, F., Rovere, M., Mercorella, A., Leidi, E., Dalla Valle, G., 2014. Geomorphology of the NE Sicily continental shelf controlled by tidal currents, canyon head incision and river-derived sediments. Geomorphology 217, 106–121.

Giosan, L., Constantinescu, S., Clift, P.D., Tabrez, A.R., Danish, M., Inam, A., 2006. Recent morphodynamics of the Indus delta shore and shelf. Cont. Shelf Res. 26, 1668–1684.

Giosan, L., Filip, F., Constatinescu, S., 2009. Was the Black Sea catastrophically flooded in the early Holocene? Quat. Sci. Rev. 28 (1), 1–6.

Giosan, L., Constantinescu, S., Filip, F., Deng, B., 2013. Maintenance of large deltas through channelization: nature vs. humans in the Danube delta. Anthropocene 1, 35–45.

Goodbred Jr., S.L., Kuehl, S.A., 2000. The significance of large sediment supply, active tectonism, and eustasy on margin sequence development: Late Quaternary stratigraphy and evolution of the Ganges–Brahmaputra delta. Sediment. Geol. 133 (3), 227–248.

Goodbred, S.L., Kuehl, S.a., Steckler, M.S., Sarker, M.H., 2003. Controls on facies distribution and stratigraphic preservation in the Ganges–Brahmaputra delta sequence. Sediment. Geol. 155, 301–316.

Hampson, G.J., 2010. Sediment dispersal and quantitative stratigraphic architecture across an ancient shelf. Sedimentology 57, 96–141.

Helland-Hansen, W., Gjelberg, J.G., 1994. Conceptual basis and variability in sequence stratigraphy: a different perspective. Sediment. Geol. 92 (1), 31–52.

Helland-Hansen, W., Hampson, G.J., 2009. Trajectory analysis: concepts and applications. Basin Res. 21, 454–483.

Hernández-Molina, F.J., Somoza, L., Rey, J., Pomar, L., 1994. Late Pleistocene–Holocene sediments on the Spanish continental shelves: model for very high resolution sequence stratigraphy. Mar. Geol. 120, 129–174.

Heward, A.P., 1981. A review of wave-dominated clastic shoreline deposits. Earth Sci. Rev. 17 (3), 223–276.

Hiscott, R.N., Aksu, A.E., Yaşar, D., Kaminski, M.A., Mudie, P.J., Kostylev, V.E., MacDonald, J.C., Isler, F.I., Lord, A.R., 2002. Deltas south of the Bosphorus Strait record persistent Black Sea outflow to the Marmara Sea since ~10 ka. Mar. Geol. 190 (1), 95–118.

Hori, K., Saito, Y., Zhao, Q., Wang, P., 2002. Architecture and evolution of the tide-dominated Changjiang (Yangtze) River delta, China. Sediment. Geol. 146, 249–264.

Jouet, G., Berné, S., Rabineau, M., Bassetti, M.A., Bernier, P., Dennielou, B., Sierro, F.J., Flores, J.A., Taviani, M., 2006. Shoreface migrations at the shelf edge and sea-level changes around the Last Glacial Maximum (Gulf of Lions, NW Mediterranean). Mar. Geol. 234, 21–42.

Kuehl, S.A., DeMaster, D.J., Nittrouer, C.A., 1986. Nature of sediment accumulation on the Amazon continental shelf. Cont. Shelf Res. 6 (1), 209–225.

Kuehl, S., Levy, B.M., Moore, W.S., Allison, M.A., 1997. Subaqueous delta of the Ganges–Brahmaputra river system. Mar. Geol. 144, 81–96.

Labaune, C., Jouet, G., Bernè, S., Gensous, B., Tesson, M., Delpeint, A., 2005. Seismic stratigraphy of the deglacial deposits of the Rhône prodelta and of the adjacent shelf. Mar. Geol. 222–223, 299–311.

Lascaratos, A., 1993. Estimation of deep and intermediate water mass formation rates in the Mediterranean Sea. Deep-Sea Res. II Top. Stud. Oceanogr. 40 (6), 1327–1332.

Lericolais, G., Guichard, F., Morigi, C., Minereau, A., Popescu, I., Radan, S., 2010. A post Younger Dryas Black Sea regression identified from sequence stratigraphy correlated to core analysis and dating. Quat. Int. 225 (2), 199–209.

Liu, J.P., Milliman, J.D., 2004. Reconsidering melt-water pulses 1A and 1B: global impacts of rapid sea-level rise. J. Ocean Univ. China 3 (2), 183–190.

Liu, J.P., Milliman, J.D., Gao, S., Cheng, P., 2004. Holocene development of the Yellow River's subaqueous delta, North Yellow Sea. Mar. Geol. 209, 45–67.

Liu, J.P., Xue, Z., Ross, K., Wang, H.J., Yang, Z.S., Li, A.C., Gao, S., 2009. Fate of sediments delivered to the sea by Asian large rivers: long-distance transport and formation of remote alongshore clinothems. Sediment. Rec. 7 (4), 4–9.

Lobo, F.J., Fernández-Salas, L.M., Moreno, I., Sanz, J.L., Maldonado, A., 2006. The sea-floor morphology of a Mediterranean shelf fed by small rivers, northern Alboran Sea margin. Cont. Shelf Res. 26 (20), 2607–2628.

Lowe, J.J., Blockley, S., Trincardi, F., Asioli, a., Cattaneo, a., Matthews, I.P., Pollard, M., Wulf, S., 2007. Age modelling of late Quaternary marine sequences in the Adriatic: towards improved precision and accuracy using volcanic event stratigraphy. Cont. Shelf Res. 27, 560–582.

Lykousis, V., Karageorgis, A.P., Chronis, G.T., 2005. Delta progradation and sediment fluxes since the last glacial in the Thermaikos Gulf and the Sporades Basin, NW Aegean Sea, Greece. Mar. Geol. 222, 381–397.

Maselli, V., Trincardi, F., Cattaneo, A., Ridente, D., Asioli, A., 2010. Subsidence pattern in the central Adriatic and its influence on sediment architecture during the last 400 kyr. J. Geophys. Res. 115, B12106.

Maselli, V., Hutton, E.W., Kettner, A.J., Syvitski, J.P.M., Trincardi, F., 2011. High-frequency sea level and sediment supply fluctuations during Termination I: an integrated sequence-stratigraphy and modeling approach from the Adriatic Sea (Central Mediterranean). Mar. Geol. 287, 54–70.

Mellere, D.O., Plink-Bjorklund, P., Steel, R., 2002. Anatomy of shelf deltas at the edge of a prograding Eocene shelf margin, Spitsbergen. Sedimentology 49, 1181–1206.

Michels, K.H., Kudrass, H.R., Hu, C., 1998. The submarine delta of the Ganges–Brahmaputra: cyclone-dominated sedimentation patterns. Mar. Geol. 149, 133–154.

Mitchum Jr., R.M., Vail, P.R., Thompson III, S., 1977. Seismic stratigraphy and global changes of sea level; part 2. The depositional sequence as a basic unit for stratigraphic analysis. In: Payton, C.E. (Ed.), Seismic Stratigraphy; Applications to Hydrocarbon Exploration. Memoir 26. American Association of Petroleum Geologists, Tulsa, pp. 53–62.

Morris, J.E., Hampson, G.J., Johnson, H.D., 2006. A sequence stratigraphic model for an intensely bioturbated shallow-marine sandstone: the Bridport Sand Formation, Wessex Basin, UK. Sedimentology 53, 1229–1263.

Nittrouer, C.A., Kuehl, S.A., Demaster, D.J., Kowsmann, R.O., 1986. The deltaic nature of Amazon shelf sedimentation. Geol. Soc. Am. Bull. 4, 444–458.

Nittrouer, C.A., Kuehl, S.A., Figueiredo, G., Allison, M.A., Sommerfield, C.K, Rine, J.M., Faria, T.L.E.C., Silveira, O.M., 1996. The geological record preserved by Amazon shelf sedimentation. Cont. Shelf Res. 16, 817–841.

Orton, G.J., Reading, H.G., 1993. Variability of deltaic processes in terms of sediment supply, with particular emphasis on grain size. Sedimentology 40, 475–512.

Palamenghi, L., Schwenk, T., Spiess, V., Kudrass, H.R., 2011. Seismostratigraphic analysis with centennial to decadal time resolution of the sediment sink in the Ganges–Brahmaputra subaqueous delta. Cont. Shelf Res. 31, 712–730.

Patruno, S., Hampson, G.J., Jackson, C.A.L., 2015. Quantitative characterisation of deltaic and subaqueous clinoforms. Earth Sci. Rev.

Pirmez, C., Pratson, L.F., Steckler, M.S., 1998. Clinoform development by advection-diffusion of suspended sediment: modeling and comparison to natural systems. J. Geophys. Res. Solid Earth (1978–2012) 103 (B10), 24141–24157.

Piva, A., Asioli, A., Trincardi, F., Schneider, R.R., Vigliotti, L., 2008. Late-Holocene climate variability in the Adriatic Sea (Central Mediterranean). The Holocene 18, 153–167.

Posamentier, H.W., Allen, G.P., 1999. Siliciclastic sequence stratigraphy: concepts and applications. Soc. Sediment. Geol. Concepts Sedimentol. Paleontol. 7 (204 pp.).

Pratson, L.F., Nittrouer, C.A., Wilberg, P., Steckler, M.S., Swenson, J.B., Cacchione, D.A., Karson, J.A., Murray, A.B., Wolinsky, M.A., Gerber, T.P., Mullenbach, B.L., Spinelli, G.A., Fulthorpe, C.S., O'Grady, D.B., Parker, G., Driscoll, N.W., Burger, R.L., Paola, C., Orange, D.L., Field, M.E., Friedrichs, C.T., Fedele, J.J., 2007. Seascape evolution on clastic continental shelves and slopes. In: Nittrouer, C.A., Austin, J.A., Field, M.E., Kravitz, J.H., Syvitski, J.P.M., Wiberg, P.L. (Eds.), Continental Margin Sedimentation: From Sediment Transport to Sequence Stratigraphy. IAS Special Publication 37. Blackwell, pp. 339–380.

Rhoads, D.C., Boesch, D.F., Zhican, T., Fengshan, X., Liqiang, H., Nilsen, C., 1985. Macrobenthos and sedimentary facies on the Changjiang delta platform and adjacent continental shelf, East China Sea. Cont. Shelf Res. 4 (1/2), 189–213.

Ridente, D., Trincardi, F., 2002. Eustatic and tectonic control on deposition and lateral variability of Quaternary regressive sequences in the Adriatic basin (Italy). Mar. Geol. 184, 273–293.

Salzmann, L., Green, A., Cooper, J.A.G., 2013. Submerged barrier shoreline sequences on a high energy, steep and narrow shelf. Mar. Geol. 346, 366–374.

Schattner, U., Lazar, M., Tibor, G., Ben-Avraham, Z., Makovsky, Y., 2010. Filling up the shelf—a sedimentary response to the last post-glacial sea rise. Mar. Geol. 278 (1), 165–176.

Slingerland, R., Driscoll, N.W., Milliman, J.D., Miller, S.R., Johnstone, E.a., 2008. Anatomy and growth of a Holocene clinothem in the Gulf of Papua. J. Geophys. Res. 113, F01S13.

Sømme, T.O., Piper, D.J.W., Deptuck, M.E., Helland-Hansen, W., 2011. Linking Onshore–Offshore sediment dispersal in the Golo source-to-sink system (Corsica, France) during the Late Quaternary. J. Sediment. Res. 81 (2), 118–137.

Steckler, M.S., Mountain, G.S., Miller, K.G., Christie-Blick, N., 1999. Reconstruction of Tertiary progradation and clinoform development on the New Jersey passive margin by 2-D backstripping. Mar. Geol. 154, 399–420.

Steel, R., Rasmussen, H., Eide, S., Neuman, B., Siggerud, E., 2000. Anatomy of high-sediment supply, transgressive tracts in the Vilomara composite sequence, Sant Llorenç del Munt, Ebro Basin, NE Spain. Sediment. Geol. 138 (1), 125–142.

Swenson, J.B., Paola, C., Pratson, L., Voller, V.R., Murray, A.B., 2005. Fluvial and marine controls on combined subaerial and subaqueous delta progradation: morphodynamic

modeling of compound-clinoform development. J. Geophys. Res. Earth Surf. 110, 0148–0227.
Ta, T.K.O., Nguyen, V.L., Tateishi, M., Kobayashi, I., Tanabe, S., Saito, Y., 2002. Holocene delta evolution and sediment discharge of the Mekong River, southern Vietnam. Quat. Sci. Rev. 21 (16), 1807–1819.
Taviani, M., Angeletti, L., Campiani, E., Ceregato, A., Foglini, F., Maselli, V., Morsilli, M., Parise, M., Trincardi, F., 2012. Drowned karst landscape offshore the Apulian margin (Southern Adriatic Sea, Italy). J. Cave Karst Stud. 74, 197–212.
Trincardi, F., Correggiari, A., 2000. Quaternary forced regression deposits in the Adriatic basin and the record of composite sea-level cycles. Geol. Soc. 172, 245–269.
Trincardi, F., Correggiari, A., Roveri, M., 1994. Late Quaternary transgressive erosion and deposition in a modern epicontinental shelf: the Adriatic Semienclosed Basin. Geo-Mar. Lett. 14, 41–51.
Trincardi, F., Asioli, A., Cattaneo, A., Correggiari, A., Langone, L., 1996. Stratigraphy of the late-Quaternary deposits in the Central Adriatic basin and the record of short-term climatic events. Mem. Ist. Ital. Idrobiol. 55, 39–70.
Trincardi, F., Cattaneo, A., Correggiari, A., 2004. Mediterranean prodelta systems. Oceanography 17 (4), 34.
Trincardi, F., Foglini, F., Verdicchio, G., Asioli, A., Correggiari, A., Minisini, D., Piva, A., Remia, A., Ridente, D., Taviani, M., 2007. The impact of cascading currents on the Bari Canyon System, SW-Adriatic Margin (Central Mediterranean). Mar. Geol. 246 (2), 208–230.
Trincardi, F., Argnani, A., Correggiari, A., 2011. Note illustrative della carta geologica dei mari italiani alla scala 1:250.000, S.EL.CA, fogli Ancona NK 33–1/2, Bari NK 33–6 e Vieste NK 33–8/9.
Trincardi, F., Campiani, E., Correggiari, A., Foglini, F., Maselli, V., Remia, A., 2013. Bathymetry of the Adriatic Sea: the legacy of the last eustatic cycle and the impact of modern sediment dispersal. J. Maps 10 (1), 151–158.
Vail, P.R., Mitchum Jr., R.M., Thompson III, S., 1977. Seismic stratigraphy and global changes of sea level, part 3: relative changes of sea level from coastal onlap. In: Payton, C.E. (Ed.), Seismic Stratigraphy — Applications to Hydrocarbon Exploration. American Association of Petroleum Geologists Memoir 26, pp. 63–81.
Vigliotti, L., Verosub, K.L., Cattaneo, A., Trincardi, F., Asioli, A., Piva, A., 2008. Palaeomagnetic and rock magnetic analysis of Holocene deposits from the Adriatic Sea: detecting and dating short term fluctuations in sediment supply. The Holocene 18, 141–152.
Vilibich, I., Supich, N., 2005. Dense water generation on a shelf: the case of the Adriatic Sea. Ocean Dyn. 55, 403–415.
Walsh, J.P., Nittrouer, C.A., 2009. Understanding fine-grained river-sediment dispersal on continental margins. Mar. Geol. 263 (1), 34–45.
Walsh, J.P., Nittrouer, C.a., Palinkas, C.M., Ogston, a.S., Sternberg, R.W., Brunskill, G.J., 2004. Clinoform mechanics in the Gulf of Papua, New Guinea. Cont. Shelf Res. 24, 2487–2510.
Wrigth, L.D., Coleman, J.M., 1972. River delta morphology: wave climate and the role of the subaqueous profile. Science 176, 282–284.
Xue, Z., Liu, J.P., DeMaster, D., Van Nguyen, L., Ta, T.K.O., 2010. Late Holocene evolution of the Mekong subaqueous delta, southern Vietnam. Mar. Geol. 269 (1), 46–60.
Yang, Z.S., Liu, J.P., 2007. A unique Yellow River-derived distal subaqueous delta in the Yellow Sea. Mar. Geol. 240, 169–176.
Yi, S., Saito, Y., Zhao, Q., Wang, P., 2003. Vegetation and climate changes in the Changjiang (Yangtze River) Delta, China, during the past 13,000 years inferred from pollen records. Quat. Sci. Rev. 22, 1501–1519.
Zecchin, M., Ceramicola, S., Gordini, E., Deponte, M., Critelli, S., 2011. Cliff overstep model and variability in the geometry of transgressive erosional surfaces in high-gradient shelves: the case of the Ionian Calabrian margin (southern Italy). Mar. Geol. 281 (1), 43–58.

6) Contourite deposits and clinoform growth

First introduced to define marine sediments deposited in the deep-sea by contour-parallel bottom thermohaline currents (Heezen and Hollister, 1964), the use of the term *contourite* has been broadened through time to embrace a larger spectrum of sediments that accumulate in a wide range of water depths by different types of bottom currents (Rebesco et al., 2014 for a review). Bottom current produce a variety of deposits and erosional features; the largest deposits are called “contourite drifts”. Based on their overall external morphology and taking into account different geological and oceanographic settings, drift systems can be classified in elongated drifts, mounded drifts, sheeted drifts, channel-related drifts, confined drifts, patch drifts, infill drifts, fault-controlled drifts, and mixed drift systems (Fig. 6.1; Rebesco et al., 2014).

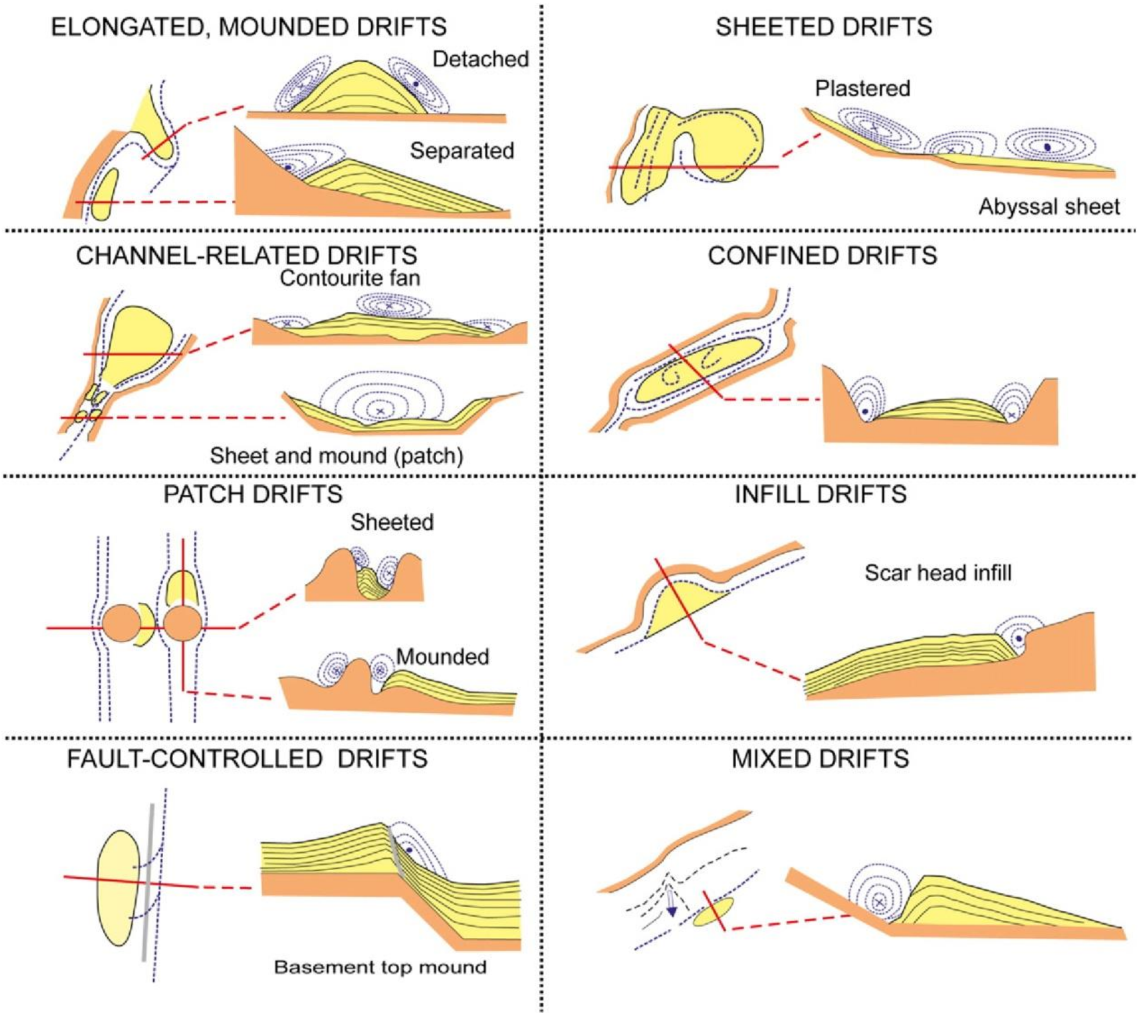

Figure 6.1: drift systems types and inferred bottom-current paths from Rebesco et al. (2014).

The basal unconformity of a contourite drift is commonly revealed by a continuous high-amplitude reflector that may widen beyond the limits of the drift system, and which represents non-deposition or erosion produced by bottom-currents (Faugères et al., 1999); indeed, these bottom current are characterized by an average velocities well above threshold for deposition (Mulder et al., 2013). Within contourites, reflectors often display low-angle downlap onto the basal unconformity while tend to be characterized by toplap truncations against the upper unconformity (Stow et al., 2002). The overall internal seismic character of a drift is the typical pattern of continuous reflectors that tend to follow the gross drift morphology. This pattern reflects the long-lasting, semi-stable conditions that are the prerequisite for building up a large contourite drift, however, large temporary changes in current strength and sediment supply may occur during the lifetime of the contourite, causing shift between erosional and depositional environments (e.g. "out of phase drift" in Verdicchio and Trincardi, 2008; moat migration in Llave et al., 2011).

Contourite depositional systems contain an association of erosional and depositional sedimentary features, which are driven through a complex interaction of bottom currents and sediment supply, reflecting the oceanographic response on the variable atmospheric processes (Hernandez-Molina et al., 2014 among others). During the last decade, reflection-seismic investigations of contourite depositional systems have benefited greatly from the increased interest in deep-water area by the petroleum industry, which has lead to improved technologies and quality seismic data; for example a higher awareness of the contourite paradigm has revealed more small-scale examples along the ocean margins, as well as in shallow water environments and even within lakes (Fig. 6.2).

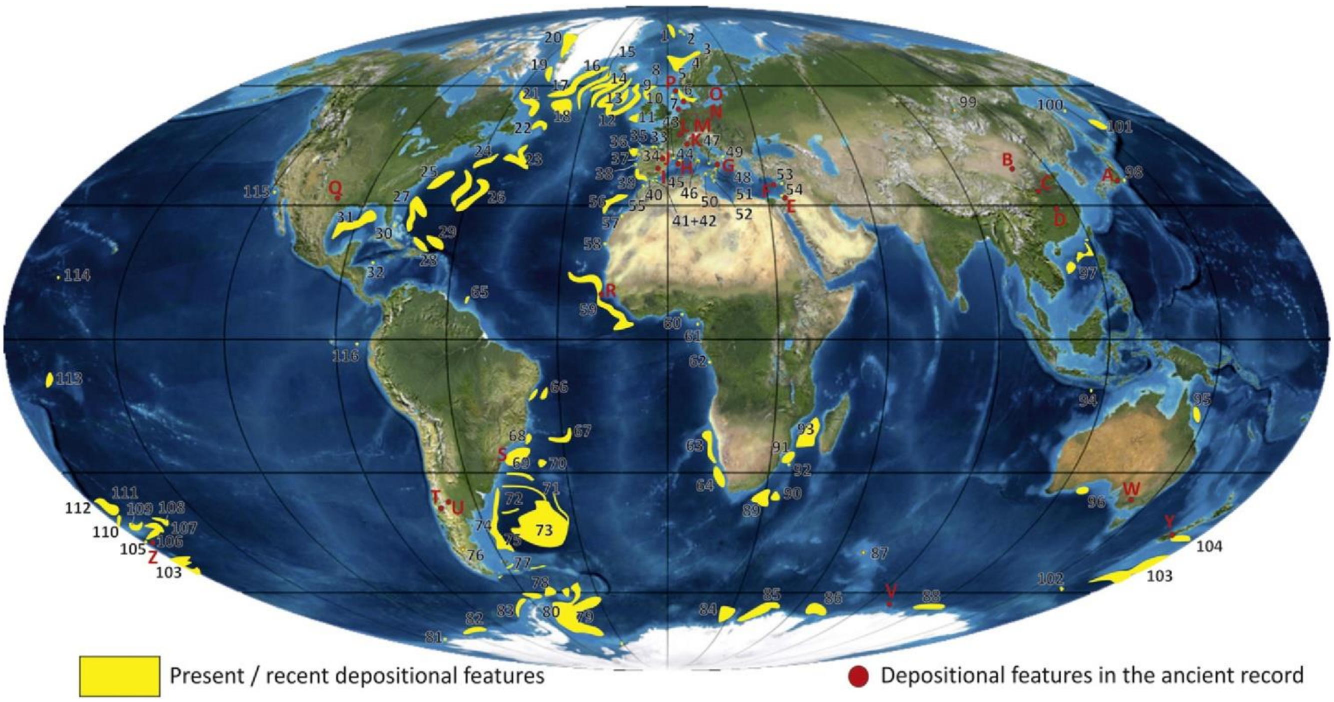

Figure 6.2: Location of contourite deposits in the modern ocean basins (yellow areas) and in the ancient sedimentary record (black points; from Rebesco et al., 2014). For number and letters references see Rebesco et al. (2014).

Contourites are well established and described from recent and sub-recent deposits although the same cannot be said for their identification in ancient sedimentary series exposed on land (Rebesco et al., 2014), because of the difficulty in depicting the low angle of fossil contourite strata and related moat, because of the lack of the three dimensions of the contourite system, and because of the lack of information regarding the paleoceanographic regime (Stow et al., 2008).

Although most of the large present-day contourite drifts have been initiated within the Neogene, they all experienced an intensification since the beginning of the Quaternary, whereas some responded even more vigorously with respect to the early to middle Pleistocene transition (Miramontes et al., 2015, among others); while stable isotope and sortable silt grain-size analysis highlight changes in the bottom current inflow and competence and variation in sediment supply on Milankovitch to millennial time-scale (Toucanne et al., 2007; Minto'o et al., 2015). Furthermore, a geotechnical approach highlighted the association between contourite deposits and marine landslide (Bryn et al., 2005; Masson et al., 2006; Cattaneo et al., 2014).

Regarding the south-western Adriatic margin, earlier publications highlighted the presence of contourite deposits, both in the basin and on the outer shelf, through the analysis of surficial stratigraphy and sediment cores (Verdicchio et al., 2007; Verdicchio and Trincardi, 2008; Foglini et al., 2015). Based on their orientation, on their overall up-slope migration and based on their patchy distribution, contourite deposits in the Adriatic Sea have been interpreted as related to the interplay of the down-slope North Adriatic Dense Water, and the along-slope Levantine Intermediate Water (Verdicchio et al., 2007; Trincardi et al., 2007). The formation of these contourite deposits seem to be incentivized by an overall decreasing in bottom current velocity at the down-current sector of the Gargano Promontory (Martorelli et al., 2010). During time, these contourite deposits reflected changes in oceanographic setting and thermohaline circulation affecting the whole Mediterranean Sea; in particular these contourite deposits were less active during glacial periods probably because of the inhibition in the production of the North Adriatic Dense Water due to the subaerial exposure of the northern Adriatic shelf (Verdicchio and Trincardi, 2008), and the less intense production of the Levantine Intermediate Water in the Western Mediterranean compare to the present interglacial (Myers et al. 1998).

Until nowadays the timing of, and the factors leading to, the onset and subsequent evolution of contourite deposits in the Adriatic Sea remained unknown. The next chapter aims to reports the regional stratigraphic architecture of the Pliocene-Quaternary contourite depositional system, its spatio-temporal evolution and a long-term perspective on the variation of the bottom-current regime. This case history shows the onset of contourite deposits within the Pliocene succession where a sediment drift developed on the flank of a structural carbonate anticline, and may represent an example of source/seal hydrocarbon play. The findings from the south-western Adriatic margin not only shows that contourite drifts contributes to creation of the stratigraphic architecture of the margin, but also that contourites may form the bulk of shelfal progradational sequences. This finding highlights that far from a feeding system, lateral advection and current deposition may became the dominant mechanisms of progradation promoting the accretion of sediment drift within clinoforms, that in turn govern the final architectural motif of the margins.

6.1) Manuscript IV

"Pliocene–Quaternary contourite depositional system along the south-western Adriatic margin: changes in sedimentary stacking pattern and associated bottom currents"

Authors: Claudio Pellegrini (Istituto di Scienze Marine, ISMAR-CNR, Università di Bologna, Dipartimento di Scienze della Terra e Geologico-Ambientali, Bologna, Italy)

Vittorio Maselli (Istituto di Scienze Marine, ISMAR-CNR, Bologna, Italy)

Fabio Trincardi (Istituto di Scienze Marine, ISMAR-CNR, Bologna, Italy)

Status: Published in *Geo-Marine Letter*, edited by B.W. Flemming and M.T. Delafontaine, pages 1-13, doi 10.1007/s00367-015-0424-4.

Geo-Mar Lett
DOI 10.1007/s00367-015-0424-4

ORIGINAL

Pliocene–Quaternary contourite depositional system along the south-western Adriatic margin: changes in sedimentary stacking pattern and associated bottom currents

Claudio Pellegrini[1,2] **· Vittorio Maselli**[1] **· Fabio Trincardi**[1]

Received: 27 August 2015 / Accepted: 18 September 2015

Abstract The Pliocene–Quaternary history of the south-western Adriatic margin, represented by a complex contourite depositional system, records the palaeoceanography of the basin and the interactions between oceanographic processes and the uneven slope morphology that resulted from tectonic deformation. Three main stages can be recognized: (1) during the Pliocene, a giant sediment drift formed on the southern flank of the slope-transverse Gondola anticline that focused and accelerated the flow of slope-parallel bottom currents; (2) since the early to middle Pleistocene transition, a reorganization of bottom-current pathways led to a sharp change in the sedimentary architecture of the margin that became dominated by the growth of contourite deposits; (3) as of 350 ka, landward-migrating contourites on the outer shelf (less than 120 m water depth) reflect the presence of bottom currents also in shallow waters. This analysis of the sedimentary stacking pattern of the contourite depositional system that developed along the south-western Adriatic margin since the Pliocene enables disentangling the processes that controlled changes in bottom-current activity, demonstrating that bottom-current deposits constitute the bulk of depositional sequences at the Milankovitch timescale.

✉ Claudio Pellegrini
claudio.pellegrini@bo.ismar.cnr.it

[1] ISMAR-CNR, Istituto di Scienze Marine, Via Gobetti 101, 40129 Bologna, Italy

[2] Dipartimento di Scienze della Terra e Geologico-Ambientali, University of Bologna, Piazza di Porta San Donato 1, 40126 Bologna, Italy

Introduction

The importance of contourite deposits as a key component of deep ocean environments was recognized since the seminal papers of Heezen and Hollister (1964) and Heezen et al. (1966). Over the last decades, contourite deposits have increasingly been identified in more shallow-water settings, from the base of the slope to the outer shelf (e.g. Fulthorpe and Carter 1991; Howe 1996; Stow et al. 1998; Verdicchio et al. 2007; Rebesco and Camerlenghi 2008; Van Rooij et al. 2010; Rebesco et al. 2014; Hanebuth et al. 2015). Viana et al. (1998) introduced the term "*shallow-water contourite*" to describe shelfal bottom-current deposits (water depths of 50 to 300 m) in contexts where the impact of waves and tides is negligible compared to a dominant contour-parallel geostrophic circulation.

In the Mediterranean Sea and particularly along its gateways, several examples of contourite deposits have been identified where long-lasting oceanographic regimes (maintained over timescales of 10^6 years) are constrained to preferential pathways. Prime examples are the middle slope of the Gulf of Cadiz (Hernández-Molina et al. 2006; Brackenridge et al. 2013), the Mediterranean Gibraltar gateway (Hernández-Molina et al. 2014), the outer shelf off south-western Mallorca (Vandorpe et al. 2011), the Corsica channel (Roveri 2002; Cattaneo et al. 2014; Miramontes et al. 2014), the Sicily channel (Marani et al. 1993; Verdicchio and Trincardi 2008a; Martorelli et al. 2011), the Apulian continental margin (Savini and Corselli 2010), and the south-western Adriatic margin (Verdicchio and Trincardi 2008b; Martorelli et al. 2010).

On the south-western Adriatic margin (SAM), previous studies explored the complex seafloor morphology and surficial stratigraphy, and highlighted the presence of contourite deposits and sediment drifts in both proximal and distal

Published online: 29 September 2015

settings (Trincardi et al. 2007a; Verdicchio and Trincardi 2008b). The present study attempts to document the timing of, and the factors leading to, the onset and subsequent evolution of a long-lasting contourite depositional system on the SAM. Focusing on a sector of the basin where the interactions between oceanographic processes and seafloor morphology are maximal, this paper aims to establish (1) the regional stratigraphic architecture of the Pliocene–Quaternary contourite depositional system, (2) its spatiotemporal evolution and (3) a long-term perspective on the variation of the bottom-current regime and its impact on changes in the depositional style of the system throughout time.

Geological setting

The modern seafloor morphology of the SAM reflects the interaction between long-term tectonic deformation and eustatic oscillations that controlled repeated changes in bottom-current circulation and sediment dispersal. The main offshore tectonic feature is the south Gargano deformation belt (Argnani et al. 1993) that includes an asymmetric relief called the Gondola anticline (Fig. 1). This compressional structure affects the shelf, the shelf edge and the slope, where it passes into the Dauno Seamount. The Dauno Seamount, at a height of up to 250 m from the basin floor, rises from the central sector of the SAM.

The south-western Adriatic continental shelf is up to 80 km wide in the Gulf of Manfredonia and becomes narrower further to the south (Fig. 1; less than 30 km), with dip gradients reaching up to 4% at the shelf break. The SAM shows an uneven seafloor morphology due to the presence of multiple mass-transport deposits (buried and exposed), testifying recurrent sediment failure (Minisini et al. 2006; Dalla Valle et al. 2015), and depositional/erosional sedimentary structures, including contourites, sediment drifts, furrows and scours that record the impact of energetic bottom currents today exceeding 60 cm/s (Fig. 1; Verdicchio and Trincardi 2008b; Foglini et al. 2015).

Stratigraphic setting

The stratigraphic architecture of the Mesozoic–early Cainozoic sedimentary succession of the SAM has been investigated through seismic profiles and exploration boreholes (Fig. 2). Two main seismic horizons can be detected and correlated at a regional scale: the M and Q reflectors. The M reflector is associated to the Miocene erosional surface (Fig. 2; Argnani et al. 1993), and marks the boundary between the Miocene carbonate succession below and the siliciclastic Pliocene–Quaternary succession above. The Q reflector represents the boundary between the Pliocene and the Quaternary succession (Fig. 2).

The chronostratigraphic framework of the late Quaternary succession in the Adriatic Sea was defined by the borehole PRAD 1.2 in the central Adriatic basin (Piva et al. 2008a, b). In this area, as in the SAM, the upper four depositional sequences, each bounded by an erosional surface of regional extent formed during sea-level lowstand, have been correlated to 100,000 year Milankovitch cyclicity (Ridente and Trincardi 2002; Ridente et al. 2009; Maselli et al. 2010).

Oceanographic setting

The SAM is affected by distinct water masses that include the Levantine Intermediate Water (LIW) and the seasonally modulated North Adriatic Dense Water (NAdDW) flowing along and across the slope (Fig. 1; Artegiani et al. 1997a, b). Both the LIW and the NAdDW are characterized by annual and inter-annual fluctuations in density, flow strength and sediment transport capacity (Turchetto et al. 2007). The LIW forms in the Levantine Basin through evaporation during the summer and cooling during the winter (Lascaratos et al. 1999). This salty water mass (29.0 kg/m^3) enters the southern Adriatic through the Otranto Strait and follows a cyclonic path, with a water depth interval of 200–700 m (Fig. 1; the so-called South Adriatic Gyre: e.g. Artegiani et al. 1997a, b; Mantziafou and Lascaratos 2008).

The NAdDW forms on the shallow northern Adriatic shelf and its density increases (29.8 kg/m^3) through winter cooling and evaporation associated with local wind forcing (Bora events). This cold water mass moves southwards along the Italian margin, flowing around the main capes (Ancona Cape and the Gargano Promontory), then cascades obliquely across the south-western Adriatic slope along the steepest sector reaching below the depth range impacted by the contour-parallel LIW (Trincardi et al. 2007b; Canals et al. 2009). Due to its dynamical properties (buoyancy and kinetic energy), a portion of the NAdDW remains trapped on the shelf, flowing as a contour-parallel bottom current over several hundreds of kilometres (Fig. 1; Benetazzo et al. 2014; Bonaldo et al. 2015).

Both the contour-parallel LIW and the NAdDW interact with the seafloor morphology, including the Gondola structure, the Dauno Seamount and the Bari Canyon. This leads to the formation of both depositional and erosional features in water depths between ca. 100 and 1,200 m (Fig. 1; Verdicchio et al. 2007; Foglini et al. 2015).

Materials and methods

The SAM has been investigated using (1) a dense grid of low-resolution multichannel seismic lines, property of the Italian Ministry of the Development, tuned with exploration boreholes, which allowed the regional correlation of the Pliocene–

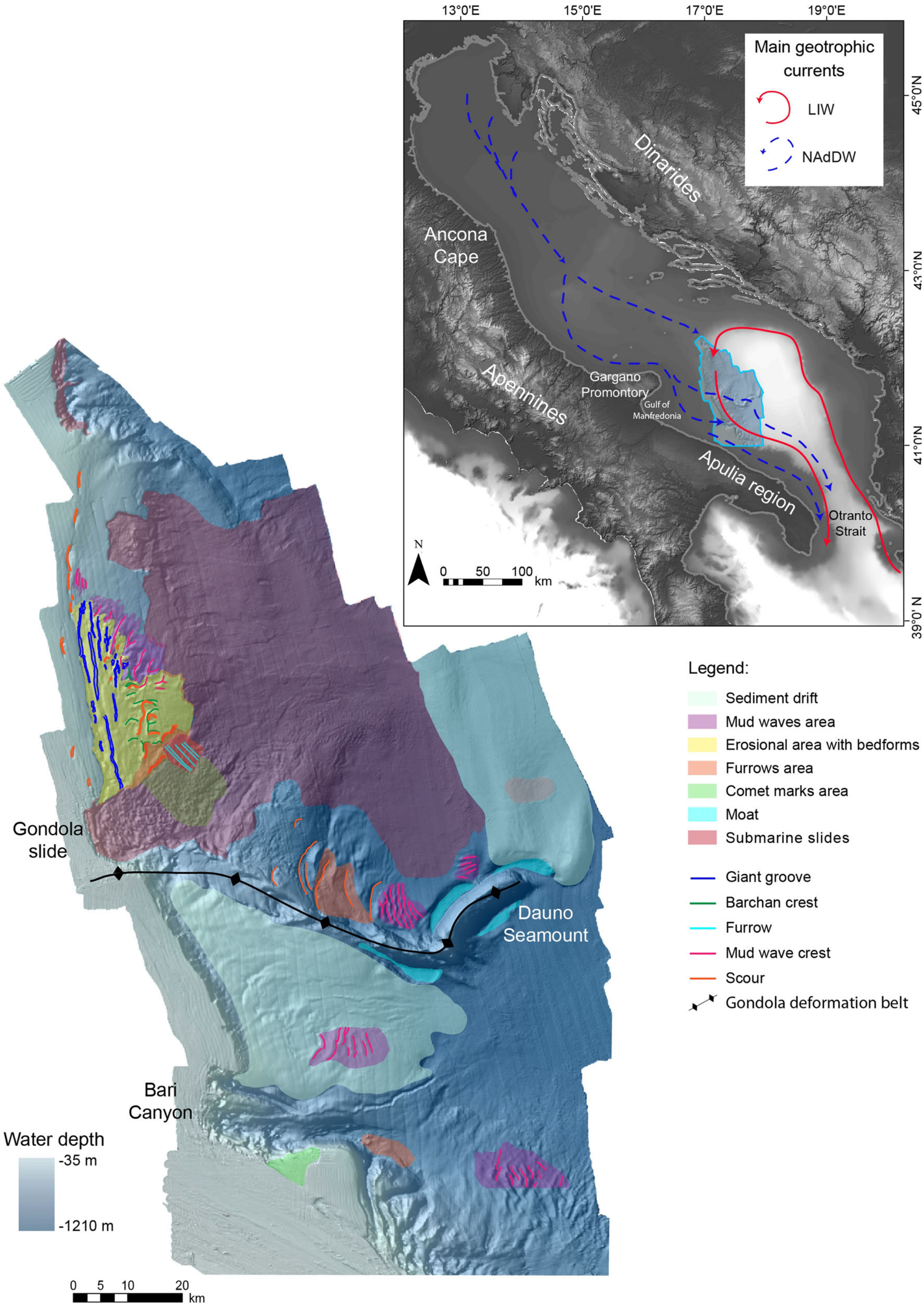

Fig. 1 *Top* Pathways of North Adriatic Dense Waters (NAdDW) and Levantine Intermediate Waters (LIW) in the Adriatic Sea. *Bottom* Multibeam bathymetry of the study area (modified from Foglini et al. 2015), showing the erosional and depositional sediment features of the SAM contourite system. Note the trace of the Gondola deformation belt with an E–W to NW–SE hinge line swivelling to SW–NE in its slope sector, the Dauno Seamount

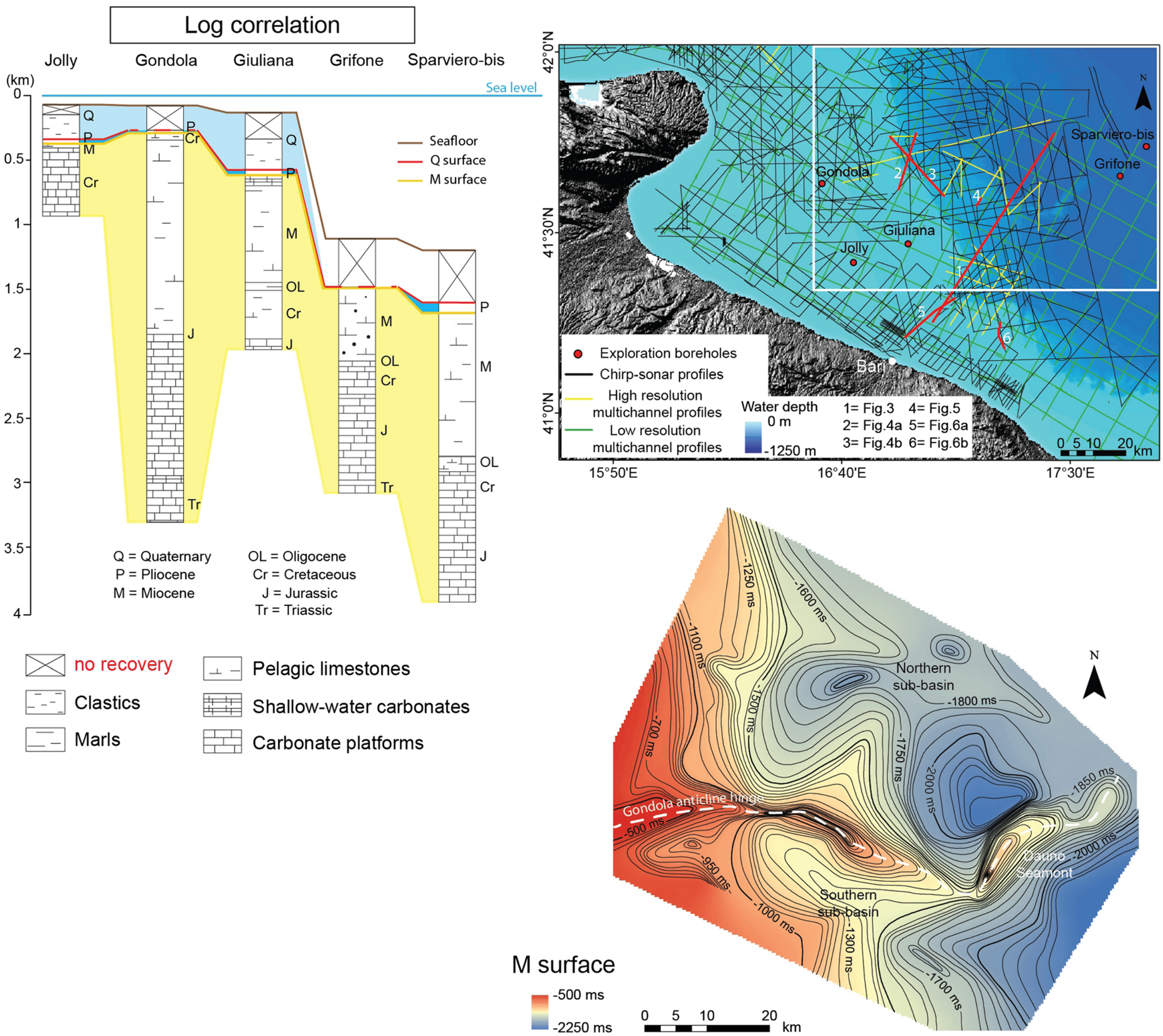

Fig. 2 *Top left* Shelf–basin correlation of exploration boreholes illustrating the depth of the Mesozoic–late Cainozoic carbonate successions and the overlying Pliocene–Quaternary succession. Note the disappearance of Miocene deposits in the Gondola well drilled on top of the Gondola anticline (modified from Argnani et al. 2009). *Top right* Locations of seismic lines and boreholes; *white box* mapping area of surface at the top of the carbonate succession (M surface). *Bottom* Isochronal map of the M surface showing the slope transverse structural relief, its irregular topography and the accompanying synclinal basins (northern and southern basins) that reach depths of up to 2,250 ms

Quaternary succession and the construction of the structural map of the M surface (Fig. 2); (2) a high-resolution multibeam bathymetry of the study area and dense grid of chirp-sonar profiles acquired by ISMAR-CNR during the last 10 years (Trincardi et al. 2014); and (3) a set of high-resolution multichannel and chirp seismic lines newly acquired by ISMAR-CNR during the ADRIASEISMIC 2009 and INVAS 2012 surveys.

Multichannel seismic lines were acquired by means of a water gun Sercel-S15 source and a teledyne mini-streamer with 24 channels (80–500 Hz frequency content). Chirp-sonar profiles were gathered using a hull-mounted 16-transducer source with a sweep modulated 2 to 7 kHz outgoing signal.

Results

Seismic stratigraphy

The stratigraphic boundaries M, Q, and the seafloor define three main successions from bottom to top: Mesozoic–early Cainozoic succession, below the M reflector; Pliocene succession and Quaternary succession, respectively below and above the Q reflector (Figs. 2 and 3). The M surface is highlighted by a very high-amplitude and high-continuity reflector and marks the top of the Mesozoic–early Cainozoic succession (Figs. 2 and 3). The isochronal map of the M reflector shows an uneven topography characterized by regional-scale convex-up and convex-down geometries with anticline and syncline structures in the slope-basin area that encompass the Gondola anticline (Fig. 2). The Gondola anticline displays a northward orientation and a NW–SE hinge line on the slope switching to a NE–SW orientation at the base of the slope (Dauno Seamount). Northwards and southwards of the Gondola anticline, two syncline structures form local topographic lows with bases deepening from 1.2 s to 2.1 s from the shelf edge towards the basin (Fig. 2).

The Q reflector is highlighted by subtle downlap terminations and locally cuts the underlying strata documenting intensified bottom-current erosion (Figs. 3 and 4a, b). This surface separates the Pliocene deposits from the Pleistocene–Holocene succession (Argnani et al. 1993, 2009; de Alteriis 1995; Billi et al. 2007). Within the Quaternary succession, the ES8 unconformity is characterized by a high-amplitude reflector that cuts the underlying strata and marks a sharp change in the stacking pattern of stratigraphic successions (Fig. 3).

SAM Pliocene succession

The Pliocene succession is bounded by the M and Q reflectors at the base and top respectively (Figs. 3, 4a, b). The configuration of the Pliocene succession is characterized by sub-parallel reflectors (Fig. 3). The lateral continuity of the reflectors within the Pliocene succession is interrupted by the growth of the Gondola anticline structure where seismic reflectors are characterized by truncations and onlap terminations (Figs. 3, 4a, b). The configuration and geometry of these seismic facies varies laterally. Southwards of the Gondola anticline, the Pliocene succession shows lateral low-amplitude and discontinuous reflectors to continuous and high-amplitude reflectors (Fig. 3). Locally, the Pliocene succession is characterized by truncated reflectors with a vertical displacement in the order of 10 ms, and a divergent reflector configuration. The seismic reflector stacking pattern changes vertically, highlighting the increasing presence of mounded reflector geometries in the upper part of the Pliocene succession (Fig. 4b). In this upper portion, the Pliocene succession can be subdivided into mounded-parallel reflector packages of 15 ms thickness and characterized by a convex-up reflector geometry, onlapping the southern flank of the Gondola anticline. Both the convex-up crest and convex-down low show an up-dip

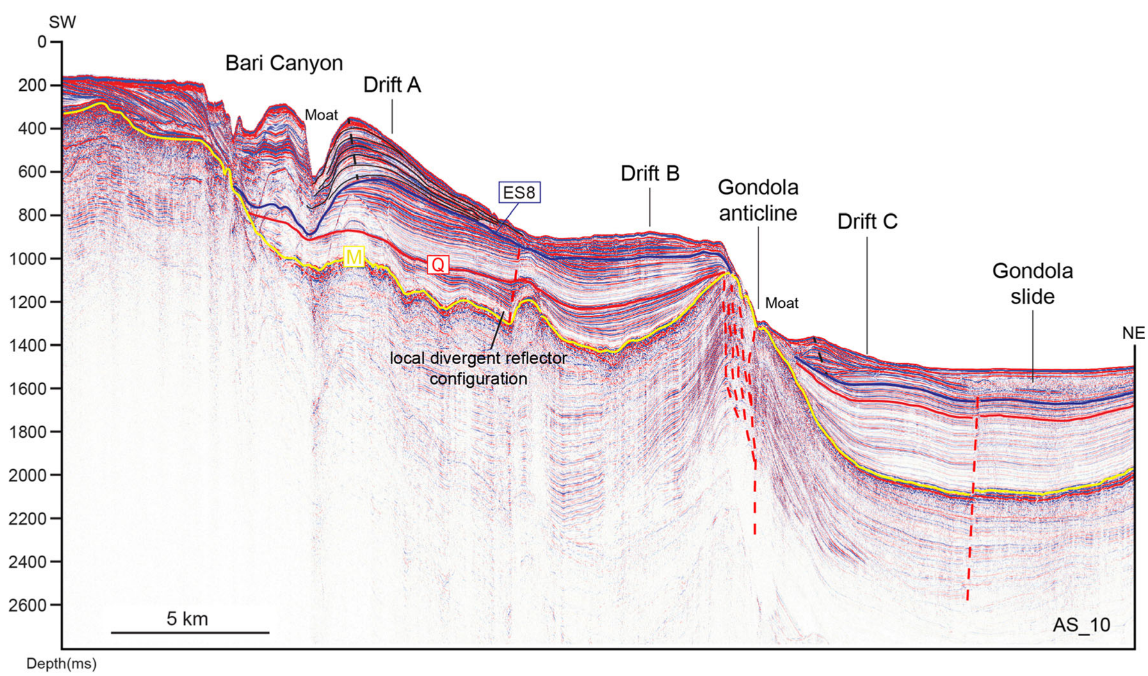

Fig. 3 Multichannel profile showing the deformed carbonate succession and the overlying Pliocene–Quaternary succession (*M reflector* top of carbonate succession, *Q reflector* base of Quaternary succession, *ES8* unconformity within Quaternary sequence). The *ES8* unconformity indicates strong erosion of the underlying strata and a net change in the stacking pattern of the stratigraphic succession. *Red dashed lines* Faults; in the Gondola anticline, fault scarps reach the seafloor. The Pliocene growth strata border the Gondola anticline and local small-scale structural high. The Quaternary succession is composed of sediment drifts of regional extent. Drift A forms the northern flank of the Bari Canyon. Note the upslope migration of the drift A and C complexes (*black dashed lines*)

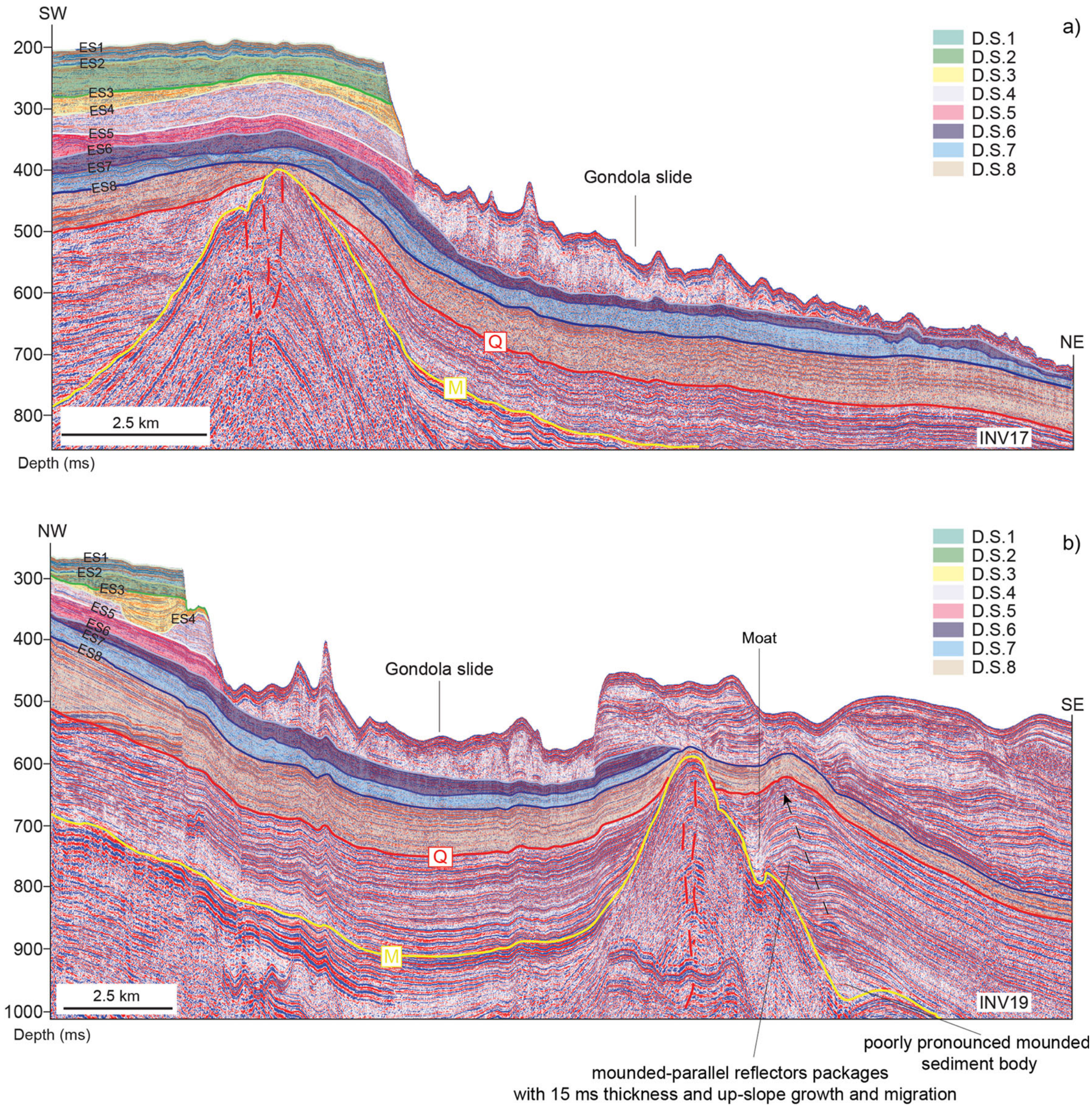

Fig. 4 **a** Multichannel seismic profile INV17 showing the influence of the Gondola anticline on the stacking pattern of the Pliocene–Quaternary succession. Depositional sequences 6 and 7 extend towards the basin whereas the overlying five depositional sequences reach the shelf edge and are truncated by the scarp of the Gondola slide. **b** Multichannel seismic profile INV19 showing a sediment drift formed against the southern flank of the Gondola anticline during the deposition of the Pliocene succession. *Red dashed lines* Faults. Note the change within the Pliocene succession from poorly pronounced mounded reflectors to mounded reflectors, the increasing number of bedforms within the Quaternary succession above the *ES8* unconformity, and the complex stacking pattern of the sequences on the shelf. The upper four depositional sequences coincide with those recognized by Ridente et al. (2007) on the Apulian shelf and in the central Adriatic (*D.S.* depositional sequence)

lateral migration towards the Gondola anticline crest (Fig. 4b).

The Pliocene succession fills the topographic lows of the Mesozoic–early Cainozoic succession and shows a predominantly mounded external geometry. The Pliocene succession appears to reflect the structural configuration, resulting in lateral variations in thickness from a few milliseconds on the Gondola anticline flanks, up to 400 ms towards the northern syncline lows (Figs. 3 and 4a, b).

SAM Quaternary succession

The Quaternary succession is bounded at the base by the Q reflector and by the modern seafloor on top (Figs. 3 and 4a, b). On the shelf and upper slope, the late Quaternary succession is internally subdivided by eight erosional unconformities labelled ES8 to ES1 progressively up-section. In the basin, only the deepest three depositional sequences (8 to 6) are preserved (Fig. 4a, b).

Depositional sequence 8, between the Q reflector and the ES8 unconformity, is characterized by sub-parallel and semi-continuous reflectors that show a vertical change from low- to high-amplitude seismic facies (Fig. 4a, b). Locally, the lateral continuity of the reflectors is interrupted by the presence of the Gondola anticline (Fig. 4b).

The depositional sequences 7 and 6, bounded respectively by ES8–ES7 and ES7–ES6 unconformities, are similar to depositional sequence 8 in terms of seismic amplitude and internal reflector geometry, with the exception that they cannot be correlated basinwards beyond the Gondola anticline (Fig. 4b). Depositional sequence 5 is bounded by the ES6 and ES5 unconformities at the base and top respectively, and is characterized by a high-amplitude seismic facies on the outer shelf with continuous and sub-parallel reflectors (Fig. 4a, b). Landwards, the reflectors of depositional sequence 5 display toplap truncations, while basinwards they are truncated by the head scarp of the Gondola slide. The Gondola slide cuts the margin sequences down to the ES6 unconformity, above which the slide deposit is characterized by low-amplitude seismic facies and discontinuous to chaotic reflectors (the Gondola slide; Fig. 4a, b).

On the slope and in the basin, the Quaternary succession is characterized by an overall sigmoidal to oblique reflector configuration and includes elongated mounds (drifts A, B and C in Fig. 3). Regional stratigraphic correlation between drifts A, B and C with depositional sequences developed on the shelf was hampered by the lateral discontinuity of the reflectors (Figs. 3 and 4a, b). Drift A is characterized by high-amplitude seismic facies passing to low-amplitude seismic facies in the trough area (Fig. 3). This drift has upward-convex reflectors with downlap terminations on the northern flank and truncated terminations on the southern flank, suggesting decreasing deposition and locally enhanced erosion. Internally, drift A is characterized by repeated downlap terminations that help identify packages of mounded-parallel reflectors. The crests of the mounded reflector packages have axes verging towards a moat (Fig. 3). Drift A has a thickness of up to 300 ms constituting the northern flank of the Bari Canyon (Fig. 3).

Drift B is characterized by high-amplitude seismic facies deposits with sub-parallel reflectors of overall mounded geometry (Figs. 3 and 5). Internally, this drift shows packages of discontinuous to chaotic reflectors interlayered with packages of continuous mounded reflectors (Fig. 5). Drift B is located on the southern flank of the Gondola anticline and reaches a maximum thickness of 150 ms (Fig. 5).

Drift C is characterized by high-amplitude seismic facies passing to low-amplitude seismic facies in the trough and toe areas (Fig. 3). This drift has mounded-parallel reflectors. Locally, the data reveal packages of undulating reflectors with wavelengths of up to 1.3 km and amplitudes of 50 ms, and with crests that show an upslope-verging axis. Drift C is located on the northern flank of the Gondola anticline and reaches a thickness of up to 200 ms (Fig. 3).

Unconformities ES4 to ES1 correlate with those recognized by Ridente et al. (2007) on the Apulian shelf and in the central Adriatic, and the depositional sequences 4 to 1 of the present work also coincide with those of Ridente et al. (2007). Depositional sequence 4 is bounded by the ES5 and ES4 unconformities at the base and top respectively (Fig. 4a, b). This depositional sequence is characterized by shingled continuous reflectors that are truncated basinwards against the modern edge scarp (Figs. 4a, b and 6a, b). There is a remarkable change in the stacking pattern from units 8–4 to units 3–1 resting above the pronounced erosional ES4 unconformity (Fig. 4b). The depositional sequences 3 to 1 are bounded by the ES4–ES3, ES3–ES2 and ES2–ES1 unconformities respectively (Figs. 4a, b and 6a, b). These depositional sequences are characterized by the presence of shingled, seaward-dipping reflectors and wavy reflectors locally truncated by the overlying unconformity (Fig. 6a, b). The wavy reflectors are characterized by a 100-m-scale wavelength and a 10-m-scale amplitude. The crests have landward-verging axes that document a consistent upslope migration of the sedimentary features. The reflectors dip and onlap consistently landwards compared to the incisions (towards W/SW; Fig. 6a, b).

Discussion

SAM contourite depositional system

Based on their seismic facies, internal stacking pattern, external drift morphology (Faugères et al. 1999; Rebesco and Stow 2001; Rebesco et al. 2014), as well as existing knowledge on the oceanographic setting and regional bathymetry (Trincardi et al. 2007b, 2014), the sedimentary bodies recognized along the SAM can be interpreted as contourite deposits. A large variety of erosional features are associated with contourite deposits, including large drift moats, scours and widespread discontinuities (Figs. 1, 3 and 6a, b). Contourite deposits and related erosional features have developed in the basin, along the slope and on the outer shelf, and include mounded drifts, separated drifts and shallow-water contourites (Figs. 3 and 6a, b).

The Pliocene succession is composed of a giant sediment drift, adjacent to a moat (Fig. 4b) that developed on the southern flank of the Gondola anticline at the modern water depth of 460–660 m (Fig. 7a). Comparable bottom-current deposits were recognized at the toe of structural highs in different continental margins, where an increase in shear stress and velocity is related to confinement of the flow against an obstacle (e.g. Van Rooij et al. 2010: Le Danois drift, Cantabrian margin; Martorelli et al. 2011: south-western seamount, Tunisian

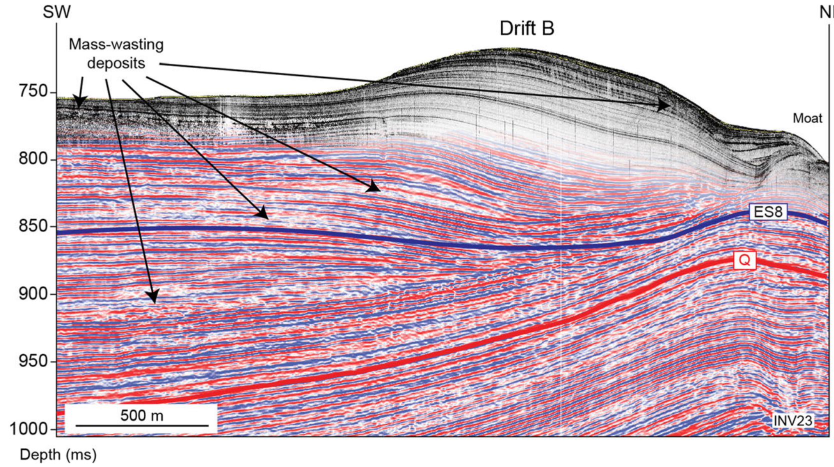

Fig. 5 Detail of sediment drift B on multichannel and chirp profiles. The superimposition of the two profiles helps identify the seismic facies of mass-transport deposits at depths not reached by the chirp profile (see Fig. 2 for profile location)

margin). As testified by their external geometry and orientation, drifts A, B and C are interpreted as upslope-migrating sediment drifts. Similar Quaternary examples come from different settings where, due to topographic constrictions, bottom currents reached velocities sufficient to erode and redistribute fine-grained sediments (Faugères et al. 1999; Roveri 2002; Ercilla et al. 2002; Verdicchio and Trincardi 2008a; Van Rooij et al. 2010). Drift A developed on the slope and is part of the northern flank of the Bari Canyon where cascading dense shelf water currents are laterally confined (Trincardi

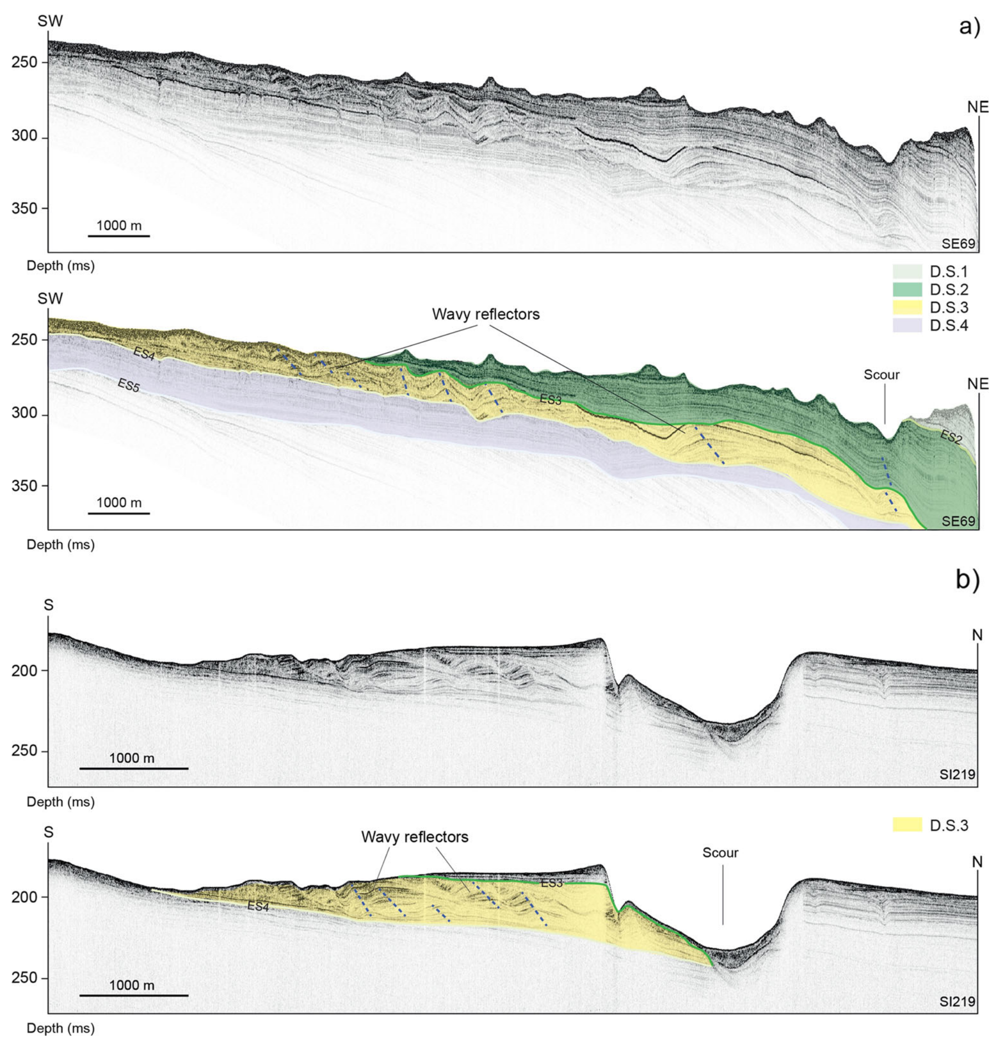

Fig. 6 **a, b** Chirp seismic profiles showing wavy and mounded reflectors within depositional sequences 3 and 2. Note the oblique-parallel reflectors within sequences older than sequence 3 (see Fig. 2 for profile locations). Also note the decreasing thickness of depositional sequences landwards (southwards), and the scour reflecting erosion by bottom currents. The upper four depositional sequences coincide with those recognized by Ridente et al. (2007) on the Apulian shelf and in the central Adriatic (*D.S.* depositional sequence)

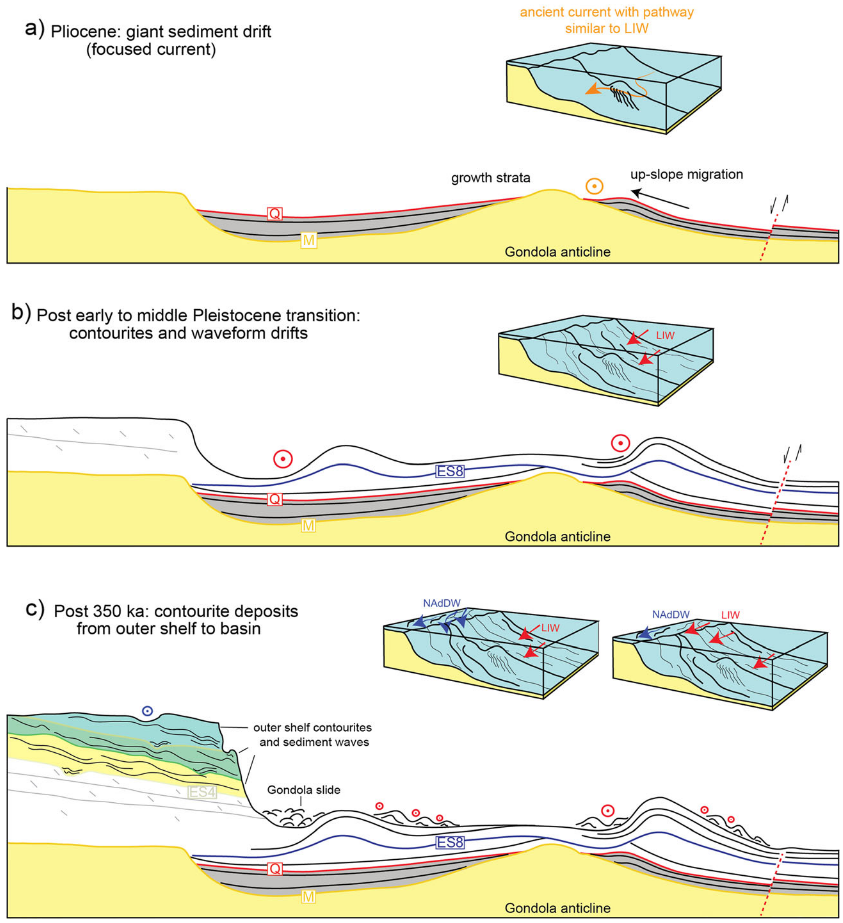

Fig. 7 Conceptual scheme of the Pliocene to Quaternary depositional history of the south-western Adriatic margin in a section from the outer shelf to the basin across the Gondola anticline. **a** Sediment drift within the Pliocene succession related to the onset of a bottom current (*orange arrow*) flowing close to the southern flank of the Gondola anticline. Note the contrasting stratal geometries within the Pliocene succession in the two sub-basins and their interaction with tectonics. **b** Change in the stacking pattern of Quaternary deposits above the ES8 unconformity (*blue line*). Note the growth of the contourite depositional system in a broader margin area, ascribed to the interplay of along-slope and down-slope currents (LIW and NAdDW respectively). **c** From the time of deposition of sequence 3, the bottom currents begin to affect a large portion of the outer shelf. Note that in this sector of the margin the bottom-current deposits constitute the bulk of the depositional sequences

et al. 2007b). Drifts B and C occur on both flanks of the Gondola anticline (Fig. 3); these separated drifts developed after the formation of the fault-generated relief of the Gondola anticline, a major obstacle in the travel of bottom waters towards the basin (Benetazzo et al. 2014). The presence of erosional features within drifts indicates repeated variations in the current intensity associated with oceanographic/climatic changes and local seafloor obstacles.

On the outer shelf the internal architecture of the depositional sequences reveals the presence of sediment wave deposits (Fig. 6a, b). These display a pronounced landward migration pattern and are interpreted as contour sediment waves of 100 m wavelength.

The complete system of contourite deposits and related erosional features of the SAM present characteristics similar to those of contourite depositional systems found worldwide on continental margins, and are the result of strong interactions between bottom-hugging current activity and irregular seafloor morphology. Key examples include the US Atlantic continental rise (Locker and Laine 1992), the Weddell Sea, Antarctica (Maldonado et al. 2005), the Argentina slope (Hernández-Molina et al. 2009), the Gulf of Cadiz (Llave et al. 2007) and the north Iberian margin (Van Rooij et al. 2010).

Pre-contourite depositional phase

The Pliocene succession immediately above the M surface shows a low-amplitude reflector deposit with a poorly pronounced mounded external geometry (Fig. 4b). This deposit records a pre-contourite depositional phase developed under weaker bottom-current activity. Similar deposits were recognized in the Algarve margin and interpreted as being associated with a pre-contourite sedimentation phase in the Early Pliocene succession (Llave et al. 2011), where the influence of down-slope sedimentary transport can not be excluded (Brackenridge et al. 2013).

Onset of bottom-current deposits and their evolution

Based on the available regional stratigraphic correlations, the onset of the bottom-current deposits along the SAM occurred during the Pliocene. The Pliocene sediment drift developed on the southern flank of the Gondola anticline and is characterized by packages of mounded-parallel reflectors that highlight the presence of contourite units (Fig. 4b). The stacking pattern of the contourite units with a typical thickness of 15 ms may suggest changes in bottom-current velocity and related sediment deposition, or intervals of oscillations in sediment supply with constant current activity (Mulder et al. 2013).

The upslope migration of the moat indicates a current flowing close to the southern flank of the Gondola structure, while the progressive increase in relief of the drift induces the upslope deflection of the bottom-current pathway. The development of the sediment drift is ascribed to a current with an anticlockwise pattern that, as a result of the Coriolis effect, was deflected towards the "right" side (i.e. against the flank of the Gondola anticline; Fig. 7a). The internal and external geometries of the Pliocene successions in the two sub-basins located north and south of the Gondola anticline (showing tabular packages and growth strata in the former setting, and contourite deposits in the latter) suggest contrasting bottom-current regimes affecting the two sub-basins, with a bottom-hugging current activity focused on the southern sub-basin (Fig. 7a).

The ES8 unconformity marks a major change in the stratigraphic evolution of the SAM, as suggested by the erosion of the underlying strata (especially in the Bari Canyon area; Fig. 3) and the spread of contourite deposits that are characterized by mounded and wavy strata (Figs. 4b and 7b). Assuming that the unconformities older than ES5 reflect sea-level oscillations at the Milankovitch scale with a 100,000 year periodicity, as recognized in the central Adriatic Basin (Ridente and Trincardi 2002; Ridente et al. 2009), the ES8 unconformity formed close to the early to middle Pleistocene transition at ca. 730/750 ka. Above the ES8 unconformity, a marked growth of large-scale mounded drifts characterized by an upslope migration highlights a major change in the stacking pattern of depositional sequences, plausibly explained by a change in the hydrodynamics of the basin (Fig. 7b). At a regional scale, these changes are associated with the onset and progressive increase in relief of drifts A, B and C at water depths of 300, 750 and 1,100 m respectively (Fig. 3). The upslope migration of the three drifts since the early to middle Pleistocene transition may be related to the modification of the LIW due to climatic/eustatic changes at Milankovitch timescales, as quantified for the Corsica channel area through sortable silt and stable isotope analyses (Toucanne et al. 2012).

The evidence of truncated and deformed reflectors in both sub-basins (on the northern flank of the Gondola anticline and beneath the Gondola slide; Fig. 3) confirms the tectonic activity during the Pleistocene and suggests a strong interaction between the Gondola slide and tectonic activity as highlighted by previous works (Minisini et al. 2006; Ridente et al. 2007). A close view of drift B reveals the presence of mass-wasting deposits interfingered with contourite units (Fig. 5). As interpreted in other settings, rapidly accumulated contourite drifts have often been associated with slumping phenomena due to the high water content, critical angle of deposition and the presence of weak layers (e.g. Laberg et al. 2003; Bryn et al. 2005; Kvalstad et al. 2005; Masson et al. 2006; Berndt et al. 2012; Ai et al. 2014; Cattaneo et al. 2014). In the case of drift B, moreover, the failure of the contourites may also be related to the activity of the Gondola anticline and related fault system, suggesting multi-event Pleistocene–Holocene tectonic activity. An extreme example is represented by drift C, which is almost entirely destroyed by the Gondola slide (Fig. 3).

These findings highlight an overall change of bottom-current activity through the Pliocene–Quaternary, with the development of multiple and perhaps more interchangeable current pathways impacting on a broader basin area (Fig. 7b). This current activity reflects a significant climatic reorganization after the early to middle Pleistocene transition when the 100,000 year cyclicity became dominant (Ruddiman et al. 1989). Furthermore, as pointed out by Selli (1965), an intensification of alpine glaciations occurred approximately 800 ka ago and records the onset of the so-called glacial Pleistocene in the Mediterranean region. On the SAM, the pacing of global Pleistocene climate oscillations is likely associated with changes in the strength and behaviour of thermohaline currents. These changes are highlighted by the progressive adjustment in the architectural pattern and by the changing growing style of the contourite and waveform deposits that developed in progressively shallower depths compared to the Pliocene drift deposit (Figs. 4b and 7b).

Onset of shallow-water contourites and their evolution

On the south-western Adriatic margin, the late Quaternary succession is composed of progradational deposits, each several tens of meters thick and separated by shelf-wide unconformities related to 100,000 year glacio-eustatic cycles (Ridente and Trincardi 2002; Ridente et al. 2009). The internal architecture of the three uppermost depositional sequences (D.S.1 to D.S.3, from top to bottom) shows, in particular, that shallow-water contourites constitute the bulk of each sequence, contributing significantly to the margin architecture and to the development of the south-western Adriatic contourite depositional system (Figs. 6a, b and 7c). The internal geometries of each depositional sequence, characterized by short-distance lateral variability in sedimentary architecture, may be related to changes in the strength and direction of bottom currents on the outer shelf in response to Quaternary climatic and oceanographic turnovers. As pointed out by several authors, sea-level changes at 100,000 year cyclicity governed the strength of the thermohaline circulation (e.g. Myers et al. 1998) and indirectly played a fundamental role in the development of shallow-water contourites (e.g. Viana et al. 1998; Verdicchio and Trincardi 2008b; Vandorpe et al. 2011).

In the SAM, in particular, the stratal pattern may reflect enhanced dense water formation in the northern Adriatic basin, and/or intervals of enhanced intrusion of the LIW towards the outer shelf with a lateral shift of the LIW–NAdDW interface. The shift of this interface towards shallower depths could be governed by eustatic cycles (Rogerson et al. 2012), which in turn affected the shift towards a shallower depth in the area where NAdDW is entrained with the LIW. Moreover, the internal complexity of each depositional sequence developed on the outer shelf may be related to changes in bottom-current strength and/or decrease in sediment supply. The presence of unconformities above each depositional sequence highlights the substantial reduction of accommodation space during relative sea-level fall, in turn leading to shallow-water erosion of contourite deposits accumulated during the preceding sea-level highstands (Fig. 6a, b). Moreover, these findings suggest the onset of current pathways similar to modern conditions, where the interplay of along-slope and down-slope (cascading) dense shelf water masses, impacting on a progressively broader margin area (extending to deeper and shallower depths), led to the development of sediment drifts with a patchy distribution (Fig. 7c).

Conclusions

The sequence stratigraphic analysis of bottom-current deposits along the Mediterranean margin and Mediterranean gateways helps identify the onset and evolution of sediment drifts, from which the associated bottom-water circulation can be inferred. These bottom-current deposits developed after the restoration of open marine conditions in the Mediterranean following the Messinian salinity crisis. On the south-western Adriatic margin, the formation of a contourite depositional system has been magnified in an area of complex slope morphology, where tectonic activity during the Pliocene–Quaternary has given rise to the slope-transverse Gondola anticline. This shows that:

- since the Pliocene a giant sediment drift migrated upslope, recording the ancestral LIW activity focused on the southern flank of the Gondola anticline;
- close to the early to middle Pleistocene transition, the impact of bottom currents spread to a broader slope area, leading to the generation of large-scale contourite deposits as well as upslope-migrating sediment waves and associated erosional moats;
- starting from ca. 350 ka (i.e. since the deposition of sequence 3), bottom currents affected for the first time a large portion of the outer shelf in shallow-water and more proximal settings, and bottom-current deposits constitute the bulk of the depositional sequences at Milankovitch timescales.

The progressive adjustment in the architectural pattern and the growing style of contourite deposits with a patchy distribution and different orientations seem to be related to the onset of a bottom-current pathway similar to the modern one that impacted on a broader and uneven seafloor morphology. It is possible that these bottom-current deposits reflect the activity of the Levantine Intermediate Water (today confined between 200 and 600 m but capable of intruding shallower shelf environments) and the onset of preferential pathways of the NAdDW that in part remains on the shelf without cascading obliquely to the slope.

Acknowledgements We would like to thank Giovanni Bortoluzzi and Valentina Ferrante for the acquisition and processing of the multichannel seismic lines Adriaseismic 2009. We are grateful to the editors B.W. Flemming and M.T. Delafontaine for their thoughtful comments that improved the readability of the manuscript, and to A. Viana and an anonymous reviewer for their comments on an earlier version of this article. This work was funded by the Flagship Project RITMARE - The Italian Research for the Sea, coordinated by the Italian National Research Council and funded by the Italian Ministry of Education, University and Research as part of the National Research Program 2011–2013. This is ISMAR-CNR contribution number 1875.

Conflict of interest The authors declare that there is no conflict of interest with third parties.

References

Ai F, Strasser M, Preu B, Hanebuth TJJ, Krastel S, Kopf A (2014) New constraints on oceanographic vs. seismic control on submarine landslide initiation: a geotechnical approach off Uruguay and northern Argentina. Geo-Mar Lett 34(5):399–417

Argnani A, Favali P, Frugoni F, Gasperini M, Ligi M, Marani M, Mattietti G, Mele G (1993) Foreland deformational pattern in the Southern Adriatic Sea. Ann Geofis 36(2):229–247

Argnani A, Rovere M, Bonazzi C (2009) Tectonics of the Mattinata fault, offshore south Gargano (southern Adriatic Sea, Italy): implications for active deformation and seismotectonics in the foreland of the Southern Apennines. Geol Soc Am Bull 121(9-10):1421–1440

Artegiani A, Paschini E, Russo A, Bregant D, Raicich F, Pinardi N (1997a) The Adriatic Sea general circulation. Part I: air–sea interactions and water mass structure. J Phys Oceanogr 27:1492–1514

Artegiani A, Paschini E, Russo A, Bregant D, Raicich F, Pinardi N (1997b) The Adriatic Sea general circulation. Part II: Baroclinic circulation structure. J Phys Oceanogr 27:1515–1532

Benetazzo A, Bergamasco A, Bonaldo D, Falcieri FM, Sclavo M, Langone L, Carniel S (2014) Response of the Adriatic Sea to an intense cold air outbreak: dense water dynamics and wave-induced transport. Progr Oceanogr 128:115–138

Berndt C, Costa S, Canals M, Camerlenghi A, de Mol B, Saunders M (2012) Repeated slope failure linked to fluid migration: the Ana submarine landslide complex, Eivissa Channel, Western Mediterranean Sea. Earth Planet Sci Lett 3(19):65–74

Billi A, Gambini R, Nicolai C, Storti F (2007) Neogene-Quaternary intraforeland transpression along a Mesozoic platform-basin margin: the Gargano fault system, Adria, Italy. Geosphere 3(1):1–15

Bonaldo D, Benetazzo A, Bergamasco A, Campiani E, Foglini F, Sclavo M, Trincardi F, Carniel S (2015) Interactions among Adriatic continental margin morphology, deep circulation and bedform patterns. Mar Geol (in press). doi:10.1016/j.margeo.2015.09.012

Brackenridge RE, Hernández-Molina FJ, Stow DAV, Llave E (2013) A Pliocene mixed contourite–turbidite system offshore the Algarve

Margin, Gulf of Cadiz: seismic response, margin evolution and reservoir implications. Mar Pet Geol 46:36–50

Bryn P, Berg K, Forsberg CF, Solheim A, Kvalstad TJ (2005) Explaining the Storegga slide. Mar Pet Geol 22:11–19. doi:10.1016/j.marpetgeo.2004.12.003

Canals M, Danovaro R, Heussner S, Lykousis V, Puig P, Trincardi F, Calafat A, de Madron XD, Palanques A, Sánchez-Vidal A (2009) Cascades in Mediterranean submarine grand canyons. Oceanography 22(1):26–43

Cattaneo A, Jouet G, Charrier S, Théreau E, Riboulot V (2014) Submarine landslides and contourite drifts along the Pianosa Ridge (Corsica Trough, Mediterranean Sea). In: Krastel S, Behrmann JH, Völker D, Stipp M, Berndt C, Urgeles R, Chaytor J, Huhn K, Strasser M, Harbitz CB (eds) Submarine mass movements and their consequences. Springer, Berlin, pp 435–445

Dalla Valle G, Gamberi F, Foglini F, Trincardi F (2015) The Gondola Slide: a mass transport complex controlled by margin topography (South-Western Adriatic Margin, Mediterranean Sea). Mar Geol 366:97–113

de Alteriis G (1995) Different foreland basins in Italy: examples from the central and southern Adriatic Sea. Tectonophysics 252(1):349–373

Ercilla G, Baraza J, Alonso B, Estrada F, Casas D, Farran M (2002) The Ceuta Drift, Alboran Sea, southwestern Mediterranean. Geol Soc Lond Mem 22(1):155–170

Faugères J-C, Stow DAV, Imbert P, Viana A (1999) Seismic features diagnostic of contourite drifts. Mar Geol 162(1):1–38

Foglini F, Campiani E, Trincardi F (2015) The reshaping of the South West Adriatic Margin by cascading of dense shelf waters. Mar Geol. doi:10.1016/j.margeo.2015.08.011

Fulthorpe CS, Carter RM (1991) Continental-shelf progradation by sediment-drift accretion. Geol Soc Am Bull 103(2):300–309

Hanebuth TJJ, Zhang W, Hofmann AL, Löwemark LA, Schwenk T (2015) Oceanic density fronts steering bottom-current induced sedimentation deduced from a 50 ka contourite-drift record and numerical modeling (off NW Spain). Quat Sci Rev 112:207–225

Heezen BC, Hollister CD (1964) Deep sea current evidence from abyssal sediments. Mar Geol 1:141–174

Heezen BC, Hollister CD, Ruddiman WF (1966) Shaping of the continental rise by deep geostrophic contour currents. Science 152:502–508

Hernández-Molina FJ, Llave E, Stow DAV, García M, Somoza L, Vázquez JT, Lobo F, Maestro A, Del Río VD, León R, Medialdea T, Gardner J (2006) The contourite depositional system of the Gulf of Cadiz: a sedimentary model related to the bottom current activity of the Mediterranean outflow water and its interaction with the continental margin. Deep-Sea Res II Top Stud Oceanogr 53(11):1420–1463

Hernández-Molina FJ, Paterlini M, Violante R, Marshall P, de Isasi M, Somoza L, Rebesco M (2009) Contourite depositional system on the Argentine Slope: an exceptional record of the influence of Antarctic water masses. Geology 37(6):507–510

Hernández-Molina FJ, Stow DAV, Alvarez-Zarikian CA, Acton G, Bahr A, Balestra B, Ducassou E, Flood R, Flores JA, Furota S, Grunert P, Hodell D, Jimenez-Espejo F, Kim JK, Krissek L, Kuroda J, Li B, Llave E, Lofi J, Lourens L, Miller M, Nanayama F, Nishida N, Richter C, Roque C, Pereira H, Sanchez Goñi MF, Sierro FJ, Singh AD, Sloss C, Takashimizu Y, Tzanova A, Voelker A, Williams T, Xuan C (2014) Onset of Mediterranean outflow into the North Atlantic. Science 344(6189):1244–1250

Howe JA (1996) Turbidite and contourite sediment waves in the northern Rockall Trough, North Atlantic Ocean. Sedimentology 43(2):219–234

Kvalstad TJ, Andresen L, Forsberg CF, Berg K, Bryn P, Wangen M (2005) The Storegga slide: evaluation of triggering sources and slide mechanics. Mar Pet Geol 22(1):245–256

Laberg JS, Vorren TO, Mienert J, Haflidason H, Bryn P, Lien R (2003) Preconditions leading to the Holocene Trænadjupet slide offshore Norway. In: Locat J, Mienert J, Boisvert L (eds) Submarine mass movements and their consequences. Springer, Dordrecht, pp 247–254

Lascaratos A, Roether W, Nittis K, Klein B (1999) Recent changes in deep water formation and spreading in the eastern Mediterranean Sea: a review. Progr Oceanogr 44(1):5–36

Llave E, Hernández-Molina FJ, Somoza L, Stow DAV, Del Río VD (2007) Quaternary evolution of the contourite depositional system in the Gulf of Cadiz. Geol Soc Lond, Spec Publ 276(1):49–79

Llave E, Matias H, Hernández-Molina FJ, Ercilla G, Stow DAV, Medialdea T (2011) Pliocene–Quaternary contourites along the northern Gulf of Cadiz margin: sedimentary stacking pattern and regional distribution. Geo-Mar Lett 31(5-6):377–390

Locker SD, Laine EP (1992) Paleogene-Neogene depositional history of the middle US Atlantic continental rise: mixed turbidite and contourite depositional systems. Mar Geol 103(1):137–164

Maldonado A, Barnolas A, Bohoyo F, Escutia C, Galindo-Zaldívar J, Hernández-Molina FJ, Jabaloy A, Lobo FJ, Nelson CH, Fernández JR, Somoza L, Vázquez JT (2005) Miocene to recent contourite drifts development in the northern Weddell Sea (Antarctica). Glob Planet Chang 45(1):99–129

Mantziafou A, Lascaratos A (2008) Deep-water formation in the Adriatic Sea: interannual simulations for the years 1979–1999. Deep-Sea Res I Oceanogr Res Pap 55(11):1403–1427

Marani M, Argnani A, Roveri M, Trincardi F (1993) Sediment drifts and erosional surfaces in the central Mediterranean: seismic evidence of bottom-current activity. Sediment Geol 82:207–220

Martorelli E, Falcini F, Salusti E, Chiocci FL (2010) Analysis and modeling of contourite drifts and contour currents off promontories in the Italian Seas (Mediterranean Sea). Mar Geol 278(1):19–30

Martorelli E, Petroni G, Chiocci FL, the Pantelleria Scientific Party (2011) Contourites offshore Pantelleria Island (Sicily Channel, Mediterranean Sea): depositional, erosional and biogenic elements. Geo-Mar Lett 31(5-6):481–493

Maselli V, Trincardi F, Cattaneo A, Ridente D, Asioli A (2010) Subsidence pattern in the central Adriatic and its influence on sediment architecture during the last 400 kyr. J Geophys Res Solid Earth 115, B12106. doi:10.1029/2010JB007687

Masson DG, Harbitz CB, Wynn RB, Pedersen G, Løvholt F (2006) Submarine landslides: processes, triggers and hazard prediction. Philos Trans R Soc A Math Phys Eng Sci 364(1845):2009–2039

Minisini D, Trincardi F, Asioli A (2006) Evidence of slope instability in the Southwestern Adriatic Margin. Nat Hazards Earth Syst Sci 6(1):1–20

Miramontes E, Cattaneo A, Jouet G, Garziglia S, Thereau E, Gaillot A, Roubi A, Rovere M (2014) The Pianosa Contourite Depositional System (Corsica Trough, North Tyrrhenian Sea): stratigraphic evolution and possible role in slope instability. http://www.vliz.be/imisdocs/publications/263956.pdf. Accessed 10 September 2014

Mulder T, Hassan R, Ducassou E, Zaragosi S, Gonthier E, Hanquiez V, Marchès E, Toucanne S (2013) Contourites in the Gulf of Cadiz: a cautionary note on potentially ambiguous indicators of bottom current velocity. Geo-Mar Lett 33(5):357–367

Myers PG, Haines K, Josey S (1998) On the importance of the choice of wind stress forcing to the modeling of the Mediterranean Sea circulation. J Geophys Res Oceans 103(C8):15729–15749

Piva A, Asioli A, Trincardi F, Schneider RR, Vigliotti L (2008a) Late-Holocene climate variability in the Adriatic Sea (Central Mediterranean). The Holocene 18(1):153–167

Piva A, Asioli A, Schneider RR, Trincardi F, Andersen N, Colmenero-Hidalgo E, Bernard D, Flores JA, Vigliotti L (2008b) Climatic cycles as expressed in sediments of the PROMESS1 borehole PRAD1-2, central Adriatic, for the last 370 ka: 1. Integrated stratigraphy.

Geochem Geophys Geosyst 9, Q01R01. doi:10.1029/2007GC001713
Rebesco M, Camerlenghi A (eds) (2008) Contourites. Developments in Sedimentology, vol 60. Elsevier, Amsterdam
Rebesco M, Stow D (2001) Seismic expression of contourites and related deposits: a preface. Mar Geophys Res 22(5-6):303–308
Rebesco M, Hernández-Molina FJ, Van Rooij D, Wåhlin A (2014) Contourites and associated sediments controlled by deep-water circulation processes: state-of-the-art and future considerations. Mar Geol 352:111–154
Ridente D, Trincardi F (2002) Eustatic and tectonic control on deposition and lateral variability of Quaternary regressive sequences in the Adriatic basin (Italy). Mar Geol 184(3-4):273–293
Ridente D, Foglini F, Minisini D, Trincardi F, Verdicchio G (2007) Shelf-edge erosion, sediment failure and inception of Bari Canyon on the Southwestern Adriatic Margin (Central Mediterranean). Mar Geol 246(2):193–207
Ridente D, Trincardi F, Piva A, Asioli A (2009) The combined effect of sea level and supply during Milankovitch cyclicity: evidence from shallow-marine $\delta^{18}O$ records and sequence architecture (Adriatic margin). Geology 37(11):1003–1006
Rogerson M, Bigg GR, Rohling EJ, Ramirez J (2012) Vertical density gradient in the eastern North Atlantic during the last 30,000 years. Clim Dyn 39(3-4):589–598
Roveri M (2002) Sediment drifts of the Corsica Channel, northern Tyrrhenian Sea. Geol Soc Lond Mem 22:191–208
Ruddiman WF, Raymo M, Martinson DG, Clement BM, Backman J (1989) Pleistocene evolution: northern hemisphere ice sheets and North Atlantic Ocean. Paleoceanography 4(4):353–412
Savini A, Corselli C (2010) High-resolution bathymetry and acoustic geophysical data from Santa Maria di Leuca Cold Water Coral province (Northern Ionian Sea–Apulian continental slope). Deep-Sea Res II Top Stud Oceanogr 57(5):326–344
Selli R (1965) The Pliocene-Pleistocene boundary in Italian marine sections and its relationship to continental stratigraphies. Prog Oceanogr 4:67–86
Stow DAV, Faugères JC, Viana AR, Gonthier E (1998) Fossil contourites: a critical review. Sediment Geol 115:3–31
Toucanne S, Jouet G, Ducassou E, Bassetti MA, Dennielou B, Minto'o CMA, Lahmi M, Touyet N, Charlier K, Lericolais G, Mulder T (2012) A 130,000-year record of Levantine Intermediate Water flow variability in the Corsica Trough, western Mediterranean Sea. Quat Sci Rev 33:55–73
Trincardi F, Verdicchio G, Miserocchi S (2007a) Seafloor evidence for the interaction between cascading and along-slope bottom water masses. J Geophys Res Earth Surf 112, F03011. doi:10.1029/2006JF000620
Trincardi F, Foglini F, Verdicchio G, Asioli A, Correggiari A, Minisini D, Piva A, Remia A, Ridente D, Taviani M (2007b) The impact of cascading currents on the Bari Canyon System, SW-Adriatic Margin (Central Mediterranean). Mar Geol 246(2):208–230
Trincardi F, Campiani E, Correggiari A, Foglini F, Maselli V, Remia A (2014) Bathymetry of the Adriatic Sea: the legacy of the last eustatic cycle and the impact of modern sediment dispersal. J Maps 10(1): 151–158
Turchetto M, Boldrin A, Langone L, Miserocchi S, Tesi T, Foglini F (2007) Particle transport in the Bari canyon (southern Adriatic Sea). Mar Geol 246(2):231–247
Van Rooij D, Iglesias J, Hernández-Molina FJ, Ercilla G, Gomez-Ballesteros M, Casas D, Llave E, De Hauwere A, Garcia-Gil S, Acosta A, Henriet JP (2010) The Le Danois Contourite Depositional System: interactions between the Mediterranean outflow water and the upper Cantabrian slope (North Iberian margin). Mar Geol 274(1):1–20
Vandorpe TP, Van Rooij D, Stow DAV, Henriet J-P (2011) Pliocene to Recent shallow-water contourite deposits on the shelf and shelf edge off south-western Mallorca, Spain. Geo-Mar Lett 31(5-6):391–403
Verdicchio G, Trincardi F (2008a) Mediterranean shelf-edge muddy contourites: examples from the Gela and South Adriatic basins. Geo-Mar Lett 28(3):137–151
Verdicchio G, Trincardi F (2008b) Shallow-water contourites. In: Rebesco M, Camerlenghi A (eds) Contourites, vol 60, Developments in sedimentology. Elsevier, Amsterdam, pp 409–433
Verdicchio G, Trincardi F, Asioli A (2007) Mediterranean bottom-current deposits: an example from the Southwestern Adriatic Margin. Geol Soc Lond, Spec Publ 276(1):199–224
Viana AR, Faugères JC, Stow DAV (1998) Bottom-current-controlled sand deposits a review of modern shallow- to deep-water environments. Sediment Geol 115(1):53–80

7) Conclusion

This dissertation offers an improved understanding of the evolution of the Adriatic Basin during the Quaternary, in particular focusing on how changes in river hydrodynamics, accommodation (eustatism, tectonic activity and sediment compaction) and climate (sediment flux and oceanographic regime) controlled sediment transport and continental margin growth. To reach this goal, my Ph.D. work focused on four case histories along an hypothetical sediment routing system, from the modern Po River (chapter 3), down to the Adriatic continental shelf (chapters 4 and 5), and basin (chapter 6).

The first case history is a portion of the Po River used as a natural laboratory to quantify how the backwater effect created by a dam-induced reservoir controls river hydrodynamics, sediment transport and river morphodynamic evolution, without introducing assumptions on the effect of waves and tides. The data show that lateral migration rates strongly decrease across the backwater zone due to a reduction of flow velocity and bed shear stress; this hydrodynamic condition promoted the deposition of coarse-grained material, moving upstream the gravel-sand transition of the river. Further downstream, close to the dam, river bed sediments are progressively finer, up to clay size, while river bedforms become progressively wider due to a combination of decreased flow velocity and sediment grain size. The results obtained may be used for a better understanding of the morphodynamic evolution of rivers, deltas and estuaries.

In the second case history, from the central Adriatic shelf (chapter 4), the Po River lowstand wedge accumulated between 31.8 and 14.4 kyr B with a 350-m-thick succession during repeated phases of progradation, aggradation and degradation on millennial scale (1-3 kyr). Thanks to the extremely high spatial and temporal resolutions achieved, the findings from the Po River lowstand clinothems highlight that sand bypass toward the basin, expected principally during periods of sea level fall and lowstand, is not steady even on a very short-lived lowstand (ca. 15 kyr in duration): high-frequency base level oscillations may force the development of sandy deposits separated by flooding surfaces and relatively thick muddy clinothems promoting the compartmentalization of potential reservoirs.

In the third case history, from the area offshore Gargano Promontory (chapter 5), late Pleistocene to Holocene mid-shelf deposits document the first case of a compound delta developed within a short-time window during the post glacial sea level rise. The scientific literature on worldwide modern continental margin so far has documented the presence of these deposits only in highstand conditions, and so above the maximum flooding surface. Offshore the Gargano Promontory, a compound delta system (PGCD) is documented as part of a landward backstepping transgressive unit; this compound delta is characterized by a sandy coastal unit up to 10 m and by a genetically-linked subaqueous muddy clinothem up to 30-m-thick. The rapid formation of the PGCD (between ca. 11.8-12.6 kyr BP) implies that the maximum time required for the development of this kind of deltaic deposit is in the order of just few centuries. This notion may be useful when interpreting ancient stratigraphic records where a much lower chronological resolution available may lead to assume or imply much slower sediment accumulation rates. Moreover, the finding from the PGCD provides the opportunity for a comparison with modern compound systems and gives the possibility to extract information on the paleo-oceanographic regime. In this view, the PGCD may be viewed as the transgressive, smaller-scale, analogue of the modern highstand Adriatic compound delta, as both records reflect progradations influenced by similar southward-directed alongshore sediment dispersion with transport occurring dominantly along the strike of the clinoform with limited exploitment of accommodation in the topset region. The comparison of the external geometry of both systems, characterized by a vertical distance of ca. 25 m between the coastal and subaqueous rollovers, suggests that during the deposition of such compound progradations the oceanographic regime was characterized by a wave-current field similar to the modern one. Conversely to the modern Po-Adriatic compound delta that is characterized by a continuous depocenter, the PGCD and the overall distribution of the middle TST unit, highlight the presence of distinct depocenters along the Italian coast indicating that an along-shore sediment dispersal similar to the modern one was already active but either without reaching a competence similar to the modern one or not receiving enough sediment from the continent to allow the creation of a continuous depocenter along hundreds of kilometers as in the case of the late-Holocene. Finally, the finding from the PGCD, in agreement with documentation from the literature, suggests that subaqueous deltas are always connected to a coastal deposit, characterized by a coastal rollover point that may be interpreted as the genetically-linked subaerial counterpart of a subaqueous progradation. The coastal deposit may constitute the geometrically and genetically linked coarser-grained reservoir of hydrocarbons migrating from the muddy and potentially organic-rich subaqueous counterpart. This concept may be useful when interpreting lower resolution seismic profiles where the spatial relation between coastal and subaqueous correlative deposits may remain more difficult to establish.

In the fourth case history, from the southern Adriatic Basin (chapter 6), the study of the south-western Adriatic contourite depositional system developed since the Pliocene provides the opportunity to reconstruct the current pathway on a longer-term perspective. Three main phases of margin growth were recognized, each characterized by specific current pathways and, possibly, intensity: during the Pliocene a cyclonic circulation along a pattern similar to the modern Levantine Intermediate Water interacted with the paleo-morphology of the basin, characterized by two sub-basins northward and southward of the slope transverse Gondola anticline. The impact of the bottom currents was initially focused prevalently on the down-current zone, the southern sub-basin, where a sediment drift up to 230-m-thick developed; a successive phase of margin growth reflects a significant climatic reorganization during the early to middle Pleistocene transition, when bottom currents spread to invest a broader slope area, leading to the generation of large-scale contourite deposits as well as upslope-migrating sediment waves, resulting from the interplay of the Levantine Intermediate Water and the North Adriatic Dense Water. During the phase of margin growth that onset at ca. 350 kyr, bottom currents impacted on the outer shelf, likely in response to an excess in buoyancy (loss of salt content or increase in water temperature), and contourite deposits became a significant contribution to the bulk of the progradational sequences that record a 100 kyr cyclicity, promoting the shelf progradation by accretion of successive contourite drift. In conclusion, it seems that a dominant cyclonic Adriatic circulation pattern (related to a water mass like the modern Levantine Intermediate

Water) was well established by Pliocene time and during the climatic reorganization close to the early to middle Pleistocene transition. The sediment drift development was possible under this paleoceanographic regime because large volumes of sediment were introduced to the region (off-shelf marginal platform). This finding highlights that far from a feeding system, the accretion of sediment drifts within shelf-margin clinoforms may represent a significant contribution to the margin growth and in turn govern the final architectural motif of the margin. The contourite deposits of the south Adriatic margin developed during short-time intervals and with high sediment accumulation rates; this evidence, combined with the fine-grained lithology of the deposits and their very high water content, promoted the instability of the margin and the formation of repeated thin-skinned landslides, suggesting that contourite deposits contain potential weak layers or promote failure through rapid compaction and fluid escape processes. Sediment drifts located above drowned carbonate platforms, as in the case of the Pliocene sediment drift, possibly comprise an interesting hydrocarbon play. The sediment drifts, located on the flank of a structural relief, are well placed to intercept hydrocarbons migrating from underlying carbonate source beds. Furthermore, these deposits have depositional closures and may be capped by muds. If clean sands are present, drifts of this type have reservoir potential and may be worthwhile exploration targets in some basins.

In all of the three case histories focus on Adriatic depositional basins (chapter 4-6), the depositional history can be constrained by a very-high chronological framework that allows documentation of short-lived phases of extremely rapid deposition during the margin construction. A common depositional motif is the growth of clinothems, which appears as a key recorder of the interaction of the main factors introduced above, and in particular records the interplay between high-frequency base-level and paleo-oceanographic fluctuations. Moreover, the presence of thick and expanded successions (clinothems developed up to hundreds of meters in thickness during intervals of only few thousands of years), allows to depict short-lived base-level and climatic variations at sub-Milankovitch time scales. Dramatic fluctuations in sediment supply coupled with high-frequency base-level variations played a crucial role in determining stratal geometry of a river-dominated system by controlling sediment transport across the shelf, as well as phases of bypass off the shelf-edge and the timing of the storage of coarse-grained sediment in the basin (chapter 4). A short-lived increase in sediment flux during a still-stand that punctuated the post-glacial sea level rise accompanied by substantial lateral advection of sediment, played a fundamental role in determining an asymmetrical compound delta on the mid-shelf during the Younger Dryas, mimicking (in internal stratal geometry and spatial distribution) the modern Po River delta and its genetically-linked subaqueous prodelta system (chapter 5). Advection played also a crucial role on sediment routing along the outer shelf and slope of the southern Adriatic basin, promoting the development of shallow-water contourite deposits intermingled with prograding clinoforms (chapter 6).

8) References

Aksu, A.E., Hiscott, R.N., Yas, D., Is, F.I., 2002. Seismic stratigraphy of Late Quaternary deposits from the southwestern Black Sea shelf: evidence for non-catastrophic variations in sea-level during the last ca. 10,000 yr. Mar. Geol. 190, 61–94.

Alexander, C.R., DeMaster, D.J., Nittrouer, C.A., 1991. Sediment accumulation in a modern epicontinental-shelf setting: The Yellow Sea. Marine Geology 98, 51-72.

Amorosi, A., Milli, S., 2001. Late Quaternary depositional architecture of Po and Tevere river deltas (Italy) and worldwide comparison with coeval deltaic successions. Sedimentary Geology, 144 (3), 357-375.

Amorosi, A., Colalongo, M. L., 2005. The linkage between alluvial and coeval nearshore marine successions: evidence from the Late Quaternary record of the Po River Plain, Italy. Fluvial Sedimentology VII, 255-275.

Amorosi, A., Centineo, M. C., Colalongo, M. L., Fiorini, F., 2005. Millennial-scale depositional cycles from the Holocene of the Po Plain, Italy. Marine Geology, 222, 7-18.

Amorosi, A., Maselli, V., and Trincardi, F., in press: Onshore to offshore anatomy of a late Quaternary sourc to-sink system (Po Plain-Adriatic Sea, Italy): Earth Science Review.

Anderson, J. B., and Rodriguez, A., B., 2008. Response of Upper Gulf Coast Estuaries to Holocene Climate Change and Sea-Level Rise, 146 pp., Geol. Soc. of Am., Boulder, Colo.

Argnani, A., Favali, P., Frugoni, F., Gasperini, M., Ligi, M., Marani, M., Mattietti, G., Mele, G., 1993. Foreland deformational pattern in the Southern Adriatic Sea. Ann. Geofis. 36 (2), 229–247.

Argnani, A., Frugoni, F., Cosi, R., Ligi, M., Favali, P., 2001. Tectonics and seismicity of the ApulianRidge south of Salento peninsula (Southern Italy).Annals of Geophysics, 44(3).

Argnani, A., Rovere, M., Bonazzi, C., 2009. Tectonics of the Mattinata fault, offshore south Gargano (southern Adriatic Sea, Italy): Implications for active deformation and seismotectonics in the foreland of the Southern Apennines.Geological Society of America Bulletin, 121(9-10), 1421-1440.

Artegiani A, Paschini E, Russo A, Bregant D, Raicich F, Pinardi N., 1997a. The Adriatic Sea general circulation. Part I: air–sea interactions and water mass structure. J Phys Oceanogr 27:14921514.

Artegiani A, Paschini E, Russo A, Bregant D, Raicich F, Pinardi N., 1997b. The Adriatic Sea general circulation. Part II: Baroclinic circulation structure. J Phys Oceanogr 27:1515–1532.

Artegiani, A., Salusti, E., 1987. Field observations of the flow of dense water on the bottom of the Adriatic Sea during the winter of 1981. Oceanol. Acta 10 (4), 387–391.

Bard, E., Hamelin, B., Fairbanks, R. G., 1990. U-Th ages obtained by mass spectrometry in corals from Barbados: sea level during the past 130, 000 years. Nature, 346(6283), 456-458.

Benetazzo, A., Bergamasco, A., Bonaldo, D., Falcieri, F.M., Sclavo,M., Langone, L., Carniel, S., 2014. Response of the Adriatic Sea to an intense cold air outbreak: dense water dynamics and wave-induced transport. Prog. Oceanogr. 128, 115–138; doi: org/10.1016/j.pocean.2014.08.015.

Bassetti, M. A., Berne, S., Jouet, G., Taviani, M., Dennielou, B., Flores, J. A., Sultan, N., 2008. The 100-ka and rapid sea level changes recorded by prograding shelf sand bodies in the Gulf of Lions (western Mediterranean Sea).Geochemistry, Geophysics, Geosystems, 9(11).

Berger, A., Loutre, M. F., 1991. Insolation values for the climate of the last 10 million years. Quaternary Science Reviews, 10(4), 297-317.

Berné, S., Jouet, G., Bassetti, M.A., Dennielou, B., Taviani, M., 2007. Late Glacial Preboreal sea-level rise recorded by the Rhône deltaic system (NW Mediterranean). Marine Geology 245, 65–88.

Bertotti, G., Casolari, E., and Picotti, V., 1999, The Gargano Promontory: A Neogene contractional belt within the Adriatic plate: Terra Nova, v. 11, p. 168–173, doi:10.1046/j.1365-3121.1999.00243.x.

Bhattacharya, J. P. and Giosan, L., 2003. Wave-influenced deltas: geomorphological implications for facies reconstruction. Sedimentology 50, 187–210.

Billi, A., Salvini, F., 2000. Sistemi di fratture associati a faglie in rocce carbonatiche: nuovi dati sull'evoluzione tettonica del Promontorio del Gargano. Boll. Soc. Geol. It. 119, 237–250.

Blum, M. D., and T. E. Törnqvist (2000), Fluvial responses to climate and sea-level change: A review and look forward, Sedimentology, 47, 2–48, doi:10.1046/j.1365-3091.2000.00008.x.

Bonaldo, D., Benetazzo, A., Sclavo, M., Carniel, S., 2015. Modelling wave-driven sediment transport in a changing climate: a case study for northern Adriatic Sea (Italy). Regional Environmental Change, 15(1), 45-55.

Bond, G., Showers, W., Cheseby, M., Lotti, R., Almasi, P., Priore, P., Bonani, G., 1997. A pervasive millennial-scale cycle in North Atlantic Holocene and glacial climates. science, 278(5341), 1257-1266.

Bourne, A.J., Lowe, J.J., Trincardi, F., Asioli, A., Blockley, S.P.E., Wulf, S. Matthews, I.P. Piva, A., Vigliotti, L., 2010. Distal tephra record for the last ca 105,000 years from core PRAD 1-2 in the central Adriatic Sea: implications for marine tephrostratigraphy. Quaternary Science Reviews v. 29, p. 3079-3094.

Bryn P, Berg K, Forsberg CF, Solheim A, Kvalstad TJ, 2005 Explaining the Storegga slide. Mar Pet Geol 22:11–19. doi:10.1016/j.marpetgeo.2004.12.003.

Bullimore, S., Henriksen, S., Liestøl, F. M., Helland-Hansen, W., 2005. Clinoform stacking patterns, shelf-edge trajectories and facies associations in Tertiary coastal deltas, offshore Norway: Implications for the prediction of lithology in prograding systems. Norwegian Journal of Geology/Norsk Geologisk Forening, 85.

Cacho, I., Shackleton, N., Elderfield, H., Sierro, F. J., Grimalt, J. O., 2006. Glacial rapid variability in deep-water temperature and δ 18 O from the Western Mediterranean Sea. Quaternary Science Reviews, 25(23), 3294-3311.

Camoin, G. F., Seard, C., Deschamps, P., Webster, J. M., Abbey, E., Braga, J. C., Dussouillez, P., 2012. Reef response to sea-level and environmental changes during the last deglaciation: Integrated Ocean Drilling Program Expedition 310, Tahiti Sea Level. Geology, 40(7), 643-646.

Canals, M., Danovaro, R., Heussner, S., Lykousis, V., Puig, P., Trincardi, F., Calafat, A.M., de Madron, X.D., Palanques, A., Sanchez-Vidal, A., 2009. Cascades in Mediterranean submarine grand canyons. Oceanography 22 (1), 26–43.

Capuano, N., Pappafico, G., Augelli, G., 1996. Ricostruzione dei sistemi deposizionali plio-pleistocenici del margine settentrionale dell’avanfossa pugliese. Mem. Soc. Geol. It, 51(1), 273-293.

Carter, R. M., Naish, T. R., 1998. A review of Wanganui Basin, New Zealand: global reference section for shallow marine, Plio–Pleistocene (2.5–0 Ma) cyclostratigraphy. Sedimentary geology, 122(1), 37-52.

Cattaneo A., Trincardi F., 1999. The late-Quaternary transgressive record in the Adriatic epicontinental sea: basin widening and facies partitioning. Society for Sedimentary Geology Special Publication 64, 127-146.

Cattaneo, A., Correggiari, A., Langone, L., Trincardi, F., 2003. The late-Holocene Gargano subaqueous delta, Adriatic shelf: sediment pathways and supply fluctuations. Mar. Geol. 193, 61–91.

Cattaneo, A., and Steel, R. J., 2003. Transgressive deposits: a review of their variability. Earth-Science Reviews, 62 (3), 187-228.

Cattaneo, A., Trincardi, F., Asioli, A., Correggiari, A., 2007. The Western Adriatic Shelf Clinoform: Energy-limited bottomset. Continental Shelf Research 27, 506-525.

Cattaneo A, Jouet G, Charrier S, Théreau E, Riboulot V, 2014. Submarine landslides and contourite drifts along the Pianosa Ridge (Corsica Trough, Mediterranean Sea). In: Krastel S, Behrmann JH, Völker D, Stipp M, Berndt C, Urgeles R, Chaytor J, Huhn K, Strasser M, Harbitz CB (eds) Submarine mass movements and their consequences. Springer, Berlin, pp 435–445

Catuneanu, O., Abreu, V., Bhattacharya, J. P., Blum, M. D., Dalrymple, R. W., Eriksson, P. G., Winker, C., 2009. Towards the standardization of sequence stratigraphy. Earth-Science Reviews, 92(1), 1-33.

Chapman, M. R., Shackleton, N. J., 1998. Millennial-scale fluctuations in North Atlantic heat flux during the last 150,000 years. Earth and Planetary Science Letters, 159(1), 57-70.

Chappell, J., Shackleton, N., 1986. Oxygen isotopes and sea level. Nature, doi: 10.1038/324137a0.

Chatanantavet, P., M. P. Lamb, and J. A. Nittrouer, 2012. Backwater controls on avulsion location on deltas, Geophys. Res. Lett., doi:10.1029/ 2011GL050197.

Chow, V. T., 1959. Open-Channel Hydraulics, 680 pp., McGraw-Hill, New York.

Covault, J.A., and Graham, S.A., 2010. Submarine fans at all sea-level stands: tectono-morphologic and climatic controls on terrigenous sediment delivery to the deep sea: Geology, v. 38(10), p. 939-942.

Cushman-Roisin, B., Gacic, M., Poulain, P. M., Artegiani, A., 2001. Physical oceanography of the Adriatic Sea, past, present and future. Cushman-Roisin et al., eds, pp. 304.

D'argenio, B., Horvath, F., 1984. Some remarks on the deformation history of Adria, from the Mesozoic to the Tertiary. In Annales geophysicae (Vol. 2, No. 2, pp. 143-146). Gauthier-Villars.

De Alteriis, G., 1995, Different foreland basins in Italy: Examples from the central and southern Adriatic Sea: Tectonophysics, v. 252, p. 349–373, doi: 10.1016/0040-1951(95)00155-7.

Doglioni, C., Mongelli, F., and Pieri, P., 1994, The Puglia uplift (SE Italy): An anomaly in the foreland of the Apenninic subduction due to buckling of a thick continental lithosphere: Tectonics, v. 13, p. 1309–1321, doi:10.1029/94TC01501.

Emiliani C., 1955. Pleistocene temperatures. J. Geol. 63, 538- 578.

Fagherazzi, S., Howard, A.D., Wiber, P.L., 2004. Modeling fluvial erosion and deposition on continental shelves during sea level cycles. Journal of Geophysical Research 109, F03010.

Fairbanks, R. G., 1989. A 17, 000-year glacio-eustatic sea level record: influence of glacial melting rates on the Younger Dryas event and deep-ocean circulation. Nature, 342(6250), 637-642.

Fanget, A., S., Berné, S., Jouet, G., Bassetti, M.A., Dennielou, B., Maillet, G.M., Tondut, M., 2014. Impact of relative sea level and rapid climate changes on the architecture and lithofacies of the Holocene Rhone subaqueous delta (Western Mediterranean Sea). Sediment. Geol. 305, 35–53.

Faugères J-C, Stow DAV, Imbert P, Viana A. 1999. Seismic features diagnostic of contourite drifts. Mar Geol 162(1):1–38.

Florineth, D., Schluchter, C., 1998. Reconstructing the Last Glacial Maximum (LGM) ice surface geometry and flowlines in the Central Swiss Alps. Eclogae Geologicae Helvetiae, v. 91(3), p. 391-407.

Foglini, F., Campiani, E., Trincardi, F., 2015. The reshaping of the South West Adriatic Margin by cascading of dense shelf waters. Marine Geology.

Frignani, M., Langone, L., Pacelli, M., Ravaioli, M., 1992. Input, distribution and accumulation of dolomite in sediments of the Middle Adriatic Sea. Rapp. CIESM, 33, 324.

Giraudi, C., 2011. Middle Pleistocene to Holocene glaciations in the Italian Apennines. Developments in Quaternary Science, v. 15, p. 211-219.

Gervais, A., Savoye, B., Mulder, T., Gonthier, E., 2006. Sandy modern turbidite lobes: a new insight from high resolution seismic data. Marine and Petroleum Geology, 23(4), 485-502.

Ghielmi, M., Minervini, M., Nini, C., Rogledi, S., Rossi, M., Vignolo, A., 2010. Sedimentary and tectonic evolution in the eastern Po-Plain and northern Adriatic Sea area from Messinian to Middle Pleistocene (Italy). Rendiconti Lincei, 21(1), 131-166.

Goodbred Jr, S. L., Kuehl, S. A., 2000. The significance of large sediment supply, active tectonism, and eustasy on margin sequence development: Late Quaternary stratigraphy and evolution of the Ganges–Brahmaputra delta. Sedimentary Geology, 133(3), 227-248.

Goodbred, S.L., Kuehl, S. a., Steckler, M.S., Sarker, M.H., 2003. Controls on facies distribution and stratigraphic preservation in the Ganges–Brahmaputra delta sequence. Sedimentary Geology 155, 301–316.

Goff, J. A., Mayer, L. A., Clarke, J. E., Pratson, L. F., 1996. Swath mapping on the continental shelf and slope: The Eel River Basin, northern California.Oceanography.

Grant, K.M., Rohling, E.J., Bar-Matthews, M., Ayalon, A., Medina-Elizalde, M., Bronk Ramsey, C., Satow, C., Roberts, A.P., 2012. Rapid coupling between ice volume and polar temperature over the past 150,000 years. Nature 491, 744-747

Grubišič, V., 2004. Bora-driven potential vorticity banners over the Adriatic. Q. J. R. Meteorolog. Soc. 130 (602), 2571–2603. http://dx.doi.org/10.1256/qj.03.71 (Part: A).

Hays, J.D., Imbrie, J., Shackleton, N.J., 1976. Variations in the Earth's orbit: Pacemaker of the ice ages. Science 194, 1121-1132. doi: 10.1126/science.194.4270.1121.

Hampson, G.J., 2010. Sediment dispersal and quantitative stratigraphic architecture across an ancient shelf. Sedimentology, v. 57(1), p. 96-141.

Haq, B. U., Hardenbol, J., Vail, P. R., 1987. Chronology of fluctuating sea levels since the Triassic. Science, 235(4793), 1156-1167.

Heezen BC, Hollister CD, 1964. Deep sea current evidence from abyssal sediments. Mar Geol 1:141-174

Helland-Hansen, W., and Martinsen, O.J. 1996. Shoreline trajectories and sequences: description of variable depositional-dip scenarios: Journal of Sedimentary Research, v. 66(4), p. 670-688.

Helland-Hansen, W., and Hampson, G.J., 2009. Trajectory analysis: concepts and applications: Basin Research, v. 21(5), p. 454-483.

Hendershott, M.C., Rizzoli, P., 1976. Winter circulation of Adriatic Sea. Deep-Sea Res. 23 (5), 353–370. http://dx.doi.org/10.1016/0011-7471(76)90834-2.

Henriksen, S., Hampson, G.J., Helland-Hansen, W., Johannessen, E.P., and Steel, R.J., 2009. Shelf edge and shoreline trajectories, a dynamic approach to stratigraphic analysis: Basin Research, v. 21(5), p. 445-453.

Hernández-Molina, F.J., Somoza, L., Rey, J., Pomar, L., 1994. Late Pleistocene–Holocene sediments on the Spanish continental shelves: model for very high resolution sequence stratigraphy. Marine Geology 120, 129–174.

Hernández-Molina, F. J., Somoza, L., Lobo, F., 2000. Seismic stratigraphy of the Gulf of Cádiz continental shelf: a model for Late Quaternary very high-resolution sequence stratigraphy and response to sea-level fall. Geological Society, London, Special Publications, 172(1), 329-362.

Hernández-Molina, F.J., Stow, D.A.V., Alvarez-Zarikian, C.A., Acton, G., Bahr, A., Balestra, B., Ducassou, E., Flood, R., Flores, J.-A., Furota, S., Grunert, P., Hodell, D., Jimenez-Espejo, F., Kim, J.K., Krissek, L., Kuroda, J., Li, B., Llave, E., Lofi, J., Lourens, L., Miller, M., Nanayama, F., Nishida, N., Richter, C., Roque, C., Pereira, H., Sanchez Goñi, M.F., Sierro, F.J., Singh, A.D., Sloss, C., Takashimizu, Y., Tzanova, A., Voelker, A., Williams, T., and Xuan, C., 2014. Onset of Mediterranean outflow into the North Atlantic. Science, 344(6189):1244–1250.

Hunt, D., Tucker, M. E., 1992. Stranded parasequences and the forced regressive wedge systems tract: deposition during base-level'fall. Sedimentary Geology, 81(1), 1-9.

Ivančan-Picek, B., Tutiš, V., 1996. A case study of severe Adriatic bora on 28 December 1992. Tellus 48a, 357–367.

Jerolmack, D.J., Swenson, J.B., 2007. Scaling relationships and evolution of distributary networks on wave-influenxed deltas. Geophysical Research Letters 34, L23402.

Jervey, M. T., 1988. Quantitative geological modeling of siliciclastic rock sequences and their seismic expression.

Johannessen, E.P., and Steel, R.J., 2005. Shelf-margin clinoforms and prediction of deepwater sands. Basin Research, v. 17(4), p. 521-550.

Jouet, G., Berne, S., Rabineau, M., Bassetti, M. A., Bernier, P., Dennielou, B., Taviani, M., 2006. Shoreface migrations at the shelf edge and sea-level changes around the Last Glacial Maximum (Gulf of Lions, NW Mediterranean). Marine Geology, 234(1), 21-42.

Kettner, A. J., Syvitski, J. P., 2008. HydroTrend v. 3.0: A climate-driven hydrological transport model that simulates discharge and sediment load leaving a river system. Computers & Geosciences, 34(10), 1170-1183.

Korus, J. T., Fielding, C. R., 2015. Asymmetry in Holocene river deltas: Patterns, controls, and stratigraphic effects. Earth-Science Reviews, 150, 219-242.

Kuehl, S.A., DeMaster, D.J., Nittrouer, C.A., 1986. Nature of sediment accumulation on the Amazon continental shelf. Cont. Shelf Res. 6 (1), 209–225.

Kuehl, S., Levy, B.M., Moore, W.S., Allison, M.A., 1997. Subaqueous delta of the Ganges-Brahmaputra river system. Mar. Geol. 144, 81–96.

Labaune, C., Jouet, G., Bernè, S., Gensous, B., Tesson, M., Delpeint, A., 2005. Seismic stratigraphy of the Deglacial deposits of the Rhône prodelta and of the adjacent shelf. Marine Geology 222–223, 299–311.

Lane, E. W., 1957. A Study of the Shape of Channels Formed by Natural Streams Flowing in Erodible Material, U.S. Army Corps of Eng., Mo. River Div., Omaha, Nebr.

Lascaratos A., Roether W., Nittis K., Klein B., 1999. Recent changes in deep water formation and spreading in the eastern Mediterranean Sea: a review. Progr Oceanogr 44(1):5–36.

Lee, C. M., Askari, F., Book, J., Carniel, S., Cushman-Roisin, B., Dorman, C., Kuzmic, M., 2005. Northern Adriatic response to a wintertime bora wind event. Eos, Transactions american geophysical union, 86(16), 157-165.

Liu, J. P., Xue, Z., Ross, K., Wang, H. J., Yang, Z. S., Li, A. C., Gao, S., 2009. Fate of sediments delivered to the sea by Asian large rivers: long-distance transport and formation of remote alongshore clinothems. The Sedimentary Record 7(4), 4-9.

Llave E, Matias H, Hernández-Molina FJ, Ercilla G, Stow DAV, Medialdea T (2011) Pliocene–Quaternary contourites along the northern Gulf of Cadiz margin: sedimentary stacking pattern and regional distribution. Geo-Mar Lett 31(5-6):377–390

Lobo, F. J., Hernández-Molina, F. J., Somoza, L., del Río, V. D., 2001. The sedimentary record of the post-glacial transgression on the Gulf of Cadiz continental shelf (Southwest Spain). Marine Geology, 178(1), 171-195.

Lobo, F. J., and Ridente, D., 2014. Stratigraphic architecture and spatio-temporal variability of high-frequency (Milankovitch) depositional cycles on modern continental margins: An overview. Marine Geology, 352, 215-247.

Lourens, L.J. 2004. Revised tuning of Ocean Drilling Program Site 964 and KC01B (Mediterranean) and implications for the $\Delta^{18}O$, tephra, calcareous nannofossil, and geomagnetic reversal chronologies of the past 1.1 Myr. Paleoceanography, v. 19, PA3010.

Mahon, R. C., Shaw, J. B., Barnhart, K. R., Hobley, D. E., McElroy, B., 2015. Quantifying the stratigraphic completeness of delta shoreline trajectories. Journal of Geophysical Research: Earth Surface.

Marini, M., Maselli, V., Campanelli, A., Foglini, F., Grilli, F., 2015. Role of the Mid-Adriatic deep in dense water interception and modification. Marine Geology.

Martorelli, E., Falcini, F., Salusti, E., Chiocci, F. L., 2010. Analysis and modeling of contourite drifts and contour currents off promontories in the Italian Seas (Mediterranean Sea). Marine Geology, 278(1), 19-30.

Mantziafou, A., Lascaratos, A., 2008. Deep-water formation in the Adriatic Sea: interannual simulations for the years 1979–1999. Deep-Sea Res I Oceanogr Res Pap 55(11):1403–1427.

Maselli, V., Trincardi, F., Cattaneo, A., Ridente, D., and Asioli, A., 2010. Subsidence patterns in the central Adriatic and its influence on sediment architecture during the last 400 kyr. Journal of Geophysical Research: Solid Earth, v. 115, no. B12, doi: 10.1029/2010JB007687.

Maselli V., Hutton E.W., Kettner A.J., Syvitski J.P.M., Trincardi F., 2011. High-frequency sea level and sediment supply fluctuations during Termination I: An integrated sequence-stratigraphy and modeling approach from the Adriatic Sea (Central Mediterranean), Marine Geology 287, 54-70.

Maslin, M. A., Ridgwell, A. J., 2005. Mid-Pleistocene revolution and the 'eccentricity myth'. Geological Society, London, Special Publications, 247(1), 19-34.

Masson DG, Harbitz CB, Wynn RB, Pedersen G, Løvholt F, 2006. Submarine landslides: processes, triggers and hazard prediction. Philos Trans R Soc A Math Phys Eng Sci 364(1845):2009–2039

Matthews I.P., Trincardi F., Lowe J.J., Bourne A.J., MacLeod A., Abbott P.M., Andersen N., Asioli A., Blockley S.P.E., Lane C.S., Oh Y.A., Satow C.S., Staff R.A., and Wulf S. 2015. Developing a robust tephrochronological framework for Late Quaternary marine records in the Southern Adriatic Sea: new data from core station SA03-11. Quaternary Science Reviews, v. 118 p. 84-104.

McCave, I.N., 1972. Transport and escape of fine-grained sediment from shelf areas. In: Swift, D.J.P., Duane, D.B., Pilkey, O.H. (Eds.), Shelf Sediment Transport: Process and Pattern. Van Nostrand Reinhold, New York, pp. 225–248.

Mellere, D.O., Plink-Bjorklund, P., Steel, R., 2002. Anatomy of shelf deltas at the edge of a prograding Eocene shelf margin, Spitsbergen. Sedimentology 49, 1181-1206

Michels, K.H., Kudrass, H.R., Hu, C., 1998. The submarine delta of the Ganges – Brahmaputra: cyclone-dominated sedimentation patterns. Marine Geology149, 133-154.

Midtkandal, I., and Nystuen, J.P., 2009. Depositional architecture of a low-gradient ramp shelf in an epicontinental sea: the lower Cretaceous of Svalbard: Basin Research, v. 21(5), p. 655-675.

Milankovitch, M., 1930. Mathematische Klimalehre und Astronomische Theorie der Klimaschwankungen. Handbuch der Klimatologie, Band I, Teil A. Gebruder Borntraeger, Berlin, 298 pp.

Milliman, J. D., and Meade, R. H., 1983. World-wide delivery of river sediment to the oceans. The Journal of Geology, 1-21.

Milliman, J. D., and Syvitski, J. P., 1992. Geomorphic/tectonic control of sediment discharge to the ocean: the importance of small mountainous rivers.The Journal of Geology, 525-544.

Minto'o, C. A., Bassetti, M. A., Morigi, C., Ducassou, E., Toucanne, S., Jouet, G., Mulder, T., 2015. Levantine intermediate water hydrodynamic and bottom water ventilation in the northern Tyrrhenian Sea over the past 56,000 years: New insights from benthic foraminifera and ostracods. Quaternary International, 357, 295-313.

Miramontes, E., Cattaneo, A., Jouet, G., Théreau, E., Thomas, Y., Rovere, M., Cauquil, E., Trincardi, F., 2015. The pianosa contourite depositional system (northern Tyrrhenian sea): drift morphology and plio-quaternary stratigraphic evolution.Marine Geology.

Mitchum Jr, R. M., Vail, P. R., Thompson III, S., 1977. Seismic stratigraphy and global changes of sea level: Part 2. The depositional sequence as a basic unit for stratigraphic analysis: Section 2. Application of seismic reflection configuration to stratigraphic interpretation.

Mitchum, R.M.J., Van Wagoner, J.C., 1991. High-frequency sequences and their stacking patterns: sequence-stratigraphic evidence of high-frequency eustatic cyclces. Sedimentary Geology 70(2-4), 131-160. doi: 10.1016/0037-0738(91)90139-5.

Mix, A. C., Ruddiman, W. F., 1985. Structure and timing of the last deglaciation: oxygen-isotope evidence. Quaternary Science Reviews, 4(2), 59-108.

Mix, A.C., Bard, E., and Schneider, R., 2001, Environmental processes of the ice age: land, oceans, glaciers (EPILOG): Quaternary Science Reviews, v. 20(4), p. 627-657.

Mulder, T., Hassan, R., Ducassou, E., Zaragosi, S., Gonthier, E., Hanquiez, V., Toucanne, S. et al., 2013. Contourites in the Gulf of Cadiz: a cautionary note on potentially ambiguous indicators of bottom current velocity. Geo-Marine Letters, 33(5), 357-367.

Myers PG, Haines K, Josey S., 1998. On the importance of the choice of wind stress forcing to the modeling of the Mediterranean Sea circulation. J Geophys Res Oceans 103(C8):15729–15749

Neal, J., Abreu, V., 2009. Sequence stratigraphy hierarchy and the accommodation succession method. Geology, v. 37(9), p. 779-782.

Nittrouer, C.A., Kuehl, S.A., Demaster, D.J., Kowsmann, R.O., 1986. The deltaic nature of Amazon shelf sedimentation. Geological Society of America Bulletin 4, 444-458.

Nittrouer, C.A., Kuehl, S.A., Figueiredo, G., Allison, M.A., Sommerfield, C.K, Rine, J.M., Faria, T.L.E.C., Silveira, O.M., 1996. The geological record preserved by Amazon shelf sedimentation. Cont. Shelf Res. 16, 817–841.

Nittrouer, C. A., 1999. STRATAFORM: Overview of its design and synthesis of its results, Mar. Geol., 154(1–4), 3–12, doi:10.1016/S0025-3227 (98)00128-5.

Nittrouer, J. A., D. Mohrig, and M. A. Allison., 2011. Punctuated sand transport in the lowermost Mississippi River, J. Geophys. Res., 116, F04025, doi:10.1029/2011JF002026.

Normark, W. R., Posamentier, H., Mutti, E., 1993. Turbidite systems: state of the art and future directions. Reviews of Geophysics, 31(2), 91-116.

Ori, G. G., Roveri, M.,Vannoni, F., 2009. Plio-Pleistocene sedimentation in the Apenninic–Adriatic foredeep (central Adriatic sea, Italy). Foreland basins, 8, 183-198.

Paola, C., 2000. Quantitative models of sedimentary basin filling, Sedimentology, 47, 121–178, doi:10.1046/j.1365-3091.2000.00006.x.

Paola, C., R. R. Twilley, D. A. Edmonds, W. Kim, D. Mohrig, G. Parker, E. Viparelli, and V. R. Voller, 2011. Natural processes in delta restoration: Application to the Mississippi Delta, Annu. Rev. Mater. Sci., 3, 67–91, doi:10.1146/annurev-marine-120709-142856.

Paschini, E., Artegiani, A., Pinardi, N., 1993. The mesoscale eddy field of the Middle Adriatic Sea during fall 1988. Deep Sea Research Part I: Oceanographic Research Papers, 40(7), 1365-1377.

Patruno, S., Hampson, G. J., Jackson, C. A. L., Whipp, P. S., 2015. Quantitative progradation dynamics and stratigraphic architecture of ancient shallow-marine clinoform sets: a new method and its application to the Upper Jurassic Sognefjord Formation, Troll Field, offshore Norway. Basin Research.

Pirmez, C., Pratson, L. F., Steckler, M. S., 1998. Clinoform development by advection-diffusion of suspended sediment: Modeling and comparison to natural systems. Journal of Geophysical Research: Solid Earth (1978–2012), 103(B10), 24141-24157.

Piva, A., Asioli, A., Schneider, R. R., Trincardi, F., Andersen, N., Colmenero-Hidalgo, E., Dennielou, B.,. Flores, J.A., and Vigliotti L., 2008. Climatic cycles as expressed in sediments of the PROMESS1 borehole

PRAD1-2, Central Adriatic, for the last 370 ka, 1: integrated stratigraphy. Geochemistry, Geophysics, Geosystems, v. 9 (1), Q01R01, doi: 10.1029/2007GC001713.

Piva, A., Asioli, A., Trincardi, F., Schneider, R. R., Vigliotti, L., 2008. Late-Holocene climate variability in the Adriatic sea (Central Mediterranean). The Holocene, 18(1), 153-167.

Plink-Björklund, P., Mellere, D., Steel, R. J., 2001. Turbidite variability and architecture of sand-prone, deep-water slopes: Eocene clinoforms in the Central Basin, Spitsbergen. Journal of Sedimentary Research, 71(6), 895-912.

Plink-Björklund, P., Steel, R., 2002. Sea-level fall below the shelf edge, without basin-floor fans. Geology, 30(2), 115-118.

Posamentier, H. W., 1988. Eustatic controls on clastic deposition II—sequence and systems tract models.

Poulain, P. M., 2001. Adriatic Sea surface circulation as derived from drifter data between 1990 and 1999. Journal of Marine Systems, 29(1), 3-32.

Pratson LF, Nittrouer CA, Wilberg P, Steckler MS, Swenson JB, Cacchione DA, Karson JA, Murray AB, Wolinsky MA, Gerber TP, Mullenbach BL, Spinelli GA, Fulthorpe CS, O'Grady DB, Parker G, Driscoll NW, Burger RL, Paola C, Orange DL, Field ME, Friedrichs CT, Fedele JJ, 2007. Seascape evolution on clastic continental shelves and slopes. In: Nittrouer, C.A., Austin, J.A., Field, M.E., Kravitz, J.H., Syvitski, J.P.M., Wiberg, P.L. (Eds.), Continental Margin Sedimentation: From Sediment Transport to Sequence Stratigraphy. IAS Special Publication, 37. Blackwell, 339–380.

Rabineau, M., Berné, S., Ledrezen, E., Lericolais, G., Marsset, T., Rotunno, M., 1998. 3D architecture of lowstand and transgressive Quaternary sand bodies on the outer shelf of the Gulf of Lion, France. Marine and Petroleum Geology, 15(5), 439-452.

Rabineau, M., Berné, S., Aslanian, D., Olivet, J. L., Joseph, P., Guillocheau, F., Granjeon, D., 2005. Sedimentary sequences in the Gulf of Lion: a record of 100,000 years climatic cycles. Marine and Petroleum Geology, 22(6), 775-804.

Rebesco, M., Hernández-Molina, F. J., Van Rooij, D., Wåhlin, A., 2014. Contourites and associated sediments controlled by deep-water circulation processes: state-of-the-art and future considerations. Marine Geology, 352, 111-154.

Reimer P.J., Bard, E., Bayliss, A., Beck, J.W., Blackwell, P.G., Bronk Ramsey, C., Buck, C.E., Cheng, H., Edwards, R.L., Friedrich, M., Grootes, P.M., Guilderson, T.P., Haflidason, H., Hajdas, I., Hatte, C., Heaton, T.J., Hogg, A.G., Hughen, K.A., Kaiser, K.F., Kromer, B., Manning, S.W., Niu, M., Reimer, R.W., Richards, D.A., Scott, E.M., Southon, J.R., Turney, C.S.M., and van der Plicht, J., 2013. IntCal13 and MARINE13 radiocarbon age calibration curves 0-50000 years calBP. Radiocarbon, v. 55, 4, p. 1869-1887.

Ricci Lucchi, F., 1986. The Oligocene to Recent foreland basins of the northern Apennines. Foreland basins, 103-139.

Rich, J. L., 1951. Three critical environments of deposition, and criteria for recognition of rocks deposited in each of them. Geological Society of America Bulletin, 62(1), 1-20.

Ridente, D., Trincardi, F., 2002. Eustatic and tectonic control on deposition and lateral variability of Quaternary regressive sequences in the Adriatic basin (Italy). Marine geology, 184(3), 273-293.

Ridente, D., Trincardi, F., 2005. Pleistocene “muddy” forced-regression deposits on the Adriatic shelf: a comparison with prodelta deposits of the late Holocene highstand mud wedge. Marine Geology, 222, 213-233.

Ridente, D., Fracassi, U., Di Bucci, D., Trincardi, F., and Valensise, G., 2008, Middle Pleistocene to Holocene activity of the Gondola fault zone (southern Adriatic foreland): Deformation of a regional shear zone and seismotectonic implications: Tectonophysics, v. 453, p. 110–121, doi: 10.1016/j.tecto.2007.05.009

Ridente, D., Trincardi, F., Piva, A., Asioli, A., 2009. The combined effect of sea level and supply during Milankovitch cyclicity: Evidence from shallow-marine δ18O records and sequence architecture (Adriatic margin). Geology,37(11), 1003-1006.

Royden, L., Patacca, E., & Scandone, P., 1987. Segmentation and configuration of subducted lithosphere in Italy: an important control on thrust-belt and foredeep-basin evolution. Geology, 15(8), 714-717.

Schattner, U., Lazar, M., Tibor, G., Ben-Avraham, Z., Makovsky, Y., 2010. Filling up the shelf—A sedimentary response to the last post-glacial sea rise.Marine Geology, 278(1), 165-176.

Schlager, W., 2004. Fractal nature of stratigraphic sequences. Geology, 32(3), 185-188.

Schwarzacher, W. (2000). Repetitions and cycles in stratigraphy. Earth-Science Reviews, 50(1), 51-75.

Scrocca, D., 2006, Thrust front segmentation induced by differential slab retreat in the Apennines (Italy): Terra Nova, v. 18, p. 154–161, doi: 10.1111/j.1365-3121.2006.00675.x.

Severinghaus, J. P., Sowers, T., Brook, E. J., Alley, R. B., Bender, M. L., 1998. Timing of abrupt climate change at the end of the Younger Dryas interval from thermally fractionated gases in polar ice. Nature, 391(6663), 141-146.

Shackleton, N. J., Backman, J., Zimmerman, H., Kent, D. V., Hall, M. A., Roberts, D. G., Westberg-Smith, J., et al., 1984. Oxygen isotope calibration of the onset of ice-rafting and history of glaciation in the North Atlantic region. Nature, 307(5952), 620-623.

Siddall, M., Rohling, E.J., Almogi-Labin, A., Hemleben, Ch, Meischner, D., Schmelzer, I., Smeed, D.A., 2003. Sea-level fluctuations during the last glacial cycle. Nature 423, 853-858.

Siddall, M., Rohling, E.J., Thompson, W.G., Waelbroeck, C., 2008. Marine Isotope Stage 3 sea level fluctuations: data synthesis and new outlook. Reviews of Geophysics 46, RG4003. doi: 10.1029/2007RG000226.

Sierro, F. J., Andersen, N., Bassetti, M. A., Berné, S., Canals, M., Curtis, J. H., Schneider, R., 2009. Phase relationship between sea level and abrupt climate change. Quaternary Science Reviews, 28(25), 2867-2881.

Sømme, T. O., Piper D. J. W., Deptuck M. E., Helland-Hansen, W., 2011. Linking Onshore–Offshore sediment dispersal in the Golo source-to-sink system (Corsica, France) during the Late Quaternary. Journal of Sedimentary Research 81, 2, 118-137.

Stanley, D. J., Warne, A. G., 1994. Worldwide initiation of Holocene marine deltas by deceleration of sea-level rise. Science, 265(5169), 228-231.

Steckler, M.S., Mountain, G.S., Miller, K.G., Christie-Blick, N., 1999. Reconstruction of Tertiary progradation and clinoform development on the New Jersey passive margin by 2-D backstripping. Marine Geology 154, 399-420.

Steel, R.J., Crabaugh, J., Schellpeper, M., Mellere, D., Plink-Björklund, P., Deibert, J., and Loeseth, T., 2000. Deltas vs. rivers on the shelf edge: their relative contributions to the growth of shelf-margins and basin-floor fans (Barremian and Eocene, Spitsbergen). Deepwater Reservoirs of the World, v. 33, p. 981-1009.

Steel, R.J., and Olsen, T., 2002. Clinoforms, clinoform trajectories and deepwater sands. Sequence Stratigraphic Models for Exploration and Production. Evolving Methodology, Emerging Models and Application Histories, p. 367-381.

Stow, D. A., Faugères, J. C., Howe, J. A., Pudsey, C. J., Viana, A. R., 2002. Bottom currents, contourites and deep-sea sediment drifts: current state-of-the-art. Geological Society, London, Memoirs, 22(1), 7-20.

Stow, D. A. V., Hunter, S., Wilkinson, D., Hernández-Molina, F. J., 2008. The nature of contourite deposition. Developments in Sedimentology, 60, 143-156.

Stuiver M. and Reimer P.J., 1993. Extended 14C data base and revised CALIB 3.0 14C age calibration program. Radiocarbon, v. 35, p. 215-230.

Swenson J. B., Paola C., Pratson L., Voller V. R., Murray A. B., 2005. Fluvial and marine controls on combined subaerial and subaqueous delta progradation: Morphodynamic modeling of compound-clinoform development. Journal of Geophysical Research: Earth Surface, 110, 0148-0227.

Teatini, P., Tosi, L., and Strozzi, T., 2011. Quantitative evidence that compaction of Holocene sediments drives the present land subsidence of the Po Delta, Italy. Journal of Geophysical Research, v. 116, B08407, doi: 10.1029/2010JB008122, 2011.

Torre, M., Di Nocera, S., Ortolani, F., 1988. Evoluzione post-tortoniana dell'Appennino meridionale. Mem. Soc. Geol. Ital, 41, 47-56.

Toucanne, S., Mulder, T., Schönfeld, J., Hanquiez, V., Gonthier, E., Duprat, J., Zaragosi, S., 2007. Contourites of the Gulf of Cadiz: a high-resolution record of the paleocirculation of the Mediterranean outflow water during the last 50,000 years. Palaeogeography, Palaeoclimatology, Palaeoecology, 246(2), 354-366.

Trincardi, F., Asioli, A., Cattaneo, A., Correggiari, A., Langone, L., 1996. Stratigraphy of the late-Quaternary deposits in the Central Adriatic basin and the record of short-term climatic events. Memorie Istituto Italaliano Idrobiologia 55, 39-70.

Trincardi, F., Correggiari, A., 2000. Quaternary forced regression deposits in the Adriatic basin and the record of composite sea-level cycles. Geological Society, London, Special Publications, 172(1), 245-269.

Trincardi F, Foglini F, Verdicchio G, Asioli A, Correggiari A, Minisini D, Piva A, Remia A, Ridente D, Taviani M. 2007. The impact of cascading currents on the Bari Canyon System, SW-Adriatic Margin (Central Mediterranean). Mar Geol 246(2):208–230.

Toucanne, S., Jouet, G., Ducassou, E., Bassetti, M. A., Dennielou, B., Minto'o, C. M. A., Mahmi, M., Touyet, N., Charlier, K., Lericolais, G., Mulder, T., 2012. A 130,000-year record of Levantine Intermediate Water flow variability in the Corsica Trough, western Mediterranean Sea. Quaternary Science Reviews, 33, 55-73.

Vail, P. R., Mitchum Jr, R. M., Thompson III, S., 1977. Seismic Stratigraphy and Global Changes of Sea Level: Part 4. Global Cycles of Relative Changes of Sea Level.: Section 2. Application of Seismic Reflection Configuration to Stratigraphic Interpretation.

Vail, P. R., 1987. Seismic stratigraphy interpretation using sequence stratigraphy: Part 1: Seismic stratigraphy interpretation procedure.

Vail, P.R., Audemard, F., Bowman, S.A., Eisner, P.N. and Perez-Cruz, G., 1991. The stratigraphic signatures of tectonics, eustasy and sedimentation: an overview. In: A. Seilacher and G. Eisner (Editors), Cycles and Events in Stratigraphy, II. Springer-Verlag, Tiibingen, in press

Van Wagoner, J. C., 1988. An overview of the fundamentals of sequence stratigraphy and key definitions.

Venditti, J.G., Church, M., 2014. Morphology and controls on the position of a gravel-sand transition: Fraser River, British Columbia. Journal of Geophysical Research 119, 1959-1976.

Verdicchio G, Trincardi F, Asioli A. 2007. Mediterranean bottom-current deposits: an example from the Southwestern Adriatic Margin. Geol Soc Lond, Spec Publ 276(1):199–224.

Verdicchio G, Trincardi F, 2008. Mediterranean shelf-edge muddy contourites: examples from the Gela and South Adriatic basins. Geo-Mar Lett 28(3):137–151.

Vilibič, I., Orlič, M., 2001. Least squares tracer analysis of water masses in the South Adriatic (1967–1990). Deep-Sea Res. I 48, 2297–2330.

Walsh, J.P., Nittrouer, C.a., Palinkas, C.M., Ogston, A.S., Sternberg, R.W., Brunskill, G.J., 2004. Clinoform mechanics in the Gulf of Papua, New Guinea. Cont. Shelf Res. 24, 2487–2510.

Wheatcroft, R. A., Sommerfield, C. K., Drake, D. E., Borgeld, J. C., Nittrouer, C. A., 1997. Rapid and widespread dispersal of flood sediment on the northern California margin. Geology, 25(2), 163-166.

Whipple, K., X., Hancock, G., S., and. Anderson, R., S., 2000. River incision into bedrock: Mechanics and relative efficacy of plucking, abrasion, and cavitation, Geol. Soc. Am. Bull., 112(3), 490–503, doi:10.1130/0016-7606(2000)112<490:RIIBMA>2.0.CO;2.

Yi, S., Saito, Y., Zhao, Q., Wang, P., 2003. Vegetation and climate changes in the Changjiang (Yangtze River) Delta, China, during the past 13,000 years inferred from pollen records. Quaternary Science Reviews, 22(14), 1501-1519.

Zhu, Y., Bhattacharya, J. P., Li, W., Lapen, T. J., Jicha, B. R., Singer, B. S., 2012. Milankovitch-scale sequence stratigraphy and stepped forced regressions of the Turonian Ferron Notom Deltaic Complex, South-Central Utah, USA. Journal of Sedimentary Research, 82(9), 723-746.